NASA CONTRACTOR REPORT

NASA CR-25
C. 1

NASA CR-252

DETERMINATION OF OPTICAL TECHNOLOGY EXPERIMENTS FOR A SATELLITE

by Herbert F. Wischnia, Harold S. Hemstreet, and John G. Atwood

Prepared under Contract No. NAS 8-11408 *by*
PERKIN-ELMER
Norwalk, Conn.
for

NATIONAL AERONAUTICS AND SPACE ADMINISTRATION • WASHINGTON, D. C. • JULY 1965

DETERMINATION OF OPTICAL TECHNOLOGY EXPERIMENTS FOR A SATELLITE

By Herbert F. Wischnia, Harold S. Hemstreet, and John G. Atwood

Prepared under Contract No. NAS 8-11408 by
PERKIN-ELMER
Norwalk, Conn.

for

NATIONAL AERONAUTICS AND SPACE ADMINISTRATION

For sale by the Clearinghouse for Federal Scientific and Technical Information
Springfield, Virginia 22151 – Price $7.00

TABLE OF CONTENTS

Section	Title	Page
I	INTRODUCTION	1-1
	1.1 Some Requirements of Optical Communication in Space	1-3
	1.2 System Trade-Offs	1-12
	1.3 A Forecast of the Role of Optical Communications in Space Exploration	1-16
	1.4 How Much Channel Capacity is Enough?	1-18
	1.5 Adequacy of Planned Experiments	1-19
	1.6 Summary	1-20
II	OPTICAL COMMUNICATIONS/TECHNOLOGY EXPERIMENT RECOMMENDATIONS	2-1
	2.1 Summary Descriptions of the Recommended Atmospheric Effects Experiments	2-2
	2.2 Brief Description of an Eye-Hand Loop Experiment	2-3
	2.3 Summary Descriptions of the Recommended Heterodyne Experiments	2-4
	2.4 Summary Descriptions of the Recommended Tracking and Acquisition Experiments	2-5
	2.5 Communications Experiments	2-8
	2.6 Optics Technology Experiments	2-8
	2.7 Experiment Definition Reports	2-10
	2.8 Recommendation on the Aperture Diameter for the Optical Technology Satellite	2-36
III	ATMOSPHERIC EXPERIMENTS DISCUSSION	3-1
	3.1 Characterizing the Transmission Channel in Space-To-Space Optical Communications Through the Atmosphere	3-1
	3.2 Laser Signal Perturbations	3-3
	3.3 Background	3-30
IV	HETERODYNE AND INTENSITY DETECTION OF LASER LIGHT	4-1
	4.1 Comparison of Optical Detection with Microwave Detection	4-1
	4.2 Effect of Atmospheric Turbulence on Optical Heterodyne Detection	4-2
	4.3 Optical Heterodyne Detection and Intensity Detection	4-4

TABLE OF CONTENTS (Continued)

Section	Title	Page
V	ACQUISITION EXPERIMENTS DISCUSSION	5-1
	5.1 The Effect of Background Illumination on Down-Looking Acquisition and Tracking	5-1
	5.2 Acquisition to 1 Degree	5-4
	5.3 The Acquisition Experiment	5-12
VI	TRACKING EXPERIMENTS DISCUSSION	6-1
	6.1 Tracking Accuracy Dependence on SNR	6-1
	6.2 Tracking to 1/10 of an Arc-Second	6-8
	6.3 Tracking in the Presence of Spacecraft Motion Disturbance	6-21
	6.4 Suspension Systems Comparison	6-26
	6.5 Focus and Alignment Techniques	6-28
	6.6 Optics Technology Experiments	6-34
VII	PHOTOMETRY CONSIDERATIONS	7-1
	7.1 Maximum Achievable Signal-To-Noise Ratio	7-3
	7.2 Background Light Level	7-10
	7.3 Detectors	7-24
	7.4 Acquisition Photometry	7-33
VIII	OPTICAL COMMUNICATIONS	8-1
	8.1 General Considerations Applicable to Deep-Space and Satellite Communications	8-1
	8.2 Information Capacity of an Optical Channel	8-2
	8.3 Signal and Noise Levels at the Optical Receiver	8-4
	8.4 Selection of Optical System Parameters	8-7
	8.5 Modulation System Considerations	8-9
	8.6 Communications in Deep Space	8-32
	8.7 Communications with a Synchronous Satellite	8-49
	8.8 A Communication Approach for the Optical Technology Satellite	8-57
	REFERENCES	9-1

TABLE OF CONTENTS (Continued)

Appendices	Title	Page
A	FLOW CHART SHOWING METHOD OF PERFORMING PHASE I TASKS	A-1
B	ORBITAL CONSIDERATIONS	B-1
C	REFLECTOR STUDY	C-1
D	COMMUNICATIONS SYSTEMS AND PROBABILITY FORMULAE	D-1
E	ATMOSPHERIC EFFECTS ON SIGNAL WAVEFORMS	E-1

LIST OF ILLUSTRATIONS

Figure	Title	Page
1-1	Space Communication Elements	1-4
1-2	Laser Communication Performance	1-15
3-1	General Optical Communication Link	3-2
3-2	Turbulent Effects Encountered at Various Altitudes	3-9
3-3	Quantitative Analysis of Image Degradation Due to Atmospheric Turbulence	3-10
3-4	Atmospheric Refraction Displaces True Angular Position of Spacecraft	3-13
3-5	Number of Uplooking Transmissions to Acquire Spacecraft Depends on Uncertainty in Beam Position	3-17
3-6	Average Spatial Coherence Versus Lateral Separation Distance	3-23
3-7	Lines R(2) of the 2-0 Bands of HCl^{35} and HCl^{37} at Two Gas Pressures	3-27
4-1	Optical Heterodyne Detection	4-3
5-1	Acquisition Subsystem	5-13
5-2	Received Power Versus Range	5-15
5-3	Tracking Subsystem	5-22
5-4	Optical Arrangement for Evaluation of Beacon Acquisition Mechanisms	5-24
5-5	A Mechanism for Beacon Acquisition	5-24
6-1	Single Axis Tracking Sensor	6-2
6-2	Fraunhofer Diffraction at a Circular Aperture	6-2

LIST OF ILLUSTRATIONS (Continued)

Figure	Title	Page
6-3	Image Light Energy On One Side Of a Knife-Edge Boundary	6-5
6-4	Rate of Energy Transfer Across a Knife Edge in the Image Plane	6-6
6-5	Energy Transfer Across a Knife Edge At The Image Plane Of A Circular Aperture	6-9
6-6	Optical Technology Satellite - Basic "32-Inch System" - Block Diagram (Telescope 1)	6-10
6-7	Optical Technology Satellite - 1 Meter Aperture - Basic Block Diagram (Telescope 2)	6-11
6-8	Transmit Beam Deflector Subsystem Utilizing Transfer Lens Principle	6-19
6-9	Deep-Space Optical Communication System Block Diagram	6-22
6-10	Optical Technology Satellite Ground Station, Basic Block Diagram	6-23
6-11	Stratoscope II Focusing Technique	6-29
6-12	Alignment Techniques	6-31
7-1	Probability Density Curve and Probability of Measurement Uncertainty Exceeding Incremental Signal Magnitude Change of Interest	7-4
7-2	Power Density Versus Range for Transmitter Power Equal to 1.0 Watt	7-6
7-3	Photons/Sec Versus Wavelength for Power of One Watt	7-7
7-4	S/N Ratio Versus Bandwidth and Average Photon Arrival Rate	7-8
7-5	Angle Versus Time of a Space Vehicle Along a Hohmann Elliptical Trajectory to Mars From The Earth	7-11

LIST OF ILLUSTRATIONS (Continued)

Figure	Title	Page
7-6	Calculated Maximum Irradiance From the Earth at the Moon	7-12
7-7	Calculated Maximum Total Irradiance From the Earth at the Moon	7-12
7-8	Earthshine Intensity Varies as Cosine θ When Viewed From Vehicle	7-13
7-9	Radiant Intensity of Earth as a Function of Phase of Illumination	7-14
7-10	Earthshine Radiance Distribution Varies as Cos θ	7-16
7-11	Solar Irradiance Curve From 0.2 to 3μ	7-17
7-12	Coronal Radiance, B_{cor}, Normalized by Photospheric Radiance $B_{\odot}$ Expressed as a Function of Distance r in Terms of the Sun's Radius $R_{\odot}$	7-18
7-13	Calculated Spectral Irradiance From Planets and Brightest Stars at the Top of the Atmosphere	7-19
7-14	Probable Spectral Irradiance From a One Square Degree Starfield In or Near the Galactic Plane	7-23
7-15	Calculated Maximum Irradiance From Mercury Outside the Earth's Atmosphere	7-25
7-16	Calculated Maximum Irradiance From Venus Outside the Earth's Atmosphere	7-25
7-17	Calculated Maximum Irradiance From Mars Outside the Earth's Atmosphere	7-26
7-18	Calculated Maximum Irradiance From Jupiter Outside the Earth's Atmosphere	7-26
7-19	Calculated Maximum Irradiance From Saturn Outside the Earth's Atmosphere	7-27

LIST OF ILLUSTRATIONS (Continued)

Figure	Title	Page
7-20	Calculated Maximum Irradiance From Uranus Outside the Earth's Atmosphere	7-27
7-21	Calculated Maximum Irradiance From Neptune and Pluto Outside the Earth's Atmosphere	7-28
7-22	Calculated Maximum Irradiance From the Full Moon Outside the Earth's Atmosphere	7-28
7-23	Calculated Irradiance From Fifteen of the Brightest Stars Outside the Earth's Atmosphere	7-29
7-24	Detectivity Versus Wavelength for the Best Detectors	7-30
7-25	Optimum Spectral Detectivities of Infrared Detectors Prepared by Santa Barbara Research Center	7-31
7-26	Spectral Response Characteristics	7-32
7-27	Photomultiplier Photocathode Dark Current Equivalent Watts	7-34
8-1	Pulse Position Modulation Error Rate Comparison	8-11
8-2	Pulse Position Modulation - Highest Pulse Error Rates, 32 Resolvable Positions	8-14
8-3	Pulse Position Modulation - Highest Pulse Error Rates, 64 Resolvable Positions	8-15
8-4	Pulse Position Modulation - Highest Pulse Error Rates, 128 Resolvable Positions	8-16
8-5	Pulse Position Modulation - Highest Pulse Error Rates, 256 Resolvable Positions	8-17
8-6	Pulse Code Modulation Error Rates, Five-Bit Code	8-18
8-7	Pulse Code Modulation Error Rates, Six-Bit Code	8-19
8-8	Pulse Code Modulation Error Rates, Seven-Bit Code	8-20

LIST OF ILLUSTRATIONS (Continued)

Figure	Title	Page
8-9	Pulse Code Modulation Error Rates, Eight-Bit Code	8-21
8-10	Equal Equivocation Curves for PCM and PPM-Large Error Rates	8-24
8-11	Equal Equivocation Curves for PCM and PPM-Small Error Rates	8-25
8-12	Comparison of Pulse Code Modulation - Polarization With Pulse Position Modulation - Highest Pulse	8-27
8-13	Three-Pass Modulator Optical Diagram	8-54
8-14	Prototype Multipass Modulator	8-55
8-15	Multipass Modulator With Resonant Line Exciter	8-56
8-16	Synchronous Detector	8-64
8-17	Block Diagram - Communication System - Uncoded	8-66
8-18	Correlator and Synchronizer for Bicoded Signals	8-67
8-19	Block Diagram - Communication System - Coded	8-69

CR-252

LIST OF TABLES

Number	Title	Page
3-1	Fractional Transmission Through Atmosphere Versus Wavelength and Zenith Angle	3-5
3-2	Refraction Angle Versus Apparent Zenith Angle	3-14
3-3	RMS Angle of Arrival Fluctuations Versus Zenith Angle θ and Receiving Aperture Diameter	3-20
3-4	Albedo of Various Planets	3-32
3-5	Spectral Radiances of Typical Optical Noise Sources	3-34
3-6	Irradiance Values Just Outside the Earth's Atmosphere for Several Sources	3-37
5-1	Assumed Deep-Space Parameters	5-8
5-2	Assumed Satellite System Parameters	5-9
5-3	Comparison of Deep-Space and Satellite System Signal-to-Noise Ratios	5-11
5-4	Relative Stellar Light Input	5-15
5-5	Signal-to-Noise Ratio Degradation Due to Earthshine	5-16
5-6	Beacon Power Required to Simulate 10^8 Mile Condition at 20 x 10^3 Miles with Transmitter Beamwidth of 5 Arc-Seconds	5-18
7-1	Calculation of Total Visible Star Irradiance Per Square Degree in or Near Galactic Plane	7-21
7-2	Spectral Distribution of Stars by Color Class	7-22
7-3	PMT Performance Summary for S20 RCA 7265 (as Measured by Perkin-Elmer)	7-35
7-4	Relative Power Levels at Photodetector for 6328Å Operation	7-37

LIST OF TABLES (Continued)

Number	Title	Page
7-5	Relative Power Levels at Photodetector for 8400Å Operation	7-42
8-1	Comparison of Simple Coding and Error or Correcting Coding	8-30
8-2	Design Parameters for Laser Communications Between a Deep-Space Probe and Earth	8-33
8-3	Laser Communications Performance Between a Deep-Space Probe and Earth	8-47
8-4	Design Parameters for Laser Communications Between Satellite in Synchronous Orbit and Earth	8-50
8-5	Laser Communications Performance Between Satellite in Synchronous Orbit and Earth	8-51

CR-252

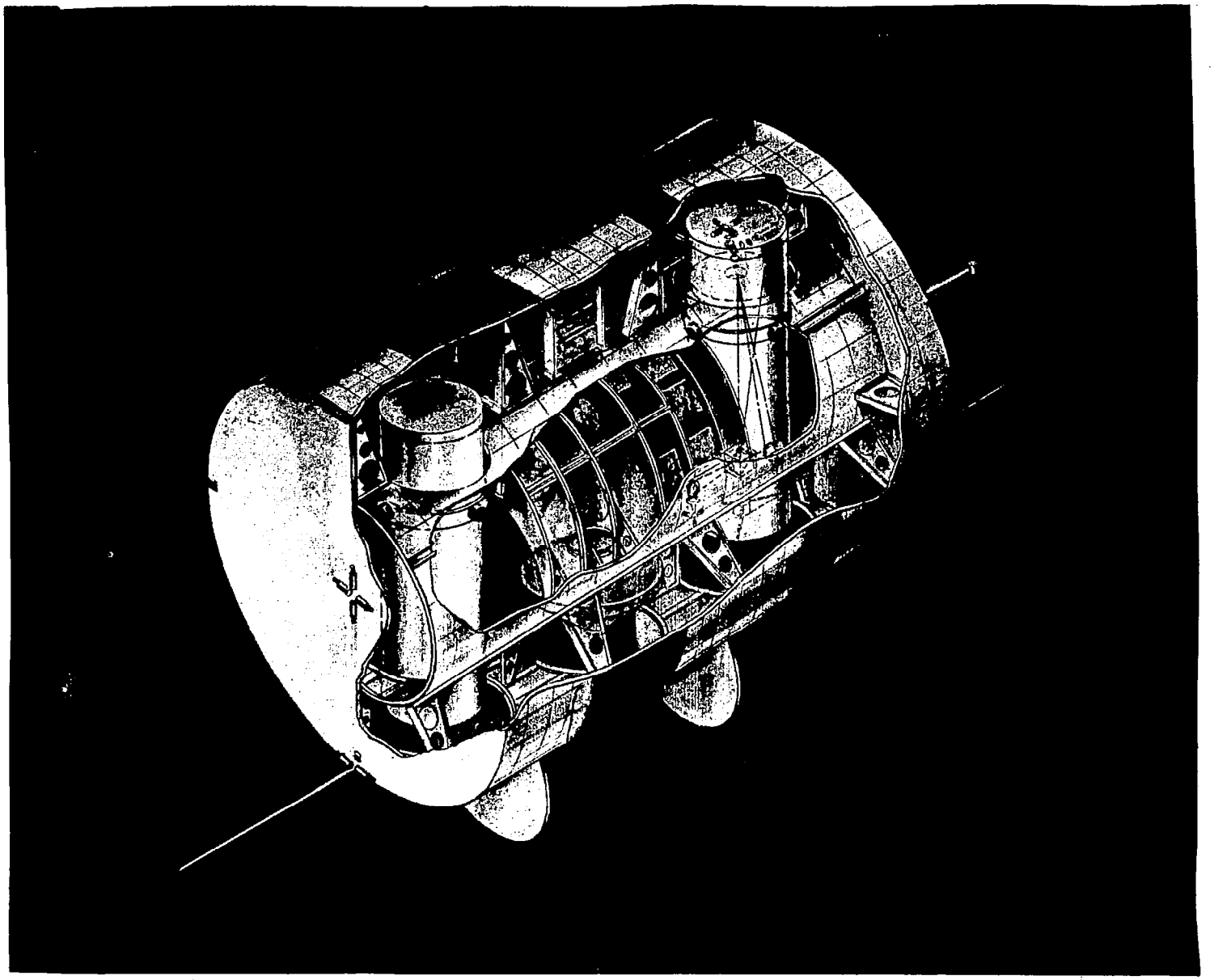

Optical Technology Satellite

SECTION I

INTRODUCTION

The purpose of this study is to recommend a set of experiments to be conducted in an earth satellite vehicle which will best advance the development of optical technology in space.

In order to make a wise choice of these experiments we must look ahead into the next ten year period of space exploration. We must attempt to forecast those important uses of optical technology in space for which a satellite experiment program now will be most rewarding. We must also attempt to foresee the unanswered technical questions and the difficult engineering performance levels required in these uses. We can then aim the experiments at securing quantitative answers to the questions and at exploring the engineering difficulties.

In conducting the study, we have limited our field of consideration to optical communication and certain closely related general aspects of optical astronomy and optical scientific instrumentation in space. Important applications such as reconnaissance and mapping, optical radar, re-entry communication through the ion sheath, etc., have not been considered. One reason for this limitation is that the specialized aspects of these fields of optical technology are being thoroughly explored by major NASA programs now underway.

There is another reason for the limitation. Our study shows that the concentration of experimental effort on the communication use of optics in

space is not really a narrow limitation on the general usefulness of the results. For example, some of the key issues concerning space astronomy are:

(1) diffraction-limited performance of large apertures

(2) guidance to fractions of an arc-second

(3) isolation from vehicle disturbances

(4) ground-controlled testing and adjustment of the system.

The list of key issues in space laser communication includes each of these as well as others. In fact, it appears that the only major technical issue in space astronomy which should not be included at present in a study of space optical communications is the very special problem of developing a technique which will permit launching 100-inch (and larger) giant aperture telescopes and maintaining their performance to diffraction limits.

It is fairly clear that apertures this large will not be economically justifiable in optical communications systems for a long time, even though they will be justifiable for astronomy as soon as they are technically feasible.

Diffraction-limited apertures of 100 inches have not been achieved on the ground, and are now far from being achieved in space without several years of ground-based research effort and component development. In contrast, virtually all the system and component technology necessary for a wide range of space laser communication systems with apertures up to 1 meter diameter is now in existence in ground-based form. Thus, planning for optical communication experiments in space can be done on a realistic basis at the present time.

Finally, numerous studies[1,2] show that when the need arises for communication channels of the order of 10^4 to 10^7 bits/second capacity at interplanetary distances, laser communication techniques appear to be the system of choice. This should remain true at least until the era of large nuclear electrical power plants in spacecraft.

For all these reasons, it is sound to place the major stress in planning the Optical Technology Satellite on the problems of optical communication. These include most of the important optical technology questions of satellite astronomy which are ready for space experimentation and are not being explored by other NASA programs.

The first part of our study of the Optical Technology Satellite was directed at the questions from this technical strategy viewpoint. We have developed a fairly plausible picture of some roles of optical communication in space exploration. This picture will be presented, for it sets the background for many of the choices of experiments we describe in later sections.

1.1 SOME REQUIREMENTS OF OPTICAL COMMUNICATION IN SPACE

There are some basic facts about optical communication systems in space which are not entirely obvious, but which dominate their design. Consider a system as shown schematically in Figure 1-1. Here for purposes of discussion the vehicle is shown as having separate transmitting and receiving antennae. It sends signals to a receiver on the Earth's surface which it locates by tracking an adjacent beacon transmitter. It may also receive signals on the beacon beam. Some facts about a practical system of this sort are as follows:

---

[1] References can be found starting on page 9-1.

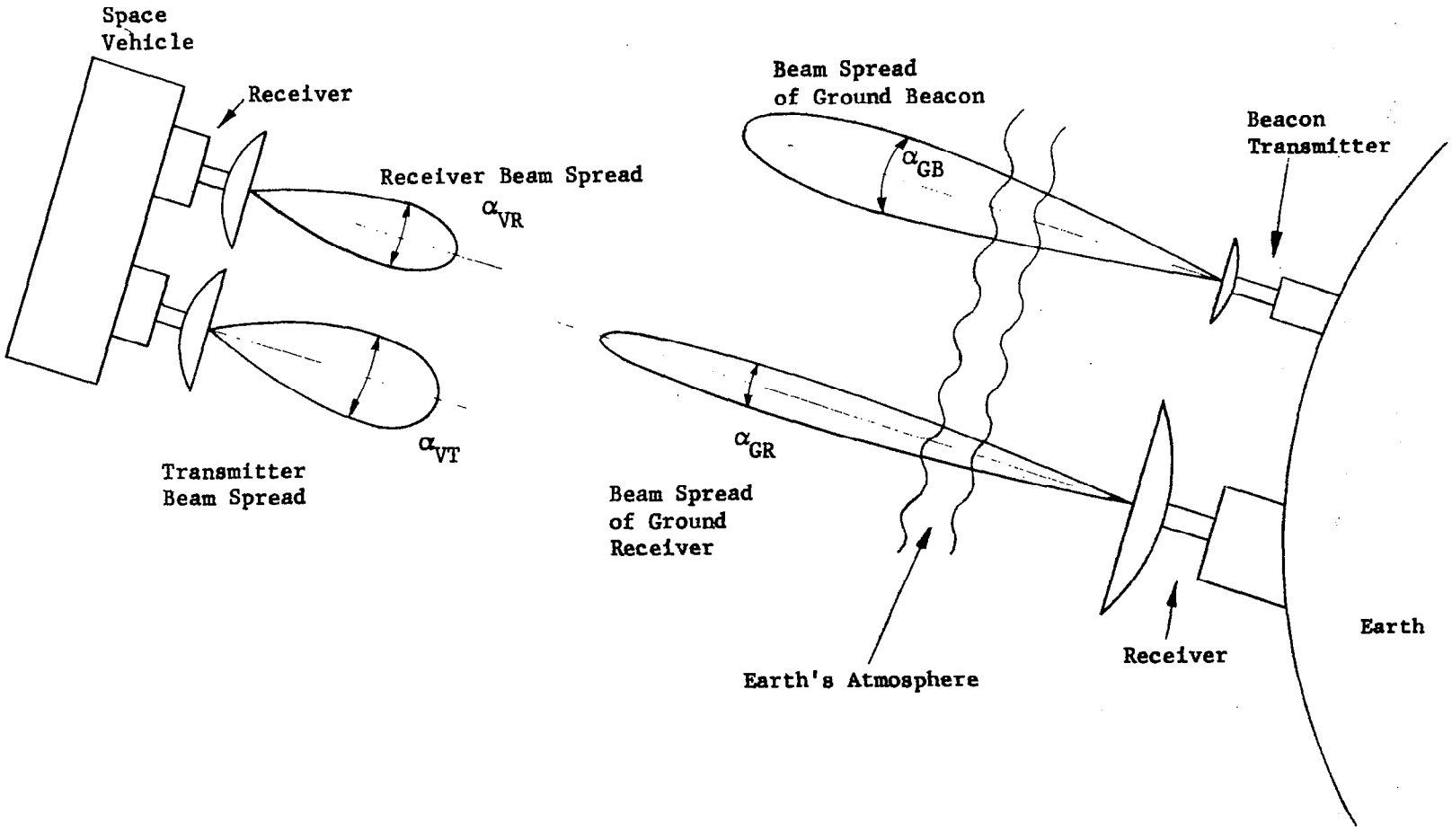

Figure 1-1. Space Communication Elements

(1) Only the downward communication requirement is difficult. The vehicle to Earth (downgoing) communication capacity must be much larger than the upgoing capacity. All the technical difficulty is associated with this requirement.

There are two reasons for this. First, large communication rates are primarily required for the transmission of pictorial information. Virtually all the reasonably foreseeable Earth to vehicle (upgoing) command and control messages can be transmitted over far narrower bandwidths.

Second, it is economically sound to provide far more transmitter power on the ground to transmit commands and control signals upward than is feasible in the vehicle for the downgoing transmission of scientific data.

(2) The vehicle transmitter is always diffraction limited. In a practical laser communication system, the vehicle transmitter's antenna is always, without exception, diffraction limited, and is always pointed at the receiver with an angular pointing error which is small in comparison with the diffraction beam spread. This is so because if the vehicle's transmitter beam spread or the pointing error is larger than the diffraction limit

of its aperture, then it is always possible to make a smaller aperture system which has the same beam spread but in which diffraction sets the beam spread, rather than errors of construction.

This leads to the need for exceedingly small pointing errors if large transmitter apertures are used. About 0.3 arc-second goes with a 5-inch aperture. A 36-inch aperture requires 0.05 arc-second. Pointing errors this small can be achieved with a coarse-fine pointing system in which a coarse system points the whole antenna, and the fine system moves a small optical component to adjust its line of sight a small amount.

A major group of experiments chosen for the Optical Technology Satellite is aimed at solving the difficulties of attaining diffraction-limited performance and pointing, in a reasonably large aperture, under typical conditions of use in space.

(3) The boresighting error between transmitter and receiver must be small compared to the diffraction angle of the transmitter antenna.

This leads to such a severe requirement in the case of 4- to 40-inch apertures that as a practical matter it can only be achieved by making the receiver and transmitter share the same antenna. Thus, the transmitting and receiving mirror antenna on the vehicle are compelled to be the same.

This causes no disadvantages for the following reason. It is sufficient that the diameter of the receiving antenna be the same as that of the transmitting antenna, in which case it will have at worst the same beam spread, and is well able to tell the transmitter where to point.

To merely receive control messages, however, the antenna need not be any larger than the transmitting antenna, because the bandwidth of the receiver control signals is much smaller than the bandwidth of those transmitted. Moreover, the beacon source power on the ground can be far greater than the transmitter power in the vehicle. In spite of the fact that the beacon beam directivity is limited by the Earth's atmosphere, and the fact that the Earth station receiver antenna can be very much larger than the vehicle receiver antenna, it turns out that the vehicle receiver is not required to have a larger antenna than the transmitter in typical cases. Consequently, they may share the same antenna even in an optimum system.

This sharing gains the advantages of smaller size and weight, as well as simplification of the boresighting of receiver and transmitter. However, it is necessary to take the precaution of operating the Earth beacon and the vehicle transmitter on different laser frequencies so that transmission and reception at the

vehicle can occur simultaneously without interference from scattered light or other pernicious effects.

The need to relate the directions of a transmission and reception path with such incredibly small angular boresighting error is a new problem, unique to optical communication. It does not occur in the guidance of astronomical telescopes on stars. It will require that a special self-alignment feature be built into the optical system to maintain the boresight alignment through launch and the space environment. A group of experiments has been chosen to obtain quantitative measures of the boresight error in space conditions, and of the value of the self-adjusting systems' work to correct it.

(4) For deep-space trajectories a deliberate offset or point-ahead angle must be added to the boresight adjustment to compensate for the motion of the Earth relative to the vehicle, between the time when the beacon signal leaves the Earth and the transmitter signal returns to the Earth.

At close ranges, this is not a serious problem, since the transmitted beam can be broadened to include the point-ahead angle. But for the deep-space case it poses

a very serious problem which has been considered by some investigators to set a total bar to the use of optical communication from interplanetary space.

For these conditions, the point-ahead angle required may be 300 times the beam spread of the transmitter; hence, it must be introduced with an accuracy of 1 part in 300.

It can not be introduced with a servo loop from the earth by sending a continuous error signal to operate the pointing system, because such a loop would have many minutes of transport lag inside it, and almost certainly can not have enough loop gain for the needed tight control of the pointing error.

A workable method is to compute the offset (it will be a very slowly varying function of time) and introduce it on an open loop basis at the vehicle. To maintain the necessary accuracy of this open loop offset system, it can be calibrated once per day or so by an extremely slow closed loop system.

A special case of this open loop offset occurs when it is desired to transfer the downward beam accurately to a different receiver on Earth while still tracking the same beacon. This is required when weather or Earth's rotation requires switching to another ground station.

An especially critical group of experiments is aimed at gaining experience with pointing ahead and transfer to another ground station.

(5) Acquisition of contact from deep space after a long signal dropout requires special planning and procedures.

Since mutual contact between a distant vehicle and Earth will be possible only with extremely narrow beams and fields of view, reacquisition will require the execution of special acquisition modes of operation for both vehicle and ground station.

Simulating these conditions experimentally in a satellite close to Earth is one of the most difficult parts of the program. Several experiments are devoted to it.

(6) Optics of the atmosphere are extremely important in planning an overall system.

For reasons to be set forth later, it is almost certain that the Earth-end of most space optical communication systems will be on the surface, not in orbit. The losses, transverse coherence lengths, signal disturbances, and background radiation introduced by the atmosphere are major factors in the choice of laser frequencies, type of modulation, and laser power levels. Especially important is the influence of these factors on the choice

between optical heterodyne detection with post-detection filtering or intensity detection with pre-detection filtering to discriminate against background signals. Daytime sky background seen by the ground station receiver, and the earthshine seen by the beacon tracker in the vehicle are both serious factors influencing system design because they force the use of narrow tracking fields of view.

Virtually all that we need to know about the atmosphere is already known from astronomical and other data to a degree adequate for planning a useful experimental system. However, to refine and optimize future designs, and to probe for unexpected effects, a group of atmospheric experiments has been chosen.

(7) A carefully planned set of ground-controlled image examination points and adjustment actuators must be provided to permit testing and alignment of the optical system in orbit.

It is a universal truth about large high performance optical systems of any kind, that it is not possible to make and assemble them so that they will stay aligned under the extreme stresses of launching and the thermal shocks of the space environment, to say nothing of the long-time drift of component characteristics. Although

a certain amount of automatic adjustment equipment will have to be included in any practical large aperture optical system, the design of a generally self-corrective (adaptive) large aperture system is totally beyond the present state-of-the-art even for a ground based system. Clearly, human intervention is required to maintain such systems to their designed diffraction-limited performance. The REMOTE MANUAL OPTICAL ALIGNMENT experiment (Number (3) on page 2-16) discusses the specific reasons why manual adjustment is required and presents a scheme for evaluating possible methods. The results of this experiment are crucial to all aspects of optical space technology.

1.2 SYSTEM TRADE-OFFS

The previous discussion has prepared us to discuss the critical trade-offs in a laser communication system design. We must understand these to choose satellite experiments wisely.

First, we must always recall that all trade-offs of one design aspect against another are purely economic matters, not technical ones.

A group of proposed space missions requires a certain communication rate in bits per second under certain conditions of range, duration, timing, etc. These requirements can be met by competing designs, or indeed by entirely different competing methods, each at a certain overall cost.

An optical communication system will only play a role if it minimizes the overall cost of the group of missions in which it is used.

In this Phase I report we cannot do in detail all the quantitative cost comparisons necessary to choose an optimum design, but we can foresee the general nature of the solution well enough to plan the satellite experiments.

For example, a few aspects concerning aperture sizes stand out strongly. Clearly, for a given downward information rate, aperture diameter at the transmitter can be exchanged for aperture diameter at the receiver on a 1:1 basis, so far as performance is concerned, but the cost of enlarging the aperture diameter in space beyond the 40-inch range is very high because:

(1) total weight and size go up dramatically;

(2) tolerable pointing error decreases;

(3) open-loop point-ahead offset error required becomes a smaller fraction of the total offset;

(4) the chance that a partial failure of any component will degrade the system to an intolerable degree increases rapidly; this necessitates more backup units which are costly.

The cost of receiver area on the ground also increases as its own size increases. But if a whole set of missions will require 6 ground stations (for diversity reception) to be used with 30 space vehicles, each increment of area on the ground can cost five times as much as it saves per space vehicle and still be a good buy.

Very rough estimates we have made indicate that, for Martian distances (10^8 miles) and 10^7 bits/sec capacity, a typical solution comes out with the space aperture near 40 inches and the ground-based aperture (a low resolution energy catching system) 400 inches.

The graph of Figure 1-2 shows these rough relationships. Channel capacity for earth reception versus range is shown for the minimum capacity 8-inch diameter system and the 39-inch diameter system mentioned earlier.

The influence of daytime sky brightness is shown by the dashed sections of each curve.

The calculation is based on the use of a 5-bit pulse code modulation system utilizing polarization change to mark the binary digits.

The calculation ignores the effects of loss of spatial coherence at the receiving aperture caused by the mirrors imperfection and the turbulence effects of the atmosphere.

Discrepancies between experimental measurements and this simple theory may be an interesting result of the experiments.

Similar trade-offs of solar cell power versus transmitter and receiver aperture must be averaged over the cost of launching solar collectors for powering a large number of units versus larger ground receiver area.

Similarly, the cost of the best cryogenic cooled detectors on the ground,which will have the unity quantum efficiency assumed in these examples, and the cost of a very powerful ground beacon are returned in comparison with the cost of less laser power and detector cooling on the spacecraft.

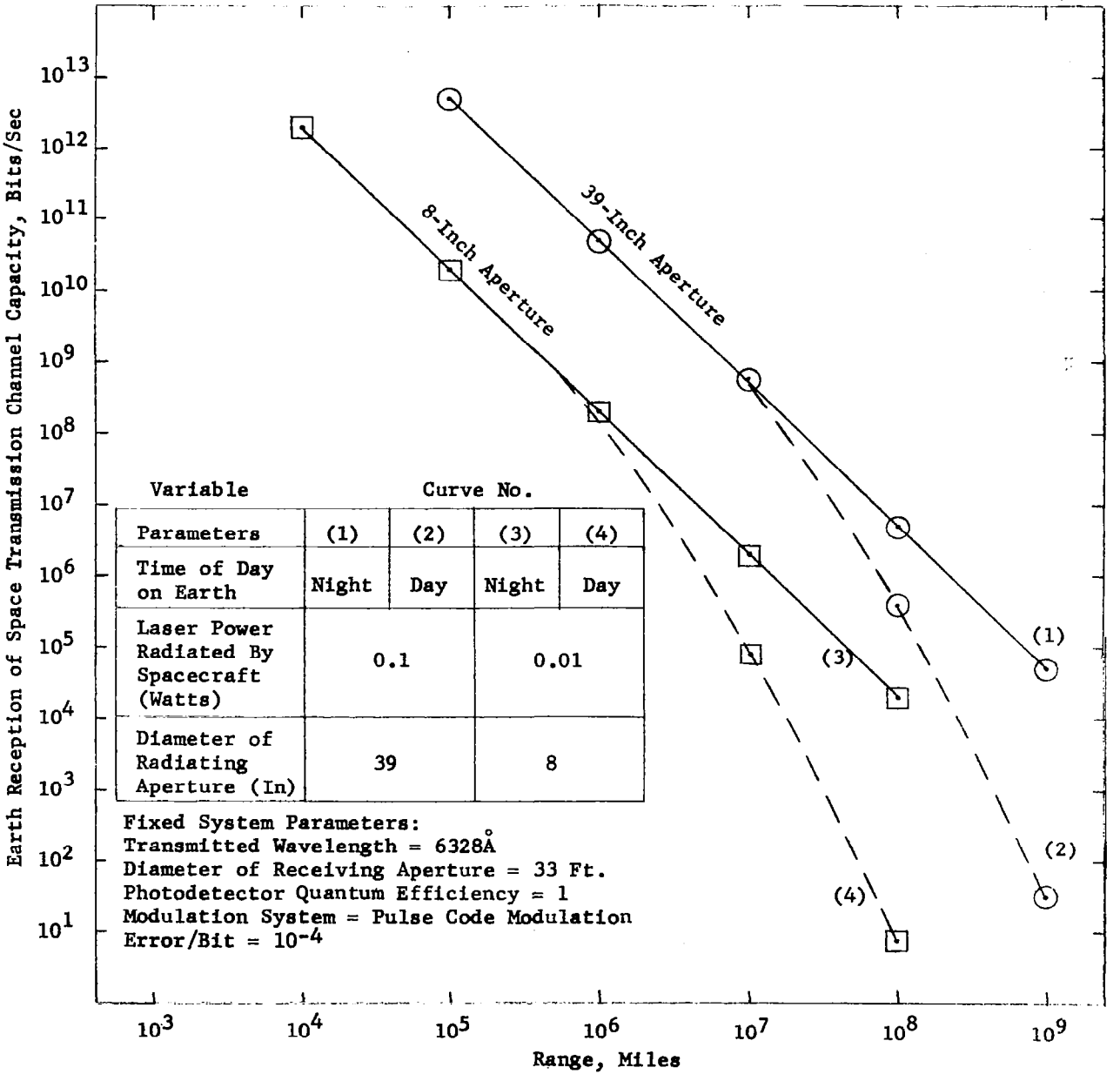

Figure 1-2. Laser Communication Performance

Power conversion efficiency of operation of the laser and modulator in the spacecraft is of course at a premium. An order of magnitude advance in efficiency, however, would probably be traded mostly for smaller aperture, more reliable, and less costly transmitter systems.

Clearly, the trend of cost pressure in these optimizations is to extremely large, high performance ground stations and to the smallest, most simple modules aloft. This is the reason why orbiting of a receiving relay station near the earth is impractical. The gain in performance it would give can almost certainly be achieved at lower overall cost for a number of missions by many large ground stations.

1.3 A FORECAST OF THE ROLE OF OPTICAL COMMUNICATIONS IN SPACE EXPLORATION

The upper bound of size and weight for laser communication systems of the foreseeable future might be forecast as follows.

With the advent of the reliable boosters of the Saturn family, there has been a quantum jump in the size of payloads that could be made available for deep-space scientific missions. No longer are we constrained to 1000-pound payloads; now, plans to send payloads of over 6000 pounds to the vicinity of the planets are realistic. A laser communication system of 40-inch aperture in space and 400 inches on the ground could provide a bandwidth of over 1 megacycle with a 30-db signal-to-noise ratio at 100 million miles; the system weight is envisioned at 1000 to 1500 pounds. Thus, in broad terms, approximately 15 percent of the deep-space payload could be allocated to communication, while the balance of the weight would be distributed between the scientific sensors and the housekeeping subsystems of the spacecraft. The power input requirements for this

1-megacycle laser communicator would be modest, perhaps 200 watts. This level of power input could be obtained through the use of solar collectors within the present technology. The cost of such a communication system will be a substantial fraction of the total, but it will not completely dominate the mission cost.

Moreover, what about the lower bound of practical size and weight? This can be roughly estimated as follows:

To operate and modulate adequately almost any laser communicator at all takes some minimum power, say 50 watts, and for this one can get some 10 milliwatts of modulated radiation as the minimum plausible amount. Trying for less than this would not save much cost or weight.

We can also make the transmitting aperture very small, but reducing it to less than eight inches does not really save much cost or weight in a typical mission. Already we have reduced the pointing error problem to one which can probably be handled without a coarse-fine system, and we have reduced the accuracy required in the point-ahead problem.

It is interesting to note, then, that such a system will provide a bandwidth of 50 megacycles at 30-db SNR using a typical modulation scheme at a range of 0.25×10^6 miles!

This suggests that, at the lunar distance, even the 8-inch system of minimum size and weight gives a communication capacity so large that only missions requiring extraordinary bandwidths could usefully employ it. For more modest bandwidths, the all-weather microwave system would probably save overall mission cost.

It appears, then, that the most attractive region for optical communication is at interplanetary distances and on missions where very large channel capacity is absolutely essential.

1.4 HOW MUCH CHANNEL CAPACITY IS ENOUGH?

This may appear to be a senseless question, but it is not. More communication than we have today in space would be better, but at some point, more capacity will cost much more money. There must, therefore, be a limit to economically justifiable channel capacity for nearly all missions which can be launched in the next decade. It is important to make some effort, however rough, to estimate what this limit is.

One kind of thinking which helps to localize the economically justifiable level of performance runs as follows.

A quick study of the output systems of all types of scientific instruments shows that, for example, recording spectrophotometers generate, at the most, 10 bits per second. X-ray diffraction apparatus, exposing one plate per ten minutes, generate about 10^4 bits per second average rate. In a 6000-pound vehicle with a 1000-pound communicator module there might be, at the most, 2000 pounds of assorted instruments comprising 20 types. These would scarcely be capable of generating a bonafide information rate exceeding 10^6 bits per second.

An exception exists when one or more of the instruments is a real-time television camera generating a typical 5×10^6 bits/sec. Suppose that this is the case. The next question, then, is at what does it look?

If the television operates full time, sending 30 frames per second, any scene which is not rapidly changing will be redundantly transmitted. Pictures of stationary scenes become redundant at once, unless a human at the receiver is using the television picture as visual feedback in controlling a remote slave manipulator in an eye-to-hand servo loop. However, if there is a round trip transport lag exceeding a few seconds in the loop, the operator's normal coordination will be interrupted. He will operate in short bursts of open loop activity, the results of which are observed one transport lag later. Consideration of this type of activity indicates that the highest rate of new pictorial information the operator can really use is in the order of ten new pictures per transport lag period. More pictures than this are essentially redundant. If there is a typical Martian transport lag of 15 minutes, ten television frames using this period average 1.6×10^3 bits/sec.

1.5 ADEQUACY OF PLANNED EXPERIMENTS

We have made some rough estimates of the range of channel capacities which seem technically feasible with optical communications. A rough check as to the range of missions for which these would be adequate is interesting. Scientific instruments seldom generate more than a few tens of bits per second unless they take photographic pictures. At one 2 x 2-inch frame per ten minutes, this averages 10^4 bits per second. Real time television generates 5×10^7 bits per second, but the number of cases in which the full 30 frames per second is not highly redundant is rare. One such case is high resolution mapping of a planet in a close flyby.

Thus, except for extensive mapping missions, the capacities available from optical communicators appear to exceed or are matched to the needs.

Thus, we need not expect great pressure for as much as 10^7 bits/sec except in rare instances and on mapping missions.

The experiments we describe later are thus, in general, not aimed far below requirements of the next decade.

1.6 SUMMARY

This is a Phase I Report and, as such, the output of the activity is the recommendation of important experiments to aid the development of the optical and communications technologies. We have presented these recommendations in Section II in as concise a manner as possible. The following sections of this report offer more detailed discussions of each recommended experiment. The experiments are arrayed together in logical groups: pointing, acquisition, atmospherics, and heterodyning. This report considers the experiments in near-earth orbit as an assessment operation for feasible deep-space communication approaches. Appropriate back-up in the form of calculations is presented where applicable.

SECTION II

OPTICAL COMMUNICATIONS/TECHNOLOGY EXPERIMENT RECOMMENDATIONS

As a consequence of a series of meetings among the technical staff at Perkin-Elmer, a list of thirty experiments was developed. This group was divided into five sub groups: atmospheric experiments (paragraph 2.1), eye-hand loop experiment (2.2), heterodyning experiments (2.3), tracking and acquisition experiments (2.4), and the communications experiments (2.5). Each of the thirty experiments identified in the list was evaluated in accordance with the flow diagram, Figure A-1, and a concise experiment definition report was developed for each experiment to assist in the selection process (see pages 2-11 to 2-35). The experiments which should be conducted to further optical communications technology were reduced to those which could be best conducted from a satellite. It was found that some of the experiments could be executed on the ground (or from aircraft or balloons). These were culled from the lists. Certain experiments were found to lend themselves to combination with others on the lists, and the experiment sheets and experiment procedures were modified to reflect this combination. Some experiments were too remote from prospective benefits to laser communications and/or optical technology.

Thus, the list of thirty experiments was reduced to a group of thirteen to be analyzed further in the Phase II activity of this Project. These experiments are discussed in a brief summary form in the following material.

2.1 SUMMARY DESCRIPTIONS OF THE RECOMMENDED ATMOSPHERIC EFFECTS EXPERIMENTS

(1) Is there scintillation of a coherent light beam coming to the earth from space after passing through the atmosphere? What is the variation of percent modulation as a function of aperture (or an array of small apertures)? What is the difference between day and night measurements? What is the difference between slanted and vertical beams?

Atmospheric Scintillation Experiment: Measure the amplitude and frequency distribution of light intensity from a coherent source as sensed after passing through the whole atmosphere. This should be done both from the earth to the satellite and from the satellite to the earth, for (at least) two aperture sizes, for (at least) two laser frequencies, for day and night conditions, and for various weather conditions and slant angles.

(2) Does the atmosphere change the polarization of coherent light beams? Note the changes and losses in polarization.

Atmospheric Effects on Polarization Experiment: Detect and measure any effects the atmosphere may have on plane and circularly polarized

light, with particular emphasis on depolarization, for both the up- and down-looking directions.

In recent years, the sun's magnetic field has been inferred from the polarization of light from sunspots. The polarization does not change with slanting look angles through the atmosphere. In addition, measured polarization in the light from the Crab Nebula and other nebulae tends to confirm the physical theory which says that the atmosphere has no significant effect on the polarization of transmitted light. Hence, we expect that no major rotational effects will be found. However, the experiment is easy to perform and requires little equipment. A few percent of depolarization may be discovered and be of interest. The depolarization would probably be more important as the number of scattering particles in the atmosphere increases, since scattered sunlight is partially polarized by haze, particularly in rainbows.

2.2 BRIEF DESCRIPTION OF AN EYE-HAND LOOP EXPERIMENT

(3) Conduct a video viewing operation of optical technology experiments on the satellite and provide the earth-based optician or astronomer with a series of servo controls to conduct an experimental sequence based on observations.

Remote Manual Optical Alignment: The broad bandwidths which optical communication makes available in downward transmission from space vehicles

may permit sending real time television pictures. An outstanding scientific and engineering benefit derived from this possibility is the closing of the eye-to-hand servo loop of a human operator using the optical communication link. This permits a scientist on Earth to carry out operations in the spacecraft which require eye-to-hand coordination. He visually monitors the motions of slave manipulators which he controls from the ground. The objective is to explore the feasibility and equipment requirements of conducting, in the unmanned spacecraft, an optical technique type laboratory procedure which requires eye-to-hand coordination.

For example, the effects of weightlessness on the optical elements and the alignment of mirrors and lenses for diffraction-limited performance can be anticipated. But if an automaton of limited capability could be placed aboard the satellite and a TV link established between the work areas and the tool areas, a highly skilled astronomer or optician on the ground could function as if he himself were in the satellite and personally performing the tasks which would take place in an observatory or on an optical bench. The communication transport lag on human performance would have to be evaluated.

2.3 SUMMARY DESCRIPTIONS OF THE RECOMMENDED HETERODYNE EXPERIMENTS

(4) Optical Heterodyne Detection in the Satellite Experiment: In detecting and tracking the earth beacon, one of two methods of reduction of background noise due to earthshine is heterodyne detection in the spacecraft. The other method involves the use of a narrow pre-detection filter.

One purpose of this experiment is to develop sufficient engineering experience with design and operation of a space-borne heterodyning system so that its feasibility, reliability, performance, and cost can be evaluated relative to pre-detection filter systems which achieve the same purpose.

A second purpose of the experiment is to evaluate the utility of Doppler velocity measurements made using the Doppler shift of the optical carrier in comparison with other methods of obtaining such velocity information, such as the shift of a narrow-band microwave signal or the shift of a narrow-band, radio frequency, intensity modulation on the optical carrier

(5) Optical Heterodyning on Earth Experiment: Verify the theoretical prediction that the signal-to-noise ratio in heterodyne detection in the atmosphere is limited by the transverse coherence diameter in the atmosphere.

A second objective is to measure this transverse coherence diameter.

2.4 SUMMARY DESCRIPTIONS OF THE RECOMMENDED TRACKING AND ACQUISITION EXPERIMENTS

(6) 0.1 Arc-Second Tracking Demonstration Experiment: This will be an engineering demonstration of angular tracking using lasers on a satellite in a synchronous orbit. Measurements will be made of the beam pattern as received on earth from the diffraction-limited optical system in the space environment.

Angular rates due to variations of the orbital location shall simulate relative angular rates between the earth tracking station and a deep-space vehicle. Tracking accuracy shall be measured as a function of SNR. Angular jitter, zero drift, pointing stability, velocity error, acceleration error, and dynamic range of control are to be measured.

(7) Point-Ahead Experiment: The point-ahead problem for laser communications in deep space is the difficulty associated with the precise placement of the beam at the location of the moving ground station (due to the earth's orbit around the sun) when the transit time of the light beam is substantial. In many ways, the problem is similar to the classical fire control system that must point ahead of the target so that the projectiles intercept the anticipated position of the moving target. Here the transmit photons from the space-borne laser beam are analagous to the projectiles. Light will take 7 1/2 minutes to traverse 10^8 miles. During this period of time, the earth is moving in its orbit around the sun, the earth station is rotating about the axis of earth rotation and the space vehicle is moving along its trajectory. The Point-Ahead Experiment evaluates the proposed solution to this most difficult problem. The solution proposed by Perkin-Elmer is based upon a logical extension of the five years of scientific and hardware development work on the Stratoscope II Telescope.

(8) Space-to-Ground-to-Space Loop Closure Experiment: At synchronous altitudes, the time delay due to the transit time of the optical beam is small (although not negligible). A feasible closed loop system test of the pointing system will provide the standard by which to assess the necessary open loop modes of the laser communication system.

(9) Tracking Demonstration in the Presence of Spacecraft Motion Disturbances Experiment: Measure the capability of the tracking system to maintain pointing operations with perturbations of motion present in the satellite's three rotational degrees of freedom. The experiment objective is to demonstrate that satellite motions about each individual axis and combinations of motions can be accommodated without significantly degrading the tracking performance. The range of velocities and accelerations will include values that can be anticipated for an instrumented deep-space probe.

(10) Suspension Systems Comparison Experiment: This test should yield comparative performance data on at least two promising spacecraft telescope suspension arrangements and the associated hardware performance. The suspension hardware (i.e., flexure bearings with torquers or magnetic suspension devices) must decouple the telescope line of sight from motion disturbances present in the spacecraft and yet provide the reaction base for telescope steering torques.

(11) Tracking Transfer Demonstrations from Ground Station A to Ground Station B Experiment: Following the period of time during which the satellite has been tracking Station A, the optical communication link must be shifted to Station B (an angular displacement of some 8 arc-seconds). This demonstration will simulate the condition in deep space when the vehicle has locked its receive optical system into the apparent line of sight of the ground station and is now faced with the problem of transferring communication to another ground station.

(12) Earthshine Effects on Acquisition and Tracking Experiment: When viewing the ground from the satellite, demonstrate acquisition for a 1-degree field of view and determine the acquisition and tracking degradation that will take place in the presence of anticipated natural variations of earthshine. Earthshine variations that must be evaluated in terms of acquisition and tracking performance will include the conditions of nighttime operations without moonlight (at the ground beacon) through the conditions of high-noon sun illumination in desert areas. Dependent upon cooperation from natural weather phenomena, the effects of other high albedo conditions, such as water glint, snow fields, high white scattered clouds or glint from ice particles in clouds, should be measured.

2.5 COMMUNICATIONS EXPERIMENTS

(13) Communication at 10^7 CPS Experiment: Demonstrate a communication system with a bandwidth of 10 megacycles and employing various modulation techniques, such as amplitude modulation or polarization modulation of the laser beam. For example, the light might be video detected in a photomultiplier tube (AM) or in a pair of photomultiplier tubes (polarization modulation). The demonstration should confirm the SNR and data error rates theoretically predicted for that modulation method and hardware and for the selected communication technique.

2.6 OPTICS TECHNOLOGY EXPERIMENTS

The combination of a moderately large aperture optical system operating at or near its diffraction limit in space with a suitable laser light source is an extremely powerful tool for the development of future large aperture

optical systems in space. This combination permits the collection of engineering data on how well the nearly perfect optical system performs under the controlled variation of parameters, such as thermal input, velocity and acceleration disturbances, and gravity-free environments. The Orbiting Astronomical Observatory series of payloads are the largest aperture systems presently in hardware for space flight (although not in orbit until 1967). These optical apertures are 38 inches in diameter with a planned figure of 1/4 wave (the Goddard Experiment) and 32 inches with a planned figure of 1/10 wave (the Princeton Experiment). 1/4-wave performance and even 1/10-wave performance are not the performance capability bounds of the present state of the art in figuring a large mirror system. Stratoscope II represents a closer approach to the limit of optical perfection with its figure of 1/50-wave performance. However, Stratoscope II is a balloon-borne payload rather than a space-borne payload and the mechanical configuration that was applicable to that very soft launch operation is not suitable for the more difficult rocket launch operations of a space optical system. Moreover, Stratoscope II operates in the presence of gravity while a space optical system would not have that constraint.

It, therefore, seems advantageous to utilize the space laser communications equipment of the Optical Technology Satellite to conduct experiments on the measurement of performance of the space optical system. Adjustable and "tunable" elements in the optical system (i.e., in-flight alignment and focus as described on pages 6-28 through 6-34) and perhaps even some

controllable figure systems for the primary mirror can be evaluated using the laser at the focus of the telescope.

2.7 EXPERIMENT DEFINITION REPORTS

The description of each recommended experiment has been expanded in the following sheets to provide the reader with: (1) an understanding of the basic experimental hardware which would be required to conduct the experiment, (2) a brief description of how the experiment would be conducted, and (3) the data forms that the experiments would produce.

(1) SCIENCE EXPERIMENT: ATMOSPHERIC SCINTILLATION

Experiment Objective(s): To measure the amplitude and frequency distribution of light intensity from a coherent source as sensed after passing through the whole atmosphere. This should be done both from the earth to the satellite and from the satellite to the earth, for (at least) two aperture sizes, for (at least) two laser frequencies, for daytime and nighttime conditions, for various weather conditions and slant angles.

Basic Experiment Hardware: Optics Technology Communications Systems

On the Satellite

Narrow-band filters

1 large telescope

Aperture stops or small telescope

Visible laser

IR laser

Real time return transmission to ground

On Ground

1 large telescope

Recorder

Laser transmitter with variable antenna aperture

1 channel microwave

Receiver and control (signal amplitude and AGC data)

Experiment Procedure: Record the received laser signals at various positions in the beam spot for the conditions mentioned under Objectives. Analyze the recordings for amplitude spatial distribution and frequency distribution. Cross

correlation between scintillation and pointing errors would be useful in servo system analysis.

Form of the Data to be Collected: Recordings of received signals on ground and of signals from space. There will be statistical data processing computer time involved.

Optical Communication Technology Benefits: The data is very important for predicting noise levels and useful in determining maximum aperture size. This data will help determine feasibility of heterodyne and homodyne detection systems and other coherent detecting systems.

Scientific Windfalls: This data will contain the first measurements ever made of atmospheric scintillation from the satellite to the ground on a coherent source and the comparisons with measurements of starlight scintillation from the ground to the satellite will be utilized in a better understanding of the atmosphere.

(2) SCIENCE EXPERIMENT: ATMOSPHERIC EFFECTS ON POLARIZATION

Experiment Objective(s): Attitude control of a vehicle and optical communications are two problems which can possibly be solved by methods utilizing the 100-percent polarization of a laser source. For instance, the torsional alignment of a vehicle about the line of sight may be determined (to within one of two positions) by locating the plane of polarization of its laser beam. This can be accomplished by finding the crossed position of a polarizing prism for null transmission. The accuracy of the alignment system is limited by the sharpness of the null, which is in turn limited by any depolarization of the beam. Also, any optical communications system which depends on some form of polarization modulation may be adversely affected by depolarization of the beam.

The interaction of a magnetic field (such as the Earth's magnetic field) with a material medium (such as the atmosphere) causes a rotation of the plane of polarization of transmitted light. This is the Faraday effect. For the Earth's atmosphere a Faraday rotation of the order of 1 arc-minute may be observed. Faraday rotation is, therefore, probably unimportant to communications and attitude control, but there may be other (unknown) effects.

In recent years the sun's magnetic field has been inferred from the polarization of light from sunspots. The polarization does not change with slanting look angles through the atmosphere. In addition, measured polarization in the light from the Crab Nebula and other nebulae tends to confirm the physical theory which says that the atmosphere can have

no more than small effects on the plane and degree of polarization of light. For the case of optical communication, small amounts of depolarization of the transmitted light will probably not cause serious degradation of the signal, in comparison with the effects of unpolarized background radiation. However, the proposed attitude control system is sensitive to slight losses of polarization of the source, since the losses will broaden the position of the null. Such loss of polarization or rotation of polarization might be related to the number of scattering particles in the atmosphere, if they are aligned anisotropically by some preferred direction mechanism such as wind or gravity. The existence of the effect would itself be of scientific interest.

The measurement can not be made using a retrodirecting reflector of the S-66 satellite type.

Basic Experiment Hardware:

Optics Technology Communications Systems

Analyzers and quarter-wave plates

Suitable encoding equipment in the satellite.

Experiment Procedure: Transmit CW laser light in both directions and measure its polarization with the analyzers and quarter-wave plates. When light is received at the satellite, encode the measurements and transmit the data to earth. Integrate readings over a sufficient period to eliminate atmospheric scintillation effects. It will be of particular interest to compare results for linearly and circularly polarized light.

Form of the Data to be Collected: Intensity measurements as a function of polarization angle.

Optical Communication Technology Benefits: Results will help to determine the limitations of an attitude control system using polarization. If no large effects are observed, confidence in modulation systems using polarization will be increased.

Scientific Windfalls: Probable confirmation of general theory and perhaps the discovery of weak effects.

(3) SCIENCE EXPERIMENT: REMOTE MANUAL OPTICAL ALIGNMENT

Experiment Objective(s): The wealth of optical fabrication experience indicates that a large aperture optical system cannot maintain diffraction-limited performance over a long period of time in an environment as hostile as the space environment without occasional testing and adjustment. The adjustment problem is made formidable by the multitude of possible misalignments, the required precision of alignment, and the amount of information about image quality necessary to determine what adjustments should be made. It is difficult to design a mechanically actuated alignment system with a set of independent adjustments sufficient to cope with all possible misalignments and difficult to gather the necessary performance data with a reasonable number of photosensors. Even if these problems are solved, the observed aberrations of the image may not correspond in any 1:1 fashion with the procedure required for correcting them. General alignment of large optical systems is, therefore, virtually never accomplished without some human intervention. This alignment is usually performed in an earth-based test tunnel.

One area of experimentation crucial to all aspects of optical space technology is the area of remote manual optical alignment. Although most such alignment problems may be simulated in ground-based laboratories, the additional freedoms and constraints imposed by a zero-gravity environment cannot. Space-borne experiments are also required to increase confidence in the ability to maintain the performance of optical instruments in space.

The experiment will explore the equipment requirements and the feasibility of re-aligning a large aperture system in space. The performance of both the remote control system and the human operators will be evaluated. Since the operator will need information about system performance which is essentially visual (i.e., the image quality at various places in the optical path), the real time television capability of the Optical Technology Satellite will be utilized. The communication transport lag of a deep-space vehicle may be simulated easily with ground equipment, and its effects on human performance may be evaluated.

Basic Experiment Hardware:

On the Satellite

Television camera and suitable viewing aparatus

Test source

Remote control actuator system for positioning optical elements

Communications equipment for transmitting television signals and receiving control system commands.

On the Ground

Operator's console with controls and video presentation

Communications equipment

Means for inserting variable transport lags into the control loop

Experiment Procedure: A broadband real time television picture sent to the ground console provides an input which roughly matches the information rate of the human operator's visual perception system.

Under the supervision of psychologists and optical scientists, the operator performs a series of re-alignments by adjustment of the console controls. Transport lags of up to fifteen minutes are inserted (corresponding to the maximum range for real time TV transmission with presently envisioned optical communications systems) and their effects on human performance are checked.

Optical Communications Technology Benefit: The experiment is a demonstration of one of the special advantages of optical communications. Successful completion of the series of experiments will greatly increase confidence in remote optical alignment techniques.

Scientific Value: This experiment is a first attempt to place a man on earth in eye-and-hand contact with objects in space. The opportunity to project not merely a human operator, but in effect, any of the world's leading scientists into a laboratory or observation platform in space is one of the richest values that space optical communications has to offer.

Scientific exploration of space will be vastly facilitated especially in fields like biology and geology where it is difficult to build preprogrammed automatic laboratories which are able to report unequivocal results over narrow-band communications channels.

(4) ENGINEERING EXPERIMENT: OPTICAL HETERODYNE DETECTION IN THE SATELLITE

Experiment Objective(s): In detecting and tracking the earth beacon, one of two competing methods of reduction of background noise due to earthshine is to employ heterodyne detection in the satellite. The other method is the use of a narrow pre-detection filter.

One purpose of this experiment is to develop sufficient engineering experience with design and operation of a spaceborne heterodyning system so that its feasibility, reliability, performance and cost can be evaluated relative to pre-detection filter systems which achieve the same purpose.

A second purpose of the experiment is to evaluate the utility of Doppler velocity measurements made using the Doppler shift of the optical carrier in comparison with other methods of obtaining such velocity information, such as shift of a narrow-band microwave signal and shift of a narrow-band radio frequency intensity modulation on the optical carrier.

Basic Experiment Hardware:

On the Satellite

Small tracking receiver telescope

Frequency stabilized local oscillator laser

Beam combining optics in receiver

Broadband photodetector, up to 5 kmc bandwidth

Broadband amplifier and frequency discriminator

Real time return transmission to ground

On Ground

High power frequency stabilized laser

Tracking transmitter telescope for laser beacon

Receiver for vehicle return transmission

Experimental Procedure: Track the earth beacon with the tracking receiver telescope. Heterodyne signal is sent to frequency discriminator which develops a modulation signal for the return transmission.

Signal-to-noise ratio, tracking performance and frequency shift are recorded.

Form of Data to be Collected: Recordings of return transmission.

Optical Communication Technology Benefits: Helps settle engineering choice of intensity versus heterodyning systems on vehicle.

Scientific Windfalls: Effects of atmosphere on frequency spectrum of upward-propagating coherent source measured.

(5) ENGINEERING EXPERIMENT: OPTICAL HETERODYNING ON EARTH

Experiment Objective(s): Verify theoretical prediction and that signal-to-noise ratio in heterodyne detection in the atmosphere is limited by the transverse coherence diameter in the atmosphere.

Basic Experiment Hardware:

On the Satellite

Frequency stabilized CW laser boresighted with earth beacon tracker

On Ground

Tracking telescope with aperture variable from about 1 to 24 inches

Frequency stabilized local oscillator laser

Broadband photodetector and amplifier

Signal recording and analysis equipment

Experimental Procedure: The satellite laser tracks the earth beacon and also transmits signal to the heterodyne receiver telescope. This receiver tracks the vehicle. The heterodyne signal-to-noise is recorded while the receiver aperture diameter is varied.

Form of Data to be Collected: Recordings of heterodyne signal with simultaneous meteorological observation and coherence diameter measurements on starlight.

Optical Communication Technology Benefits: Verifies theoretical predictions that behavior of laser light is the same as starlight so far as propagation of transverse coherence is concerned. This verification will help confirm engineering choice of ground-based detection system.

Scientific Windfalls: Measures transverse coherence progapation in the atmosphere under daytime conditions in which the use of starlight is difficult.

(6) ENGINEERING EXPERIMENT: 0.1 ARC-SECOND TRACKING DEMONSTRATION

Experiment Objective(s): This will be an engineering demonstration of angular tracking using lasers on a satellite in a synchronous orbit. Measurements will be made of the beam pattern as received on earth of the diffraction-limited optical system in the space environment. Angular rates due to variations of the orbital location shall simulate relative angular rates between the earth tracking station and a deep-space vehicle (refer to Appendix B). Tracking accuracy shall be measured as a function of SNR. Angular jitter, zero drift, pointing stability, velocity error, acceleration error, and dynamic range of control are to be measured.

Basic Experiment Hardware:

On the Satellite

32-inch aperture reflecting telescope

10-mw 6328 A He-Ne laser

20-cps transfer lens beam deflector

S-1 PMT receiver for 8400Å

4-quadrant detector

Narrow-band filters

Acquisition subsystem

On Ground

0.5 -watt GaAs ground beacon

Four 12-inch aperture reflecting telescopes

Acquisition subsystem

Neutral density filters

Narrow-band filters

S-20 PMT receiver for 6328Å

Point-ahead system

4-quadrant detector

Experiment Procedure: Point the ground beacon to the vicinity of the satellite and proceed through acquisition operations. On the spacecraft lock onto the ground beacon. Use a ground station array of 4 telescopes so that the received signal on the ground can be detected as a function of spacecraft beam deflection. Use this data in a closed loop procedure (space-earth-space) to establish optimum pointing of the space beam. In order to measure the diffraction limit capability of the 32-inch optical system in the space environment, vary the beam angular pointing using a conical scan pattern to determine intensity as received on the ground as a function of pointing angle.

Form of the Data to be Collected: Measure the intensity of the received signal on the ground when it is unattenuated and then attenuated by the neutral density filters at the ground receiver array. The beam from the 32-inch system is measured and correlated with scan pattern data sent down by telemetry.

Optical Communication Technology Benefits: The first practical demonstration of 1/10 arc-second pointing and tracking from the satellite to the earth with laser beams will reveal the feasibility of future optical communications systems in space. The ability of maintaining diffraction-limited performance in a large space-borne telescope is also determined and measured.

(7) ENGINEERING EXPERIMENT: POINT-AHEAD DEMONSTRATION

Experiment Objective(s): This is a test of the spacecraft point-ahead subsystem. After locking onto the beam from a ground station, the transmit beam from the spacecraft must point ahead by an appropriate angle to intercept the same ground station. This is due to Bradley effect and transit time effects. During the increment of time of transit of light, the earth moves in its orbit around the sun, the spacecraft moves in its trajectory, and the earth spins about its axis. Therefore, even when the spacecraft is receiving the ground station signal, the transmit signal to that same ground station must be advanced to the proper angle (point ahead $\sim$ 36 arc-seconds). This test will demonstrate the performance of the Point-Ahead Subsystems to step off precise angles in the necessary direction.

Basic Experiment Hardware: In addition to all basic communication gear on both satellite and ground station, a second complete ground station is required located 3 2/3 miles away. This second station (Station D) will transmit at frequency f_D. For this test all computational equipment will be located on the ground at Station A. The satellite must have the equipment on board to receive and store commands of point ahead angle and must have an optical beam displacement subsystem for the transmit beam which will point away from the received line of sight (LOS) in the necessary direction and amount.

Experiment Procedure: This operation will proceed after the satellite has locked its receive beam onto the ground station transmitter. The ground station sends up the command on its own beacon to move the space-borne transmit beam ahead (i.e., 36 arc-seconds in azimuth). These angles are set up about

a reference for the rotation of the LOS determined by polarization measurements from A. The satellite transmit beam will be measured and recorded at Station D. The experiment should be repeated frequently for the various conditions of day and night operations (satellite time). Space-earth-space loop closures should be executed for ground measurements of satellite pointing errors.

(8) ENGINEERING EXPERIMENT: SPACE-TO-GROUND-TO-SPACE LOOP CLOSURE

Experiment Objective(s): This is an instrumentation test which will be used to determine the accuracy of space transmitting beams. Therefore, the objective of the experiment is to demonstrate the effectiveness of this instrumentation loop. The utility of the loop at longer ranges (with corresponding increases in the time delay for the information from the ground to get up to the spacecraft) should be determined. Transport delays of up to 15 minutes can be simulated.

Basic Experiment Hardware: (In addition to the complete optical communications equipment required for both the satellite and the ground station). Ground station arrays have a receiver system which can be correlated with the orientations of the spaceborne beam. These spatially correlated signals must then be converted into commands for the satellite beam steering subsystem. Tape recorders with movable read heads will be used for time delay simulation.

Experiment Procedure: After the satellite has locked onto a ground beam, the space-earth-space loop operation is commenced. The receive signals on the ground are measured and the location of the space-borne beam relative to the ground station is determined. Once the beam errors are established, they can be translated into satellite steering commands to reduce these errors towards zero. The procedure requires simulating the operation of the space-earth-space loop for variable time delays. The variable time delay subsystem is used on the ground to simulate these delays. Tape recorders in a run-stop-run mode can simulate the long time delays (over a minute) while these same tape recorders can be used for the shorter duration time delay simulation by varying the location of the read heads with respect to the write heads.

(9) ENGINEERING EXPERIMENT: TRACKING DEMONSTRATION IN THE PRESENCE OF SPACECRAFT MOTION DISTURBANCES

Experiment Objective(s): Measure the capability of the tracking system to maintain pointing operations with perturbations of motion present in the three rotational degrees of freedom of the satellite. The experiment objective is to demonstrate that motions about each individual axis and combinations of motions (in the range of values that can be anticipated for an instrumented deep-space probe and also for a manned deep-space vehicle) will not cause the tracking performance to deteriorate below a required level.

Basic Experiment Hardware: The equipment aboard the satellite must include motion disturbance producing devices in the three rotational degrees of freedom. In addition, angular rate measuring sensors are required to monitor the motions produced. The motions must be controllable in amplitude, frequency and/or rise time. In addition to the basic tracking equipment, the three orthogonal sets of inertia wheels or the reaction jets must be used.

Experiment Procedure: After the optical communication tracker has proceeded through the acquisition and tracking procedures, and while tracking in space lock mode and monitoring tracking performance, the external torque disturbances are introduced into the spacecraft one axis at a time and with varying frequencies at some preset amplitude (harmonic frequency response test). Step inputs of varying levels are inserted in a similar manner. After single degree of freedom data on degradation of tracking performance are obtained for these conditions, the tests are repeated for the three axes' disturbances simultaneously.

Form of the Data to be Collected: Tracking accuracy as measured on the ground as a function of amplitude and frequency of the disturbances generated aboard the vehicle.

Optical Communication Technology Benefits: Practical demonstration of the tracking system performance in the presence of measured disturbances to the three rotational axes of the vehicle will permit extrapolation of the data to permit the design of future manned and unmanned optical communication units. The data should also permit the measurement of tracking performance during anticipated vehicle maneuvering operations.

(10) ENGINEERING EXPERIMENT: SUSPENSION SYSTEMS COMPARISON

Experiment Objective(s): This test should yield comparative performance data on two promising spacecraft telescope suspension arrangements and associated hardware. The suspension hardware must decouple the telescope line of sight from motion disturbances present in the spacecraft and yet provide the reaction base for telescope steering torques.

Basic Experiment Hardware: Instrumentation must be added to the telescope to measure the amounts of telescope motion disturbances which are originally generated in the vehicle.

Experiment Procedure: This experiment is performed in conjunction with "Tracking Demonstration in the Presence of Spacecraft Motion Disturbances". Instrumentation is added to measure the telescope motion responses in the presence of vehicle disturbances. The procedure is otherwise identical to the aforementioned demonstration.

Form of the Data to be Collected: Angular velocities and accelerations about the three rotational axes as a function of the vehicle inputs.

(11) ENGINEERING EXPERIMENT: TRACKING TRANSFER DEMONSTRATION FROM GROUND STATION A TO GROUND STATION B

Experiment Objective(s): Following the period of time during which the satellite has been tracking Station A, the optical communication link must be shifted to Station B (an angular displacement of some known number of arc-seconds). This demonstration will simulate the condition in deep space when the vehicle has locked its receive optical system onto the apparent position of the ground station and is now faced with the problem of transferring communication to a different ground station.

Basic Experiment Hardware: In addition to all basic communication gear on both the satellite and the ground station, a second complete ground station is required located 4650 feet away (this distance represents 8.2 arc-seconds which, in turn, represents some 4,000 miles at 10^8 mile range). While this second station (Station B) does not have to be exactly 4650 feet away, the exact distance should be known for future measurements. Station A and Station B will have ground laser transmitters operating at different frequencies. The spacecraft will have pointing subsystems at each frequency. There will be a space-borne transfer arrangement whereby the receiving subsystem can shift from laser frequency f_A to laser frequency f_B on command. An additional space-borne subsystem is required to control the rotation about the LOS to an accuracy of .05°.

Experiment Procedure: This is an engineering test to demonstrate the transfer of communications from ground Station A to Station B (separated by some known distance equal to an angular subtense of some 8 arc-seconds). While tracking Station A is operating at laser frequency f_A, the transmitter of tracking Station B is beamed up at its frequency f_B. Station B is within the field of

view. Based upon receipt of the A station polarization, the rotational control subsystem aboard the spacecraft will operate to control the roll gimbals about the LOS. Upon receipt of ground station command to change the pointing from Station A to Station B, the pointing subsystem will use the Station B incoming beam as the pointing reference instead of the Station A beam. These tests simulate the transfer of the deep-space tracking from one ground station to the next. This is a necessary operation since the earth rotates about its axis and blocks off the communication path between an earth station and a deep-space vehicle.

(12) ENGINEERING EXPERIMENT: EARTHSHINE EFFECTS ON ACQUISITION AND TRACKING

Experiment Objective(s): When downlooking, determine the acquisition and tracking degradation that will take place in the presence of anticipated natural variations of earthshine. Variations of earthshine that must be evaluated in terms of acquisition and tracking performance will include conditions of nighttime operations without moonlight (at ground beacon) through the conditions of high noon sun illumination on adjacent desert areas. Other high albedo conditions should be considered such as water glint, snow fields, high white scattered clouds or glint from ice particles in clouds.

Basic Experiment Hardware: The planned equipment for the optical communications system aboard the OTS is adequate to gather the data, together with the ground equipment, rather than adding space-borne gear. The ground equipment would consist of various neutral density filters to attenuate the ground laser beacon so that the received signal on the satellite can be varied in the presence of various situations of earthshine to simulate anticipated conditions of signal and noise in deep space.

Experiment Procedure: Following the basic acquisition and tracking demonstrations which would take place at night (no earthshine), the acquisition and tracking operations would be performed at different times of the day and night to introduce the variations of adjacent area illumination into the system. Then, ground beacon signal levels would be reduced to simulate deep-space signal/background noise conditions. Acquisition and tracking performance for the reduced signal levels would be evaluated against the nighttime operations.

For the acquisition approach that utilizes a 1-degree field of view, a space-borne collimator* could be transferred into position so that the effects of a 1-degree star field would be inserted into the down looking beam. Acquisition procedures are executed and performance measured for this arrangement.

Form of the Data to be Collected: SNR measurements for various signal levels of the ground beacon are measured on the spacecraft in the presence of different conditions of earthshine at the ground station. The effects on the SNR measurements with the 1-degree star field inserted into the main optical beam are measured.

Optical Communication Technology Benefits: Practical demonstrations of acquisition and tracking in the presence of the various levels of earthshine.

*The additional complexity of this collimator in the satellite does not warrant its inclusion. Therefore, in accordance with discussions held with NASA MSFC, this collimator will not be included in the Phase II efforts since the data that would be obtained do not justify the additional equipment.

(13) ENGINEERING EXPERIMENT: COMMUNICATION AT 10^7 CPS

Experiment Objective(s): Demonstrate a communication system with a bandwidth of 10 megacycles and employing either amplitude modulation or polarization modulation of the laser beam. The light will be video detected in a photomultiplier tube (AM) or in a pair of PM tubes (polarization modulation). The demonstration should confirm the SNR and data error rates predicted by theory.

Basic Experiment Hardware: Optical Communications System

In addition, the following ground facilities will be needed for development operations prior to space equipment development:

Telescope	Correlator (electronic)
Laser	Receiver
Modulator	Printer
Retroreflector	Error recorder
Code generator	

Experiment Procedure: The space experiments will produce communication data, per se, to verify SNR and data error rates. The ground tests will have the following procedure prior to space hardware freeze:

Modify purchased telescope (12-inch aperture) for coaxial illumination of distant (10 n.m., unfolded path length - 20 n.m.) retroreflector.

Procure hardware for 10-megacycle (5-megacycle information bandwidth) bandwidth system.

Send binary data so that bit error rates can be recorded automatically.

Modify code characteristic so that information rate can be controlled in optimum manner while maintaining 10-megacycle bandwidth.

Adjust geometric loss in transmission to simulate communication at various ranges in space where geometric loss is the only loss mechanism. Also adjust range to include effects of 1 atmosphere for absorption measurements.

Form of the Data to be Collected:

Analog tapes before decoding

Digital tapes after decoding

Radiometric data

Meteorologic data.

Optical Communication Technology Benefits:

Reduction to practice of a communications system which is categorically general and probably optimum. The resulting data will assist in predicting tracking system performance. The system lends itself to adaptive control of the coding characteristic to suit the error rate. For example, critical information would be held to low data rates while less critical data would use the higher rates. Thus, as the signal-to-noise ratio drops off due to increased noise or increased distance, the most important data are preserved since they are coming through the system at the lower data rate.

2.8 RECOMMENDATION ON THE APERTURE DIAMETER FOR THE OPTICAL TECHNOLOGY SATELLITE

The factor which most significantly affects the payload volume for the satellite is the size of the basic telescope primary mirror. A 32-inch diameter system is indicated in numerous sections of this report and the configuration indicated on the frontispiece illustrates a general arrangement for a satellite which contains two telescopes of this size. Admittedly, at this time in the program, there is a considerable amount of judgment involved in the identification of a payload of this size.

The question of aperture diameter can be approached from two bounds, i.e., by considering both larger and smaller systems. From the optical technology point of view, the larger the diameter of the primary system the greater will be the usefulness of the experimental data in determining the performance limits for future generations of astronomical instruments and reconnaissance systems. However, the constraint that is imposed is the "state of the art" capability of the instrument makers of today. Large optical systems can be manufactured, but, the techniques of manufacturing large diffraction-limited optical systems in sizes much greater than the recommended size are on tenuous grounds. Yet, future space-borne optical systems for laser communications, planetary reconnaissance or astronomical observations will need the diffraction-limited performance (which can only be utilized to advantage in the large diameters when in space). Therefore, the question can be asked...."What is the largest aperture diffraction-limited system which is within the "state of the art"? The answer to this question is that a space worthy optical system could be figured and utilized in the size range of 36 to 50 inches in diameter. Thus, an upper bound for the optical system diameter is available to guide our judgment.

The answer to the question of the lower bound is a more difficult problem. As the diameter of the optical system is decreased, the technical interest level for the reconnaissance and astronomical groups likewise decreases. For a laser communication system, the decrease in aperture diameter lowers the available bandwidth of the channel. On the other hand, the decrease in primary mirror diameter has a marked effect on the weight and volume of the laser communication system. A decrease in diameter by a factor of two would cause a weight decrease of about eight in the primary mirror. There would be significant decreases in the weight of the overall payload as the primary diameter and weight decrease. Now, it can be observed that the requirement of a mission for an operational laser communication system may actually increase if size and weight are decreased at the expense of bandwidth. The channel capacity of a laser communication system must be evaluated with respect to the weight, volume, complexity, cost and power for a particular mission. At this point in the project efforts, we cannot predict these trades. However, for the Optical Technology Satellite, we have based our analysis on the 32-inch aperture as the size to proceed with for the experiments, since it can provide a bandwidth which is the upper extreme of mission needs known to us. This bandwidth is 10^7 bits/second.

A further justification for the 32-inch aperture choice is that this size system would identify clearly the nature of the difficult engineering problems.

As a corollary, we do not recommend the inclusion of additional small aperture communicators despite the knowledge that the smaller size may

better satisfy present mission needs. The scientific and engineering experiments which we recommend will provide the basis for scaling the systems downward in size.

SECTION III

ATMOSPHERIC EXPERIMENTS DISCUSSION

3.1 CHARACTERIZING THE TRANSMISSION CHANNEL IN SPACE-TO-EARTH OPTICAL COMMUNICATIONS THROUGH THE ATMOSPHERE

The material which follows presents the considerations bearing on the recommended science experiments (1) and (2) and engineering experiments (4) and (5).

A laser beam traversing the earth's atmosphere suffers various disturbances which will be described in some detail in the next section. A basic problem inherent in the study of laser beam propagation through the atmosphere is the characterization and evaluation of these various disturbances in a generalized model of a nonreciprocal channel.

If suitable models for the atmosphere could be found, then attention could be focused on the design of optimal encoders and decoders as well as optical signals to insure that the transmission disturbance effects are minimized. Refer to Figure 3-1 for a sketch of a generalized optical communication link.

If the case of laser transmission from space to earth is similar to starlight transmission, then the wealth of astronomical data already accumulated over the years on atmospheric visibility can be brought to bear on the problem. One of the purposes of the scientific experiments is to see if indeed this correlation exists, and also to gather additional new data on two-way laser beam propagation between earth and deep space.

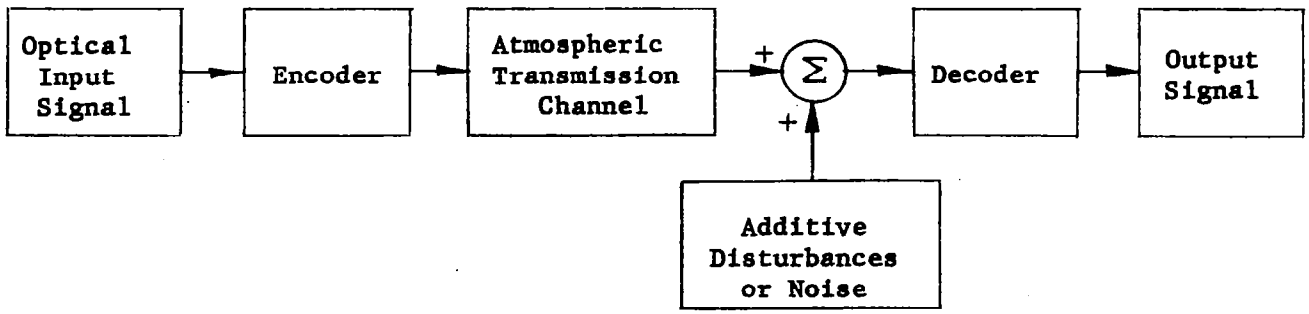

Figure 3-1. General Optical Communication Link

For purposes of establishing rough estimates on some of the deleterious effects of atmospheric turbulence on laser beam propagation for the up-looking link, it will be assumed that laser light behaves in a manner similar to starlight.

Additive disturbances will also be present in the output of the communication link, even in the absence of a desired input signal, and they may be caused by a wide variety of sources. The following noise sources will be discussed in Section 3.3:

(1) Background - photon noise, thermal noise

(2) Background - source fluctuations

(3) Detector noise.

Finally, combining the signal disturbances and additional noise sources allows one to assess the relative merits of various optical detection systems.

3.2 LASER SIGNAL PERTURBATIONS

As mentioned in Section 3.1, a laser signal suffers various forms of degradation as it passes through a communication channel. Attention in this discussion will be given to the earth reception link.

The following signal perturbations or changes will be discussed in some detail.

(1) Atmospheric absorption, Rayleigh and Mie scattering

(2) Intensity fluctuations of laser beam due to atmospheric turbulence

(3) Angle of arrival fluctuations of laser beam - steady state refraction effects, dynamic refraction effects

(4) Loss of lateral coherence

(5) Loss of polarization

(6) Polarization rotation

(7) Antenna diffraction pattern

(8) Doppler frequency shift

(9) Signal photon noise

(10) Anomalous dispersion.

Atmospheric Absorption, Rayleigh and Mie Scattering[3,4] - Scattering and absorbing smoke, smog, dust, salt particles, pollen, haze, and tenuous ice and water

droplet clouds are widely distributed throughout the troposphere even when the sky is, meteorologically speaking, clear. Tables of attenuation of visible and infrared radiation under model "clear standard atmospheric" conditions are available.[4] These tables are useful because of the spectral and altitude ranges covered and the inclusion of realistic aerosol distributions. Both Rayleigh (molecular) and aerosol attenuation coefficients are tabulated. For example, at 0.7μ the Rayleigh coefficient is 8.157×10^{-3} km^{-1} and the aerosol coefficient is 1.50×10^{-1} at the surface level. This is based upon aerosol concentration measurements under or adjusted to conditions when visibility is 20.25 kilometers. Therefore, at least in the lower atmosphere, the clear air attenuation is much more sensitive to particulate than molecular concentration, especially since molecular concentration is relatively constant at any given level.

Long (Reference 5, pages 859-860) has specified gaseous attenuation at ruby wavelengths in an analysis of attenuation versus wavelengh over the probable operational bandwidth (as controlled by temperature) of this type of laser. Several atmospheric absorption bands due to oxygen and water vapor have been noted.

Ligda[3] has suggested that when it becomes possible to construct practical filters with a bandpass of a fraction of an angstrom, attention may focus on exploitation of a solar absorption line with attendant noise reduction. One strong (55 percent) absorption line a few tenths of an angstrom wide due to iron in the solar atmosphere lies at about 0.6945μ (close to a laser ruby wavelength).

Transmission through the atmosphere versus wavelength and zenith angle is shown in Table 3-1. This information[6] includes the effects of

molecular scattering, water vapor, ozone absorption, and dust in fairly clear conditions for a normal atmosphere.

Clouds and fog present the most serious attenuation factors along an extended path. This degradation may even be exceeded by localized dense smoke plumes and dust concentration.

TABLE 3-1

FRACTIONAL TRANSMISSION THROUGH ATMOSPHERE VERSUS WAVELENGTH AND ZENITH ANGLE

Wavelength in Angstroms	Zenith Angle in Degrees				
	90	85	80	60	0
3000	3.16×10^{-75}	3.99×10^{-21}	1.13×10^{-11}	1.23×10^{-4}	.0110
4000	2.58×10^{-8}	8.32×10^{-3}	.0760	.400	.630
5000	1.59×10^{-4}	.0913	.276	.633	.795
6000	2.19×10^{-3}	.166	.382	.710	.844
7000	.0313	.384	.600	.835	.911
8000	.0872	.512	.698	.882	.939
9000	.147	.590	.755	.906	.952
10,000	.336	.650	.794	.923	.961

Clouds range tremendously in thickness and particle concentration. The cloud cover problem must be anticipated for an earth/deep space laser communication system. The tradeoffs between probability of deep-space-vehicle observability and number of earth receiving stations must be carefully studied from a logistics and economic point of view. Factors such as longitude and

latitude of earth sites, longitude coverage, statistical mean number of days per month that cloud cover over a station is less than or equal to some prescribed threshold must be evaluated. Data from Tiros and Nimbus cloud cover pictures should also provide insight to the problem.

Precipitation away from clouds may not seriously attenuate a laser beam if there is a relatively low concentration of drops per unit volume. Snow probably attenuates more than rain because of the larger particle size and lower forward scattering factor.

It is felt that both Rayleigh and Mie scattering cause transmission loss which is a very slowly varying function of wavelength, so that they are not likely to be different for laser beams than for ordinary light because of the laser's monochromaticity.

However, when considering scattering of a laser beam as opposed to scattering of starlight, the finite dimensions of the laser beam wavefront must be considered. This differs from the astronomical case where the wavefront from a star is of infinite extent. In the latter case, there is essentially the same amount of light scattered into the receiving aperture as there is scattered out, whereas for the finite diameter beam there is a greater outward loss.

It is believed that both forward and backward scattering effects will not be significantly different for laser beams than for other collimated beams.

The aforementioned scattering effects can probably be predicted adequately for laser beams from known data. Therefore, unless gross anomalies in the scatter effects attendant on absorption measurements are discovered, we do not intend to study them explicitly as part of the OTS program.

Analysis of Image Degradation Due to Atmospheric Turbulence - It has been well established by various research workers in the field of atmospheric turbulence that the effect of turbulence on astronomical "seeing" is a serious problem.[7,8] Turbulence in the atmosphere between a point object and an optical imaging system causes the image of that point object to be degraded in various ways. The image will fluctuate randomly in sharpness (image blur), intensity (scintillation), and position (angle of arrival fluctuations).

Turbulence in the atmosphere, especially near the earth's surface, can also severely limit the performance of laser optical communications systems. The disturbance causes local variations in the refractive index of the air in the form of blobs or "turbulons." These turbulons move with the wind and give rise to the aforementioned phenomenon of scintillation and angle of arrival jitter. In addition, there exist random phase differences among the light wavefronts in various parts of the receiving telescope aperture due to turbulence.

It has been demonstrated from various theoretical and experimental investigations that, as the diameter of a receiving aperture increases, the magnitude of intensity fluctuations decreases. With a decrease in diameter of a receiving aperture there is a shift of scintillation frequency to higher values.

It has been postulated that scintillation is due primarily to turbulent atmospheric elements at some distance from the observer as opposed to image dancing and pulsation which are due to turbulent elements closer to the observer. From high-altitude experimental flights it has been noted that scintillation is highly correlated with winds near the tropopause and that scintillation frequency is a function of wind velocity near the tropopause and of turbulon size.

A list of the pertinent atmospheric environmental factors appears below. Refer to Figure 3-2 for a sketch of the turbulent effects encountered at various altitudes above the earth.[9] Figure 3-3 shows a sketch of the steps necessary to give a quantitative analysis of image degradation due to atmospheric turbulence.

Scintillation is also dependent upon the time of day. A maximum of scintillation occurs at noon; a minimum near sunset and sunrise. A secondary maximum which is substantially less than the daytime case occurs at night. Seeing also shows fluctuations with weather systems. The poorest seeing usually occurs during cyclone (low) conditions.

Environmental Parameters -

(1) Seeing conditions - seeing disc diameter

(2) Index of refraction correlation function

(3) Atmospheric structure function

(4) Inner and outer scale lengths of turbulence

(5) Shadow band pattern

(6) Temperature gradients.

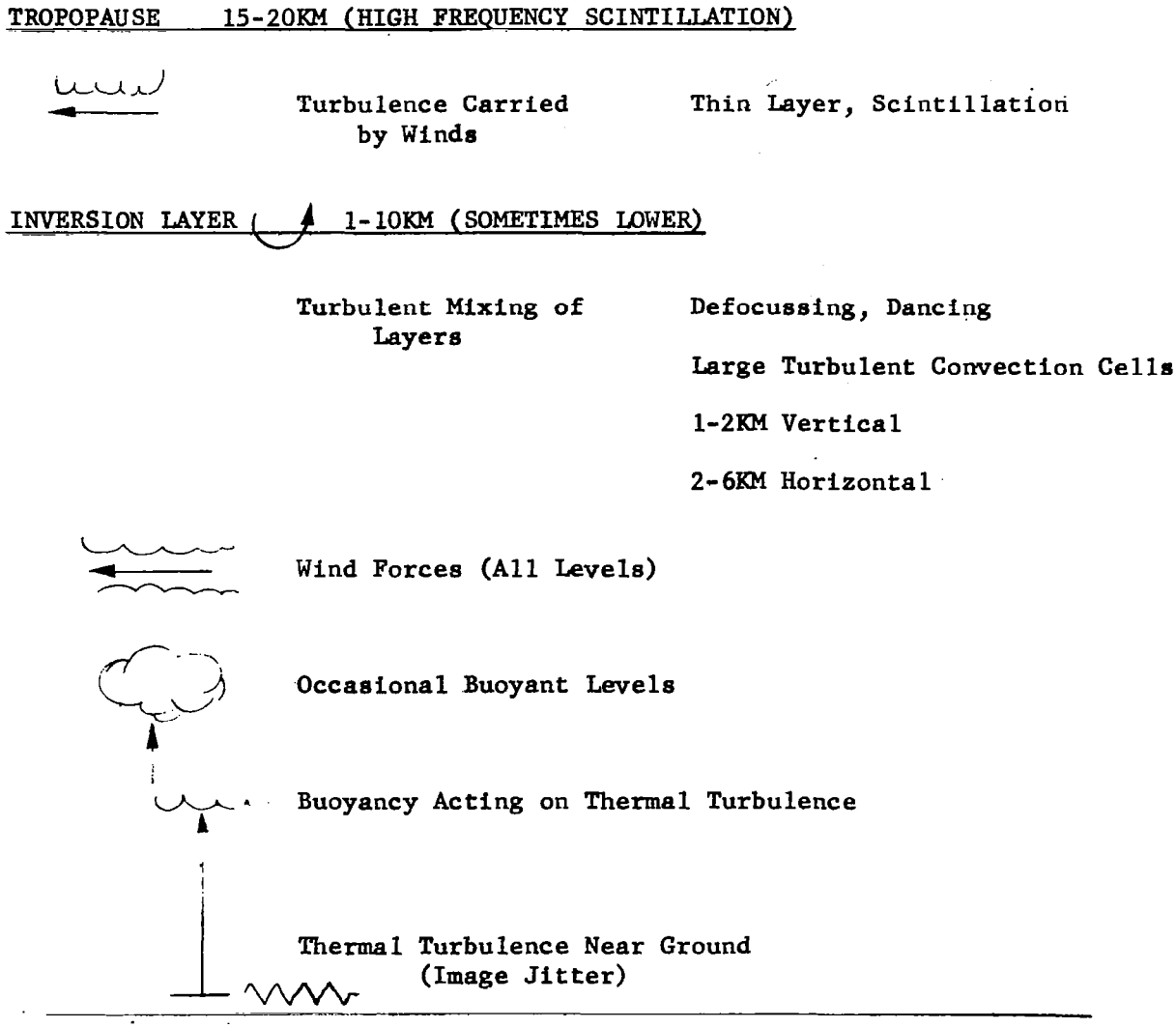

Figure 3-2. Turbulent Effects Encountered at Various Altitudes

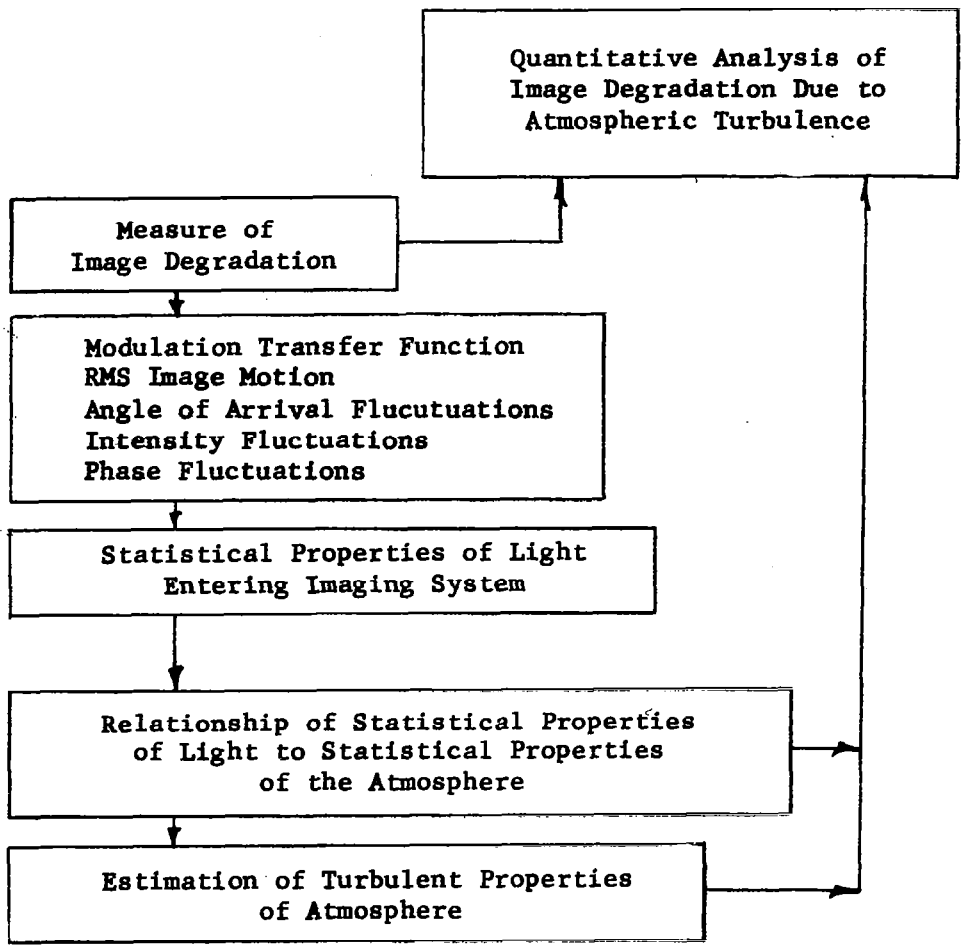

Figure 3-3. Quantitative Analysis of Image Degradation Due to Atmospheric Turbulence

(7) Pressure, humidity, air density

(8) Wind velocity, shear, Richardson number

(9) Season, time of day

(10) Observer altitude

(11) Terrain

(12) Lapse rate, gravity waves.

Sources of Poor Seeing - The following list of four sources of poor seeing will establish the environmental conditions under which an earth-based observatory may have to work:

(1) Turbulence caused by convection currents - daytime phenomenon - can occur at night in poorly chosen locations.

(2) Winds give rise to turbulence near the surface of the ground - day or night phenomenon.

(3) Strong temperature inversion and motion of air. Wavelike turbulence exists at the interface of two air masses.

(4) Turbulence caused by air moving past an obstacle such as an observatory dome.

Intensity Fluctations of Laser Beam Due to Atmospheric Turbulence - (Science Experiment 1) - The temporal variations in light intensity (scintillation) due to atmospheric turbulence cause effects analogous to rapid fading in radio channels. Since the OTS communication channel is polychromatic, i.e., it

contains information bearing sidebands, it is necessary to consider the effect of atmospheric turbulence on the sideband transmission. The primary effects result from the fact that the random intensity and wavefront variations due to atmospheric turbulence are frequency dependent.

If the optical index of refraction of air depends on the intensity of the transmitted light, then the above effects will be non-linear, relative to the propagated light intensity.

Some initial work has been done at Perkin-Elmer in improving a theory as given by Tatarski.[7] It is known that intensity modulation of approximately 100 percent can and often does occur for polychromatic light (stars) and that the modulation can be even greater for highly monochromatic light (Reference 7, pages 256-257). Thus, scintillation is highly significant. The scintillation power spectrum extends to 500 cps and beyond.

One can expect significant selective fading under certain conditions for the following reasons: For non-zenith light paths atmospheric dispersion will cause the rays to traverse different regions of the atmosphere and, hence, to be statistically partially independent. For normal starlight this effect is observed for $\Delta\lambda$ = 1000A, (e.g., red-yellow-green-blue twinkling of stars) in which the refractive index differs only by a few parts in 10^6. For laser light a similar index change can be observed over a $\Delta\lambda \approx$ .01A, if one operates near a narrow atmospheric absorption resonance line.

These deleterious effects can influence the channel capacity of a modulated laser beam.

Science experiment (1), page 2-11, has as its goal the meas-measurement of the amplitude and frequency distribution of light intensity from a coherent source as sensed after passing through the whole atmosphere. The data obtained from this experiment will be useful for predicting anticipated noise levels and in establishing maximum useful aperture size for the OTS system.

Angle of Arrival Fluctuations of Laser Beam - Steady State Refraction Effects - A light ray traveling between earth and a spacecraft will be deflected through a slight angle because of atmospheric refraction. Refer to Figure 3-4. This effect has long been studied by astronomers since it produces a discrepancy

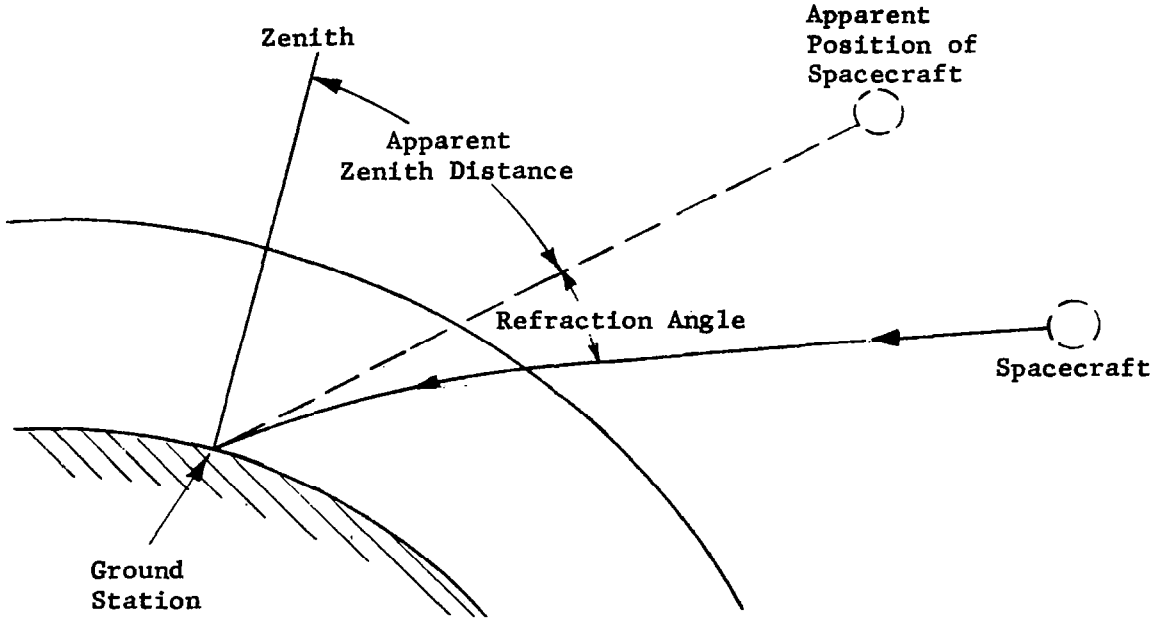

Figure 3-4. Atmospheric Refraction Displaces True Angular Position of Spacecraft

between the apparent and the true position of stars. Table 3-2 (taken from Reference 10, page 453) shows that the angular difference between the apparent and true zenith distances of a star is strongly dependent on how far off the zenith one is looking. At the zenith no refraction takes place, while at the horizon the refraction angle exceeds 30 arc-minutes. The magnitude of the refractive error can be seen to increase very rapidly as a zenith angle of 90 degrees is approached.

TABLE 3-2

REFRACTION ANGLE VERSUS APPARENT ZENITH ANGLE

Apparent Zenith Angle (Degrees)	Refraction Angle (Minutes & Seconds of Arc)	Apparent Zenith Angle (Degrees)	Refraction Angle (Minutes & Seconds of Arc)
0	0 0.0	70	2 35.7
5	0 5.0	75	3 30.0
10	0 10.1	80	5 13.1
15	0 15.3	81	5 46.0
20	0 20.8	82	6 26.0
25	0 26.7	83	7 15.0
30	0 33.0	84	8 19.0
35	0 35.7	85	9 40.0
40	0 47.9	86	11 31.0
45	0 57.1	87	14 7.0
50	1 8.0	88	17 55.0
55	1 21.4	89	23 53.0
60	1 38.7	90	33 51.0
65	2 1.9		

Since the index of refraction of air depends directly upon its density, it is pressure and temperature dependent and tends to decrease with increasing altitude. Extremes of atmospheric temperature and barometric pressure occurring at a ground station in the arctic versus one in the desert could cause a difference of roughly 50 percent between the minimum and maximum values of the refraction angle observed for a given zenith distance. Exact analytical expressions[11,12] have been derived relating refraction angle to zenith distance but these cannot be numerically evaluated until a density versus altitude profile has been specified. The density profile may be derived from one of several standard atmospheres or, for very accurate work, must be computed from experimental data obtained at the observing site, such as that obtained by weather balloons. However, astronomers using single air temperature and pressure measurements made at the observing site, together with semi-empirical formulas, can predict the refraction angle to within a second of arc at zenith distances up to 75 degrees.[13] If this degree of accuracy is indeed sufficient (for acquisition purposes), it eliminates the need for the extra work required to experimentally determine the local density versus altitude profile.

Only during acquisition at the transmitting ground station is it necessary to know accurately the refractive error at a given pointing direction. Initially, the position of the spacecraft in the sky is known to within a certain angular uncertainty as a consequence of the uncertainty in the computed trajectory. The earth transmitter must either floodlight or sweep out this area of uncertainty with repeated transmissions to locate the spacecraft and initiate a response. Any uncertainty in the transmitted beam direction which remains after the correction for refraction angle has been made will increase the uncertainty in intercepting the spacecraft and will lengthen operating time prior to communications.

As a simple illustration, consider the following problem. It is anticipated that the spacecraft position at any time can be predicted from trajectory measurements performed early in flight to within .001 degree (4.0 arc-seconds). This means that the spacecraft is known to be somewhere within a square "window" in the sky 4.0 arc-seconds on a side. Assume that after passing through the earth's atmosphere the transmitted beam from earth has a divergence of 3 arc-seconds. In order to guarantee striking the spacecraft, it is necessary to cover completely the 4.0-arc-second square window. This requires four transmissions with the 3.0-arc-second diameter beam (See Figure 3-5). However, if the instantaneous uncertainty in the transmitted beam direction is restricted to even 1.0 arc-second, in any direction, thirty-six transmissions are required. (Since the uncertainty in diffraction angles lies in the zenith direction only, rather than in all directions equally, the actual number of transmissions would be less than thirty-six). Obviously, it will be easiest to acquire the spacecraft when it is directly above the observing site where the refraction angle is zero. A careful analysis of this problem would consider the probability of establishing communications in view of such factors as type of search pattern, probability distribution of beam position, and probability distribution of spacecraft position.

Once acquisition is complete, correction for refraction angle is not required during tracking. The ground base telescope is locked on to the apparent position of the spacecraft during tracking and the light being transmitted from earth is aimed back close to the image of the spacecraft. It, therefore, emerges from the atmosphere refracted through nearly the same angle as the received beam from the spacecraft, and the refraction error is cancelled.

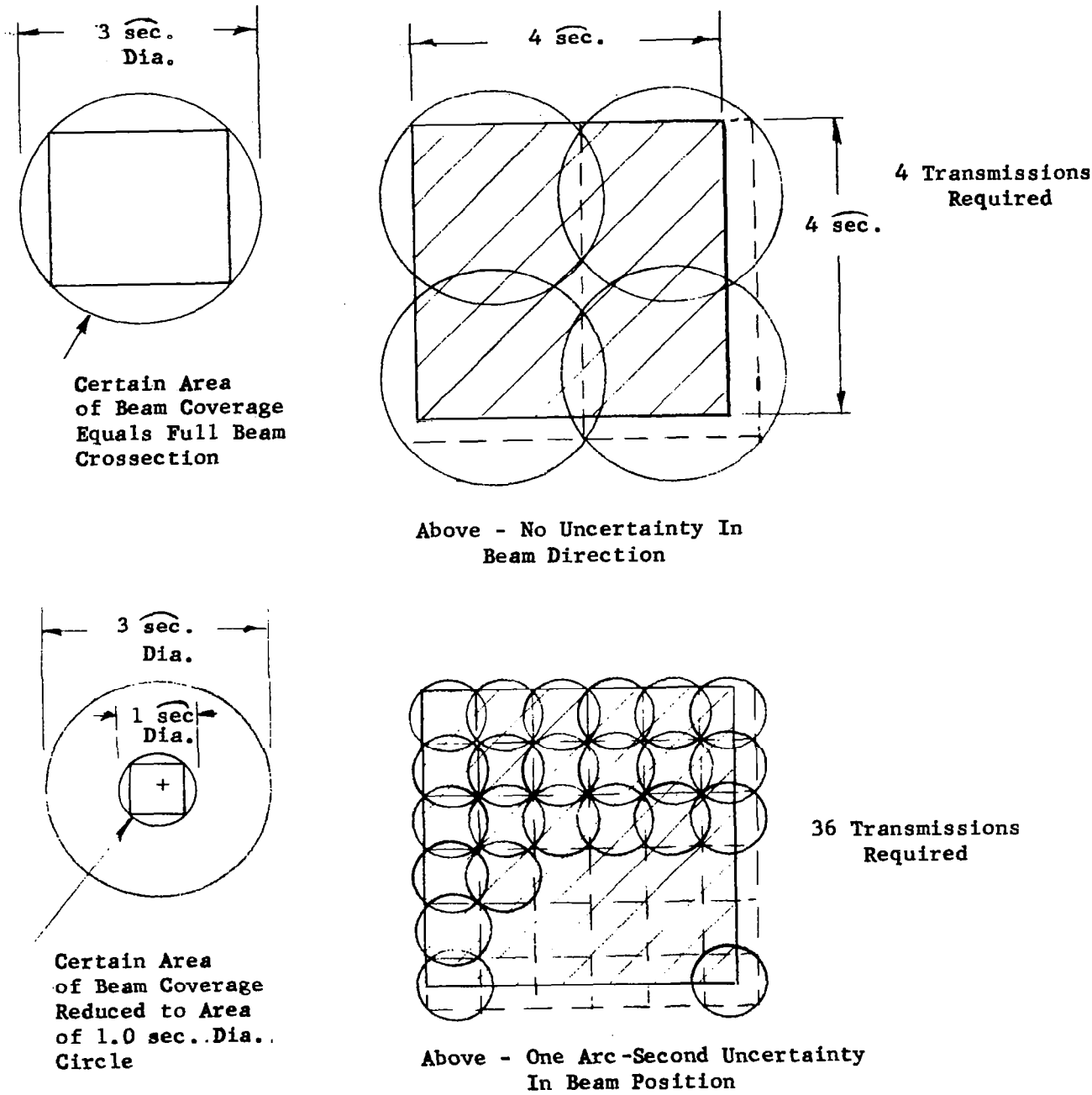

Figure 3-5. Number of Uplooking Transmissions to Acquire Spacecraft Depends on Uncertainty in Beam Position

Only at pointing directions close to the horizon at maximum lead angle might a refraction angle correction be conceivably required. For example, in order to accommodate the change in spacecraft position during the 18-minute round trip transit time at a distance of 10^8 miles, the ground transmitter may have to point ahead by as much as 30 arc-seconds. A change in zenith distance of this magnitude will cause a refraction angle change of 1 arc-second or more for zenith distances exceeding about 85 degrees. It is, however, highly unlikely that tracking will ever be maintained this close to the horizon because of the excessive signal attenuation due to the high scatter and absorption caused by the long light path.

Atmospheric refraction produces some slight lateral shift in the position of the beam received from the spacecraft. For example, at a zenith distance of 60 degrees the refraction of 100 arc-seconds shifts the beam spot along the ground by about 20 meters, which is negligible compared to an expected spot diameter of 40 miles.

Angle of Arrival Fluctuations of Laser Beam - Dynamic Refraction Effects - This section will deal with the determination of the angle of arrival fluctuations of the laser beam due to atmospheric turbulence and the dependence of these fluctuations on various system parameters.

Hufnagel[14] has shown that the rms one-dimensional position deviation (at the image plane) of the instantaneous center of gravity of the image of a point is given approximately by:

$$\sigma \cong \left(\langle s^2 (D) \rangle \right)^{1/2} \frac{F}{D}$$

where $\langle S^2 \rangle$ is a function describing the random optical path length fluctuations between the object and the image forming system;

F = focal length of the receiver optical system;

D = aperture diameter of the image forming system.

The total rms deviation in two dimensions is $\sqrt{2}\,\sigma$.

The function $\langle S^2(P) \rangle$ is the mean squared value of the fluctuation of the difference in optical path lengths as measured along straight lines from the object to two points in the entrance pupil which are separated by a distance P. $\langle S^2(P) \rangle$ can be expressed in terms of the statistics of the intervening index of refraction. The pertinent statistic is the atmospheric structure function or mean squared fluctuation of the difference in index of refraction at two points separated by a fixed distance at an average distance from the imaging system. The structure function in turn can be related to the structure constant and inner scale length of turbulence and local meteorological conditions. These parameters, which can be computed from empirical data, are averages and considerable departures may occur in individual situations, especially near atmospheric inversion layer boundaries. It should be noted that there is a rapid decrease in structure constant and a rapid increase in inner scale length at altitudes above a few kilometers.[14] This is caused mostly by the decreased atmospheric density at these elevations.

For earth-based slant path viewing of a far extra-atmospheric object (plane-wave source) it can be shown that the rms image jitter σ/F is approximately equal to:[14]

$$\frac{\sigma}{F} \cong \frac{1.3 \times 10^{-5} \sqrt{\sec \theta}}{D^{1/6}} \text{ radians}$$

where D is expressed in cm and θ is the zenith angle.

Refer to Table 3-3 for bounds on the rms angular jitter (angle of arrival fluctuations) under average seeing conditions for various zenith angles. It is assumed that diffraction-limited optics are employed and that the wavelength, λ, of the laser source is equal to 6328A.

It is important to realize that the above considerations on angular fluctuations are used only for the approximate evaluation of the earth reception laser communication link case.

TABLE 3-3

RMS ANGLE OF ARRIVAL FLUCTUATIONS VERSUS ZENITH ANGLE θ AND RECEIVING APERTURE DIAMETER

Diffraction Limited Beamwidth (Arc-Seconds)	1.0	0.1
Receiving Aperture Diameter (Meters)	0.131	1.31
Zenith Angle θ in (Degrees)	RMS Angular Jitter $\frac{\sigma}{F}$ (Arc-Seconds)	
0	1.75	0.76
30	1.88	0.82
45	2.08	0.91
60	2.45	1.08

Starlight and laser light differ to the extent that laser light is essentially monochromatic, while starlight is not. Also, the laser beam has a wavefront with finite dimensions. This differs from the astronomical case where the wavefront from a star is of infinite extent.

It is also interesting to note that the angular jitter for viewing through the entire atmosphere will be larger than that encountered from mountain top observatories, so that the data in Table 3-3 are "conservative" in this sense.

It will be useful to evaluate the crosscorrelation between scintillation and angle of arrival fluctuations and their influence on optical communications and tracking performance. Science experiment (1), page 2-11, covers this area of interest. It will provide the first opportunity to compare the scintillations of laser light with those of starlight and thus check the applicability of astronomical data to the laser communications problem.

Loss of Lateral Coherence - Another optical signal perturbation which is caused by atmospheric turbulence is the loss of lateral coherence. This effect has been shown by Hufnagel[15] to be similar to the degrading effect of blur in an image forming system.

The average lateral spatial coherence M(p) as given in Reference 15 is:

$$M(p) = \exp\left[-\frac{K^2}{2}\left\langle\left[S(p)\right]^2\right\rangle\right]$$

where p is the lateral separation distance;

k is wave number = $2\pi/\lambda$; λ = wavelength; and

$\langle [S(p)]^2 \rangle$ is a function describing the random optical path length fluctuations between the object and the receiver system.

Figure 3-6 is a plot of the coherence M(p) computed from 0.5μ collimated laser light transmitted vertically downward through the whole average earth turbulent atmosphere.

For this case $\langle [S(p)]^2 \rangle \cong 2 \times 10^{-10} p^{5/3}$ (cm^2).

Some measure of the loss of lateral coherence will be obtained from science experiment (1) by comparing reception with varying receiver aperture diameters.

Loss of Polarization - The contemplated OTS communication system and a possible alignment system depend upon the polarization of the laser beam. It is, therefore, well to consider if the whole atmosphere will cause any significant loss and change of polarization.

The degree and the direction of polarization of a laser beam can be investigated with a rotating polarizer. Important polarization parameters such as the phase difference, the polarization azimuth, and the degree of polarization can be measured using an analyzer assembly mounted in the path of the laser beam. Intensity information can also be measured photoelectrically. With the use of a quarter-wave plate the same parameters can be investigated for circularly polarized light. All of this information is of scientific as well as engineering interest. Refer to the summary of science experiment(2).

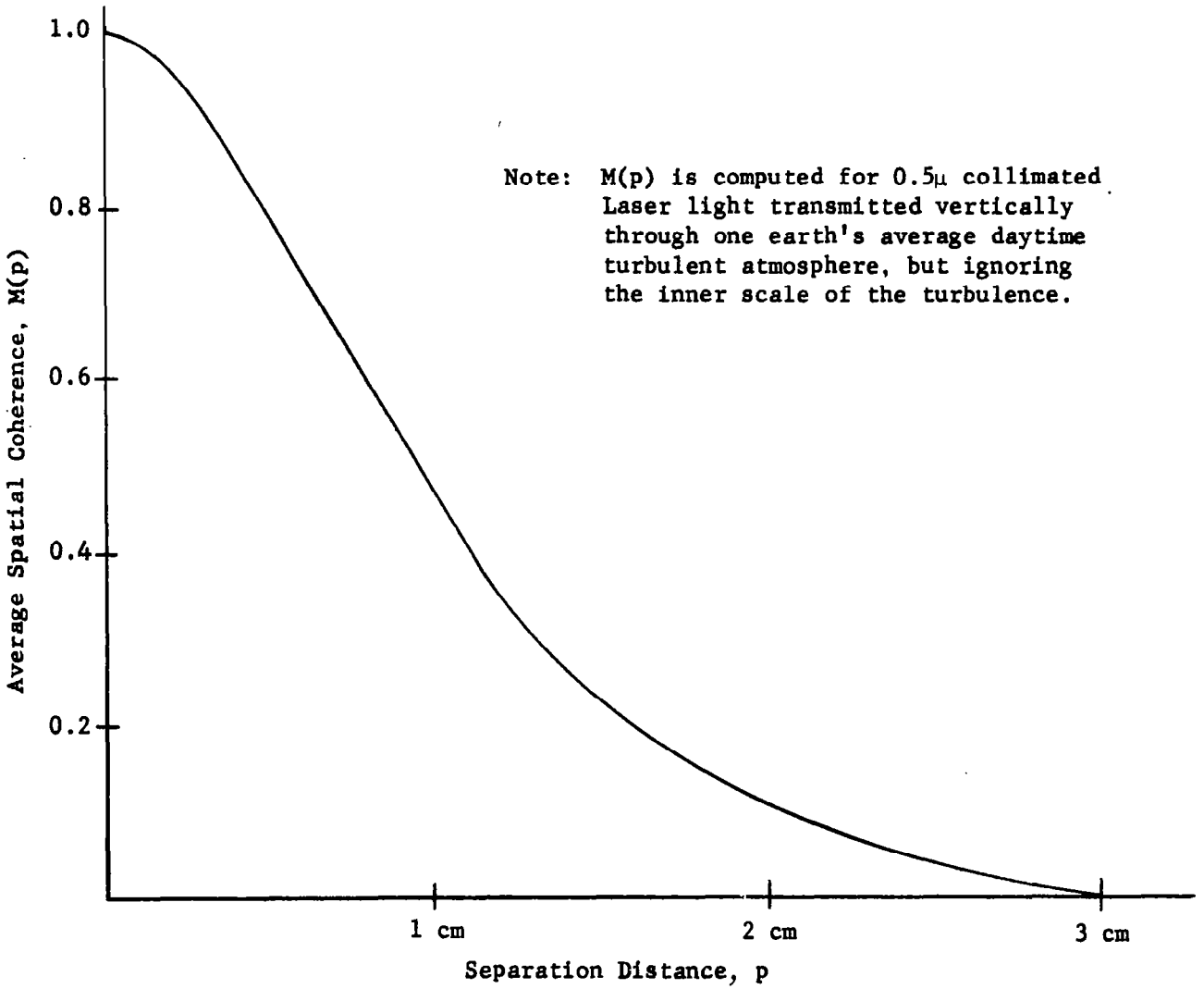

Figure 3-6. Average Spatial Coherence Versus Lateral Separation Distance

Since the atmosphere has a near-zero shear modulus* it causes near-zero changes in the polarization state of transmitted light. In recent years the sun's magnetic field has been inferred from the polarization of light originating in sunspots. The axis of the inferred field is closely aligned with the rotational axis of the sun. Also, galactic fields have been inferred from starlight. These data would tend to indicate that the atmosphere produces only slight changes (if any) in the polarization state of transmitted, partially polarized, incoherent light.

One possible source of polarization loss might be the orientation of anisotropic particles in a preferred direction by wind or gravity. Such a phenomenon might be discovered and be of interest.

Polarization Rotation - The Faraday rotation of the plane of polarization by the earth's magnetic field can be computed as follows:[16]

$$\alpha = \rho t H \cos \theta$$

where α is the angle of rotation in arc-minutes;

ρ is the Verdet's constant for the atmosphere = 6.83×10^{-6} arc-minutes at a pressure of 1 atmosphere and temperature of 0°C;

t is the thickness of the atmosphere taken as 10^6 cm;

H is the earth's magnetic field in gauss = 0.4 gauss;

θ is the angle between the light path and the earth's magnetic field, taken as 60 degrees.

*The ratio of shearing stress to shearing strain.

Therefore, the Faraday rotation α is approximately 1 arc-minute. This rotation of the plane of polarization should cause little disturbance in the envisioned optical alignment system for the OTS. Refer to the summary of science experiment (2).

Antenna Diffraction Pattern - At an earth-based receiver terminal the diffraction pattern of the space vehicle transmitter will appear to have a moving fine structure (intensity fading) which will be determined in part by the structure of the atmosphere and by the aperture size of the space vehicle laser transmitter. This fading phenomenon, similar to scintillation, is another factor that degrades optical communication. This effect is studied in science experiment (1) and engineering experiment (13).

The OTS pointing system will attempt to keep the diffraction pattern centered on the receiver telescope to within the free-space nominal beamwidth requirement. However, intensity fading may still result, due to the perturbations of the position of the diffraction pattern within this allowed limit.

Anomalous Dispersion - The gases composing the atmosphere exhibit anomalous dispersion in the vicinity of an absorption line. In this region, the index of refraction and absorption vary rapidly with frequency. The index of refraction is associated with the phase or time delay of the received wave and absorption is associated with the amplitude. An analogy may be drawn between the anomalous dispersion, absorption of the atmosphere and an electronic narrow-band rejection filter. The existence of anomalous dispersion will cause some frequency components to be delayed more than others and the absorption will cause some components to be attenuated or missing completely; the resultant signal will thus be frequency deficient and scrambled.

The index of refraction also varies with altitude since the concentration of the various gases composing the atmosphere, the temperature, pressure, and ionizing radiation vary with altitude. The relative concentrations of specific atmospheric constituents, such as the water and carbon dioxide, that are primarily responsible for the absorption lines of interest varies more rapidly than the average density of the atmosphere. A laser beam that is not perpendicular to the stratified atmosphere will be bent by the gradient of the refractive index with respect to altitude. In addition, since anomalous dispersion causes the index of refraction to vary with frequency, the degree of bending will also vary with frequency. The differential bending with frequency is analogous to chromatic aberration in optics.

Normally, one might try not to operate a laser near one of these absorption lines. However, there are many lines, closely spaced, so that a moderate change in the laser's apparent frequency, such as those caused by Doppler shifts, could cause the light beams and absorption frequencies to coincide. If frequency coincidence already occurs, small frequency shifts will perturb the actual distortion causing the signal distortion to be time-dependent. These relative frequency shifts may arise from the relative motion of the vehicle or earth to the atmosphere. The former includes Doppler and relativistic frequency shifts; the latter absorption shifts are caused by atmospheric motion, Zeeman effect and Fizeau-Fresnel drag.

As an example of atmospheric dispersive effects, consider a one-nanosecond pulse of one-micron laser light. This laser pulse duration yields sidebands extending beyond one gigacycle per second about each side of the laser center frequency. For air at one atmosphere, the average refractive index is $N = 1.0003$.

For a typical absorption line, the refractive index may vary by $\Delta N = 3 \times 10^{-5}$ over a frequency difference of about one gigacycle per second. Refer to Figure 3-7 for the variation of refractive index of a typical weak absorption line. If the laser signal and atmospheric absorption frequencies coincide, anomalous dispersion could cause the frequency components of the laser pulse, which are spread over more than one gigacycle per second, to experience time delays differing by $\Delta t = \Delta N \frac{L}{C} = 0.8$ nanoseconds; where L = 8 kilometers is the scale height of the atmosphere and C the velocity of light. Thus, anomalous dispersion in the atmosphere could easily cause the pulse width to be approximately doubled.

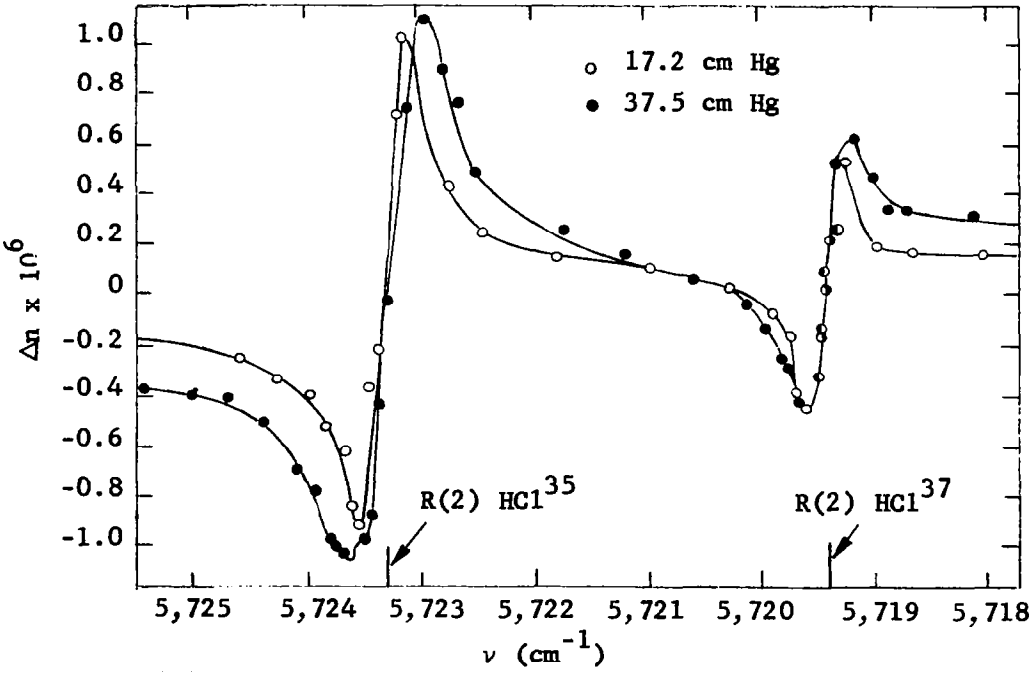

Figure 3-7. Lines R(2) of the 2-0 Bands of HCl^{35} and HCl^{37} at Two Gas Pressures

For communications purposes in the OTS program, it is unlikely that pulse widths smaller than 50 nanoseconds will be used. Commensurate bandwidths will naturally be employed. Thus, the effects of anomalous dispersion will be negligible and almost impossible to detect. There may be some other effects, but these must be several orders of magnitude greater than the largest effect anticipated from anomalous dispersion, as indicated by the discussion in Appendix E.

Doppler Frequency Shift - Since optical heterodyne detection is a candidate for the spacecraft reception technique (refer to engineering experiment (4)), it is important to consider the sources and magnitude of Doppler frequency shifts. For a low orbit, considerable Doppler shifts (of the order of gigacycles) may occur, and they will occur rapidly. In a deep-space mission there also may be considerable Doppler frequency shifts, but they occur very slowly.

The Optical Technology Satellite will be placed in a synchronous orbit in which the maximum north-south angular rate will be approximately 7.5×10^{-5} radians per second relative to the earth terminal. Thus, there is no important Doppler shift to be expected on the OTS program.

Signal Photon Noise - The maximum information capacity of the OTS communication link, or any deep-space laser communication link, is limited ultimately by the mean number of signal quanta (photo-electrons) received per second.[17] R. Clark Jones (Reference 18, pages 493-501) has shown that for the case of non-degenerate (incoherent) light the maximum information carried by a photon is one bit, provided that the *a priori* probability of the shutter being open at the transmitter is one-half. Jones' theory with some modifications may also be applied to laser light.

For a communication system using polarization to mark the binary "one" or "zero" the maximum information capacity of the photon is also one bit for a priori equally likely markings.*

For a deep-space communication channel, there will be a high-transmitted power density and, therefore, a large number of photons per transmitted bit. At the receiver there will be only a few photons to carry the information due to the attendant geometric loss. There will be even fewer photoelectrons (received signal quanta) because the quantum efficiency of a practical photomultiplier is less than unity. There may be, in addition, statistical fluctuations in the quantum efficiency. There is some probability, therefore, that no signal photons will be received at all or that the received background photons will greatly exceed the signal photons. The attendant loss of information is termed signal photon "noise".

In a microwave (or lower frequency) communications channel, signal photon noise is usually small compared with the thermal and Johnson noise. Signal photon noise, however, predominates for an optical communication link because $h\nu >> kT$.

All of the above signal perturbations must be considered in the design of a deep-space communications link.

---

* For the noiseless case it is possible to send $\log_2 3 = 1.585$ bits per photon using the following scheme. Let there be three code symbols (a_o, a_r, a_ℓ) with equal a priori probability of transmission (1/3). Let the receiver consist of an analyzer and two photomultipliers. The analyzer will send a left circularly polarized photon into the "left" channel and a right circularly polarized photon into the "right" channel. If code symbol a_o is to be transmitted, the transmitter closes its shutter. For transmission of a_r, a right circularly polarized photon is sent with some probability less than unity; similarly for a_ℓ. Then the maximum amount of information per photon is 1.585 bits.

3.3 BACKGROUND

It is possible to classify sky background noise in two ways:

(1) External background noise arising from extended sources which will fill the receiver beam;

(2) External background noise arising from small sources which do not fill the receiver beam.

It is necessary, considering these two background noise factors, to know the magnitude and spectral distribution of flux incident upon a detector from background sources. The following types of background will be considered in the order indicated:

(1) Sun
(2) Moon
(3) Earth
(4) Other planets
(5) The day sky
(6) The night sky.

The Sun - The irradiance of the sun just outside the earth's atmosphere is 1390 watts/m^2, and its spectral distribution at the earth's surface is modified by the transmittance of the atmosphere.

Sunlight Reflected from Moon, Earth, and Other Planents - The spectral distribution of reflected sunlight is identical to that of sunlight only if the reflectance of the object is independent of wavelength. This appears to be a fair approximation for several cases.

The Moon - The lunar irradiance of the full moon is approximately 1/465,000 that of the sun, or 3.0×10^{-3} watts/m^2 just outside the earth's atmosphere and its spectrum is essentially that of sunlight.[19]

The irradiance falls off rapidly as the elongation angle (phase) goes from 180 degrees (full moon) to 0 degrees (new moon). The half moon (90 degrees), though apparently half the area of the full moon, is only 11 percent as bright. This rapid fall off is due mostly to the rough character of the surface, which causes it to be more or less darkened, except when full, by shadows cast by surface irregularities. The non-uniformity of the surface is quite important when the receiver's field of view is small.

The Earth - The earth's albedo (reflection coefficient) may be determined from measurements of the earthshine on the moon, and also from estimates based on individual albedos of ground, sea, forest, snow and clouds. The actual albedo is strongly affected by cloud cover. If an albedo of 0.39 is assumed, the irradiance of the full earth at the mean moon distance is approximately 0.22 watts/m^2.

The spectrum of reflected sunlight from the earth is accentuated in the blue region. This is due to the fact that there is an increased contribution of atmospheric scattering at the shorter wavelength.

Other Planets - The albedo of various planets is presented in Table 3-4. Venus, the brightest planet seen from the earth, has an irradiance outside the earth's atmosphere of from 0.46 to 1.15 microwatts/m^2.

TABLE 3-4

ALBEDO OF VARIOUS PLANETS

Planets	Visual Albedo
Mercury	0.069
Venus	0.59
Mars	0.154
Jupiter	0.56
Saturn	0.63
Uranus	0.73

The Day Sky - The day sky will exhibit wide variations in radiance and in spectral content depending upon the sun's position, weather conditions, and receiver orientation.

When the sun is near its zenith on a clear day, the sky is predominantly blue, due to Rayleigh scattering. When the sun is near the horizon, the blue component in the sun's rays is severely attenuated from Rayleigh scattering by the time they reach an area overhead. Rays are now rich in the red-yellow portion of the spectrum. Clouds and dust particles illuminated by this light make the sky appear red or yellow in hue. The flux density per steradian of the receiver's field of view is of the order of 20 watts/m^2- steradian for a clear day sky.

Let us consider the condition when the receiver's field of view is completely filled with a fairly uniform source of radiation (gradientless sky). This background condition may be characterized by its flux density at the receiver per steradian of the receiver's field of view, i.e., the radiance B

of the background in watts/m^2 - ster. Over a wavelength interval between λ and $\lambda + d\lambda$ the spectral radiance at the receiver will be designated B_λ watts/m^2 -ster-μ. If at this λ, the radiant sensitivity of a photocathode is α and the receiver light losses are denoted by n_r, then the external background current $I_{BE(E.S.)}$ where (E.S.) denotes extended source, is given by:

$$I_{BE(E.S.)} = \omega A_R \int_0^\infty \alpha n_r B_\lambda \, d\lambda$$

where A_R is the projected area of the receiving collecting mirror and ω is the solid angle measure of the receiver's field of view. For the case of a conical search pattern, it is convenient to express ω in terms of the apex angle, ϕ. For ϕ in radians we obtain approximately:

$$\omega = \frac{\pi}{4} \phi^2$$

Therefore,

$$I_{BE(E.S.)} = \frac{\pi}{4} A_R \phi^2 \int_0^\infty \alpha n_r B_\lambda \, d\lambda.$$

For minimization of background current, it is clear that ϕ should be made as small as possible, so long as the signal itself is not degraded.

If light losses in the receiver are substantially constant over the spectrum of αB_λ, n_r can be taken outside the integral. At this point it is convenient to define a weighted value of cathode radiant sensitivity as:

$$\bar{\alpha}_{BE(E.S.)} = \frac{1}{B} \int_0^\infty \alpha B_\lambda \, d\lambda.$$

Then,

$$I_{BE(E.S.)} = \frac{\pi}{4} n_r A_R \phi^2 \bar{\alpha}_{BE} B.$$

To calculate $I_{BE(E.S.)}$, one must know B and $\bar{\alpha}_{BE(E.S.)}$ for the particular background. As an example, for clear day sky a typical B is 20 watts/m^2 - steradian.

Table 3-5 gives the radiance of several background sources. The information contained in the table is adequate for performing initial feasibility investigation of an optical communication system when limited by radiation from these background sources.

TABLE 3-5

SPECTRAL RADIANCES OF TYPICAL OPTICAL NOISE SOURCES
(In watts/cm^2-ster-angstrom)

Wavelength (A)	Sun ⊙	Moon x 10^{-6}	Zero Magnitude Star* x 10^{-15}	Sunlit Earth x 10^{-5}	Day Sky x 10^{-5}	Night Sky x 10^{-14}
3000	0.081	0.12	0.34	0.001	0.0055	1.4
4000	0.222	0.34	0.83	0.118	0.053	1.3
5000	0.310	0.47	1.16	0.170	0.035	2.0
6000	0.272	0.41	1.04	0.173	0.019	5
7000	0.214	0.33	0.80	0.157	0.012	-
8000	0.168	0.26	0.63	0.132	0.0065	-
9000	0.132	0.20	0.50	0.110	0.0032	-
10000	0.108	0.16	0.41	0.0875	0.0025	-

The Night Sky - The spatial distribution of stars has been well documented in the literature. Combining this data with some assumptions on the average spectrum of stars allows one to determine in a statistical manner the effect of this background.

*watts/cm^2-angstrom.

The stellar magnitude, M, of a star or other heavenly body is defined as:

$$M = M_o - 2.51 \log I$$

where I is a measure of the brightness of the object and M_o is a reference magnitude. This brightness measure is taken with a detector whose response peaks in the blue part of the spectrum. This formula is applicable to a visual observation of a star. To convert from stellar magnitude to photoelectric magnitude it is necessary to determine the color index for the stars of interest.

Most of the irradiance from stars comes from those whose magnitudes are larger than 5. Very bright stars contribute little to the total irradiance because there are so few of them.

The amount of light from stars is a function of galactic latitude since the density of stars is a function of galactic latitude. More than five times as much light comes from latitude 0 degrees as from any latitudes above 60 degrees.

The brightness of any star compared to the sun can be expressed as:

$$\frac{I}{I_s} = 10^{\left[\frac{M_s - M}{2.51}\right]}$$

Since the sun's visual magnitude is -27, a first magnitude star would be only 6.3×10^{-12} times as bright. The total light from a hemisphere of stars is approximately equal to that from 1440 first-magnitude stars.[20] This means that the light from a hemisphere of stars is $1440 \times 6.3 \times 10^{-12} = 9.2 \times 10^{-9}$ times that of the sun.

If the spectral irradiance of a star at the receiver is b_λ, the background current which results is

$$I_{BE(E.S.)} = A_R \int_o^\infty \alpha\, n_r\, b_\lambda\, d\lambda$$

Assuming again that n_r is flat over the spectrum of b_λ and defining the weighted cathode radiant sensitivity for the source as

$$\bar{\alpha}_{BE(E.S.)} = \frac{1}{b} \int_o^\infty \alpha\, b_\lambda\, d\lambda$$

the equation for external background current (small source case) becomes:

$$I_{BE(S.S.)} = n_r\ A_R\ \bar{\alpha}_{BE(S.S.)}\ b$$

Where b is equal to the irradiance of the star in watts/m^2. Table 3-6[20] gives irradiance for some possible discrete sources (stars of various magnitude). The irradiance values listed are for a receiver just outside the earth's atmosphere.

Background - Thermal Noise and Photon Noise - From an optical communications standpoint the major contribution of background radiation to noise is due to the fluctuations in the rate of arrival of background photons, i.e., shot noise. Thermal noise will be present whenever background radiation is received, but, at optical frequencies where $h\nu >> kT$, the thermal noise power is much less than the background shot noise power. Strandberg has shown that the total background power spectral density $\psi(\nu)$ is given by: (Reference 21, pages 617-620, and Reference 22):

$$\psi = \frac{h\nu}{\exp\left[\frac{h\nu}{kT}\right] - 1} + h\nu$$

When $h\nu \gg kT$, the first term (thermal noise) becomes much smaller than the second term (shot noise).

TABLE 3-6

IRRADIANCE VALUES JUST OUTSIDE THE EARTH'S ATMOSPHERE FOR SEVERAL SOURCES

Source	Irradiance (Watts/m^2)	Spectrum
Sun (M = 26.7)	1390	Typical Solar Spectrum
Moon	3.0×10^{-3}	Approx. Sunlight
Venus	0.4 to 1.2×10^{-6}	Approx. Sunlight
Stars		Sunlight*
M: -2.0	1.83×10^{-7}	
-1.0	7.27×10^{-8}	
1.0	1.15×10^{-8}	
3.0	1.83×10^{-9}	
5.0	2.90×10^{-10}	
7.0	4.60×10^{-11}	
9.0	7.27×10^{-12}	
11.0	1.15×10^{-12}	
13.0	1.83×10^{-13}	
15.0	2.90×10^{-14}	
17.0	4.60×10^{-15}	
19.0	7.27×10^{-16}	
21.0	1.15×10^{-16}	

*Because of the way in which magnitudes are defined and measured, the irradiance values given apply only to stars whose spectra are the same as sunlight.

The effect of shot noise on the output signal-to-noise ratio depends, of course, on the message encoding scheme. It is interesting to note that the optimum radio frequency communications system, from the point of view of noise immunity, is not necessarily the best one at optical frequencies. Reference to Figure 8-12 in this report shows that, in the presence of a given background photon reception rate, a pulse position modulation system in which the highest received pulse marks the pulse position requires far less signal power than pulse code modulation to maintain the same output signal-to-noise ratio (received error rate). This result is remarkable, since the reverse is true for radio-frequency communications. The reversal is directly traceable to the reversal of the $h\nu$ and kT inequality.

Further discussion of the effects of background shot noise will be found below. For a small background photon arrival rate Poisson statistics are preferred over Gaussian statistics for a realistic analysis. As the background photon arrival rate increases it will be noted that the minimum signal photon rate required for a given error rate asymptotically approaches a linear relationship with the square root of the background photon arrival rate. This is to be expected since the Poisson statistics approach Gaussian statistics for large means.

Background - Source Fluctuations - Another possible source of unwanted noise that can degrade the performance of an optical communication and tracking system is source fluctuation, or variation in the spectral irradiance from various celestial backgrounds.

The varying or a-c noise portion of the spectral irradiance from the various celestial backgrounds (sun, planets, satellites of planets, stars

galaxies, and clusters of stars) is passed by a receiver's a-c intermediate frequency amplifiers and its preamplifiers. This situation can be ameliorated somewhat by optical spectral filtering, pulse coding and decoding techniques, and electronic frequency filtering.

In Reference 23 experiments are described which were conducted to determine the percentage of a-c noise value (or modulation) in steady-state solar irradiance in the visible spectrum as a function of frequency. This percentage is applicable either to the sun or to the solar-reflection irradiances of planets and satellites of planets of the solar system. Modulation noise was measured over a frequency range of approximately 40 cps to 50 kilocycles. The data indicates that the noise spectrum falls off by an order of magnitude for every 100-cps increase in frequency. This result appears to be in rough agreement with work done by Chatterton (Reference 24, pages 43-44).

Typical modulation ratios of around 0.1 percent in the frequency range 50-1000 cps based on measurements by Gilmore (Reference 25, page 3) were not borne out by work reported in Reference 23. It appears that University of Michigan's measurements tend to agree more with those reported by Chatterton. Chatterton's data, derived from measurements in the infrared region of the spectrum, indicate modulation ratios smaller than 0.1 percent by one or more orders of magnitude.

It has been pointed out that frequency dependence and magnitude of the modulation indices of the observed solar modulation are very similar to that produced by scintillation.[23] It is possible that the observed modulation is due to the scintillating effect of the atmosphere and not to variations in the sun's radiance. Further experimentation is needed to determine the extent scintillation contributes to solar radiation modulation.

In any event, this possible source of background fluctuation will degrade performance of an optical communication and tracking link.

Detector Noise - Detector noise may be considered as an internal noise in a communication link. The major components of this source of noise are: Johnson noise, current noise, generation and recombination noise, and shot noise.

Johnson noise is due to the resistive component of the detector and is equal to:

$$N_J = 4K\ TR\ \Delta f$$

where Δf is the bandwidth of the circuits measuring the noise; T is the absolute temperature of the detector; and K is Boltzmann's constant. This noise can be minimized by cooling the detector.

Current noise has been shown to be related to an appropriate power of the total average current through the detector, the sensitive area of the detector, the detector thickness, and modulation frequency. This noise appears to be insignificant for high modulation rates.

Generation and recombination noise is a characteristic noise in semiconductors which is caused by the rise of valence-band electrons in the conduction band and also by the recombination of electrons and holes. This component of noise can be neglected provided that the product of modulating frequency and carrier lifetime is much greater than one.

Shot noise due to the discrete nature of the electron charge is a component that cannot be neglected. This noise depends on the total average current $\overline{I}$ through the detector, which consists of the average signal current $\overline{i}_s$, the average background noise current $\overline{i}_B$, and the average current which flows through the detector in the absence of any input, i.e., the average dark current $\overline{i}_D$. The shot noise, N_{shot}, is equal to:

$$N_{shot} = 2q \overline{I} \Delta f.$$

The dark current noise, N_D, is equal to

$$N_D = 2q \overline{i}_D \Delta f.$$

Since the nature of noise caused by background radiation and the detector is fairly well understood, it will be very interesting to compare the results of the Optical Technology Satellite experiments with the results expected from theory and the known amounts of background.

SECTION IV

HETERODYNE AND INTENSITY DETECTION OF LASER LIGHT

This section deals with a comparison of optical detection and microwave detection for both the up-and-down-looking communication links. The effect of atmospheric turbulence on optical heterodyne detection on earth is considered. An evaluation is made of the loss in received signal power produced by turbulence-induced phase fluctuations over the receiving aperture.

Finally, the pros and cons of optical heterodyne detection and intensity detection for use on earth or in space are discussed.

4.1 COMPARISON OF OPTICAL DETECTION WITH MICROWAVE DETECTION

From quantum mechanical considerations it has been shown that an ideal linear amplifier has an inherent noise of $h\nu$ watts/cps referred to the input. The total noise power spectral density $\psi(\nu)$ is given by:[22]

$$\psi = \frac{h\nu}{\exp\left(\frac{h\nu}{KT}\right) - 1} + h\nu$$

The first term is the thermal noise (one dimensional black-body radiation) from the source at temperature T. The second term represents the minimum additional noise due to quantum effects and, for the laser case, is usually ascribed entirely to spontaneous emission in the amplifying medium. For the microwave detection case $\frac{h\nu}{KT} << 1$, and, therefore, the thermal noise predominates and the system is receiver noise limited. For the optical case $h\nu/KT >> 1$

and, therefore, thermal noise virtually disappears and $\psi \rightarrow h\nu$; hence, the system is photon shot noise limited.

4.2 EFFECT OF ATMOSPHERIC TURBULENCE ON OPTICAL HETERODYNE DETECTION

Loss of Signal Power - One principal reason heterodyne reception is desirable is that it should permit narrow-band, photon-noise-limited operation with solid-state detectors.

For an earth-based reception system, heterodyne detection of transmission from a deep-space vehicle becomes difficult for large receiver telescope apertures. This is because there exist random phase differences among the light wave fronts in various parts of the telescope aperture due to atmospheric turbulence. Heterodyne reception depends upon phase coherence between the local oscillator and the signal and it is difficult to compensate for a multitude of different phases across the aperture. The heterodyne detector system, as illustrated in Figure 4-1, converts a steady signal into a much weaker and noisier signal because the voltage due to various portions of the wavefront would add and subtract randomly. Also, even assuming a uniform wavefront, there is the problem of generating a constant-amplitude local oscillator signal.

In a case similar to that of the microwave, an optical heterodyne receiver provides a signal amplitude proportional to the integral of electric field over the aperture for an undistorted wavefront. Consequently, the aforementioned random spatial variation in amplitude and phase will reduce the received signal power.

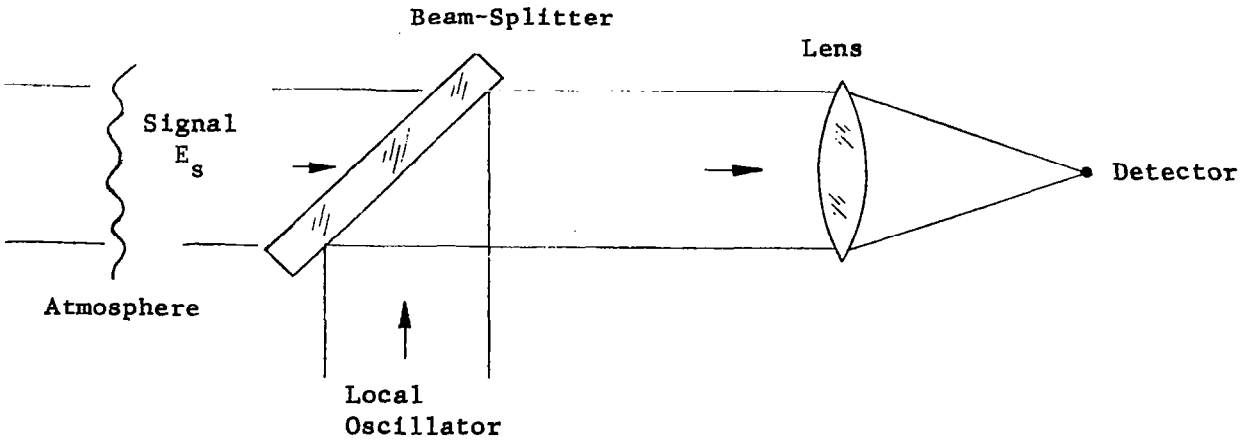

Figure 4-1. Optical Heterodyne Detection

Employing an analytical approach by Gardner[26] that was utilized to evaluate optical heterodyne detection performance for horizontal line-of-sight transmission above the earth, a modification of the analysis was made so that performance could be assessed for the case of vertical downward laser transmission at 6328Å through the atmosphere to an earth receiving station. Reference 27 provides data on the magnitude of atmospherically caused phase fluctuations for this case.

The resulting signal power loss (in db which is equal to 10 $\log_{10}(\gamma)$, where γ is defined as the ratio of the actual received detector signal power to the corresponding power received with no phase fluctuations) increases very rapidly with increasing receiving aperture.

For receiver aperture diameters D greater than approximately 7 cm the loss factor is: $\gamma \sim \alpha/D^2$

where $\alpha = 8.8 \times 10^{-3}$ and D is expressed in meters.

The results presented above tend to be in good agreement with those based on typical astronomical resolution. For the astronomical case a diameter of 10-to-15 cm is the point for which diffraction-limited resolution approximates atmospherically limited resolution.

It is of interest to note that Fried and Cloud[27] have suggested that if the local oscillator wavefront in an optical heterodyne detection system could be made to track the average tilt of the distorted wavefront, efficiency of heterodyne reception could be made to saturate at larger receiving aperture diameters than predicted.

The average signal power loss computed above neglects all effects caused by motion of transmitter and receiver. Therefore, a calculation of average signal power loss based upon this static model represents an optimistic estimate since any motion can only result in further loss of signal information. Also zenith angle dependence must be taken into account to evaluate performance under slant path conditions.

It appears from the above considerations that optical heterodyne detection, although highly attractive, may be extremely difficult to accomplish on earth with large receiving apertures. On the ground an intensity detecting receiver of large aperture may turn out to be more efficient than the optical heterodyne system.

4.3 OPTICAL HETERODYNE DETECTION AND INTENSITY DETECTION

Advantages and Disadvantages

The optical heterodyne signal-to-noise ratio will be reduced if the receiver is not diffraction-limited or if a pointing error larger than the

diffraction limit exists. This reduced value of signal-to-noise ratio is equal to that applying to a smaller diffraction-limited aperture under the same disturbing conditions. Also, the signal-to-noise ratio decreases with $\theta_{DL}/\epsilon_{MAX}$ where θ_{DL} is the diffraction-limited angle and ϵ_{max} is the maximum error angle.

Optical heterodyne detection can in principle always reach the theoretical maximum signal-to-noise ratio in deep space where diffraction-limited operation is required for other reasons, because phase front distortions are minimal. As noted above, on the earth's surface where the atmosphere disturbs the transverse coherence of the beam near the receiver, there is a maximum diameter beyond which diffraction-limited wavefronts cannot be utilized.

An intensity detecting receiver of large aperture and poor pointing accuracy may be a good choice for the earth-based receiver.

Optical heterodyne detection is attractive since the technique can reduce noise originating in the detector to a level less than the signal shot noise. Also, by using heterodyne detection, the effect of background radiation shot noise such as earthshine or sky light can be minimized by use of post-detection filtering. Doppler velocity information may also be obtained by sensing the Doppler shift of the optical carrier.

Essential elimination of detector noise is afforded in a heterodyne system by insuring that the noise due to the local oscillator is greater than the detector noise.

This is accomplished by making the local oscillator power, $\bar{P}_o$, large. The detected signal power increases linearly with local oscillator power, so the only remaining sources of noise are background noise which falls into the post-detection bandpass Δf and quantum noise, i.e., signal noise.

As an example, suppose that the received signal power, $\bar{P}_s$, is 4×10^{-12} watts rms and the detector noise power, $\bar{P}_d$, is 10^{-8} watts. The quantum efficiency is η, and $\bar{P}_b$ is the received background power. The signal-to-noise ratio is a function of local oscillator power and received background power (among other parameters) so it may be written functionally as:

$$\frac{S}{N} = \frac{S}{N}\left(\bar{P}_o\ ;\ \bar{P}_b\right)$$

According to Brinkman (Reference 28, pages 7-1 to 7-24):

$$\frac{S}{N}\left(\bar{P}_o\ ;\ \bar{P}_b\right) = \frac{\eta \bar{P}_s \bar{P}_o}{h\nu\Delta f\left[\bar{P}_s + \bar{P}_o + \bar{P}_b + \bar{P}_d\right] + \eta \bar{P}_b \bar{P}_o}$$

The ultimate signal-to noise ratio is still a function of received background power, even when the local oscillator power is increased without limit.

Thus:

$$\lim_{P_o \to \infty} \frac{S}{N}\left(\bar{P}_o;\ \bar{P}_b\right) = \frac{S}{N}\left(\infty\ ;\ \bar{P}_b\right) = \frac{\eta\ \bar{P}_s}{h\nu\Delta f + \eta \bar{P}_b}$$

Very large local oscillator power is impractical, since it will burn out the photomultiplier. One might desire to make the local oscillator power large enough to obtain a signal-to-noise ratio within m% of the ultimate.

Thus:

$$\frac{S}{N}\left(\bar{P}_o^{*};\ \bar{P}_b\right) = \frac{m}{100}\ \frac{S}{N}\left(\infty\ ;\ \bar{P}_b\right)$$

Substitution from the two preceding equations into the above yields:

$$\bar{P}_o^* = \frac{mh\nu\Delta f\left(\bar{P}_s + \bar{P}_b + \bar{P}_o\right)}{(100 - m)\left(h\nu\Delta f + \eta\bar{P}_b\right)}$$

This $\bar{P}_o^*$ is a function of $\bar{P}_b$, so it may be written $\bar{P}_o^*(\bar{P}_b)$.

Let us choose two cases when $\bar{P}_b = \bar{P}_s$ (i.e., S/N = 1) and $\bar{P}_b = 0$, and let m = 90.

One obtains: $\frac{S}{N}(\infty\,;\ 4 \times 10^{-12}) = .86$, $\bar{P}_o^*(4 \times 10^{-12}) = 1.27 \times 10^{-8}$ watts

$\frac{S}{N}(\infty\,;\ 0) = 6.2$, $\bar{P}_o^*(0) = 9 \times 10^{-8}$ watts

One notes that less local oscillator power is required to obtain 90 percent of ultimate S/N in the presence of received background noise power than when the background noise power is zero, but the S/N for the two cases is different! The natural choice is the larger local oscillator power, obtained by assuming that the background power is zero.

Turning attention to intensity detection, detector noise can be substantially reduced in the visible region by using low noise photomultipliers. In the IR region detector noise can be made negligible by employing cyrogenic cooling.

The minimization of background radiation in a heterodyning system can be accomplished by ensuring that the local oscillator power is larger than the background noise power at all signal image spots, and by the use of narrow-band post-detection filtering. The noise contributions that will remain will be the shot noise of the signal and the minimum background radiation.

The minimization of background radiation in an intensity detection scheme can be accomplished by using narrow-band pre-detection filtering, as with Lyot filters. However, reliable intensity detection with large field angle and large apertures requires sophisticated narrow-band filtering.

The anticipated Doppler shift for low orbits (in the vicinity of 100 n.m.) is from 3 to 30 kmc/s and dictates a requirement of either multi-band local oscillator or transmitter or very broadband photodetectors for a heterodyning application. In addition, mode and frequency control of the lasers would be necessary.

The engineering decision for heterodyne and intensity detection for ultimate deep-space communications will have to be made in light of the above considerations and their system implications. Engineering experiments (4) and (5) will provide sorely needed data to permit the choice of an optimal detection system.

SECTION V

ACQUISITION EXPERIMENTS DISCUSSION

5.1 THE EFFECT OF BACKGROUND ILLUMINATION ON DOWN-LOOKING ACQUISITION AND TRACKING

Ground beacon power and beam width requirements depend directly on the minimum signal-to-noise ratio at which acquisition and tracking by the spacecraft can be performed. As the spacecraft views the earth, the largest source of background noise is earthshine, or reflected (and re-emitted) solar energy. Starlight is a second noise source which is small compared to the earthshine contribution in most instances.

The amount of energy reflected from the sunlit earth towards the spacecraft varies over several orders of magnitude and depends upon many factors. Some of these factors are:

(1) The reflectance of the ground cover which can vary by a factor of 15 to 20.

(2) The extent to which reflecting surfaces act as specular or lambertian reflectors.

(3) The extent and type of cloud cover.

(4) The phase of earth illumination by the sun.

(5) Atmospheric absorption which depends upon the elevation and azimuth positions of both the spacecraft and the sun.

(6) Atmospheric scattering which depends upon the size and distributions of particles suspended in the atmosphere.

The noise due to earthshine cannot be easily computed with any exactitude because of the complexity of these factors. However, even when allowance is made for a wide margin of error, calculations make it quickly apparent that any attempt to view the ground station in the presence of earthshine will require careful steps to limit noise.

Two means are used to reduce the noise incident in the photodetectors in the laser receiver system. The first method of reducing earthshine noise is to use a pre-detection filter. The laser beam received by the spacecraft passes through a narrow-band pre-detection filter which has as narrow a bandwidth as possible. A bandwidth varying from 0.1Å to 10Å can be obtained, dependent upon the type of filter used. Lyot filters have been made with a bandwidth as narrow as 1/8Å while thin film dielectric filter bandwidths have been made as narrow as 5Å. Mica filters have a transmission passband of 1Å. A second method involves reducing the field of view of the receiving telescope to the limit imposed by servo-dynamic performance in an effort to reduce earthshine contribution to noise. This is accomplished by introducing a field stop into the very fine pointing beam. When acquisition is complete, the field of view is reduced to several seconds from the 1-degree field of view, thereby increasing the signal-to-noise ratio and the communication bandwidth. During acquisition the signal-to-noise ratio is necessarily lower due to the wider field of view required.

The extent to which acquisition and tracking will be affected by the background illumination encountered during a deep-space mission must be demonstrated by the OTS. Specifically, two questions must be answered:

(1) How large is the variation in signal-to-noise ratio due to the noise contribution of earthshine and starlight for a variety of observing conditions?

(2) How do the tracking and acquisition functions deteriorate as the signal-to-noise ratio is lowered?

In order to answer these two questions, signal-to-noise measurements should be made aboard the spacecraft and telemetered to earth. Following the basic acquisition and tracking demonstrations which will take place on a moonless night (maximum SNR), acquisition and tracking operations will be performed at different times of the day and night to determine the natural variation in signal-to-noise ratio due to the variation in earthshine.

The signal-to-noise ratio detected aboard the OTS relatively close to earth will be much higher than levels typically encountered in a deep-space mission. Two means will be used to simulate the reduced signal-to-noise ratio likely to occur at distances up to 10^8 miles from earth. Various neutral density filters can be introduced which will attenuate the ground laser beam. At no time will an appreciable star field be observable from the OTS because of the comparatively close range. In order to simulate the optical noise of the stellar background seen during acquisition in deep space, a small mechanical collimator having a 1-degree field of view could be mounted aboard the OTS

pointing away from earth. A beam-splitter might be used to transfer the stellar energy directly into the main optical beam of the spacecraft. However, the complexity involved in this apparatus does not justify its existence aboard the OTS. The noise that would be present may be calculated and simulation of the starfield will not be provided.

In addition to studying the effect of earthshine and starlight on the acquisition and tracking capabilities of the spacecraft, some attention should be given to the ground station receiver which is subject to noise from three sources. These are: sky luminance, starlight, and planetary albedo when the planet is viewed together with the spacecraft. Signal-to-noise measurements made with the ground-based receiver can be useful in determining the noise contributions of the first two of these sources, while simulation of planetary albedo background is possible with an OTS in synchronous orbit, when the earth's moon appears behind the satellite. When tracking the OTS in the vicinity of different planets with the ground-based receiver, it should be possible to make separate estimates of the noise contribution in order to accurately predict system performance in the deep-space situation.

5.2 ACQUISITION TO 1 DEGREE

Previous work indicates that the most stringent conditions for acquisition exist at maximum range (10^8 miles for a deep-space vehicle) and with maximum earthshine. These conclusions are based on the fact that signal power level is minimum and, hence, its associated quantum noise is maximum; additionally, photosensor and electronics noise is largest relative to the signal received. The addition of earthshine background adds to the quantum

noise and reduces the signal-to-noise ratio substantially even when narrow-band pre-detection filtering is incorporated. The location of the apparent position of earth could possibly be eased by detection of earthshine. However, for many portions of vehicle trajectories the phase of earth illumination may be such that earthshine is substantially reduced. Computation of the probable stellar irradiance per square degree leads to the significant conclusion that only modest S/N reductions are to be expected due to relatively large stellar fields in the earth's background. Whether an earth beacon is directly sought or, alternatively, the earth location is sought through earthshine detection followed by beacon search, the field of view during search can thus be reasonably large, the search time can be minimized, and the scanning operations simplified.

If it is now assumed that the vehicle position relative to earth can be accurately predicted prior to launch and trajectory computations refined by post launch tracking data, then it appears reasonable that the earth beacon can floodlight the expected region of vehicle position with a reasonable power density to allow detection by the vehicle. While the vehicle might search for this beacon by scanning in all directions, the scan time would be unreasonably large since there are over 40,000 regions of one square degree area in a sphere. A more logical approach, which achieves tremendous scan time reduction, involves a vehicle stored program which predicts the angular distance between the earth and the sun as a function of trajectory time. With such a program available, the vehicle would simply search for the sun, offset its optical receiver's line of sight from this reference direction by the predicted angle, and roll about the reference direction while searching for earthshine and/or earthbeacon signal.

With a one-degree search field the scanning time would be reduced to 360 rather than 40,000 sectors and the predicted angle need only be accurate to approximately one-half degree. Additional advantages of this approach are that vehicle power required for the search operation is reduced and the stored angle indicates the proximity of the earth to the sun. This latter information can be used either to avoid operations where damage to the system by direct solar power is likely or to narrow the FOV as coronal background light increases (and/or to turn off an earthshine detector if used). For the case of maximum earthshine and a range of 10^8 miles, the signal-to-noise ratio (for video detection) will be low and, since the earth subtends only 16 arc-seconds, no significant S/N improvement will result as the field is reduced from one degree to the earth's angular subtense. Further field restriction, if practical, will increase S/N ratio or alternatively allow bandwidth increase for the same S/N ratio to reduce small-amplitude higher frequency pointing errors which otherwise become more effective in producing target loss for narrower fields. Since total earthshine introduces essentially all quantum noise under the assumed conditions, a field restriction from 16 to 8 arc-seconds will reduce quantum noise by a factor of two and allow bandwidth to be increased by a factor of four. There are no apparent methods of avoiding the degrading effects of earthshine except the following:

(1) Increase the ground beacon laser power or reduced beacon beamwidth to increase received power density.

(2) Increase vehicle receiver aperture to reduce quantum noise associated with earthshine and, in addition, to obtain greater signal power at the vehicle's tracking sensor.

(3) Resort to low duty cycle high power ground laser pulses to minimize earthshine effects on S/N ratio. This approach is discussed elsewhere.

(4) Develop detectors of higher quantum efficiencies.

(5) Utilize low spectral bandwidth detectors and operate at wavelengths where earthshine contribution is reduced.

Reduction of beacon beamwidth is only possible if the vehicle position uncertainty region can be minimized. While atmospheric spreading effects will form an ultimate beamwidth reduction limitation, the position of a deep-space vehicle could be more accurately established if the vehicle could floodlight the expected position of the earth and allow earthtracker lock-on. The 0.1-arc-second beamwidth vehicle transmitter which normally transmits at a 10^7-cps data rate could be used to transmit a floodlight beam at a lower data rate of approximately 10 cps and a beamwidth 1000 times greater or 100 arc-seconds, a value clearly large enough to avoid the 36-arc-second point ahead problem. The received data would indicate, for example, non-systematic refraction angle component of the earth's atmosphere and allow ground beacon beamwidth reduction through better vehicle position determination.

Since no approaches competitive with the foregoing one have evolved in the course of this study, the following paragraphs are limited to considering the requirements for demonstrating the technique with an Optical Technology Satellite.

Let us first examine the case of a deep-space vehicle for the parameters assumed in Table 5-1.

TABLE 5-1. Assumed Deep-Space Parameters

Ground Laser	8400Å, 4 watts average power pulse operation
Earth Beacon Beamwidth	5 arc-seconds with diffraction-limited intensity distribution
Range	10^8 miles
Vehicle	1Å pre-detection filter, 33% transmission, 50% optical attenuation, 32-inch diameter aperture (0.5 meter^2)
Atmospheric Transmission	50%

The signal power density at the receiver will be 7.3×10^{-18} watts/cm^2 corresponding to a received power of 3.6×10^{-14}. The signal power at the detector is 0.6×10^{-14} watts or 2.82×10^4 photons per second. The number of photocathode electrons/sec from a 0.4 percent efficient S1 phototube will be 113, corresponding to a S/N ratio of 7 at 1 cps.* The dark current of the cooled (-70°C) photosensor (EMR 543C) will be 5×10^{-11} amp, which is equivalent to a background of 10^{-14} watts. Earthshine input at the detector will be approximately 468×10^{-14} watts, a value 780 times the signal power, which would tend to lower the S/N ratio by a factor of approximately 27.9. Operation of the beacon at 0.1 percent duty cycle (if possible) would reduce this factor to 1.6 at the cost of increased bandwidth and synchronous gating. A starfield background of 1 degree would produce an additional power input of 0.42×10^{-14} watts which, like detector dark current equivalent, is small compared to earthshine contribution and can be neglected.

*Refer to Equation 5, page 7-5 or Figure 7-14, page 7-8.

Consider next the case of a synchronous earth satellite with the assumed parameters of Table 5-2.

TABLE 5-2. Assumed Satellite System Parameters

Ground Laser	8400Å 4 watts average power pulse operation
Earth Beacon Beamwidth	5 arc-seconds with diffraction-limited intensity distribution
Range	18,000 miles
Vehicle	1Å pre-detection filter, 33% transmission, 20% optical system transmission 12-inch diameter aperture (.07 meter^2)
Albedo	0.36

Assuming a lambertian earth reflectance in a one square degree field of view, the earthshine will be 3.53×10^9 watts/steradian/Å/degree^2 and the power density at the receiver aperture will be 4.21×10^{-6} watts/meter^2/Å. The signal power density at the receiver will be approximately 2.5×10^{-6} watts/meter^2. The signal and earthshine powers at the detector will be 1.2×10^{-8} watts and 1.9×10^{-8} watts, respectively, indicating a signal-to-noise ratio of 20 at 10^6 cps without earthshine. A signal-to-noise ratio of 20 at 100 cps can be obtained with about 10^4 times less beacon power without earthshine or with about 10^2 times less power with earthshine. Hence, ground station power in the order of milliwatts should suffice from a signal-to-noise standpoint.

Practical considerations (viz: saturation of photosensor on high earthshine) may require a higher beacon power which is easily obtained from available lasers. Moreover, pulse duty cycles in the order of 50 percent through optical chopping should suffice.

The FOV restriction from 1 degree to 2 arc-minutes* should reduce earthshine by a factor of 900 to 2.11×10^{-11} watts allowing an equivalent ground station reduction in signal power to 1.33×10^{-11} watts at the detector for a S/N of 20 at 1,111 cps. An uncooled EMR 543C phototube has a dark current equivalent power of 2×10^{-8} which has the effect of maintaining photon noise constant during the foregoing signal power reduction. The S/N ratio thus drops by a factor 900 to $\frac{20}{900}$ @ 10^6 cps or $\frac{20}{9}$ @ 10^2 cps or 22 @ 1 cps or 6 @ 16 cps, a value reasonably close to the deep-space conditions, where the dark current of the phototube is used to simulate earthshine noise. PMT cooling to reduce dark current could be used to allow further degradations by higher ground signal attenuation. If cooling to -70°C is feasible, for example, and the signal is reduced by a factor of about 500, then the signal and earthshine will be approximately 4 times that for the deep-space mission, so that a degree starfield input could result in conditions where the expected S/N ratio is 1/2 @ 1 cps. These figures are summarized in Table 5-3.

Two approaches to search are possible. These are:

(1) Point at Nadir (rather than the sun) with an IR sensor and rotate about this reference with an offset of up to 10 degrees (1/2 earth's subtense for synchronous satellite). This method involves

*Corresponding to the tentative satellite implementation.

TABLE 5-3. Comparison of Deep-Space and Satellite System Signal-To-Noise Ratios

	1 Deep Space	2 Satellite	3 Satellite	4 Satellite
Signal Power at Detector (Watts)	6×10^{-14}	1.2×10^{-8}	1.33×10^{-11}	2.66×10^{-14}
PMT Equivalent Input (Watts)	10^{-14} @-70°C	2×10^{-8} @25°C	2×10^{-8} @25°C	10^{-14} @70°C
Earthshine Power at Detector (Watts)	5×10^{-12}	1.9×10^{-8}	2.2×10^{-11}	22×10^{-12}
Star Power at Detector (& FOV) (Watts)	$.42 \times 10^{-14}$ (1 deg)	$.42 \times 10^{-14}$ (1 deg)	$.42 \times 10^{-14}$ (1 deg)	1.68×10^{-14} (2^2 deg)
S/N	7/28 @1 cps	10 @10^6 cps	22 @1 cps	1/2 @1 cps
Laser Power (50% Duty Cycle)	4 watts	4 watts	4.45 mw	8.9 μw
FOV	1°	1°	2 arc-minutes	2 arc-minutes
Aperture Diameter	32"	12"	12"	12"

NOTE: If a satellite aperture diameter of 32 inches (rather than 12 inches) is considered, the power inputs for the signal, earthshine, and stellar field would increase by a factor of about 7. The effect would be to raise the indicated values of S/N (in columns 1, 2 and 4) by a factor of about $\sqrt{7}$ For the conditions of column 3, the S/N ratio would increase by a factor of 7 because of the predominating and unchanged value of PMT equivalent inputs.

low rates of change of the offset angle but requires search for the earth by an IR sensor which is undesirable.

(2) Point at the sun which is visible to the satellite over 95 percent of the time (at the synchronous altitude and at the recommended inclination angle) and scan about this reference direction. While higher offset angle rates are anticipated, the method better duplicates the proposed scheme. However, the range of the offset angle must now be 180 degrees which complicates the satellite hardware (vis: approach (1) could utilize flex bearings of limited range for implementing offset.)

The acquisition system, as illustrated in Figure 5-1, (corresponding to approach (2)) seems feasible.

5.3 THE ACQUISITION EXPERIMENT

Engineering experiment (12) addresses itself to evaluation of the ability of a deep-space vehicle to acquire a ground beacon directly and, in addition, to acquire the earth beacon once the vehicle's line of sight has been directed towards the earth.

Direct detection of the earth beacon without resort to earthshine detectors appears to be a requirement if one considers that during certain portions of a vehicle trajectory the phase of the earth's illumination may be such as to make earthshine sensing impractical. Calculations assuming the earth to be a lambertian reflector indicate that while the earth may look like a -4 magnitude star at 1AU., it can also appear to be up to 5 to 10 magnitudes less bright and can, thus, be lost among the many stars which exist in this magnitude range.

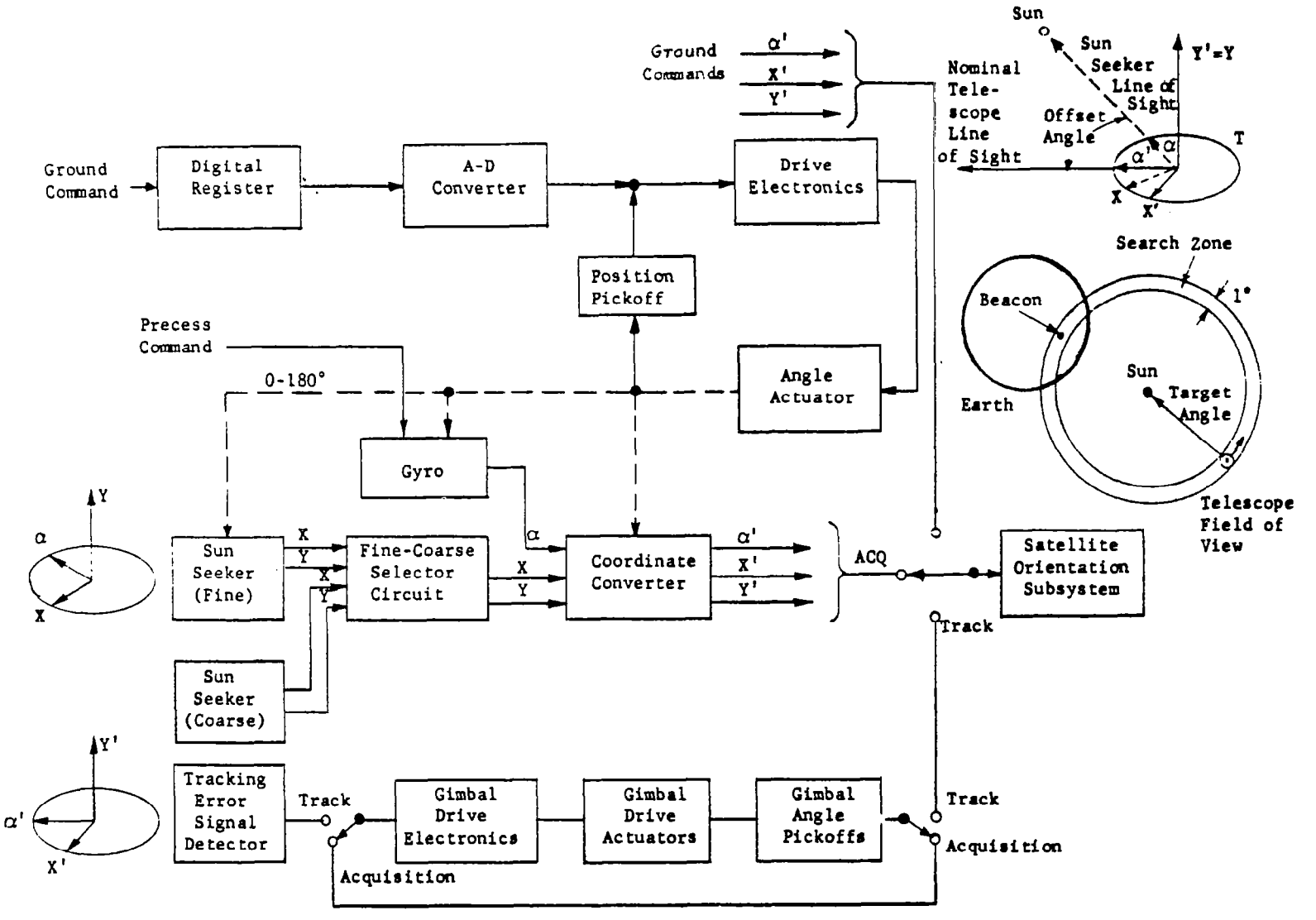

Figure 5-1. Acquisition Subsystem

Alternatively, if the earth's reflected sunlight is large, earthshine sensors are practical for earth location or coarse acquisition, but these conditions then make earth beacon detection extremely difficult due to the presence of a large background light contribution at the vehicle's beacon photosensors.

To gain some insight as to the magnitude of these problems one can consider the case of a deep-space vehicle at a range of 10^7 to 10^8 miles, a range which is reasonable if one considers vehicle trajectories to Mars or Venus which have minimum ranges of 48.5×10^6 and 64×10^6 miles, respectively.

The most adverse conditions for acquisition tend to occur at maximum range where the received beacon power is least and, therefore, quantum noise associated with the signal itself is highest and where the relative amplitude of fixed noise sources (such as from detectors) is greatest. Refer to Figure 5-2.

If it is assumed logically that good tracking must be possible without background light, then it is apparent that the ratio of signal to noise in signal must be adequately large. With this assumption on basic S/N ratio it is found that S/N reduction due to light contributions from relatively large stellar fields is modest. This is significant in that the search field utilized to detect the beacon can be extremely large, if earthshine is small, and the search time and problem reduced accordingly.

Table 5-4 shows the ratio of beacon power to stellar power at both 6328Å and 8400Å for cases wherein the signal power has been chosen to yield a S/N of 6 with no earthshine present. The results, which are given for the

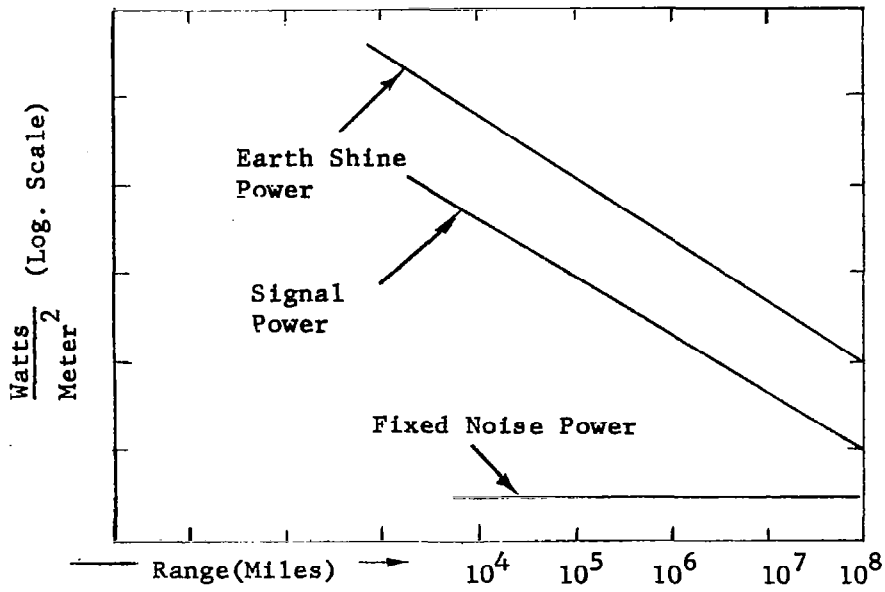

Figure 5-2. Received Power Versus Range

TABLE 5-4. Relative Stellar Light Input

Assumptions	(A) Vehicle Aperture - 32" (B) Pre-detection Filter - 1A° (C) Filter Efficiency - 33% (D) Optical Efficiency - 50%	
λ(A°)	6328	8400
Signal Power Density in w/m^2 for S/N = 6 @ 20 cps	11×10^{-12}	120×10^{-12}
Starfield (1 deg^2) w/m^2	8×10^{-14}	5×10^{-14}
Ratio $\frac{\text{Signal Power}}{\text{Stellar Power}}$	141	2400
Signal Power Density in w/m^2 for S/N = 6 @ 2 cps	1.1×10^{-12}	12×10^{-12}
Ratio $\frac{\text{Signal Power}}{\text{Stellar Power}}$	14	240

assumed cases of 20- and 2-cps bandwidth, indicate that S/N degradations due to starfield background should be small even if the stellar light contains modulation components.

The effect of earthshine on the ability to detect the beacon, however, can be substantial. Table 5-5 indicates the S/N degradation factors expected (assuming no solar modulation components) for the conditions assumed for Table 5-4 and at a range of 10^8 miles where the field of view exceeds the earth's angular subtense. For troublesome earthshine conditions, wide FOV earthshine sensors can be utilized to acquire and point the vehicle receiver LOS at the earth. The problem now becomes one of locating the beacon on the earth in the presence of earthshine, which can drastically reduce detection capability and for deep-space conditions will not vary until the field of view is reduced below the earth's subtense.

TABLE 5-5. Signal-To-Noise Ratio Degradation Due to Earthshine

Assumptions:
(A) Vehicle Aperture - 32"
(B) Range - 10^8 Miles
(C) Field of View $\geq$ 16 Arc-Seconds

λ(Å)	6328	8400
Signal Power Density in w/m^2 for S/N = 6 @ 20 cps	11×10^{-12}	120×10^{-12}
Earthshine w/m^2	11×10^{-11}	57×10^{-12}
S/N Degradation Factor	3.34	1.21
S/N Degradation Factor with Original S/N = 6 @ 2 cps	10.7	2.4

It is concluded that: (1) either earthshine seekers and/or direct beacon detectors can operate with wide field to locate Earth and provide coarse orientation; (2) with low earthshine, the beacon can be acquired directly; (3) earthshine sensors will be ineffective during low earthshine conditions; and (4) the main problem consists in locating the beacon when pointed at the earth under high earthshine conditions. Schemes for the solution of this problem basically include the following:

(1) Acquire the beacon directly and narrow the field of view to reduce earthshine input and improve S/N and, thereby, tracking accuracy.

(2) Acquire the earth with an earthseeker and scan the earth with relatively narrow field sensors to locate the beacon in the presence of reduced background light.

Whatever the approach, the prime question appears to be thus: For a given beacon sensor field of view, what value of S/N ratio will be large enough to avoid beacon loss from the field due to vehicle torque disturbances and noise in signal plus background light? And, what techniques can provide improved beacon detection ability under high earthshine conditions?

The acquisition experiment for the Optical Technology Satellite addresses itself to the simulation by an actual system operating in near space of the acquisition problems and techniques for solution corresponding to deep space.

Let us now consider the simulation aspect from the standpoint of laser power requirements, earthshine, and starfield. The basic assumption is that the beacon acting alone should produce enough power at the vehicle's tracking error sensor so that a reasonable S/N is obtained for tracking purposes. While high power will be required for the deep-space condition, much lower and more practical power levels will be required in the satellite.

Table 5-6 indicates the laser requirements to achieve a S/N of 6 at 20- and 2-cps bandwidth with no background light present. Indicated also is the power level required to attain S/N of 6 at 20 cps in the presence of one square degree of earthshine. The indicated power levels are attainable with available lasers.

TABLE 5-6. Beacon Power Required to Simulate 10^8 Mile Condition at 20 x 10^3 Miles With Transmitter Beamwidth of 5 Arc-Seconds

λ(Å)	6328	8400
Laser Beacon Power for S/N = 6 @ 20 cps	28 microwatts	240 microwatts
Laser Beacon Power for S/N = 6 @ 2 cps	2.8 microwatts	24 microwatts
Laser Power Required for S/N = 6 @ 20 cps with One Square Degree of Earthshine	21 milliwatts	66 milliwatts

It is desired to simulate the earthshine condition corresponding to a deep-space condition where the earth subtends a particular angle. This will be nearly the same as that existing in the satellite field of view corresponding to the equivalent angle. This is true if the earth is considered to be a uniformly illuminated disc since the brightness of the earth would be constant. Hence, earthshine effects are readily simulated by field stop adjustments in the satellite.

Although starfield background will not be a function of range, a minor problem will be encountered if it is desired to simulate deep-space conditions where a stellar field beacon background exists. This is because the earth's angular subtense will be 20 degrees and it will be required that the stellar background light be somehow optically superimposed on the beacon image. Since stellar light contributions have been shown to be relatively negligible, the evaluation of stellar degradation effects by the satellite experiments is considered unnecessary.

The experiment shall evaluate: (1) the ability to locate the beacon directly using large search field for various conditions of earthshine, albedo, and S/N ratio; (2) the ability to acquire the beacon (or to stay acquired) as a function of earthshine conditions for various transmitted power levels (or S/N) and for various fields of view equal to the earth's subtense corresponding to deep-space conditions; and (3) methods of improving acquisition capability under adverse conditions of earthshine.

Let us now consider the proposed equipment for performing the direct beacon detection evaluations. The scan method proposed is essentially

one that is possible with a deep-space vehicle which points at the sun, offsets its receiver line-of-sight from this reference direction by a predicted angle, and rolls about the reference axis while the telescope searches for the beacon in a 1-degree wide angular region of the sky. The predicted angle corresponds to the expected angular position of the earth with respect to the sun. For the deep-space case the predicted angle could be derived from an on-board computer but for the satellite it shall be provided by ground command. The engineering implementation for the satellite is presented by the block diagram in Figure 5-1.

The telescope is either caged or operated as shown to maintain itself along a particular vehicle axis direction. This axis is pointed at the sun by means of a conventional sun seeker arrangement which supplies pointing error signals to the satellite orientation subsystem. Rather than offsetting the telescope line-of-sight to the predicted search angle, the fine sun sensor is rotated by the illustrated ground control loop through this angle, causing the whole vehicle to move with respect to the sun seeker LOS, as the vehicle is controlled to maintain the fine sensor directed at the sun. When the correct angle is achieved, a ground precess command is introduced into the gyro whose output causes the vehicle to move through the circular search zone indicated. When beacon power is sensed by the telescope beacon sensors, the error signals from these sensors are utilized to control subsequent telescope orientation. When this occurs the satellite orientation subsystem receives commands from the telescope gimbal angle sensors and the vehicle is oriented to follow the telescope. This maintains the telescope gimbal bearings within their restricted motional range.

The telescope is now receiving a beacon image at a wide field of view error sensor consisting of an image splitting prism and a group of associated phototubes. The optical arrangement shown in Figure 5-3 features a mirror with a hole positioned at a point of low effective focal length. This allows use of reasonably sized elements to provide a wide field of view sensing. More important, the full receiver light gathering capabilities are harnessed by the wide field sensor as would undoubtedly be required to obtain high S/N in a deep-space system. The coarse photosensors feed signal differencing electronics whose outputs could directly provide mispointing information to the telescope gimbal servo system. If the telescope gimbal system requires a proportional error signal for stabilization reasons, a deviation device (as shown), driven by the difference signals, can be incorporated. This element will move to place the beacon image at the apex of the coarse prism and the degree of motion can be detected by a pickoff and used to feed the gimbal drive servo. As the telescope moves into a position of small alignment error the deviator will return to its zero position.

When the line-of-sight error of the telescope is correct within one minute of arc, the beacon image will pass through the field stop provided in the mirror and light will reach the fine tracking sensor. This sensor will provide pointing error signals to its transfer lens which will try to acquire the beacon by centering its image upon the prism apex. Since the natural field stop provided by the mirror corresponds approximately to the earth's subtense at 10^7 miles (2 arc-minutes), beacon detection and acquisition by the fine sensor system simulates beacon detection in the presence of earthshine at this large range. Transfer lens position and the difference signals can be ground monitored to assess detection and acquisition capability.

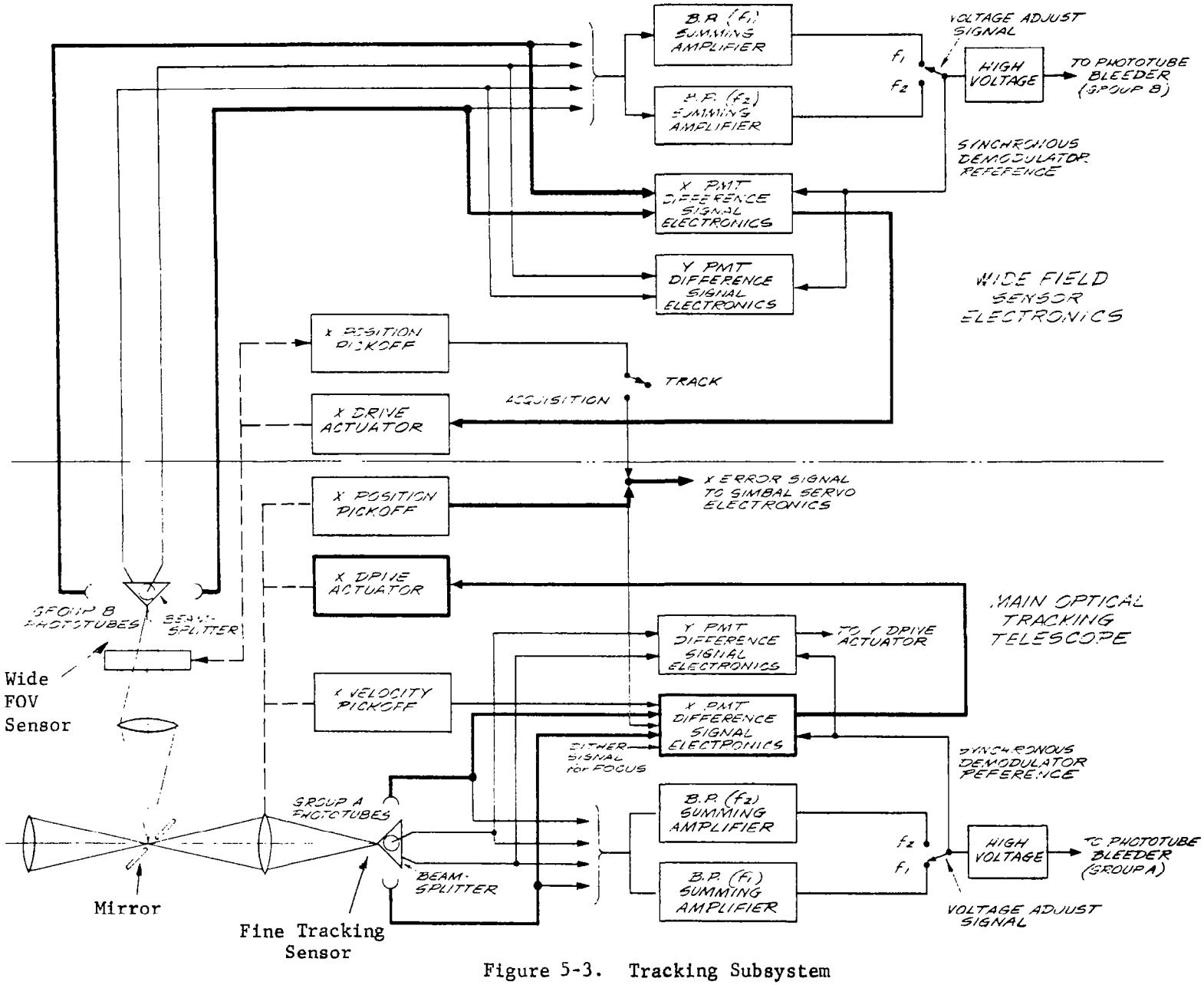

Figure 5-3. Tracking Subsystem

The same process can be repeated to simulate performance at 10^8 miles by waiting until earthshine is naturally reduced by an appropriate amount.

Subsequent to the foregoing procedure the field of view can be restricted below 2 minutes with an adjustable field stop forward of the fine splitter to assess beacon acquisition for the 10^7 mile case using field restriction techniques for moderately low S/N conditions.

Techniques for evaluating methods to improve beacon detection in the presence of high earthshine will not be simple since the earth subtends an angle of less than 2.5 minutes for deep-space conditions while the satellite will view a 20-degree earth. One approach would be to demonstrate the principles using the fine splitter and defocused beacon image to simulate an earthshine sensor which stabilizes the line of sight. (Refer to Figure 5-4). A beam-splitter forward of the fine splitter could relay the beacon image with earthshine to an image plane at a greater EFL which allows the use of reasonably sized elements required to accomplish desired ends. This method is proposed for the Optical Technology Satellite.

Of the several techniques under consideration the following seems appropriate. (Refer to Figure 5-5). An auxiliary beam-splitter, associated photosensors, and very low bandwidth circuitry could be utilized to slowly drive the auxiliary beam-splitter apex into coincidence with the beacon image. The use of low electronics bandwidth results in improved beacon detection signal-to-noise ratio at the expense of longer beacon acquisition time. With this approach, earth tracking sensors could stabilize the nominal vehicle

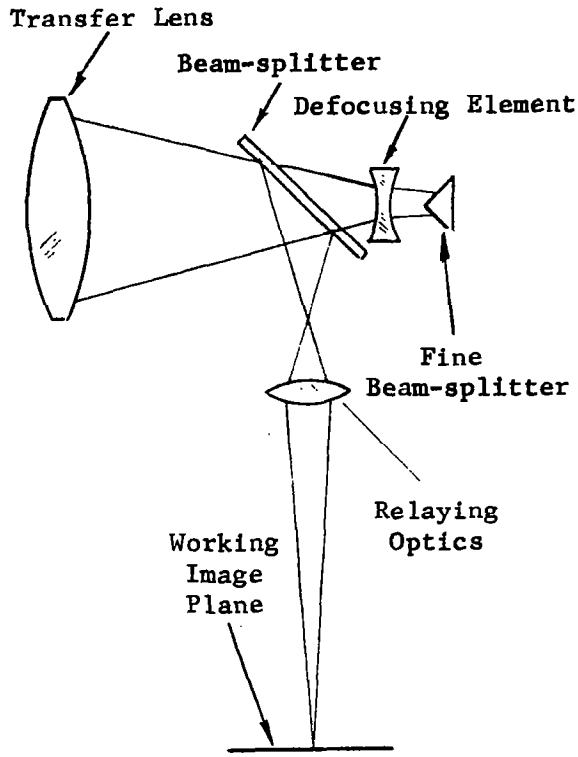

Figure 5-4. Optical Arrangement for Evaluation of Beacon Acquisition Mechanisms

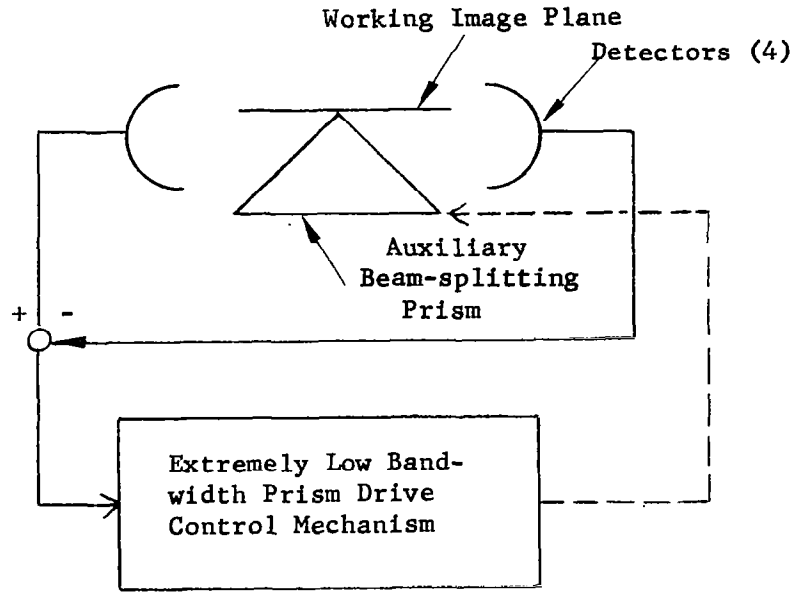

Figure 5-5. A Mechanism for Beacon Acquisition

receiver line-of-sight towards the earth and a gyro could furnish a rotation stabilization reference. In the case of the satellite, this rotational reference element might be the gyro ordinarily used during acquisition scan, provided the scan offset angle is reduced to zero prior to this operational mode.

After the auxiliary beam-splitter apex is coincident with the beacon image, an associated field stop could reduce the background light. Then, the receiver-transmitter transfer lens position can be controlled by the auxiliary beam-splitter photosensor output signals (processed by higher bandwidth circuitry) to maintain the image at the apex. Subsequent shift of the auxiliary beam-splitter back to an on-axis position can re-establish alignment between the receive and transmit lines-of-sight.

SECTION VI

TRACKING EXPERIMENTS DISCUSSION

6.1 TRACKING ACCURACY DEPENDENCE ON SNR

One of the basic questions involved in the tracking of an earth beacon by a deep space communication antenna is the relationship between receiver characteristics, power density at the receiver antenna, noise due to background illumination, photon discreteness, and detector noise contributions. This section examines the question for the case of a single-axis tracker utilizing image splitting and differencing techniques to derive pointing error signals "proportional" to the degree of mispointing. Evolved is an expression relating rms tracking error to receiver resolution and signal-to-noise ratio for a diffraction-limited system with a clear circular aperture. The result:

$$\text{RMS Pointing Error} = \frac{1.22\lambda}{D} \quad (S/N)^{-1}$$

where λ is the wavelength of light,

D is aperture diameter; and

S/N is the signal-to-noise ratio of the system,

can readily be extended to predict the ultimate limit of tracking performance for the case of centrally obscured apertures.

Consider a single-axis tracking sensor (as shown in Figure 6-1) consisting of a diffraction-limited optical system with aperture diameter D

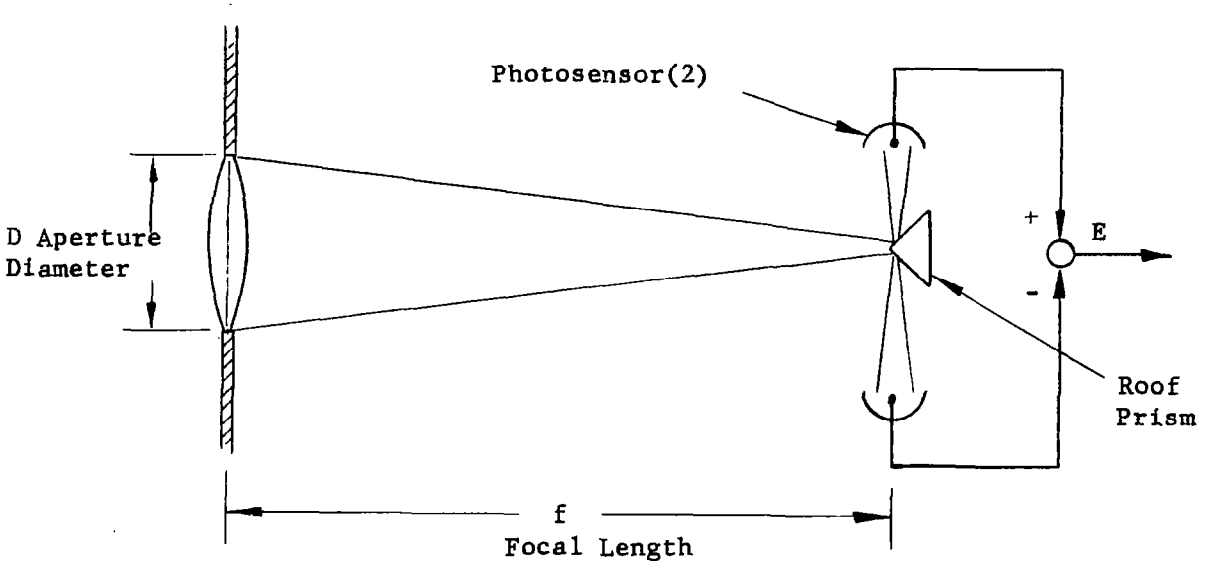

Figure 6-1. Single Axis Tracking Sensor

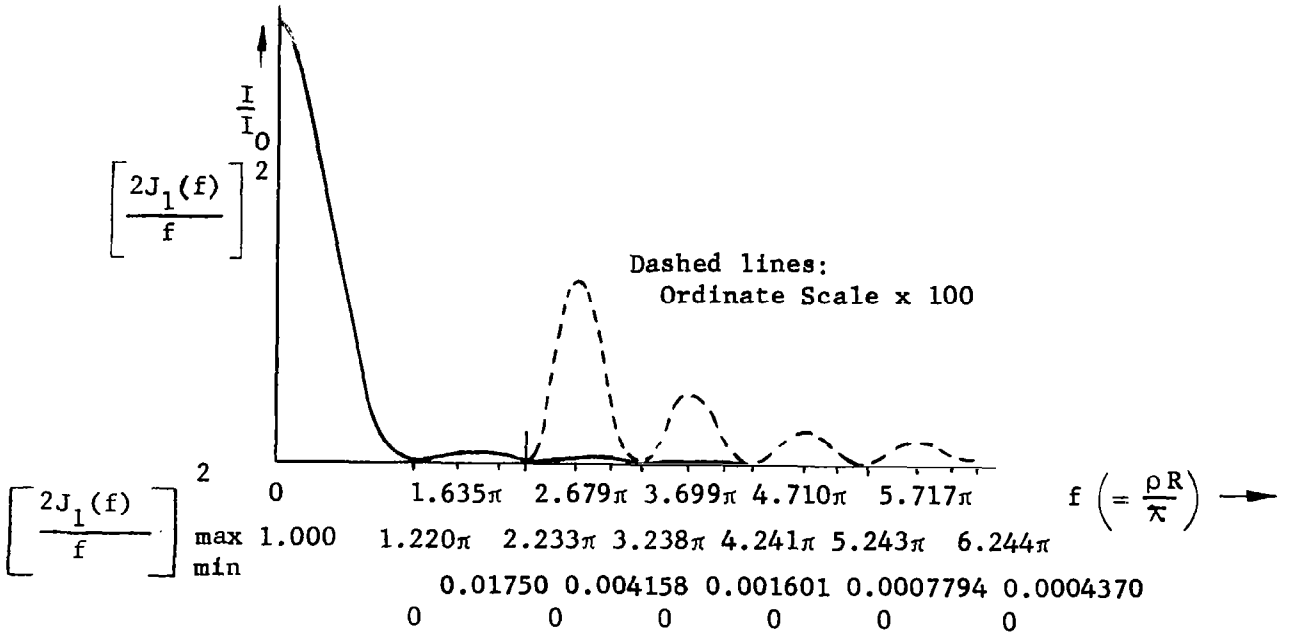

Figure 6-2. Fraunhofer Diffraction at a Circular Aperture

and focal length f, a two-sided roof prism at the focal plane, and two photosensors whose output signals are subtracted to derive the pointing error signal, E, in electrical form. Assuming that the source to be tracked is either coherent or monochromatic with an angular subtense at the receiver which is small compared with receiver resolution, then the image of the "point" source in the focal plane will be the familiar Airy diffraction pattern. Figure 6-2 indicates the variation of image light intensity for the case of a clear circular aperture: i.e. (Reference 29, pages 6-81 and Reference 30, pages 394-396),

$$(1) \qquad I_{(\rho)} = I_o \left[\frac{2J_I(f)}{f} \right]^2$$

where f equals $\rho R \frac{2\pi}{\lambda}$;

J_1 is the first order Bessel function;

R is the aperture radius;

ρ is sin θ, the sine of the angle of deviation; and

I_o is the intensity at the center of the circularly symmetrical image.

This may be expressed in rectangular coordinates

$$(2) \qquad \frac{I_{(\rho)}}{I_o} = \Delta_y = \left[\frac{2J_1 \, (u^2 + v^2)^{1/2}}{(u^2 + v^2)^{1/2}} \right]^2$$

with the y axis as the axis of symmetry, and integrated to find the amount of energy on one side of an arbitrarily positioned boundary line parallel to the U axis

$$(3) \qquad I = \int_{-\infty}^{U} \left\{ \int_{-\infty}^{+\infty} \left[\frac{2J_1\left(\sqrt{u^2 + v^2}\right)}{\sqrt{u^2 + v^2}} \right]^2 dv \right\} du$$

This result is shown graphically in Figure 6-3* while Figure 6-4 indicates the rate of energy transfer across the boundary as a function of U (the boundary location)

$$(4) \qquad \frac{dI}{dU} = \int_{-\infty}^{+\infty} \left(\frac{2J_1\left(\sqrt{U^2 + v^2}\right)}{\sqrt{U^2 + v^2}} \right)^2 dv.$$

Since the angular radius of the first dark ring of the diffraction pattern is not affected by focal length but depends simply on the aperture diameter, change of focal length simply results in proportional changes in image size.

Consider now the tracking error sensor of Figure 6-1 with a total received power S from the distant beacon and a total rms noise power N expressed in terms of equivalent beacon received power. With correct pointing, the two photosensors receive equal quantities of light and the electrical error signal output E will be null. Mispointing upsets the light division and causes the signal E to depart from null.

The sensor can be kept pointed at the beacon by incorporating a servo system which receives the signal E and acts to maintain it at null by controlling receiving antenna orientation. However, even a perfect servo cannot distinguish between fluctuations in E caused by noise, and signal fluctuations due to mispointing. The servo will, therefore, act to maintain

---

*These results have been obtained by W.H.Steel[31], who has also derived similar results for centrally obscured circular apertures.

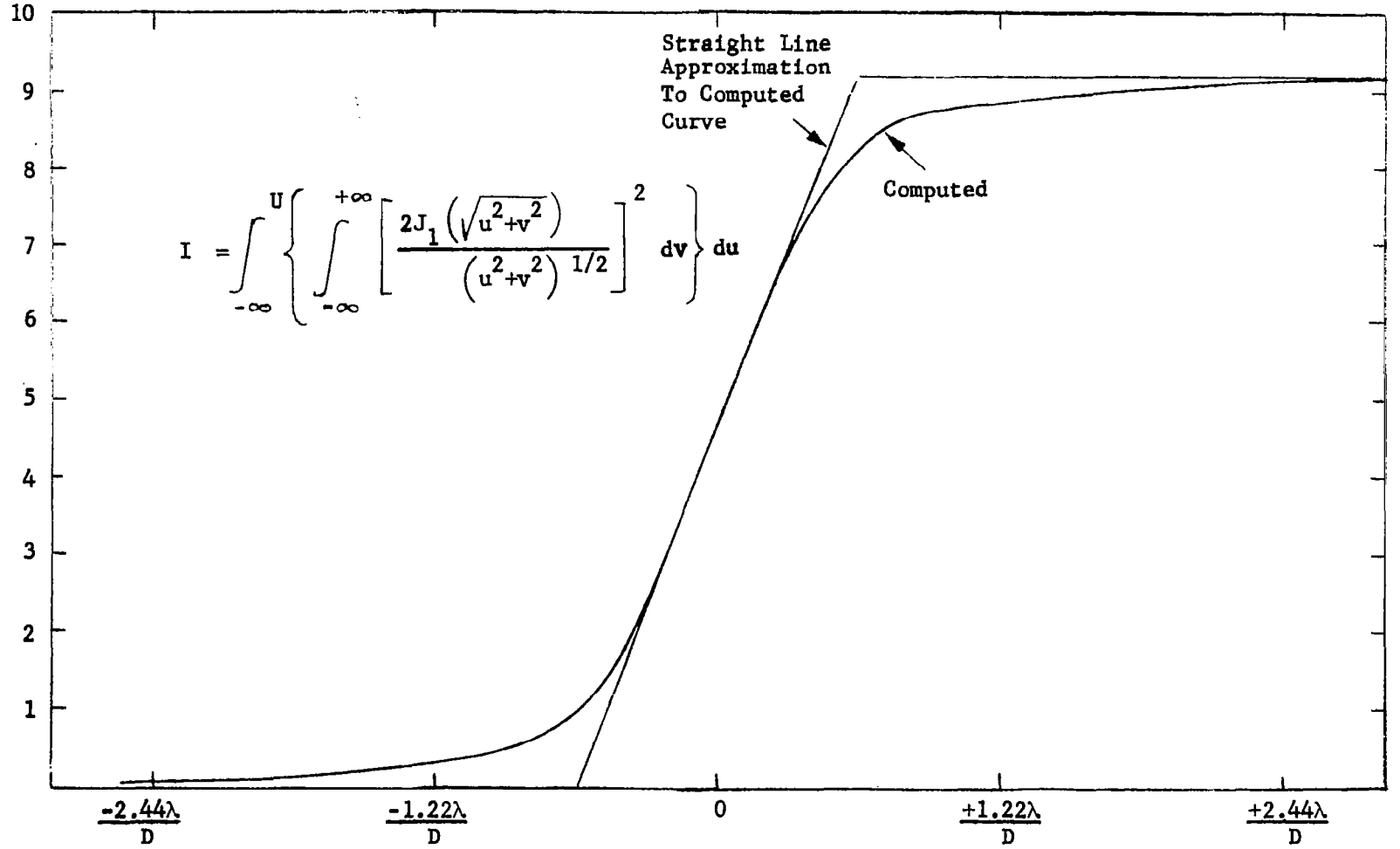

Figure 6-3. Image Light Energy On One Side Of a Knife-Edge Boundary

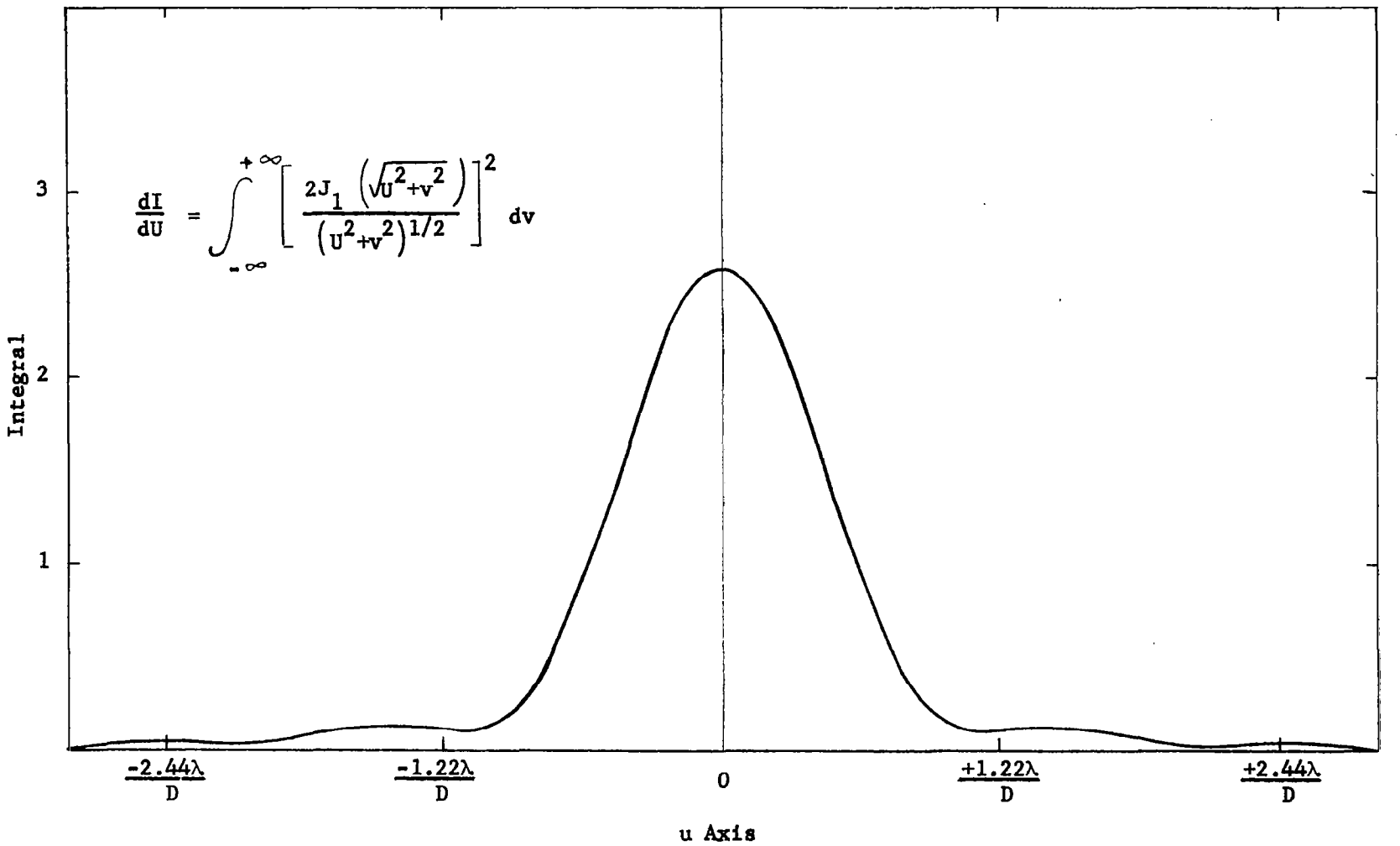

Figure 6-4. Rate of Energy Transfer Across a Knife Edge in the Image Plane

E at null regardless of the source of fluctuation and noise* will cause unwanted motions of the receiving antenna.

The magnitude of these motions can simply be determined from a knowledge of the S/N ratio and the energy transfer curve derived previously. A straight line approximation to the energy transfer curve of Figure 6-3 indicates that the transfer rate at the null position is equivalent to total energy transferred for an angular motion of approximately 1.22 λ/D. An rms noise of N, therefore, will cause the system to have an rms pointing error of:

$$E_p = \frac{1.22\ \lambda/D}{S} \quad (N) \tag{5}$$

This expression is nearly correct for reasonably high signal-to-noise ratios (viz: $S/N \geq 10$). As the S/N ratio is lowered, the expression becomes optimistic (due to greater departures of the straight line approximation from the actual energy transfer curve) and more accurate results can be obtained if desired with other than the simple slope approximation used above. The effect of aperture diameter D on system performance** is not immediately evident from equation (5) since S/N ratio may also be a function of D. Three cases shall now be considered:

(1) For systems which are limited by noise in signal (due to photon discreteness), larger apertures will act to increase

*While filtering (or bandwidth restriction) can be introduced to decrease the amount of such motion, the bandwidth cannot be reduced to zero without making the pointing system insensitive to the frequency range of expected input disturbances. A compromise bandwidth based on any of numerous criteria[32] is usually chosen to minimize noise effects while maintaining satisfactory servo response.

**The variations of aperture diameter as a function of wavelength and weight are developed in Appendix C.

S/N ratio directly with aperture so that pointing performance increases as the square of aperture diameter.

(2) For a system which is detector noise limited wherein noise is a constant, S/N ratio will increase as the square of D and, therefore, pointing performance will increase as the cube of D.

(3) For a system that is limited by distant background noise (such as may be the case for earthshine, which contains solar modulation components), the S/N ratio is unaltered by aperture diameter and pointing performance increases directly with D.

It is also clear that failure to achieve diffraction-limited operation (viz: focus errors) will degrade pointing performance through reduction of the energy transfer rate. Centrally obscured optic systems which contain a smaller fraction of their total image power in the central portion of the diffraction image will similarly suffer. Figure 5 of Reference 31 contains energy transfer curves for the cases where the obscuration diameters are 1/2 and 1/3 that of the total aperture. These are duplicated here as Figure 6-5.

6.2 TRACKING TO 1/10 OF AN ARC-SECOND

A technique for optical tracking to 1/10 arc-second is illustrated in both block diagrams shown in Figures 6-6 and 6-7. With reference to the first block diagram in Figure 6-6, it is assumed that the satellite orientation subsystem can coarse position the satellite. The commands for the satellite orientation subsystem originate in the acquisition subsystem which is discussed

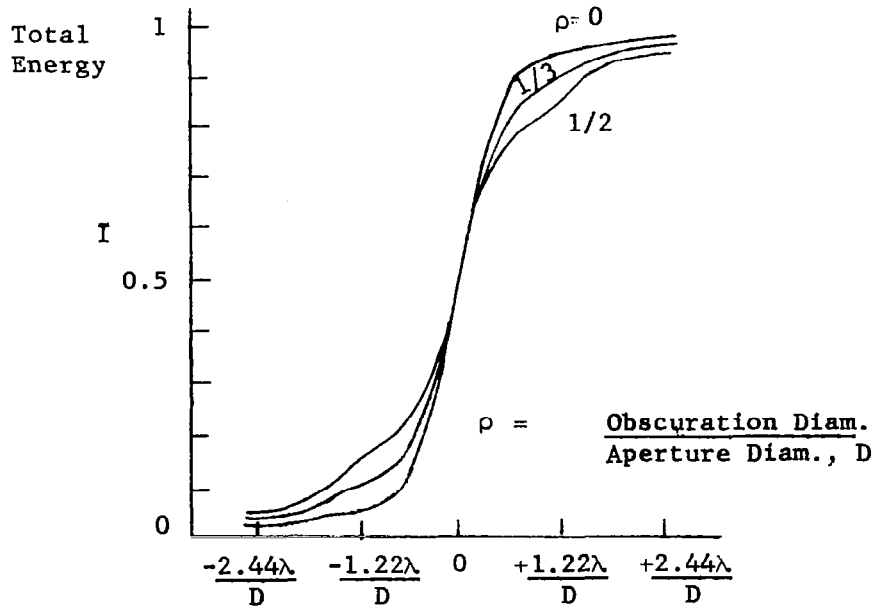

Figure 6-5. Energy Transfer Across A Knife Edge At The Image Plane Of A Circular Aperture

in more detail in Section 5 of this report. For the moment assume that it is possible to acquire the earth beacon inside a 1-degree field of view. At this point, the tracking operations are ready to begin. The angular rates that will be present during the tracking operation from the synchronous satellite will simulate the rates an operational spacecraft communication system will encounter in deep space, as shown in Appendix B. The ground laser beam will propagate through space and enter the telescope, impinge on the primary and pass through the optical element shown as the two-axis transfer lens. This received beam then is passed to the cube corner prism via the beam splitter. With the earth laser image some place within the 1-degree field of view, but not centered to a tenth of an arc-second, the ground beacom image will appear on one of the faces of the cube corner prism. The photomultiplier tubes shown schematically in the block diagram then would generate unbalanced

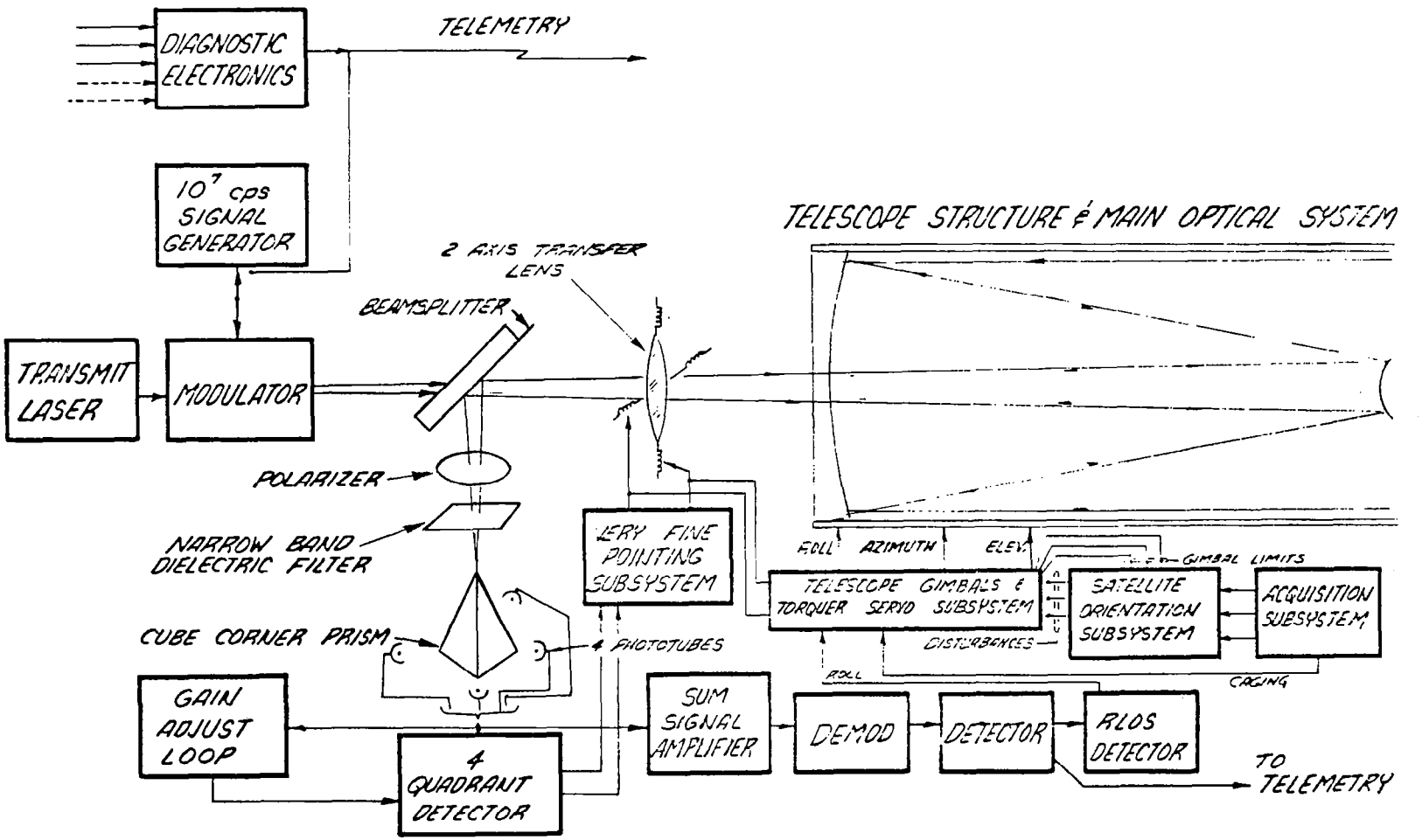

Figure 6-6. Optical Technology Satellite - Basic "32-Inch System" - Block Diagram (Telescope 1)

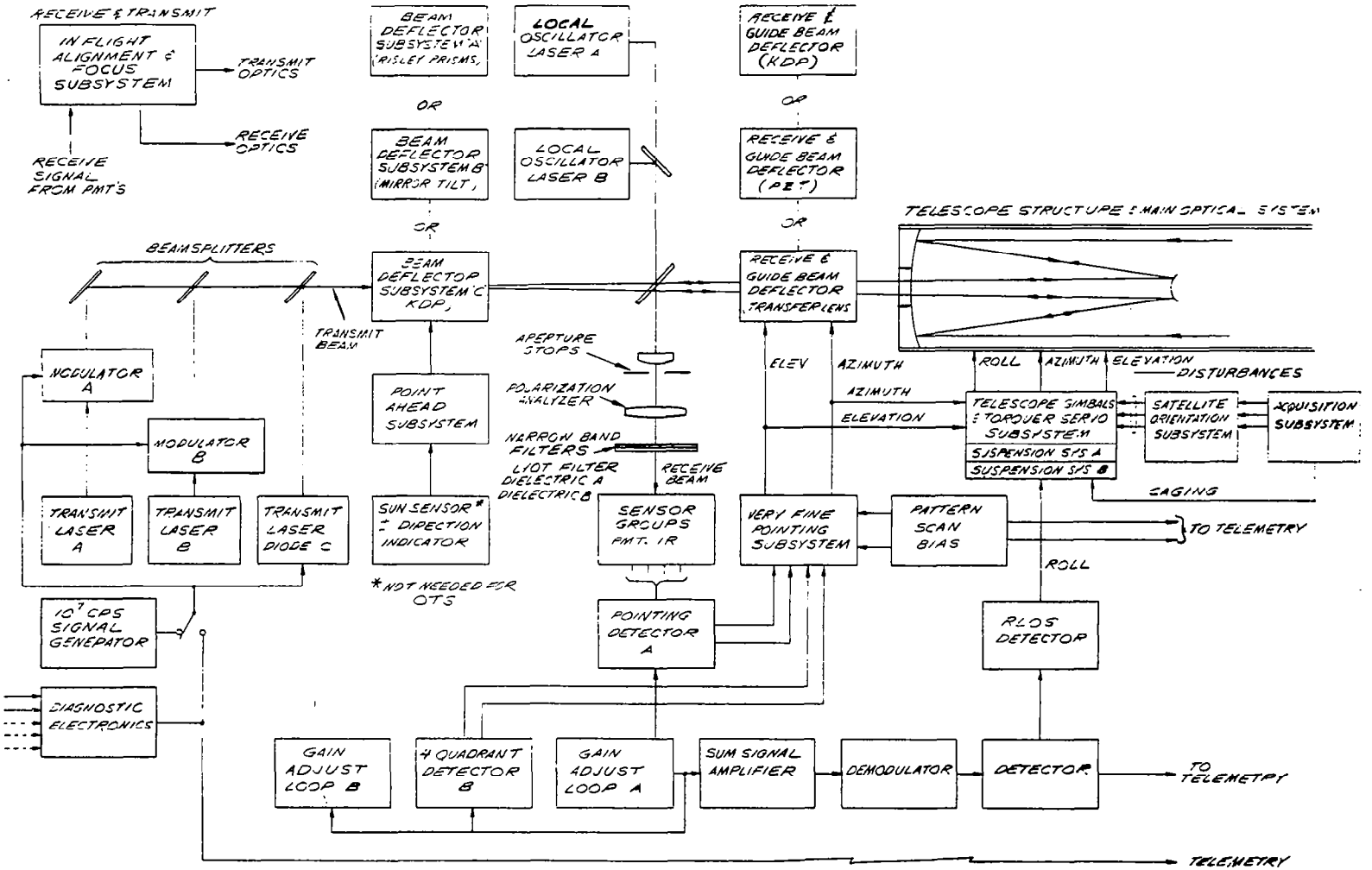

Figure 6-7. Optical Technology Satellite - 1 Meter Aperture - Basic Block Diagram (Telescope 2)

signals which, in turn, are fed to the four-quadrant detector. The four-quadrant detector processes the signals from the four photomultiplier tubes and generates up-down and left-right commands which are passed on to the very fine pointing subsystem, which in turn controls the X-Y position of the two-axis transfer lens. Thus, the ground laser image generates the signals in the four-quadrant detector to control the two-axis transfer lens motions in such a manner that the image of the ground beacon is rapidly centered on the nose of the cube corner prism. At that time, the signals from the four photomultiplier tubes are balanced and there is no up-down command or left-right command to the two-axis transfer lens. Thus, the line of sight of the received system of the telescope on the spacecraft is now pointing directly at the ground station beacon.

The degree of accuracy of this pointing system, which is identical in form to the pointing system used on the Stratoscope II, is determined by the gain of the loop from the transfer lens to the cube corner prism through the four-quadrant detector and back to the transfer lens through the very fine pointing subsystem.

The 0.1 arc-second tracking which is desired can be compared with the 1/50 of an arc-second pointing demonstrated by the Stratoscope II System.

However, in Stratoscope II the pointing signals originate in stars, while for OTS the signals originate in ground laser beacons. Also, there is no requirement for a transmit beam on Stratoscope II. Observe that with the telescope optical system lined up so that it is pointing directly at the apparent line of sight of the earth beacon, the transmit laser beam goes through the

identical two-axis transfer lens and the identical optical system. Therefore, the transmit laser should be pointing in exactly the same direction within the accuracy of alignment of the received system to the transmit system. Note that in Figure 6-6 there is no point-ahead capability. That is, the transmit laser signal is passed through the telescope optics exactly in line with the receive beam from the earth's beacon. Since the satellite is at a substantial altitude, there will be a .1-second transit time involved for the energy to get from the transmit laser on the ground to the received system on the satellite. Also, the satellite transmit beam will propagate down in a similar period of time. Due to the relative velocity of each station with respect to the other, there will be an angular displacement of the beam in each case. Thus, the beam that is transmitted down to the ground will not be centered on the ground station due to this relative motion between the earth station and the satellite station. This is the essence of the point-ahead problem for optical communications in space.

While it is possible to point the transmit beam ahead by the necessary angle (so that the transmit beam is received on the ground at the ground transmit station), the point-ahead equipment is not provided in the simple telescope. The point-ahead subsystem is in telescope 2, shown in Figure 6-7. The point-ahead equipment is intentionally excluded from telescope 1 in order to avoid complexity.

The technique for receiving the beam from space back on the ground at the receive telescope for the apparatus involves the translation of the transmit laser on the ground at an offset to compensate for the relative

motions (and transit times) between the satellite and the earth. The beam interlocking operation would then consist of translating the mobile transmitter beam until the down going beam is received at the ground telescope with maximum amplitude. This complexity in the ground station equipment is the price that is to be paid for the simplicity in telescope 1 on the satellite.

The transmit laser output is shown modulated by the modulator block before it is transmitted through the beam-splitter and the two-axis transfer lens and then down to the earth station. The input to the modulator block is shown as either a ten-megacycle signal generator or it can be the output from the diagnostic electronics equipment. This last output is normally being transmitted down to the earth on the microwave telemetry signal, but it could be switched in as the input to the modulator on command. In this manner the diagnostic information can be transmitted to the earth on the optical beam and the microwave telemetry power turned off.

In the previous discussion, it was shown that the received signal from the ground laser beacon arrives at the cube corner prism through the transfer lens to effect the fine pointing to the apparent line of sight. This same signal is transmitted through a narrow-band dielectric filter in order to filter out the unwanted earthshine background illumination. The narrow-band dielectric filter is shown in this block diagram arrangement because it is a high efficiency bandpass filter that has a high transmission within the pass band and at the same time a high rejection outside the pass band. This filter was chosen in preference to other narrow bandpass filters for this application because of its extreme simplicity. While it is true that the filter does not have a bandpass as narrow as one might desire, for the distances and powers involved in the Optical Technology Satellite, there would be adequate signal-

to-noise ratios. Other filters with a narrow pass band, such as the mica filter or the Lyot filter, would be evaluated on the more sophisticated test bed of telescope 2, which is shown in Figure 6-7.

The signal from the earth station beacon arriving at the nose of the cube corner prism also passes through a polarizer which has a fixed orientation with respect to the satellite structure. The function of the polarizer at this location in the received beam path is to develop rotational references about the line of sight to the ground beacon. It can be assumed that the ground laser has a plane of polarization which can be rotated about the line of sight to the satellite on the ground by rotating the entire laser assembly. The beam from earth which arrives at the telescope is also plane polarized, and rotation about the line of sight will cause the signal received by the satellite to vary in intensity as a function of the angular rotation about the line of sight. This is due to the polarizer element. Note that the output signal from the four photomultiplier tubes is fed to the sum signal amplifier. The output from the sum signal amplifier goes through the demodulator and detector and then to the rotational line of sight detector. The rotational line of sight detector, in turn, controls the roll gimbal so that the signal received by the detector is held at a maximum. Using this technique, the rotation about the line of sight can be held to the rotation angle commanded by the physical orientation of the plane polarized beam from the ground laser to within 0.05 degree. The degree of precision required for this rotation about the line of sight is considerably less than that required for the point ahead of the transmit beam. Based on calculations for the deep-space case, however, the precision involved for the alignment about the roll axis is this angle of 0.05 degree.

Note that when the azimuth and elevation gimbals are approaching the ends of their restricted motional range, signals should be generated and passed over to the satellite orientation system to cause the satellite to re-orient and center the gimbals within their freedom of travel. This is shown on the block diagram as output signals going from the gimbals to the satellite orientation system.

Note that during the operation of the acquisition subsystem the gimbals should be caged. This is shown on the block diagram as an output signal from the acquisition subsystem.

The earth beacon signal as received on the satellite is summed after the four photomultipliers at the sum signal amplifier and after demodulation and detection is sent back down to earth via the microwave telemetry signal for analysis on the earth.

This concludes the functional description of the basic operations of the precision tracking system as indicated by the blocks and subsystems of Figure 6-6 and in more detail in Figure 5-3. In summary, the acquisition subsystem generates the commands to the satellite orientation subsystem which points the telescope in approximately the right direction. Then the very fine pointing system takes over and controls the telescope pointing arrangement to aim the telescope to the apparent line of sight to the ground station as received in the satellite. The transmit beam, in turn, is sent parallel to the received beacon. If no transit time delays were involved, the transmit laser output from the satellite would be received at the same ground station as was used for the ground transmitter beam. However, because of transit time

delays at synchronous orbit altitudes, there is a physical separation between the beams received and transmitted by the ground station.

Note that in the description above we have the very basic principles of operation for the precise tracking operation. A ground beacon is used and the satellite has an optical receiving system so that it can line itself up with respect to the ground beacon. This is the line of sight. Then the transmit beam is passed back through the same optical system. This beam is colinear with the received beam for the rudimentary system described above. If the receiver system can hold the image of the ground beacon stably centered on the nose of the cube corner prism so that the line of sight is independent of reasonable disturbances due to vibration and motion of the telescope structure, then the transmit beam would pass out from the satellite with that same degree of stability. The fundamental problem that is not treated in this basic block diagram (Figure 6-6) system is the problem of point-ahead for the deep space communication system. As noted in the above paragraphs, the transmit laser beam from the satellite would intersect the earth's surface at some distance from the point where the transmit laser from the ground station had transmitted the signal to the satellite. For the case of the synchronous orbit, the linear translation of the satellite's transmit laser beam and the earth station's transmit laser beam is some 2,000 feet. For the distances involved in deep space, the transmit beam from the satellite would be 16 thousand miles away from the ground station if some provision were not incorporated into the pointing system to take into account the effects of the transit time. However, for the satellite demonstrations in the simple case, the point-ahead system is not included in order to keep the basic telescope arrangement as simple as possible.

The second telescope, which is shown in Figure 6-7, aboard the same satellite does have the necessary point-ahead system. Figure 6-8 illustrates in more detail the arrangement that could be used to point ahead. As shown for the satellite case, the point-ahead command arrives at the satellite from the ground via a microwave link. For a deep-space case, this same principle could be applied, or the data could arrive at the spacecraft via the earth-to-satellite optical communications channel, or it could be stored aboard the spacecraft since the point-ahead angle is a slowly changing number. The implementation of point-ahead is accomplished with a transfer lens as shown in Figure 6-8. This equipment is aboard telescope 2. Other point-ahead mechanisms are indicated in Figure 6-7 for experimental evaluation if necessary.

The number of experiments that could be conducted in the simplified optical communication arrangement shown in Figure 6-6 is limited. This is due to the basic concept of making one optical and communications telescope as simple as possible in order to obtain the highest reliability. The minimum number of experiments that would be useful for the basic demonstration is 1/10 of an arc-second of pointing and 10^7 cycles per second of communication. In contrast to this limited experiment approach, the second telescope aboard the same satellite is a sophisticated test bed and permits the conduction of a larger number of experiments to collect the engineering and scientific data which would permit the establishment of the feasibility of optical communications for deep-space applications. The block diagram (Figure 6-7) shows the general arrangement for the more sophisticated test bed. It not only provides the same basic functions as the simplified version but, in addition, has the elements necessary for the conduction of tests simulating the conditions

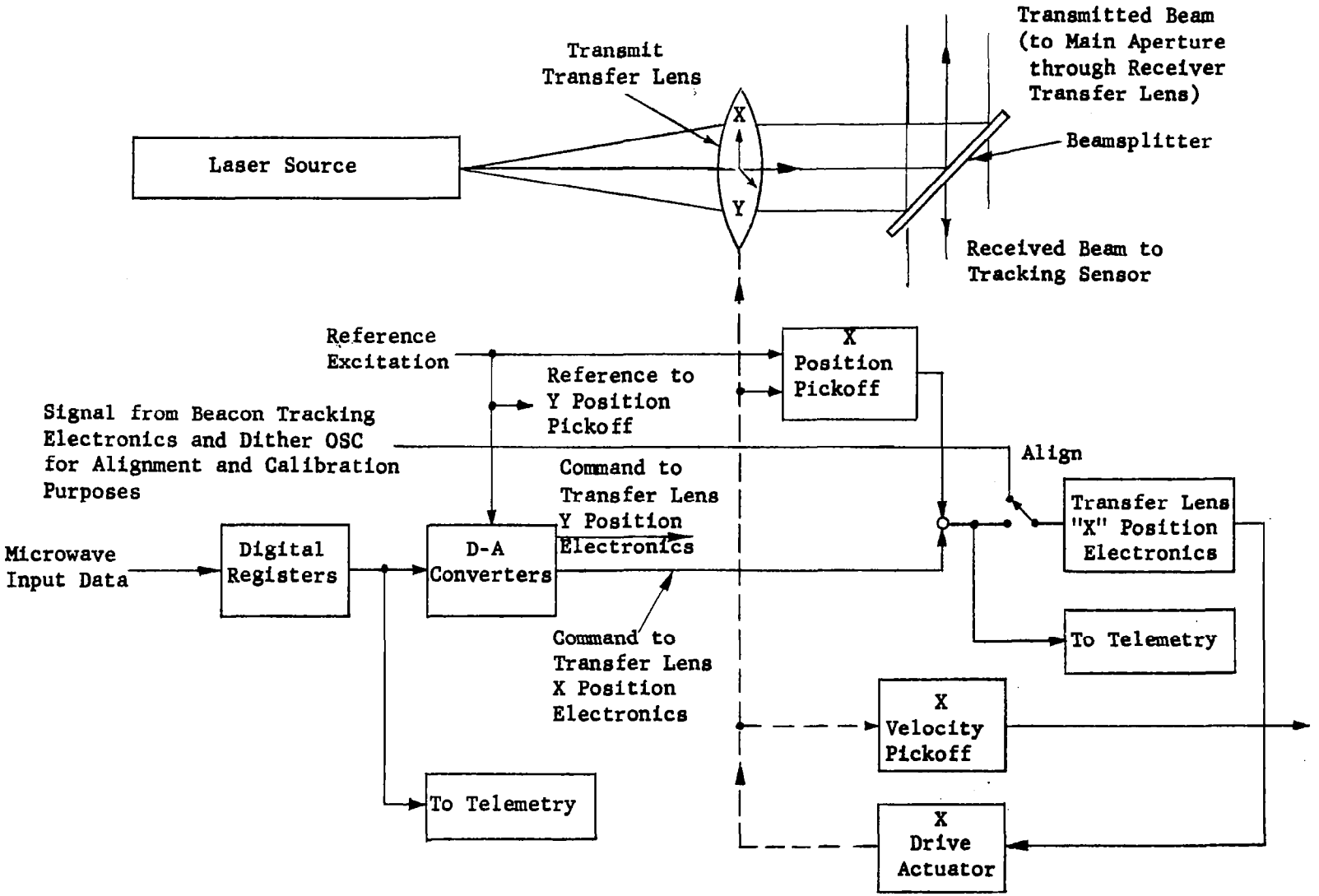

Figure 6-8. Transmit Beam Deflector Subsystem Utilizing Transfer Lens Principle

encountered for a deep-space mission. Thus, there are two fundamental differences between these two block diagrams. The block diagram in Figure 6-7 provides for point-ahead operations, which are mandatory for deep-space communications, but not required for near-space missions. The second basic difference between the two block diagram is the number of parallel subsystems. These would be evaluated on the Optical Technology Satellite whenever necessary in order to determine which of the subsystems provides the highest performance and most reliable operation over the long-term life of the satellite. For example, a number of different lasers will be used in the transmit mode from the second optical communication package while in the first optical communication package only a single laser is chosen. In a similar manner, various techniques of beam deflection, telescope suspension, pointing, LOS guidance data generation, and narrow-band filtering are indicated. The second test bed has the capability of conducting heterodyning experiments in space. Also shown in Figure 6-7 are those elements which are needed to conduct the recommended experiments. For example, different aperture stops are indicated. These would be used in the scintillation experiments.

The very fine pointing system accepts bias signals to generate a scan pattern. A precise scan pattern deflection of the transmit beam permits the performance of the optical system in space to be evaluated on the ground. In-flight alignment and focus subsystems which are necessary for deep-space missions, but which were omitted from telescope 1(Figure 6-6) for reasons of simplicity, are included in telescope 2 (Figure 6-7). The transmit optics must be aligned to the receive optics after launch and several additional times during a long duration operation in space.

Different modulation techniques are also planned as part of the experiments and therefore transmit laser A is shown with modulator A and transmit laser B is shown with modulator B. The intent here would be to evaluate the capabilities of each of the modulators and modulation techniques in terms of the most efficient operation of the communication system.

Since telescope 1 (Figure 6-6) is the design for the simplest operation of the optical communications system, it does not include all the elements necessary for a deep-space communications system; and since telescope 2 (Figure 6-7) is a test bed for a number of different experiments, neither system will be an operational one for deep-space missions. The deep-space optical communications telescope is shown in Figure 6-9. Note that this is basically the same as Figure 6-7, but the equipment for testing alternate subsystems and conducting scientific experiments has been removed.

Figure 6-10 shows the ground station block diagram. Its operational principles are identical to the space-borne telescopes 1 and 2.

6.3 TRACKING IN THE PRESENCE OF SPACECRAFT MOTION DISTURBANCE

In the environment of any space-borne laser communications systems disturbing forces which, if applied directly to the telescope, can alter the pointing direction sufficiently to degrade or disrupt communications will necessarily exist. The use of laser beams for communications across deep-space distances will be feasible only if reliable acquisition and tracking functions can be demonstrated in the presence of motion and vibration at the levels likely to be encountered.

The spacecraft will transmit disturbances to the telescope through the suspension system unless special techniques are applied to isolate the

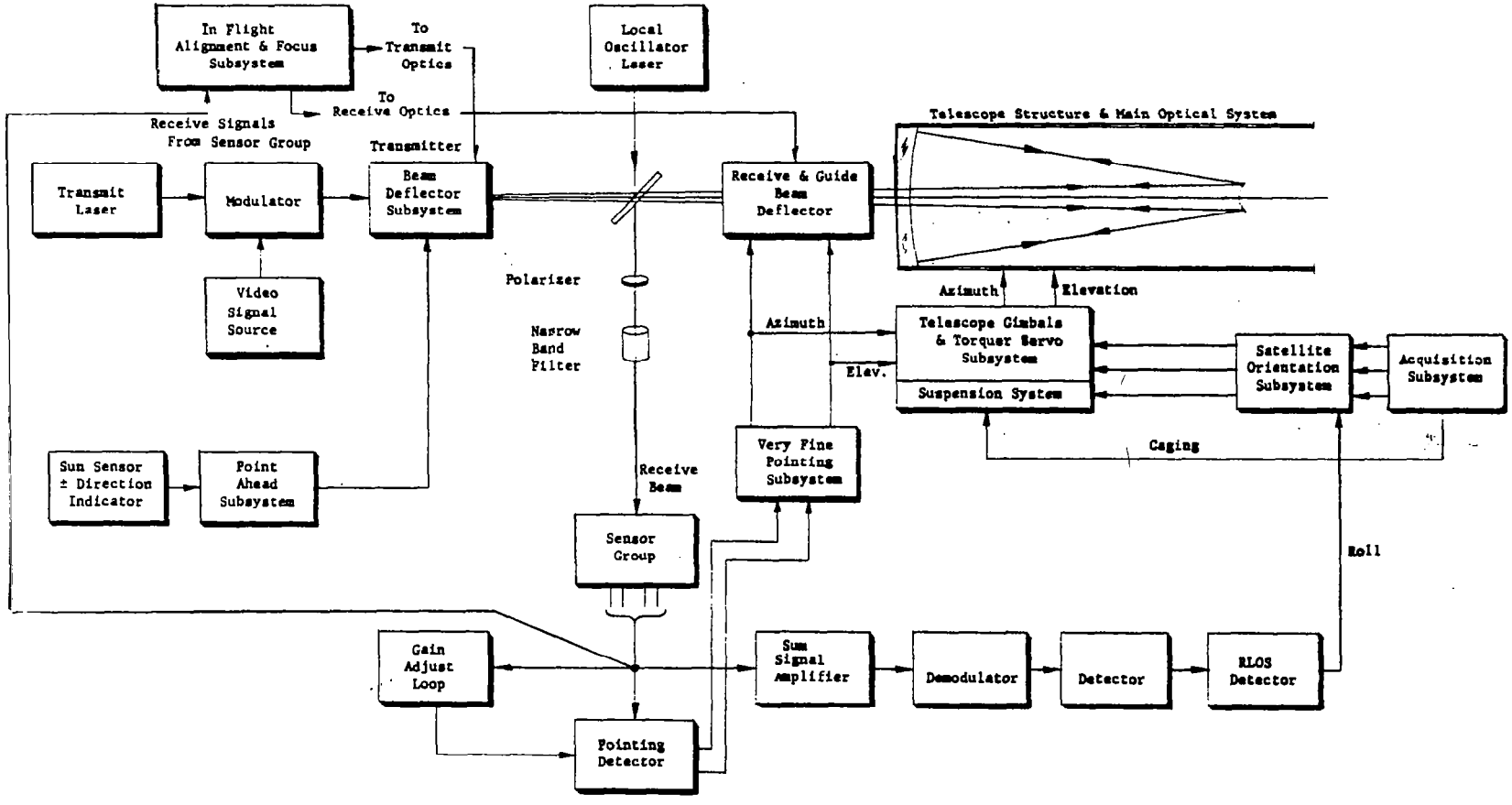

Figure 6-9. Deep Space Optical Communication System Block Diagram

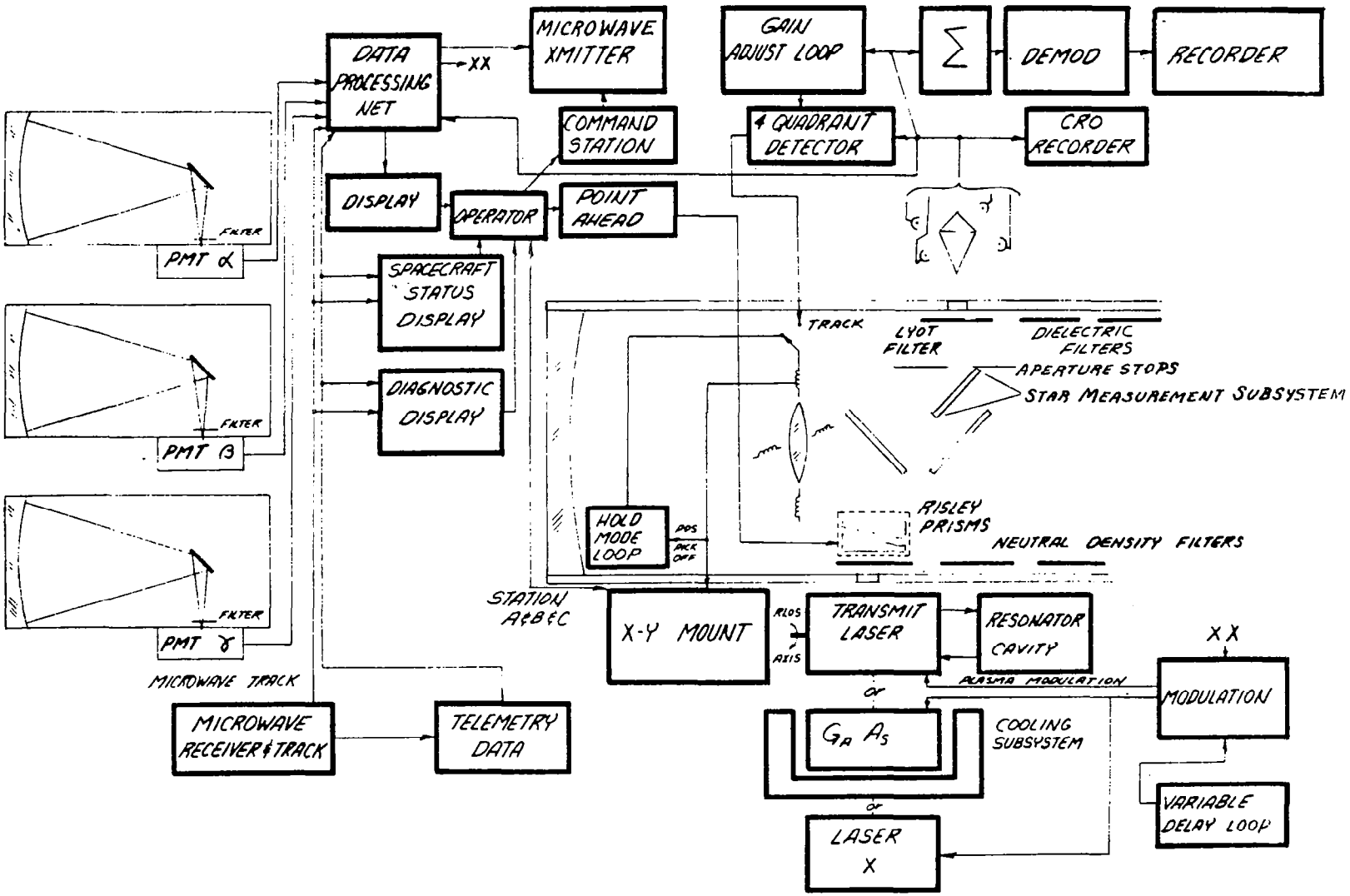

Figure 6-10. Optical Technology Satellite Ground Station, Basic Block Diagram

telescope from the structure. These disturbing forces may arise from the movement of personnel or equipment within the spacecraft or from outside environmental factors. At any given moment, these motions or vibrations may be considered as rotational accelerations applied around each of the three axes of the telescope suspension system, or as translational accelerations along each axis. The degree to which these accelerations are transmitted to the telescope depends upon the compliance of the suspension system. This system must be soft enough to isolate the telescope line of sight from motion disturbances present in the spacecraft but yet be firm enough to provide the reaction base for telescope steering torques when required.

The acquisition process is less sensitive to small disturbances in the optical pointing direction than is the tracking process, since acquisition involves a wider field of view (i.e., 1 degree). During tracking, the field of view must be reduced to a few arc-seconds, and motion disturbances of this angular magnitude are necessarily a part of the operational environment. The extent to which tracking is affected depends not only on the degree of isolation provided by the suspension system, but also on the characteristic servo response of the telescope tracking system. The response bandpass must encompass the residual motions transmitted to the telescope through its suspension system.

Experiments must be carried out with the Optical Technology Satellite equipped to simulate vehicle motion in order to determine the effect on spacecraft tracking. The satellite would have the following devices capable of producing vehicle motions in each of the three rotational degrees of freedom of the telescope suspension system. Vibrational motion could be produced

by three orthogonal electro-magnetic force transducers, similar to small conventional test shakers. These would be attached to the satellite structure at points which would maximize the acceleration applied to each rotational axis of the telescope suspension system. The amplitude and frequency of the output of the oscillator circuitry driving the shakers would be controllable. Transient step motion disturbances would be simulated by the use of inertia wheels and/or reaction jets mounted to the vehicle structure. Rise time and amplitude of the generated pulse would also be capable of variation over a given range. Angular and translational accelerometers, which would sense accelerations along and about each suspension axis, would be located on the spacecraft structure at the telescope suspension attachment points.

The microwave telemetry link would be used to select the desired motion generator and the desired output in terms of amplitude frequency or pulse shape. A pre-programmed test sequence, on the other hand, would require only an initiation command. The output from the three accelerometers would be relayed to earth for evaluation.

After the basic acquisition and tracking demonstrations have been carried out, the torque disturbances would be introduced while the satellite was in the tracking mode. A harmonic frequency response test would be conducted for one axis at a time at a constant amplitude. Next, step inputs for each individual axis would be generated by the reaction jets or inertia wheels. The angular acceleration applied to each axis would be monitored by the accelerometers.

The effect of simulated vehicle motion on tracking would be determined in a manner identical to that used in the 0.1 arc-second tracking demonstration.

An array of ground stations would be spaced to permit the measurement of the direction and extent of beam shift along the ground caused by the vehicle motion. Severe disturbance would lead to an interruption in communications and would necessitate re-acquisition.

After data on the degradation of single-axis tracking performance had been obtained, the tests would be repeated for disturbances simultaneously produced about each of the three axes of rotation.

6.4 SUSPENSION SYSTEMS COMPARISON

The suspension system required for the spacecraft telescope must meet several requirements. Ideally, the suspension would be infinitely compliant around one rotational axis in the gimbal system but would have sufficient stiffness in the other rotational directions to permit the transmission of restoring torques through the gimbals to the telescope. High compliance around the axis of rotation isolates the telescope from space vehicle motion and also reduces the torquer power required to drive the system to null.

Although the space environment introduces some limitations not normally encountered, it also opens up a number of new design approaches. Low temperatures and high vacuum make the use of lubricated bearings considerably more difficult, for example. However, greater compliance is possible since the suspension system need not be designed to carry gravity-induced loads. The spring members in a flexure suspension system could therefore be much lighter and more flexible. However, the weight component which functions usefully to offset the spring restoring force as in the Stratoscope II flexure suspension system would be absent, tending to reduce system compliance. This

opens up the possibility of using a magnetic suspension system. Many of the problems of mechanical suspension systems might be overcome in a weightless environment by the use of a magnetic suspension system.

The performance of the two most promising suspension systems considered to date for the experiments on the satellite can only be fully evaluated in a weightless environment. Several alternate means of mounting the two 32-inch telescopes aboard the OTS are possible. The flexure suspension system, which appears to be the most reliable, will be used in telescope 1, whereas a more unorthodox suspension system, such as the magnetic suspension system, would be used with telescope 2. The approach here is to mount telescope 2 on a single set of gimbals which could be alternately suspended by either flexures or magnetic fields.

Performance evaluation would consist in determining which suspension system transmitted the least vehicle motion and which system led to the least consumption of power. Rotational and translational accelerometers would be located on the telescope and the outputs from these would be compared with the measured accelerations applied to the suspension system. The torquer power would also be measured for each system in normal operation.

The comparison between suspension systems would be made in conjunction with the previously described experiment which demonstrates tracking capability in the presence of spacecraft motion disturbances.

6.5 FOCUS AND ALIGNMENT TECHNIQUES

The successful operation for both the Optical Technology Satellite communications system and an operational communications system critically depends on the ability to:

(1) Focus the vehicle receiver optics so that a sharp image is available for beacon tracking purposes;

(2) Focus the vehicle's transmitter optics to avoid widening of the transmitted beam, which would result in reduced signal power at the ground detectors; and

(3) Align the transmit and receive optical systems to each other to achieve precise zero point-ahead conditions so that point-ahead angles can be accurately referenced.

Basic techniques for doing this can closely parallel methods now in use on the Stratoscope II equipment (See Figure 6-11). When guiding on a star in Stratoscope II, the star image is formed at the nose of the pyramidal shaped prism. Pairs of photosensors receiving light from opposite faces of the prism produce electrical difference signals when the image is not centered. These difference signals are utilized to drive the transfer lens in such a direction as to center the image on the prism. When the image is sharply focused, minute motions of the transfer lens will upset the balance of light between the photosensors. For poor focus conditions, the image at the nose of the prism is larger, and hence larger transfer lens motions are required to

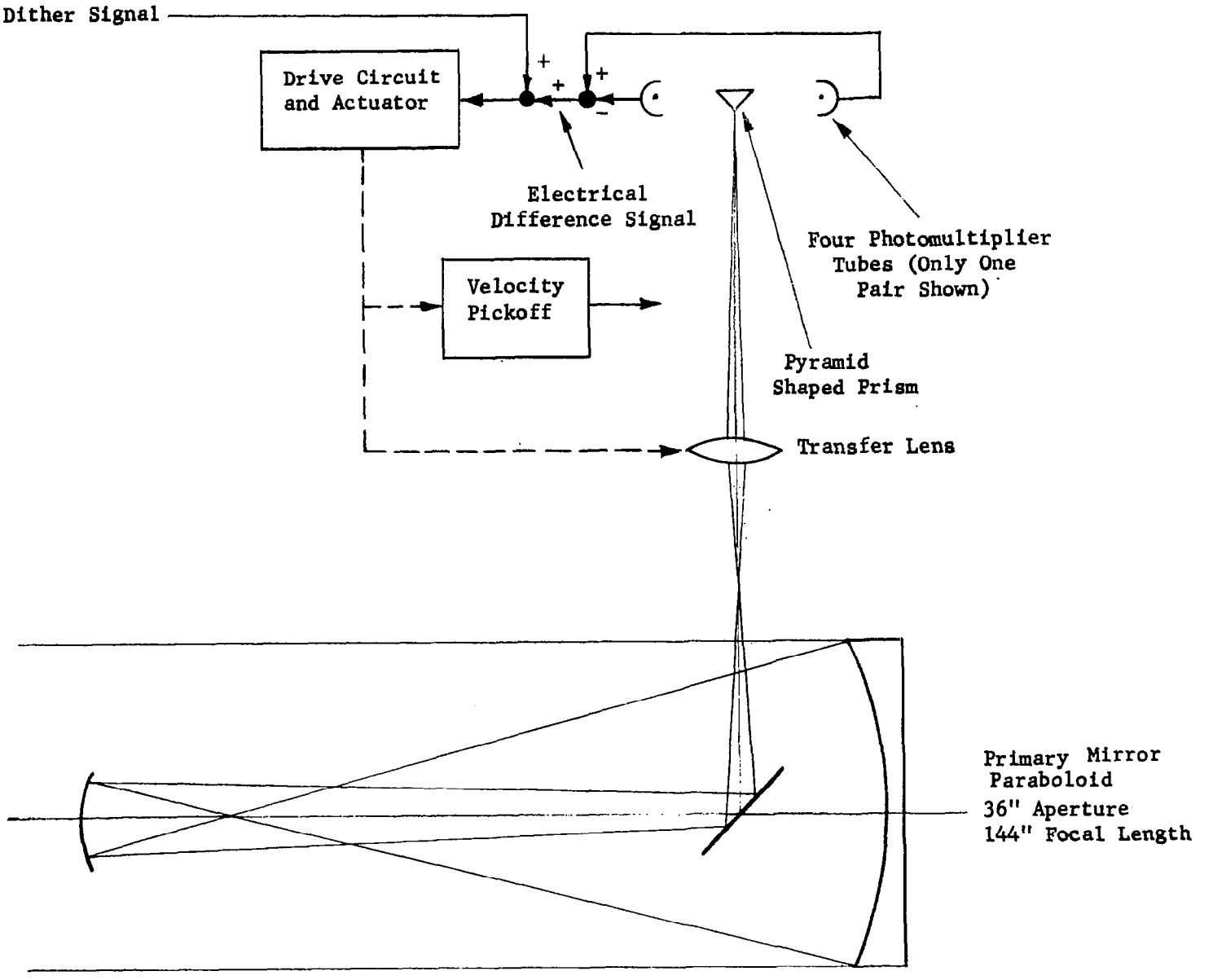

Figure 6-11.Stratoscope II Focusing Technique

produce the same light imbalance, and hence an equivalent electrical difference signal, as for a sharply focused image.

If an electrical (dither) signal of fixed amplitude and frequency is introduced into the servo loop during tracking, the transfer lens will move to maintain the net signal to the drive circuit at null. This will require the smallest transfer lens motion for conditions of best focus. Therefore, the transfer lens velocity pick-up has the smallest output at best focus and, when monitored during focus adjustment, it detects proper focus setting. This focus setting is at the precise location where the velocity signal has the smallest output amplitude for a fixed dither amplitude. On Stratoscope II, this technique achieved a focus condition corresponding to near optimum image quality. This degree of focus alignment is required by the Optical Technology Satellite.

The foregoing technique can be harnessed to align the proposed optical system.

If one considers the optical arrangement shown in Figure 6-12, three basic steps could be performed to focus both the receiving and transmitting optics and to align the two lines of sight. These steps are as follows:

1. Position the collimating adjustment lens to obtain coincidence of its focal plane with the apex of the fine beam-splitter. In principle, this can be accomplished through the use of an auxiliary slit source, the fine beam-splitter, and a controlled tilting mirror.

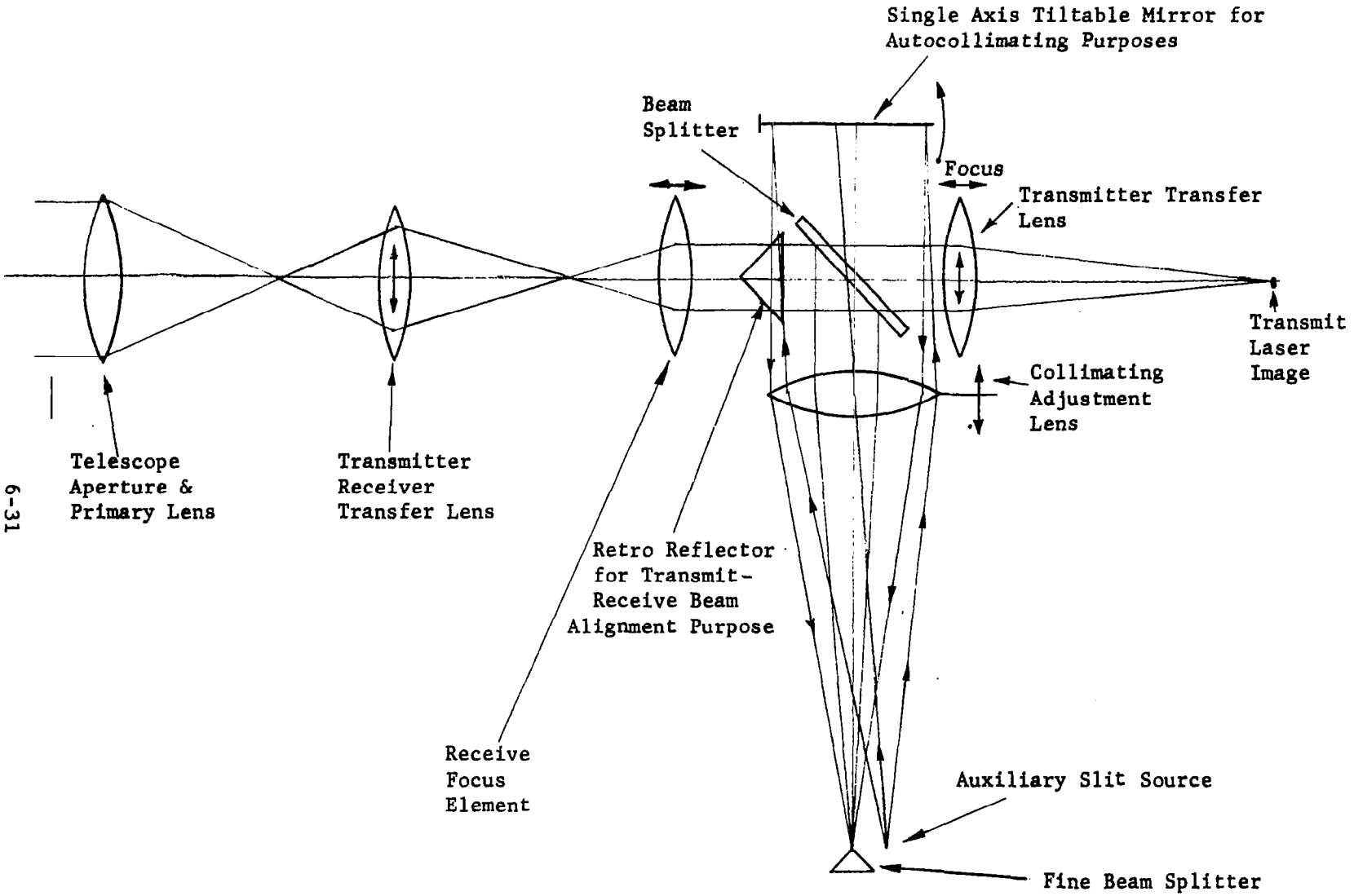

Figure 6-12. Alignment Techniques

Light from the source passing through the collimating adjustment lens will be reflected by the mirror and will pass back through the lens to form an image. If the auxiliary source and the beam-splitter lie in a plane normal to the lens axis, the image will also lie in this plane when the lens is properly positioned. Coincidence between this image and the fine beam-splitter apex can be obtained by controlling the tiltable mirror via pointing error signals generated by photosensors associated with the fine beam-splitter. Subsequent introduction of a dither signal into this control loop will cause the tilt mirror to oscillate angularly (and move the image in a manner similar to that caused by the Stratoscope II transfer lens), and best image focus is obtainable by positioning the collimating adjustment lens to obtain minimum amplitude (or rate) of mirror motion. When this condition is achieved, a beacon image will be sharply focused at the fine beam-splitter apex only when the received light forms a collimated bundle incident on the collimating adjustment lens.

The foregoing procedure is only required to permit subsequent transmitter optical system adjustment by the method to be described.

2. Focus the receiver optical system. As in Stratoscope II, this can be accomplished during tracking of a strong ground

beacon, with the fine beam-splitter controlling the transmitter-receiver transfer lens, by the introduction of electrical dither into this transfer lens loop. The receive focus element would be adjusted while the transfer lens velocity pickoff is monitored.

3. Focusing of the transmit optical system. For this operation the cube corner retroreflector introduced at the point shown in Figure 6-12 will reflect transmitter light back to the receiver prism. The transmitter transfer lens can now be controlled by the photosensors associated with the fine beam-splitter to center the laser image at the beam-splitter apex. Dithering the transmit transfer lens can now be performed as in previous cases to establish good focus conditions for the transmit system. If the dither signal is now removed the transmit transfer lens will be maintained in a position corresponding to alignment between the transmitter and receiver optical systems. This transfer lens position can be sensed and monitored by telemetry to establish the position corresponding to alignment. This is illustrated in Figure 6-8, the transmitter transfer lens control system block diagram, where the transfer lens position is controlled by the error signals (generated by the fine beam-splitter photosensors) to maintain the laser image at the beam-splitter apex. In this alignment mode, the digital register

setting can be controlled from the ground to obtain a null between its analogue voltage counterpart and the position pickoff signal. At null, the digital register setting corresponds to that required to re-establish optical alignment between the transmit and receive lines of sight when the transfer lens is later positioned to follow ground commands as introduced into the register. In this alternate mode of operation, the ground operator changes the digital register setting by an amount corresponding to the point-ahead angle desired. The analogue command derived from the D-A converter is then compared to the position pickoff signal to derive the pointing error signal required to correctly reposition the transfer lens.

These focus and alignment techniques are presented to indicate the feasibility of a system alignment in space without the need of large flats of full aperture or other arrangements which would make alignment a more formidable task than necessary. Once aligned in space, the system should not require readjustment over substantial periods of time.

6.6 OPTICS TECHNOLOGY EXPERIMENTS

Future optical instruments in space will need optical systems of large aperture. There is considerable discussion already in the technical journals[33] and in scientific committees about 100-inch diameter (and larger) diffraction-limited systems in space. Systems of the future will certainly include 1-meter diameter apertures (diffraction-limited) and may include systems in which the diameter is up to 400 inches. But the persistent question that

remains for all the individuals concerned with designs relating to large aperture optics is: "How well can one achieve diffraction-limited performance in practice in space as compared with how well can we design these systems with our mathematical modeling techniques?"

Those unknown factors which reduce the optical perfection of the system must be considered by the engineers and decision makers. To have a diffraction-limited optical system in space with a convenient and precise technique of measuring the degradation of optical performance in the presence of controlled disturbances (thermal, mechanical, dynamic and electronic), and over a period of time sufficient to measure and control degradations due to the space environment, is unquestionably a key to our rate of progress in space exploration.

The laser telescope system required aboard the Optical Technology Satellite for laser communications development is nearly identical to that required to provide such an impetus for optics technology in space. For example, the aperture size is of the right order of magnitude. With apertures much smaller than 1 meter one would generate little additional information. Apertures much greater than 1 meter present practical problems of implementation for the 1965-to-1975 period of time.

Consider the ease with which the performance of the optical system is measured when that system has a laser at the optical focus point and the laser beam is viewed on the ground. The Airy disk for the optical system is now measured by the radiated intensity pattern as received at the ground terminal. The radius of the first dark ring of this disk for the equipment

under consideration is 100 feet (for a range of 20,000 n.m. and a resolution limit determined by the aperture of 1 meter). The pattern of the intensity inside the first dark ring, and outside the first dark ring to perhaps the sixth ring, can be established as the parameters of interest are varied under ground control. The space optical beam is precisely programmed in angle from the received line of sight as indicated in the discussion of telescope 2. Simple intensity measurements on the ground angle-correlated with the deflections of the down going beam will provide the intensity profile of the beam. The point-ahead subsystem required for optical communications in deep space is used to provide the angular deflections in accordance with ground control.

Questions of basic mirror structure can be answered as the parameters are varied. Mirror configurations based on solid fused quartz designs or egg crate approaches in quartz or beryllium can be evaluated. Even pellicle mirrors can be assessed in the space environment. Much valuable data on mirror performance in gravity free environments, at varying temperatures, with varying lateral temperature gradients, and on reliability lifetimes in the presence of cosmic rays and vacuum can be obtained. There will be no scattered light from dust or gas molecules to limit performance. The instrument can be designed to limit the scattered light from the internal instrument surfaces to a value determined only by the skill of the designer. The techniques of detection which will be developed for laser communications systems will be useful in many areas of optical technology. If the quantum efficiency of detectors can be improved by the utilization of space worthy cryogenic techniques (such as passive radiant cooling or ablative cooling of the detectors), these improvements will certainly advance optical technology.

While the optical communication detectors considered for the Optical Technology Satellite do not require cryogenic cooling, the gallium arsenide laser sources may require this cooling.

Using these experimental techniques and analyzing the data collected, the sensitivity of the optical performance to the disturbances can be precisely determined in a most practical manner so that guide lines for the design of future astronomical instruments in space can be established. Transfer function responses of the optical system can be determined by reduction of this data so that future reconnaissance systems for either extraterrestrial or terrestrial missions can be developed from measured data.

SECTION VII

PHOTOMETRY CONSIDERATIONS

The problem of earth beacon acquisition and subsequent tracking from a deep-space vehicle was investigated in an effort to evolve reasonable approaches. Since the major aspect of acquisition and tracking is the ability to sense received beacon power in the presence of expected noise, the first step in the study was the preparation of several nomographs allowing rapid evaluation of the received beacon power and the expected ultimate in S/N due to noise in signal (i.e., photon discreteness effects). Subsequent to this, expected background light levels from planets, stars, sun and corona, and earthshine were reviewed to assess their effects on achievable S/N ratios. Very pertinent information in this regard was obtained from two existing documents[34,35] and has been repeated for convenience. A quick survey of existing sensors useful in the visible and into the infrared region of the spectrum revealed that very good performance summaries for infrared detectors exist[36,6] but similar summaries for sensors useful in the visible and up to one micron were not readily available. Examination of the spectral responses of photoemissive surfaces revealed that the S20 and S1 surfaces are reasonably optimum in the range of 0.32 to 1.0μ, being exceeded only by a factor of two by other available surfaces for only small portions of this range. Accordingly, measured values of dark current for the 2-inch diameter RCA 7265 S20 phototube at +25°C and -70°C were utilized to prepare a plot of "dark current equivalent

input power" versus wavelength. Also included is a similar curve, for the EMR phototube, prepared from manufacturer's published curves.

Examination of the results indicates the definite possibility of acquiring the earth beacon directly without the necessity of involved scanning operations. This conclusion is based upon the following assumptions:

(1) The earth beacon pointing direction is predictable, based upon previous tracking data, to approximately 3.6 arc-seconds and the beacon beamwidth is in the order of 10 arc-seconds (including atmospheric scattering effects).

(2) The vehicle receiver aperture area is in the order of one meter square.

(3) Approximately 10 watts of earth beacon power is reasonable.

(4) The angular position of the earth from the vehicle-sun line is known correctly within one or two degrees.

Calculations are shown for an earth beacon at the specific wavelength of 6328Å to demonstrate the feasibility of such an approach.

7.1 MAXIMUM ACHIEVABLE SIGNAL-TO-NOISE RATIO

Fundamentally, the signal-to-noise ratio of an optical communication system is limited by the photon discreteness associated with light transmission. The limiting signal-to-noise ratio so imposed decreases as the total transmitted light level is reduced.

The nature in which light level restricts performance can best be established by considering the statistical uncertainty in determining average light level by measuring the number of photons arriving at a sensor during a finite sampling time Δt. If the average signal photon arrival rate is $\bar{n}_s$, proportional to intensity of illumination, and the average background photon arrival rate is $\bar{n}_B$, the total average number of photons $\bar{N}$ is given by:

$$\bar{N} = \Delta t(\bar{n}_s + \bar{n}_B) \triangleq \Delta t(\bar{n}) \tag{1}$$

The actual number of photons N arriving during a single time interval Δt, however, can be expected to differ from the average (due to random changes in n with time) in accordance with the Gaussian probability curve of Figure 7-1. Any attempt to determine a change of signal illumination N_c ($N_c \triangleq \Delta n_s \Delta t$) from a given level ($\bar{N}_S$) is thus subject to an rms uncertainty of $\sqrt{\bar{N}}$ and, it follows that if:

$$N_c >> \sqrt{\bar{N}} \tag{2}$$

measurement errors shall be small.

A figure of merit which, therefore, expresses the ultimate quality or precision of measurement is given by:

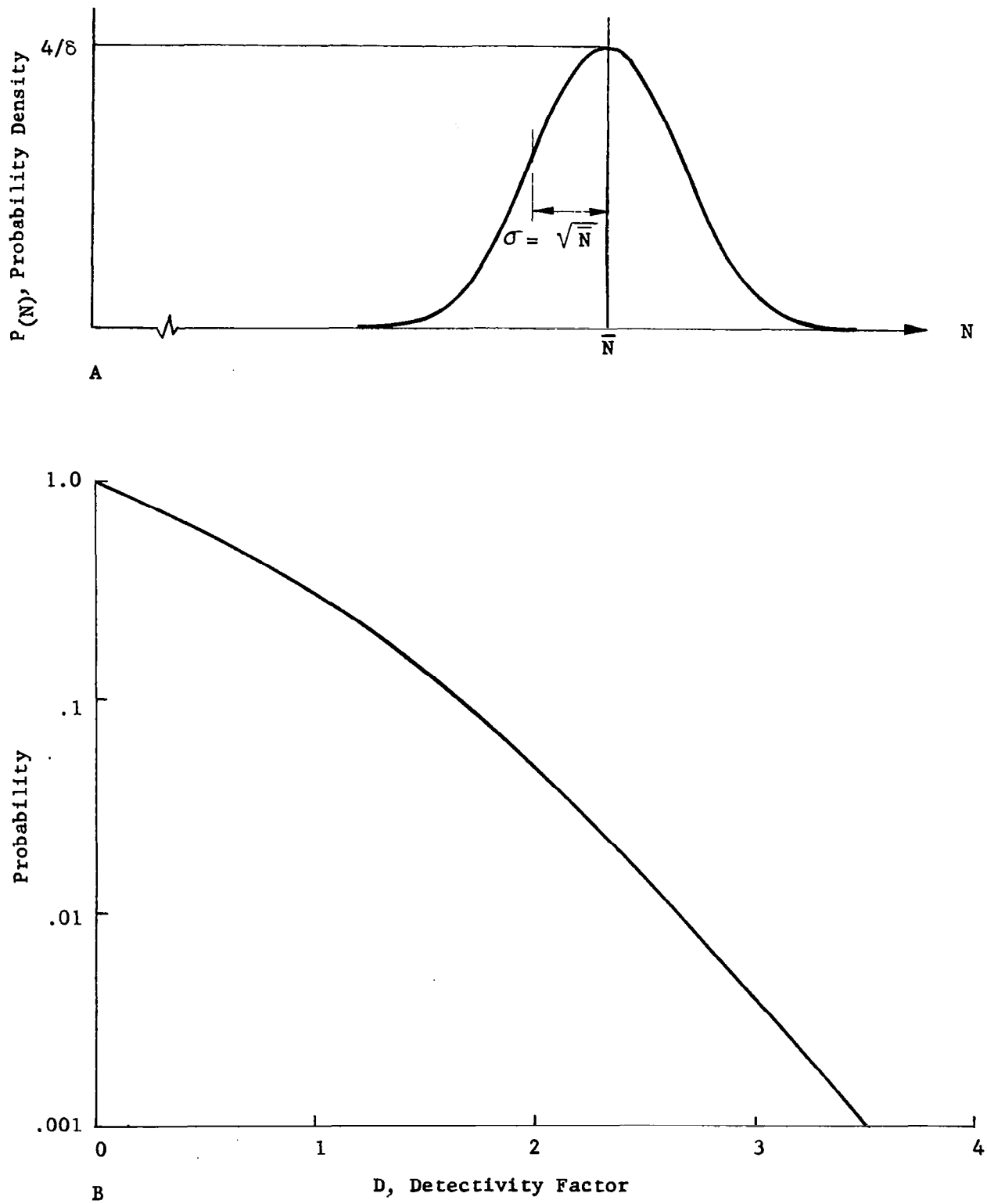

Figure 7-1. Probability Density Curve and Probability of Measurement Uncertainty Exceeding Incremental Signal Magnitude Change of Interest

(3) $$D = \frac{N_c}{\sqrt{\bar{N}}} = \frac{\Delta t(\Delta \bar{n}_s)}{\sqrt{\Delta t(\bar{n}_s + \bar{n}_B)}}$$

where D will be called "detectivity factor". The maximum value of D is obtained if it is assumed that N_c is equal to the total signal N_s and there is no background light. For this case, the preceding equation reduces to the more familiar expression for signal-to-noise ratio:

(4) $$S/N = \frac{\bar{N}_s}{\sqrt{\bar{N}_s}} = \sqrt{\bar{N}_s} = \sqrt{\bar{n}_s \Delta t}$$

or (5), $$S/N = \sqrt{\frac{\bar{n}_s}{2\Delta f}}$$

where Δf is the equivalent bandwidth related to the interval, Δt by the expression $2\Delta t = \frac{1}{\Delta f}$

For the more general case where background light exists the signal-to-noise ratio is given by:

$$S/N = \frac{\bar{N}_s}{\sqrt{\bar{N}_s + \bar{N}_B}} = \frac{\bar{n}_s}{\sqrt{(\bar{n}_s + \bar{n}_B)2\Delta f}}$$

Figures 7-2 through 7-4 were prepared to allow rapid evaluation of signal-to-noise ratio (based on Equation (5) above) for the case of an optical communications system utilizing a one-watt monochromatic beacon of specified wavelength, beamwidth, and receiver range and aperture area.

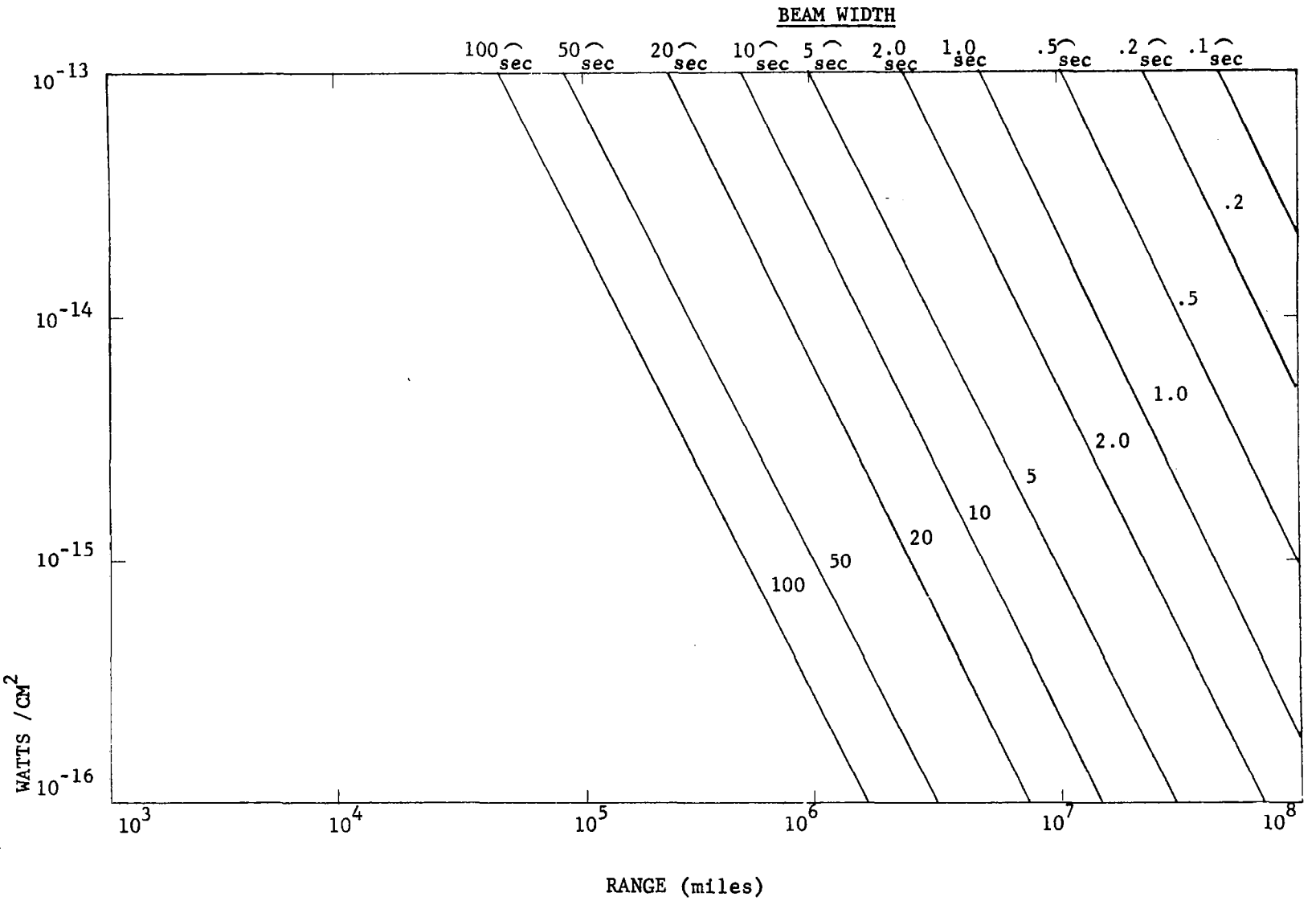

Figure 7-2. Power Density Versus Range for Transmitter Power Equal to 1.0 Watt

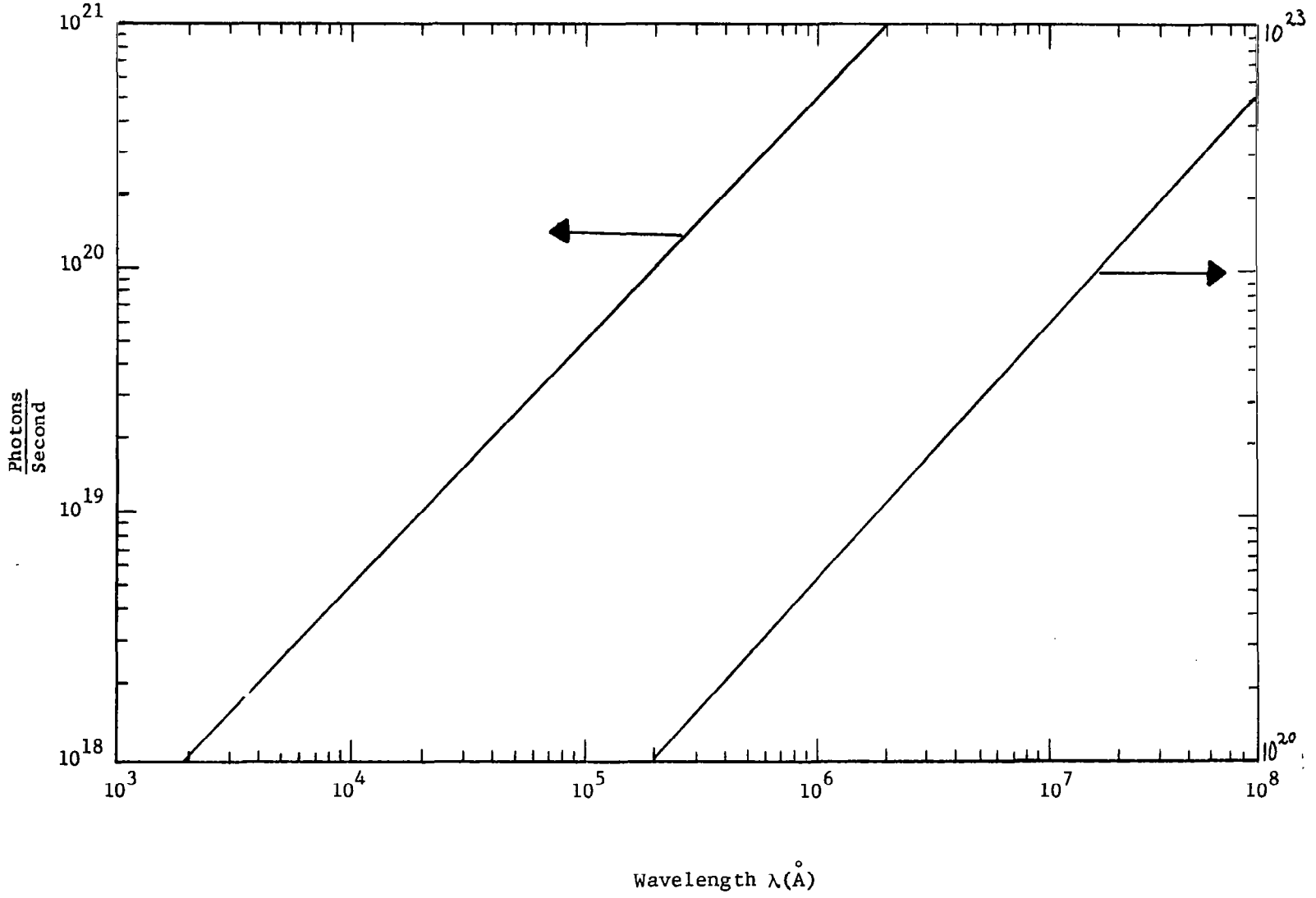

Figure 7-3. Photons/Sec Versus Wavelength for Power of One Watt

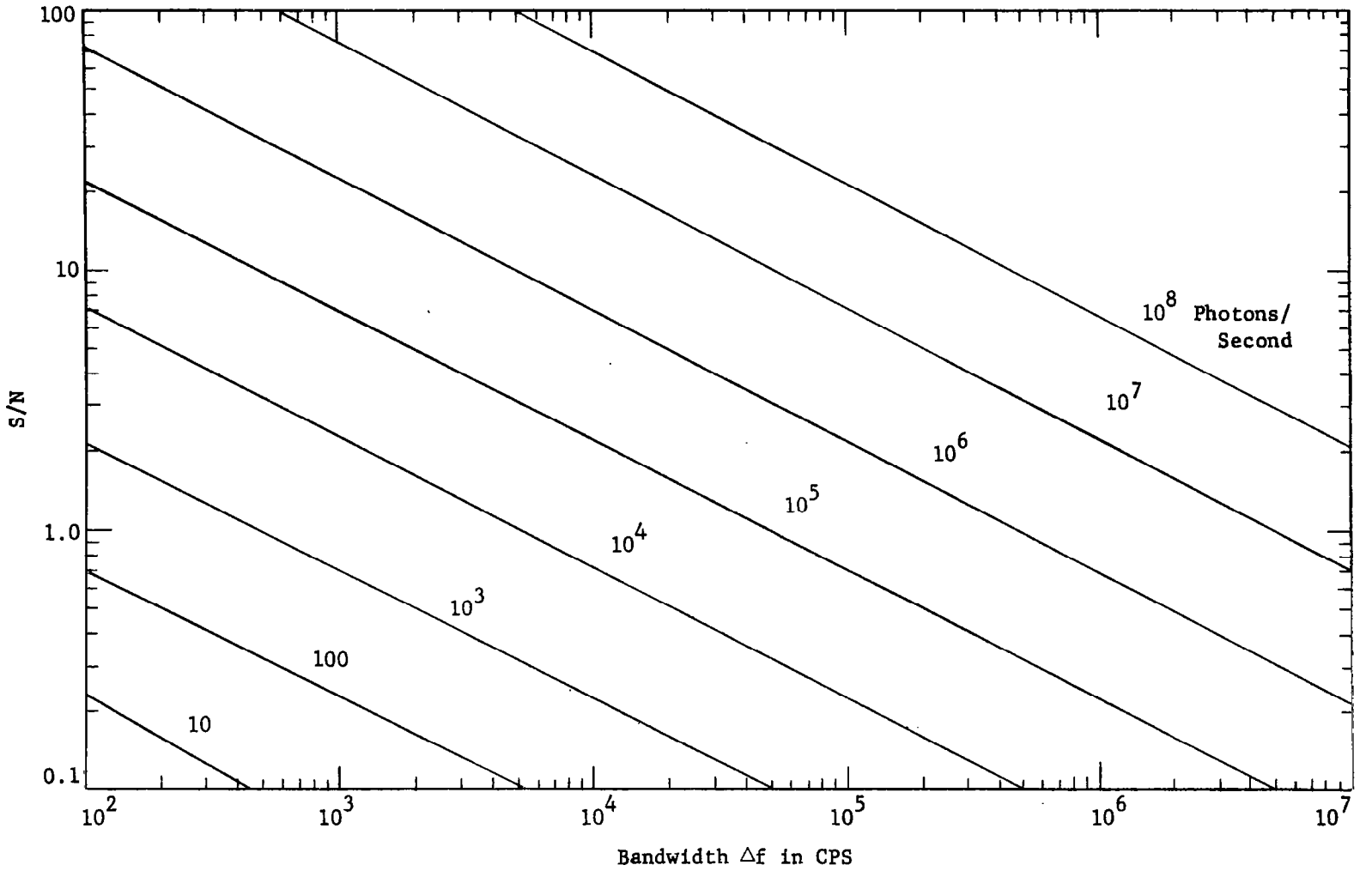

Figure 7-4. S/N Ratio Versus Bandwidth and Average Photon Arrival Rate

Figure 7-2 indicates the received signal power density in watts per square centimeter per transmitter watt as a function of range and transmitter beamwidth, assuming constant power density throughout the beam.* The equation incorporated in the preparation of these results is:

$$(6) \qquad P_R = P_T \frac{1}{(R \times \emptyset)^2 \frac{\pi}{4}}$$

where P_R is the power density at the receiver aperture in watts per square centimeter;

P_T is the total transmitter power in watts;

R is the range from the beacon to the receiver in centimeters; and

$\emptyset$ is the transmitter beamwidth in radians.

Selection of the aperture area in square centimeters allows total received power to be evaluated and converted to photons per second through the use of Figure 7-4, a graphical expression of the fact that one watt of power is equivalent to $\frac{\lambda}{10^{-7}\ hc}$ photons per second**. Knowledge of the number of

*Note: If the power density in the beam corresponds to a diffraction-limited $(\frac{\sin\alpha}{\alpha})^2$ distribution and the beamwidth is defined as $1.22\lambda/D$, the curves of Figure 7-2 are correct for approximately 2.2-watt transmitter power.

**Note: Where λ is wavelength in meters, h is Plancks constant (6.6254×10^{-27} erg sec) and C is the velocity of light in meters per second.

received photons per second and selection of a desired bandwidth Δf allows the use of Figure 7-4 to rapidly determine the S/N ratio identical to that obtainable from Equation (5).

7.2 BACKGROUND LIGHT LEVEL

While the S/N ratios of communications systems are ultimately limited by the discreteness of photon flow, practically achievable S/N ratios may be significantly lower than this due to the noise components introduced by background light (photosensors and subsequent electronics). Evaluation of degradations due to background light requires knowledge of the amount of such light that is incident upon the photodetector from each of the many sources which may appear, either wholly or in part, within the optical field of view. For a deep-space communications system, the possible sources of background light are energy from the moon, planets, the sun and its corona, the stars, and the earth and its atmosphere. The paragraphs below consider these sources and present data which is useful in estimating the degradation of S/N to be expected in a given system due to light from the aforementioned sources.

Earthshine and Earth Self Emission

A review of the orbital considerations of a deep-space vehicle reveals that the earth may appear either fully illuminated, as in the case of a vehicle near Venus, at Venus inferior conjunction, or totally dark as for a vehicle near Mars at Mars apposition. Further, a plot of a Hohman Elliptical Trajectory to Mars, Figure 7-5 (Reference 34, page 7), indicates that earthshine will vary quite markedly reaching a nearly zero value at some point on the trajectory. It is evident, therefore, that total received earthshine will

be not only a function of distance but, in addition, a function of the phase of earth illumination. For vehicle receivers with fields of view which include only a portion of the earth, received background earthlight will be a function of earthshine intensity adjacent to the earth beacon position.

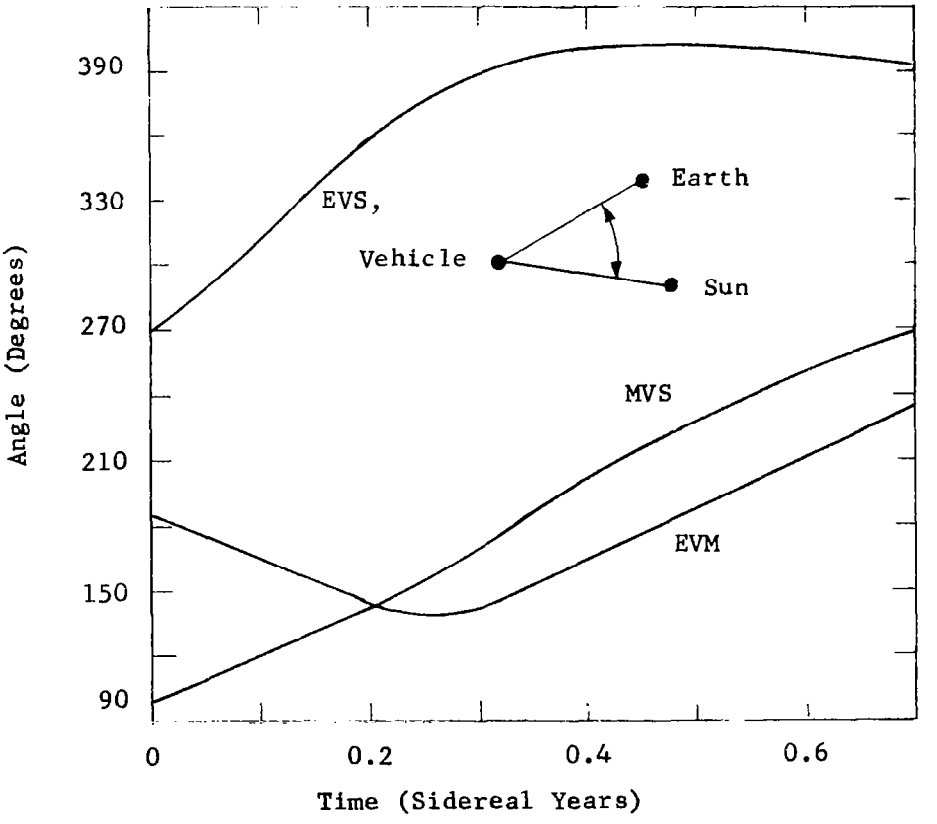

Figure 7-5. Angle Versus Time of a Space Vehicle Along a Hohmann Elliptical Trajectory to Mars From The Earth

Figures 7-6 (Reference 34, page 150) and 7-7 (Reference 34, page 34) show the maximum total estimated irradiance produced by the earth at the moon (separation distance of 238,000 miles). This data can be simply corrected, assuming a squarelaw reduction of irradiance with distance, to yield the irradiance at other distances. Assuming that the earth is a lambertian reflector also

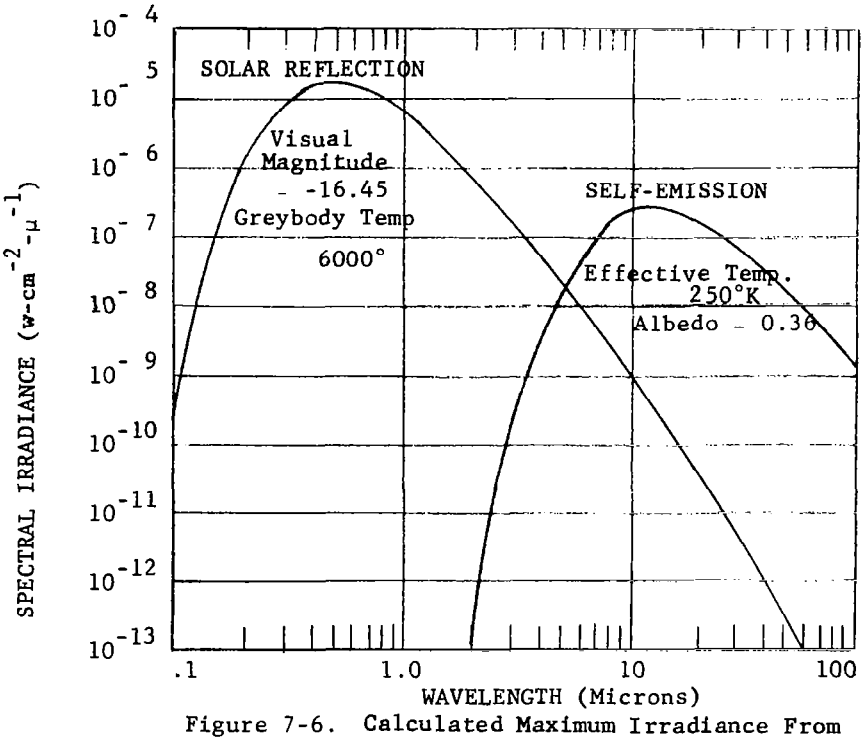

Figure 7-6. Calculated Maximum Irradiance From the Earth at the Moon (Earth to Moon at minimum distance of 384.4(10^3)km.)

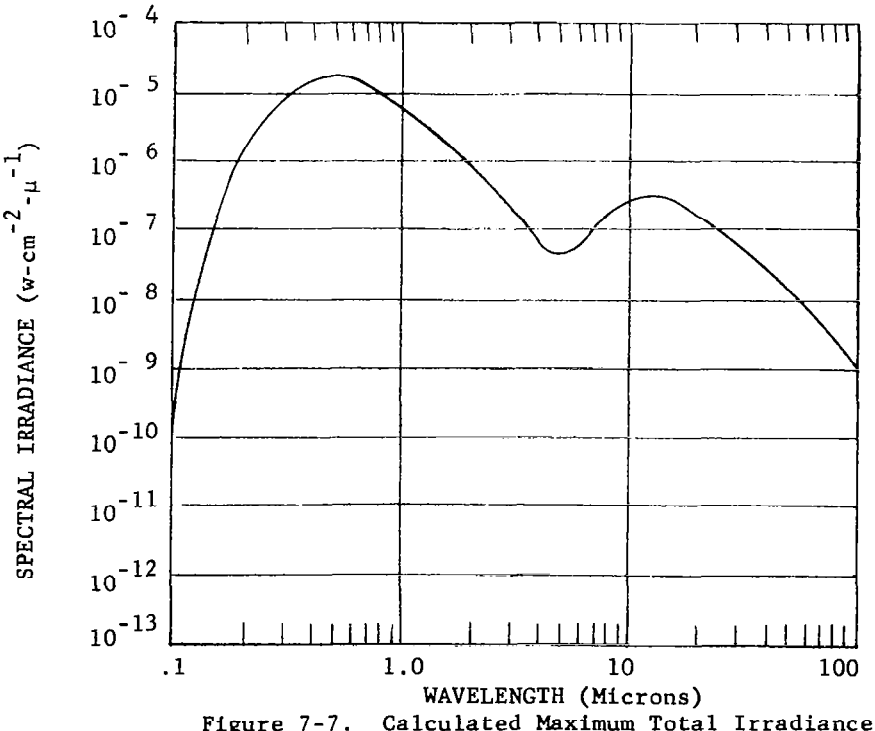

Figure 7-7. Calculated Maximum Total Irradiance from the Earth at the Moon (Total irradiance includes both the solar reflected and self-emitted blackbody irradiances from Figure 7-6)

allows use of the data for rapid estimation of the light accepted by systems with fields of view which include only a portion of the earth. For such cases it is assumed that earthshine (solar reflection) varies cosinusoidally with angle θ (see Figure 7-8).

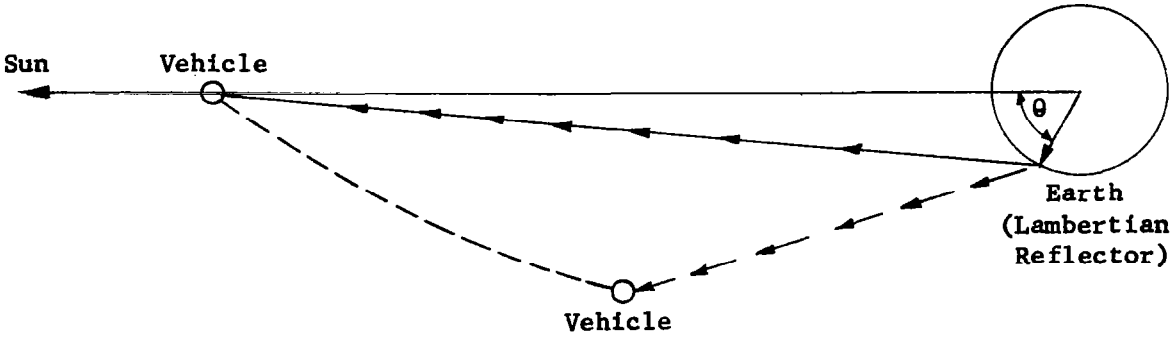

Figure 7-8. Earthshine Intensity Varies As Cosine θ When Viewed From Vehicle

Since the solar reflection curve of Figure 7-6 is applicable only for a fully illuminated earth (i.e., with vehicle between sun and earth), some correction is required for those conditions where the phase of earth's illumination, θ, is other than zero. Figure 7-9 indicates the appropriate correction factor and was computed from the formula:

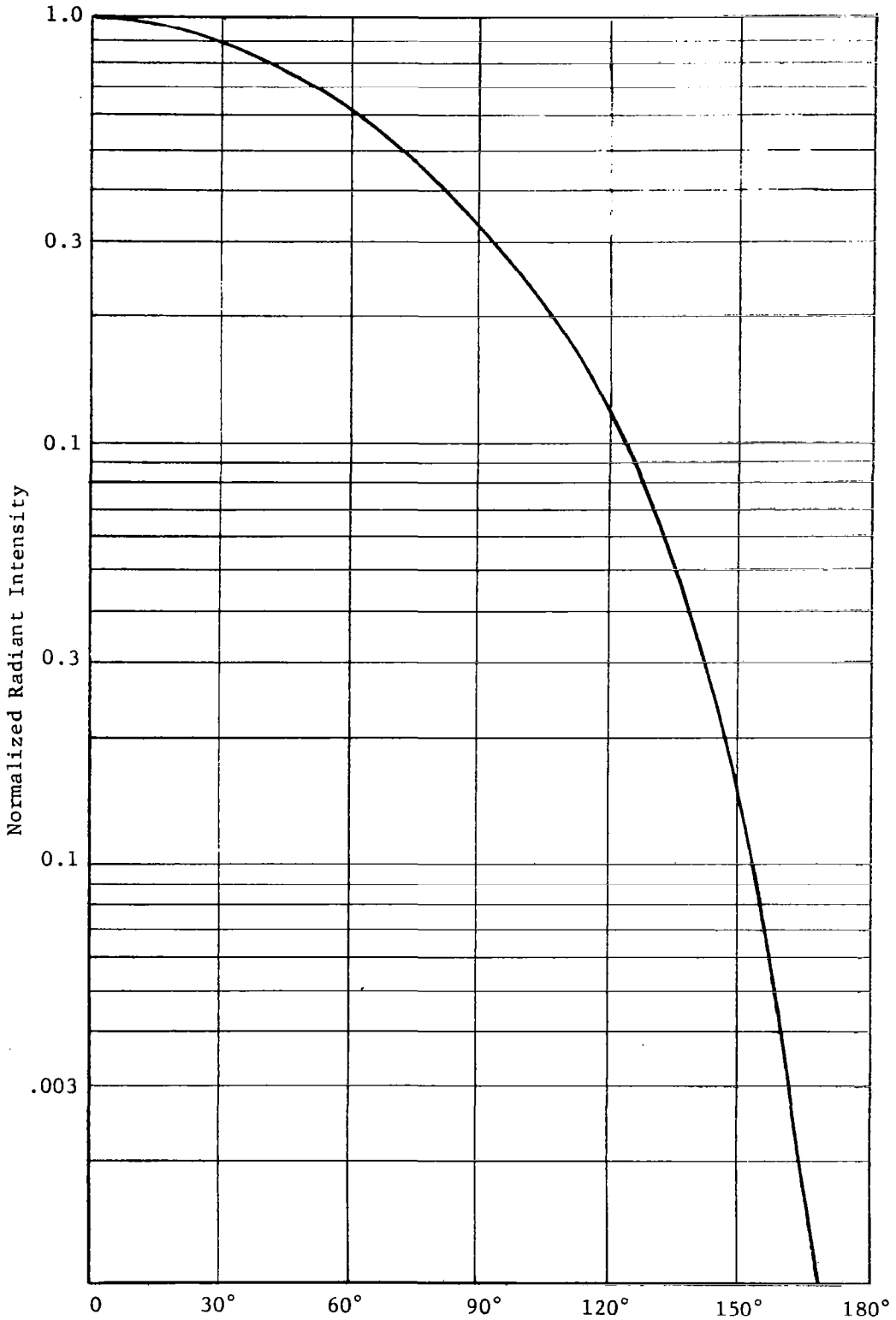

Figure 7-9. Radiant Intensity of Earth as a Function of Phase of Illumination

$$J = \frac{\rho}{\pi} H_s \frac{2}{3} a^2 \left(\left[\pi - \beta \right] \cos\beta + \sin\beta \right)$$

where

J is the apparent radiant intensity in watts/steradian;

ρ is reflectance or albedo;

H_s is the irradiance at earth due to sun in watts per square centimeter;

a is the radius of earth; and

β is the angle between sun - earth - observer (always positive).

Figure 7-10 indicates the radiance distribution, assuming lambertian reflectance, over the earth's surface and is useful in those cases mentioned previously where only a portion of the earth is within the optical field of view.

The self emission curve in Figure 7-6 can be assumed to vary only with distance in square law fashion for systems whose fields of view include the whole earth. For systems with narrower fields of view, corrections are readily computed since the radiance for a lambertian emitter is constant (viz: if the field of view subtends an angle of N times less than the earth's angular subtense, the irradiance curve for self emission, corrected for distance, is reduced by N squared).

Solar Irradiance

The irradiance as a function of spectral wavelength, λ, at one astronomical unit is shown in Figure 7-11 (Reference 34, page 136). Since the photosphere displays essentially constant radiance over its surface, background light in systems viewing 1/N of the photosphere are readily computed via a square law distance correction factor and a $\frac{1}{N^2}$ field-of-view correction factor.

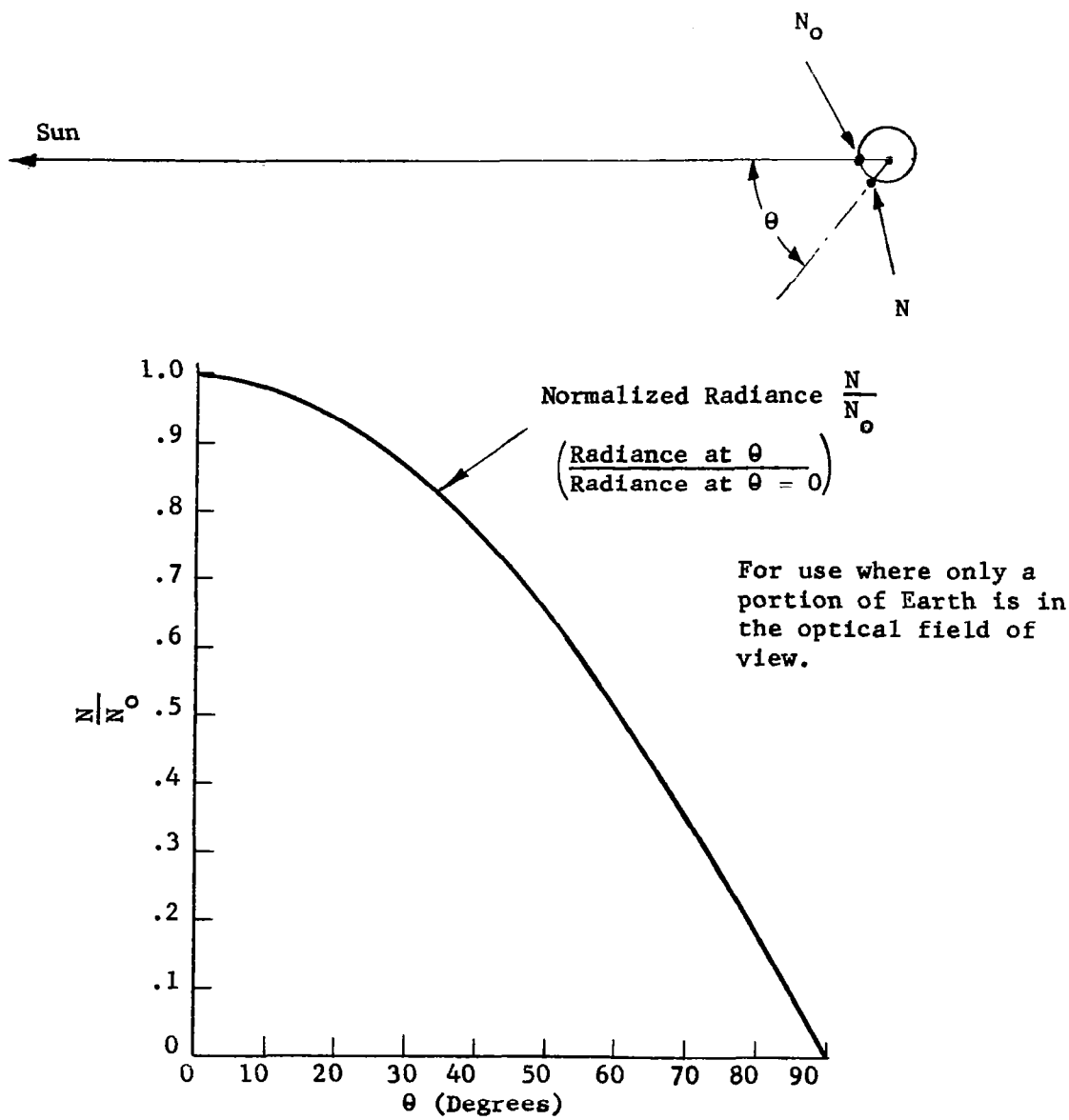

Figure 7-10. Earthshine Radiance Distribution Varies as Cos θ

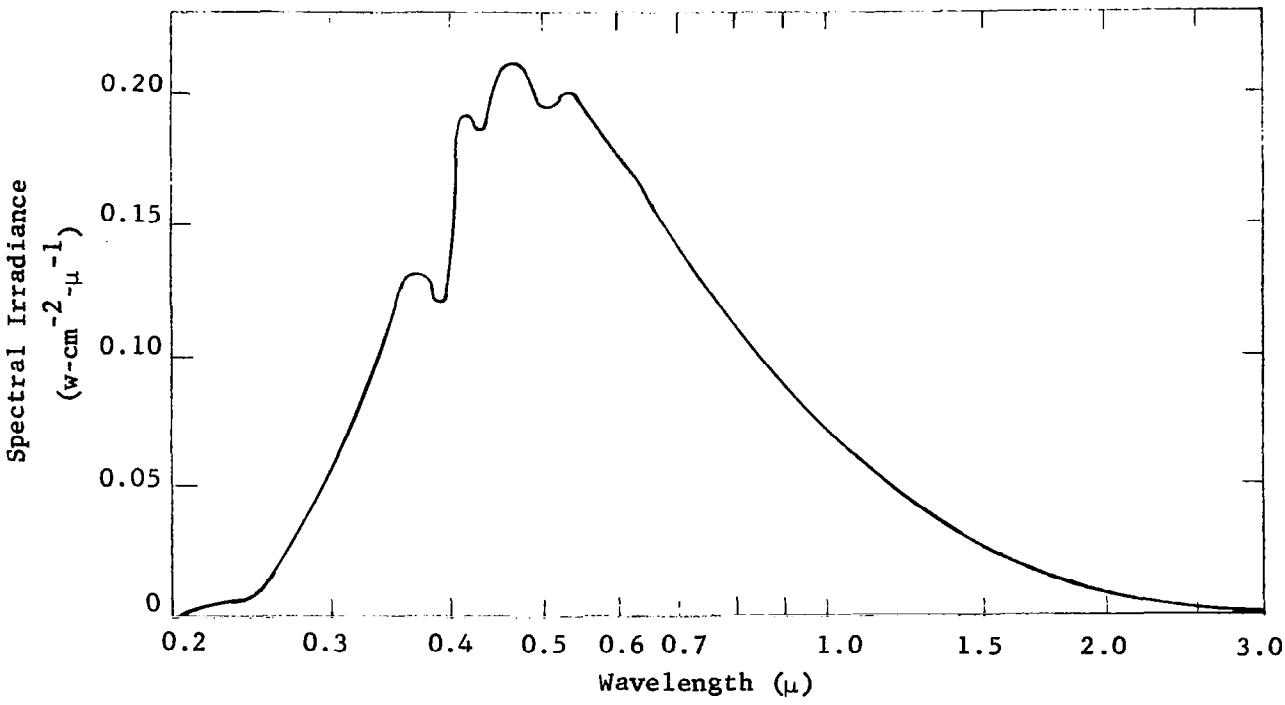

Figure 7-11. Solar Irradiance Curve from 0.2 to 3μ

The solar coronal radiance (K and F components), expressed as a fraction of the photospheric radiance, is shown by Figure 7-12 (Reference 6), and can be used, in conjunction with Figure 7-11, to ascertain light level in cases where coronal background exists. It is assumed that the spectral distribution of coronal light is essentially the same as the photosphere.

Irradiance from Planets, Stars, and Moon

References 34 and 35 provide reasonably good estimates for irradiances above the earth's atmosphere from the moon, planets, and stars. Curves from Reference 35 (page 466), which are duplicated here as Figure 7-13, are based upon published values of visible magnitude and effective temperatures and the assumption that the Planck radiation function is applicable. The self emission curves shown for planets are based upon the equation:

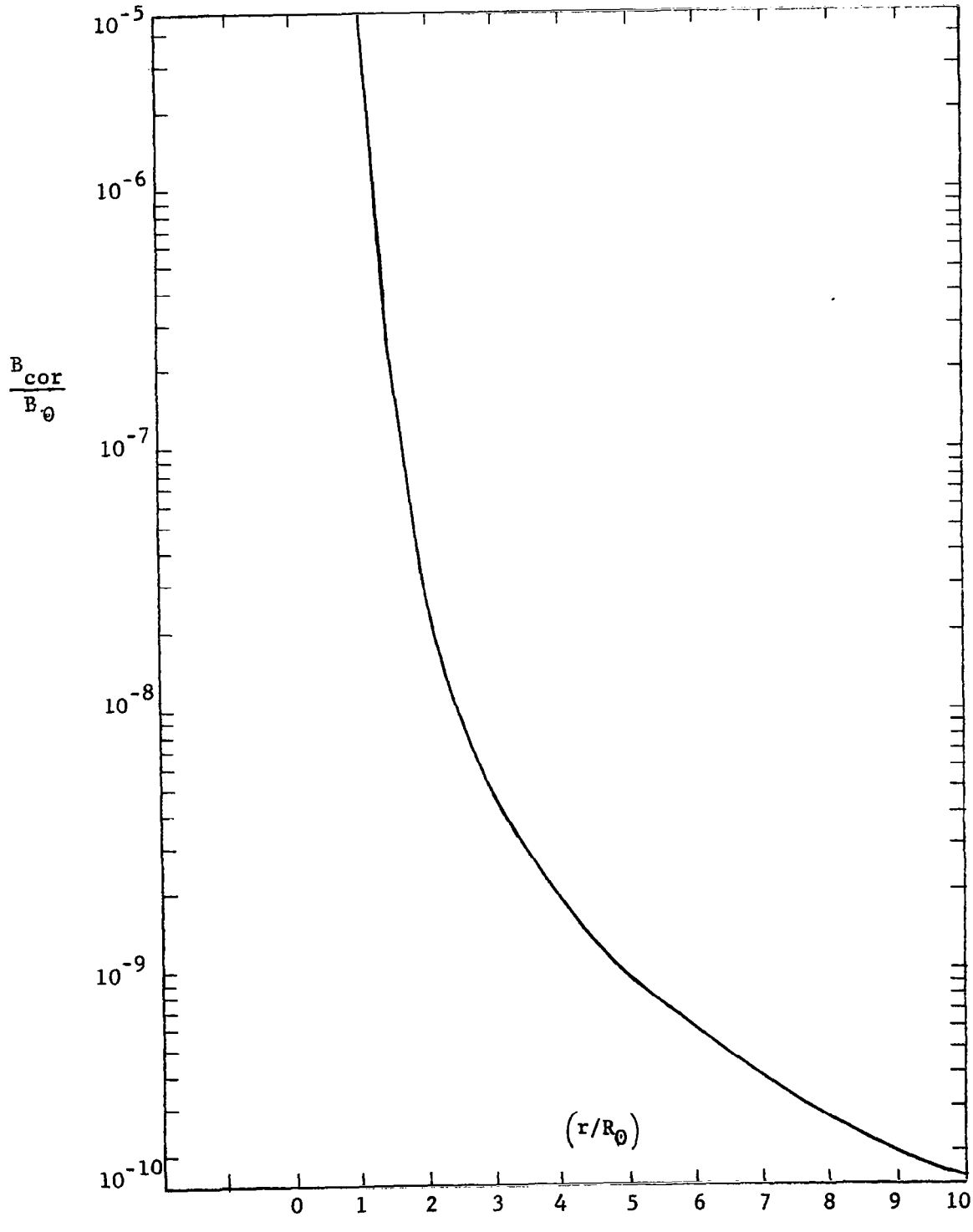

Figure 7-12 Coronal Radiance, B_{cor}, Normalized by Photospheric Radiance $B_\odot$ Expressed as a Function of Distance r in Terms of the Sun's Radius $R_\odot$

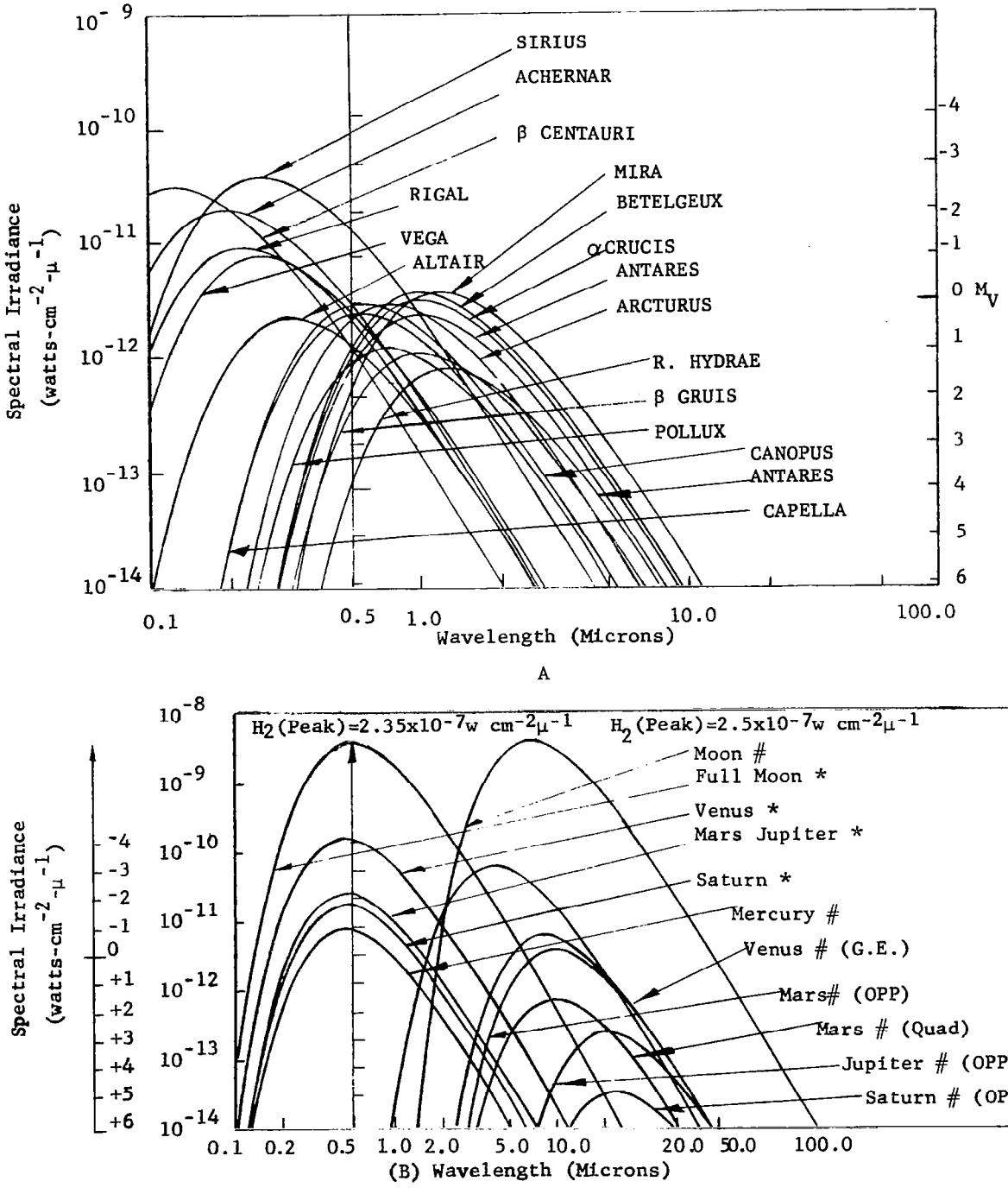

*-Calculated irradiance from planets, at brightest, due to sun reflectance only. GE- inferior planet at greatest elongation. OPP - superior planet at opposition. QUAD - superior planet at quadrature. #Calculated irradiance from planets, due to self-emission only.

Figure 7-13. Calculated Spectral Irradiance From Planets and Brightest Stars at the Top of the Atmosphere

$$H_\lambda(\text{peak}) = \frac{\omega_{\lambda max}(T)}{4\pi} \quad (1-A) \quad \frac{\pi d^2}{D^2}$$

where $\omega_{\lambda max}(T)$ is peak value of the Planck function;

$H_\lambda(\text{peak})$ is peak spectral irradiance in watts/cm^2/micron;

T is effective surface temperature of the planet;

$(1-A)$ is the assumed emissivity of the radiating body, where A is the value of the albedo in the visible region;

$\frac{\pi d^2}{4}$ is the radiating surface of the planet (d is the diameter);

D is the distance to the planet from the earth.

The methods used in Reference 35 to obtain spectral irradiance curves for the stars were used to obtain an approximation for the irradiance in watts/cm^2/micron per square degree of starfield. This was accomplished by utilizing existing probability data for the number of stars per square degree expected in or near the galactic plane for each visible magnitude range. Such data yields the probably visible irradiance due to stars in each magnitude range per square degree (refer to Table 7-1). Summation of visible irradiances for all magnitude ranges between second and twenty-second magnitude yields the total visible irradiance expected per square degree of sky as 10^{-13} watts/cm^2/micron/degree^2. The assumption that the stars in each square degree are distributed spectrally, as indicated by Table 7-2, allows the Planck radiation curve representing the contribution from each star color class to be constructed.

TABLE 7-1

Calculation of Total Visible Star Irradiance Per Square Degree in or near Galactic Plane

1	2	3	4	5	6	7	8	9	8 x 9 = 10
M	Log $N_{M_{pg}}$	$N_{M_{pg}}$	Log $N_{M_{pg}}$ $\left(N_{M_{pg}}\right)$ Mean 0 to 90° Galactic Latitude	Log N_{M_v} $\left(N_{M_v}\right)$	Correction To $N_{M_{pg}}$ $\left(N_{M_v}/N_{M_{pg}}\right)$	3 x 6 = 7 N_{M_v}		Visible Stellar Irradiance From Single Star With Average Magnitude For Magnitude Range Considered	Visible Irradiance Contribution For Magnitude Range
2	$\bar{3}.18$	.001514	$\bar{4}.96$ (.000911)	$\bar{4}.99$ (.000976)	1.07	.00162	.00613	3.2×10^{-14} watts/cm^2	19.60×10^{-17}
3	$\bar{3}.68$	.00479	$\bar{3}.4$ (.00219)	$\bar{3}.55$ (.00355)	1.62	.00775	.02175	1.25×10^{-14}	27.20×10^{-17}
4	2.25	.0178	$\bar{3}.89$ (.00776)	$\bar{2}.11$ (.0129)	1.66	.0295	.0508	5×10^{-15}	25.40×10^{-17}
5	2.72	.0525	$\bar{2}.37$ (.0234)	$\bar{2}.6$ (.0398)	1.70	.0893	.1562	2×10^{-15}	31.24×10^{-17}
6	1.18	.1514	$\bar{2}.86$ (.0724)	$\bar{1}.07$ (.1173)	1.62	.2455	.4495	8.0×10^{-16}	36.00×10^{-17}
7	1.61	.408	$\bar{1}.31$ (.204)	$\bar{1}.54$ (.347)	1.70	.695	1.295	3.2×10^{-16}	41.50×10^{-17}
8	.05	1.12	$\bar{1}.75$ (.561)	0 (1.0)	1.78	1.99	4.04	1.25×10^{-16}	50.50×10^{-17}
9	.52	3.31	.19 (1.55)	.45 (2.82)	1.82	6.03	12.53	5.0×10^{-17}	62.70×10^{-17}
10	.97	9.33	.62 (4.17)	.92 (8.3)	1.99	18.56	33.94	2.0×10^{-17}	67.88×10^{-17}
11	1.43	26.9	1.05 (11.2)	1.34 (21.9)	1.95	52.5	102.5	8.0×10^{-18}	82.00×10^{-17}
12	1.88	75.9	1.46 (28.8)	1.77 (58.9)	2.05	155.	245.	3.2×10^{-18}	78.50×10^{-17}
13	2.3	200.	1.87 (74.0)	2.17 (148)	2.00	400.	647.	1.25×10^{-19}	81.00×10^{-17}
14	2.72	5.25	2.26 (182)	2.56 (363)	1.994	1,047.	1,778.	5.0×10^{-19}	88.90×10^{-17}
15	3.12	1,320.	2.62 (416)	2.95 (890)	2.14	2,825.	2,765.	2×10^{-19}	55.30×10^{-17}
16	3.41	2,670.	2.98 (954)	3.3 (1995)	2.09	5,590.	8,170.	8×10^{-20}	65.30×10^{-17}
17	3.83	6,750.	3.33 (2140)	3.64 (4360)	2.04	13,760.	19,290.	3.20×10^{-20}	61.60×10^{-17}
18	4.2	15,800.	3.64 (4360)	3.96 (9110)	2.09	33,050.	29,950.	1.25×10^{-20}	37.50×10^{-17}
19	4.5	31,600.	3.9 (7940)	4.2 (15,830)	1.994	63,000.	32,300.	5.0×10^{-21}	16.15×10^{-17}
20	4.7	50,000.	4.17 (14,800)	4.45 (28,200)	1.906	95,300.	104,700.	2.0×10^{-21}	20.90×10^{-17}
21	5.0	100,000.	4.4 (25,100)		≈ 2.0	200,000.			
									942.17×10^{-17} w/cm^2/deg^2
									9.42×10^{-14} w/cm^2/μ/dg^2 (Since visible range is approximately 0.1μ wide)

NOTES: (1) Data in columns 1 through 5 obtained from Reference 6, page 234.

(2) Figures in parentheses in colums 4 and 5 are the values of N_m corresponding to the Log N_m shown.

(3) Column 8 indicates the probable number of stars in each magnitude range (viz: probable number of stars between 2nd and 3rd magnitude is .00613).

(4) Column 9 is the visible irradiance for the average stellar magnitude in the range considered (viz: for 2nd to 3rd magnitude the average was taken as 2.5 magnitude).

(5) $N_{M_{pg}}$ is the number of stars per square degree brighter than photographic magnitude M.

(6) N_{M_v} is similar to $N_{M_{pg}}$ and pertains to visual magnitude.

TABLE 7-2. Spectral Distribution of Stars by Color Class

Sp*	% Stars**	Assigned Effective Temperatures	Wavelength of Peak Irradiance (From Wiens Displacement Law)
B	10	25,000°K	0.116μ
A	22	12,000°K	0.2415μ
F	19	8,500°K	0.3415
G	14	6,500°K	0.446
K	32	5,000°K	0.58
M	3	3,400°K	0.853

*Sp denotes spectral classification.
**Reference 6, page 234.

Each curve peaks at the wavelength derived from Wiens Displacement Law,

$$\lambda_{max} T = 2898$$

where T is effective temperature in degrees Kelvin and λ_{max} is wavelength in microns, and each curve is drawn through $\lambda = 0.55$ microns at the value of visible irradiance, corresponding to the visible contribution of the color class (viz: for A stars at 22% x 10^{-13} watts/cm^2/micron). Figure 7-14 shows the separate curves for each of the assumed six color classes and, in addition, the total curve obtained by addition of the separate curves. It should be noted that the assumption of the Planck radiation function for the M stars is reasonably correct up to about four microns and may be appreciably in error for longer wavelengths. Hence, all curves are shown only for shorter wavelengths. Moreover, the curves do not extend below about 1500Å, a region wherein stellar atmospheric absorption effects can cause significant departures from the assumed Planck radiation characteristic.

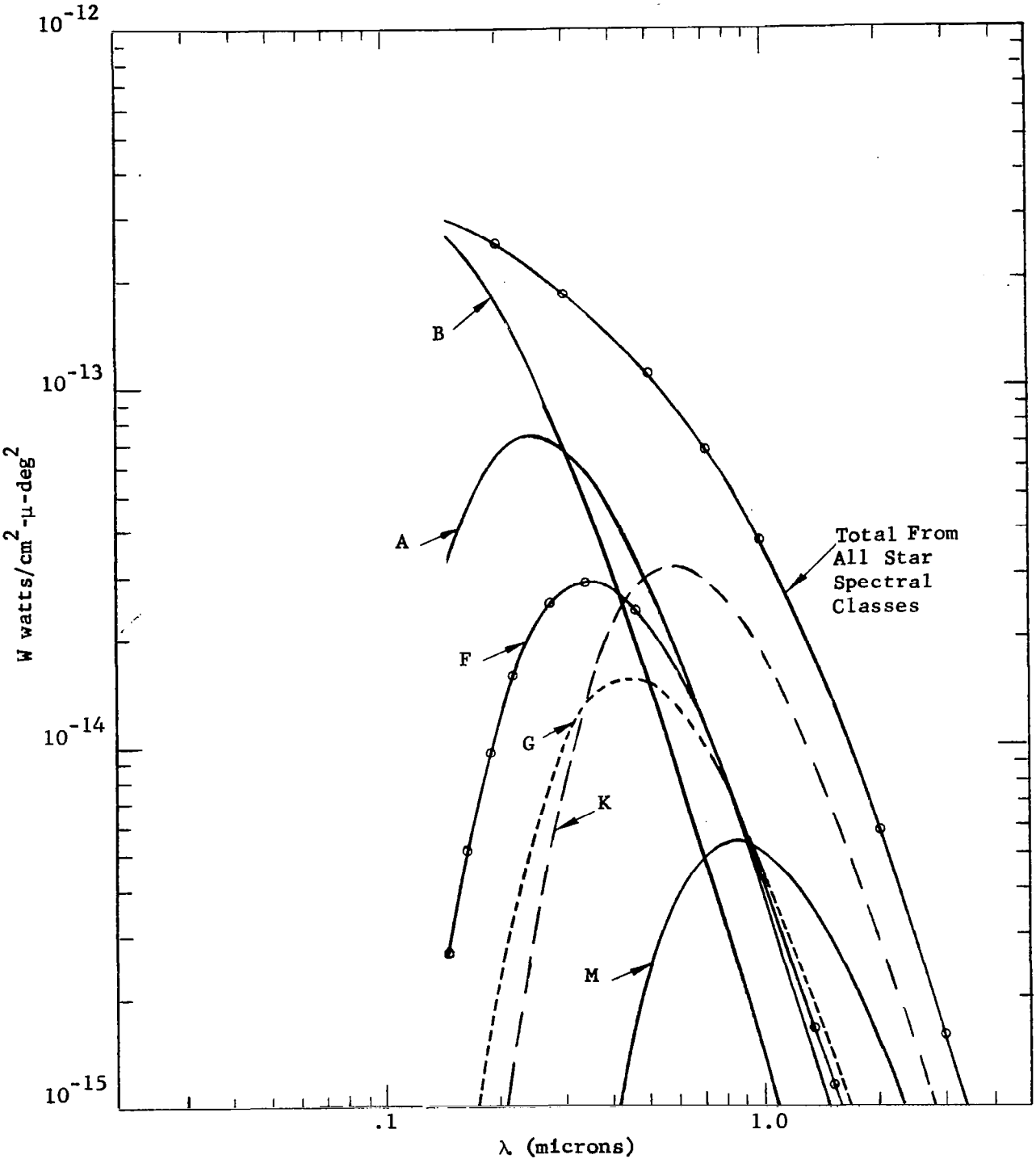

Figure 7-14. Probable Spectral Irradiance from a One Square Degree Starfield In or Near the Galactic Plane

Additional data for irradiances at the surface of the earth's atmosphere due to brighter stars and planets was obtained from Reference 34 and is duplicated here as Figures 7-15 through 7-23.

7.3 DETECTORS

Previous paragraphs have considered the effects of photon descreteness on signal-to-noise ratio both for the case of noise in signal only and for the case where background light also prevails. Also presented has been data on irradiances to be expected from earth, planets, the sun, and the stars so that S/N can be calculated for the latter case for typical communications systems. Since additional degradation of S/N can be expected due to photosensor noise contributions, a limited review of available detectors was performed to gather data relavent to photosensor performance. Because existing data* (refer to Figures 7-24 and 7-25) is relatively current and complete for the wavelength range above one micron, efforts were restricted to supplementing published data for sensors which appeared optimum for use at shorter wavelengths.

Inspection of the spectral response characteristics of available photoemissive surfaces (Figure 7-26) indicates S20 and S1 to be close to optimum for the range of 0.32 to 1.0 micron with only two other surfaces (S17 and S5) offering slightly higher quantum efficiencies over portions of this spectral range. Measured data for several RCA 7265-S20 (selected for low dark current) was tabulated (refer to Table 7-3) and utilized to obtain average expected

*Reference 34, page 67 reproduced here as Figure 7-24.
Reference 35, pages 386-483.
Reference 37, pages 386-483; page 1 reproduced here as Figure 7-25.

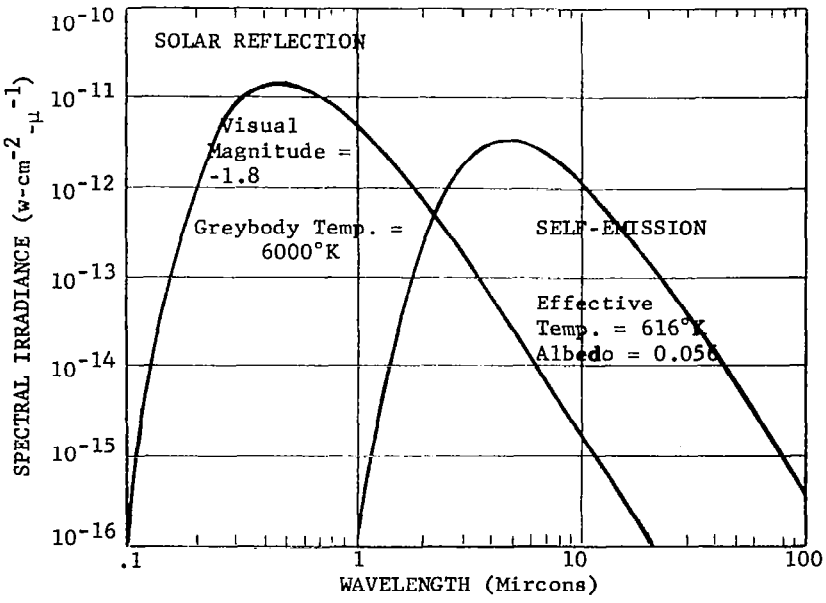

Figure 7-15. Calculated Maximum Irradiance from Mercury Outside the Earth's Atmosphere (Mercury to Earth at Minimum Distance of 137.8×10^6 km.)

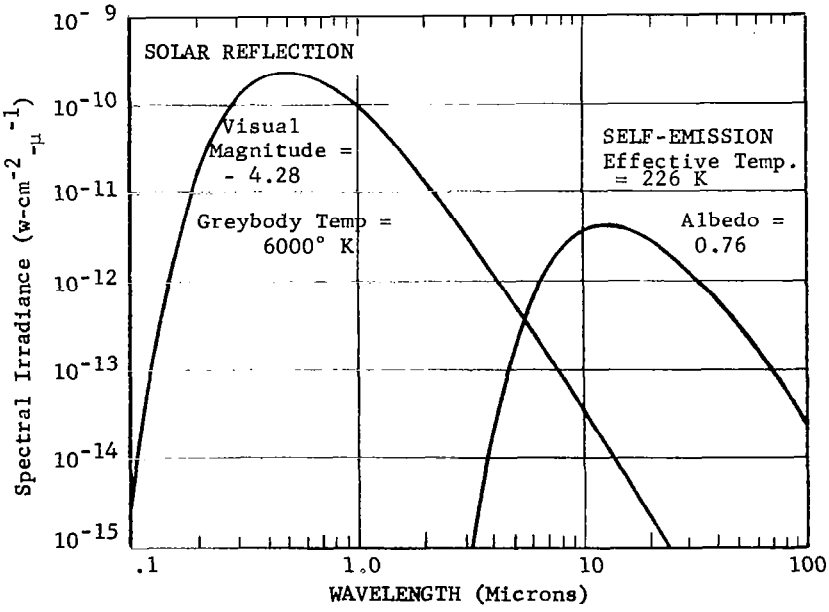

Figure 7-16. Calculated Maximum Irradiance From Venus Outside the Earth's Atmosphere (Venus to Earth at Minimum Distance of 103.3×10^6 km.)

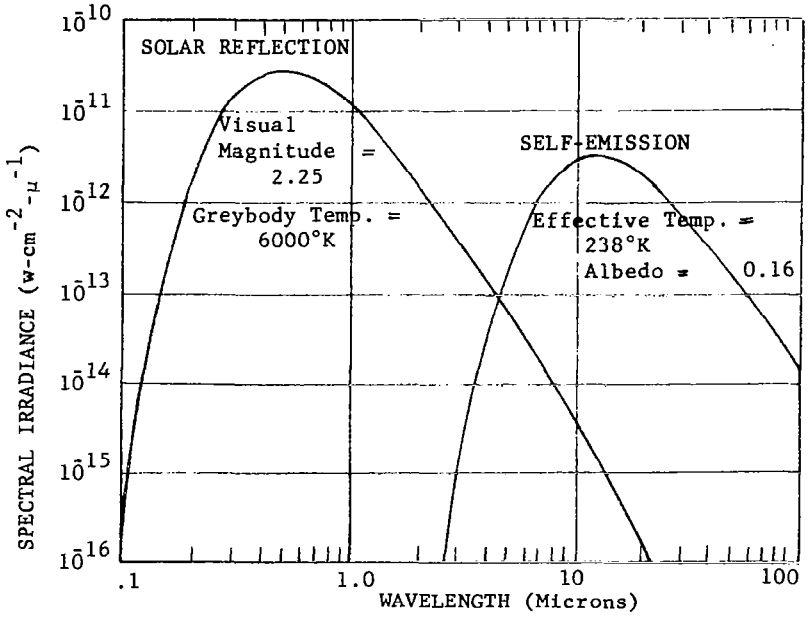

Figure 7-17. Calculated Maximum Irradiance from Mars Outside the Earth's Atmosphere (Mars to earth at minimum distance of 78.3(10^6) km.)

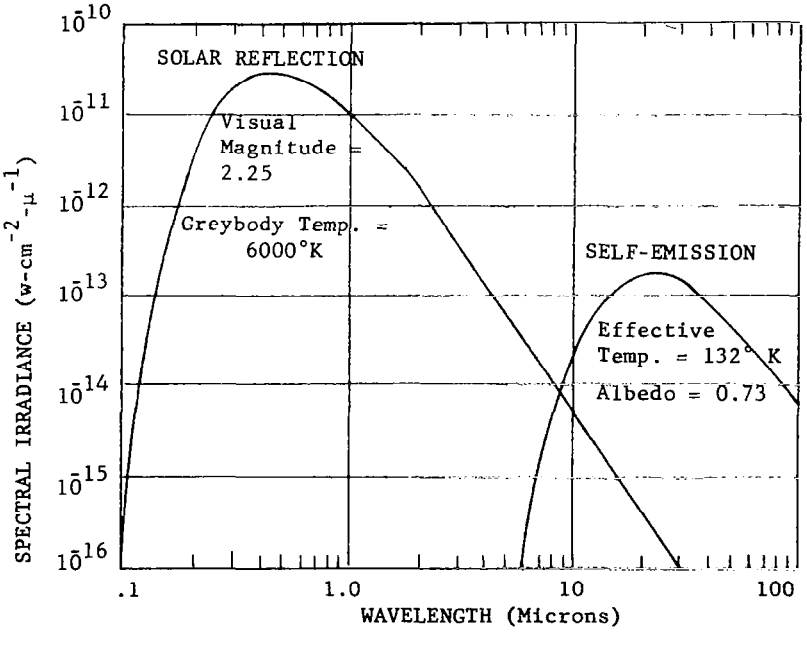

Figure 7-18. Calculated Maximum Irradiance from Jupiter Outside the Earth's Atmosphere (Jupiter to Earth at minimum distance of 628.3(10^6) km.)

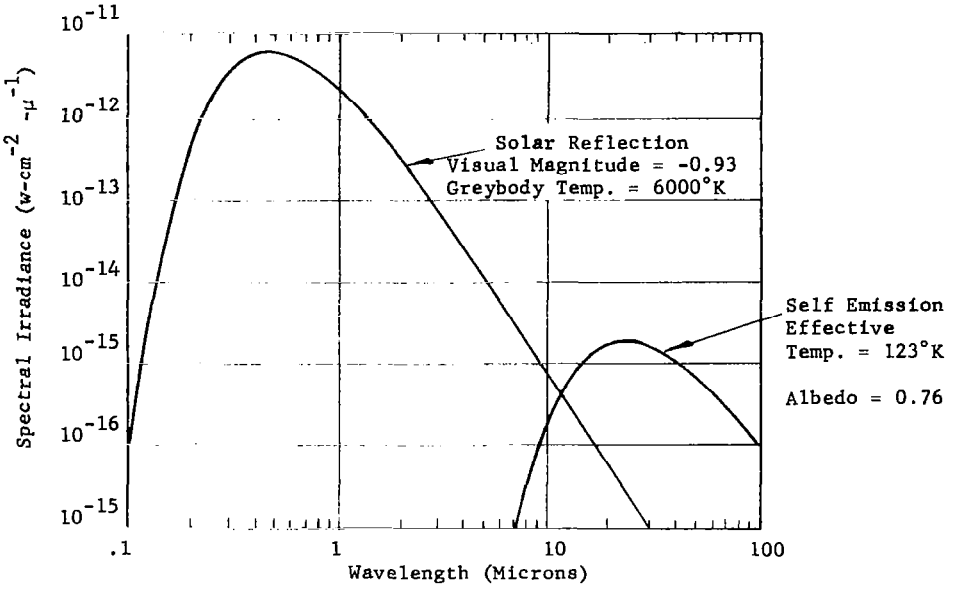

Figure 7-19. Calculated Maximum Irradiance from Saturn Outside the Earth's Atmosphere (Saturn to Earth at Minimum Distance of 1277.0 (106) km.)

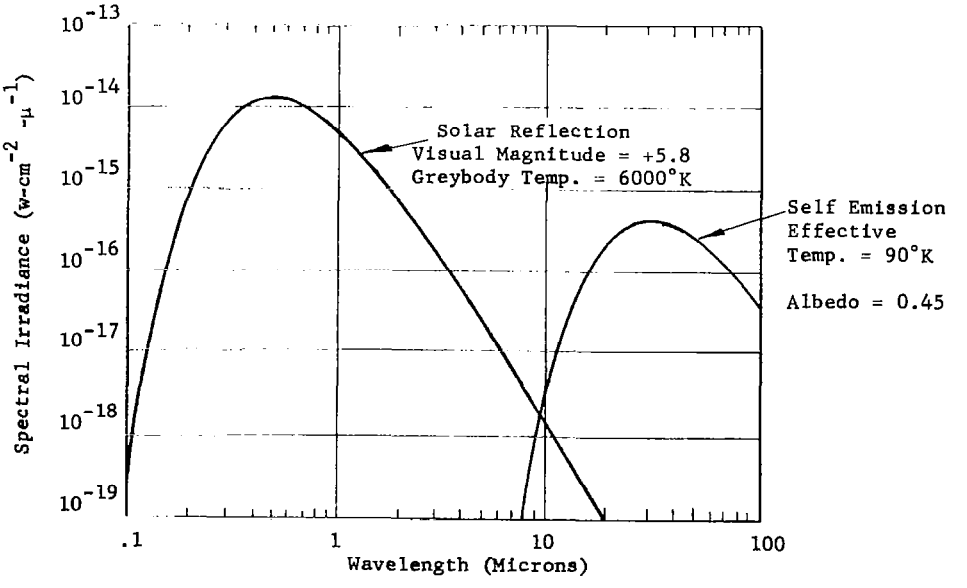

Figure 7-20. Calculated Maximum Irradiance from Uranus Outside the Earth's Atmosphere (Uranus to Earth at Minimum Distance of 2720.0 (106) km.)

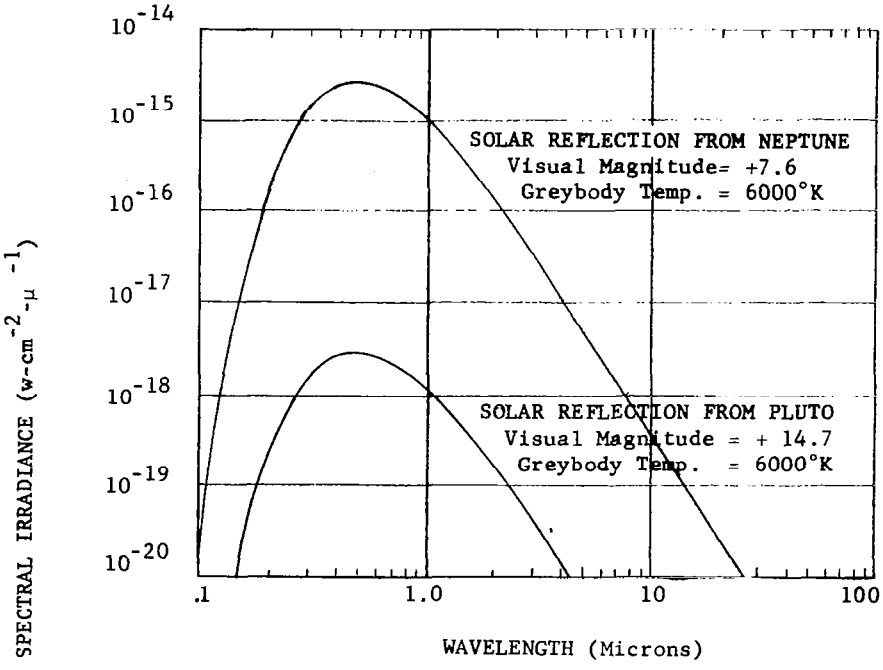

Figure 7-21. Calculated Maximum Irradiance from Neptune and Pluto Outside the Earth's Atmosphere (Self emission irradiance from Neptune and Pluto insignificant)

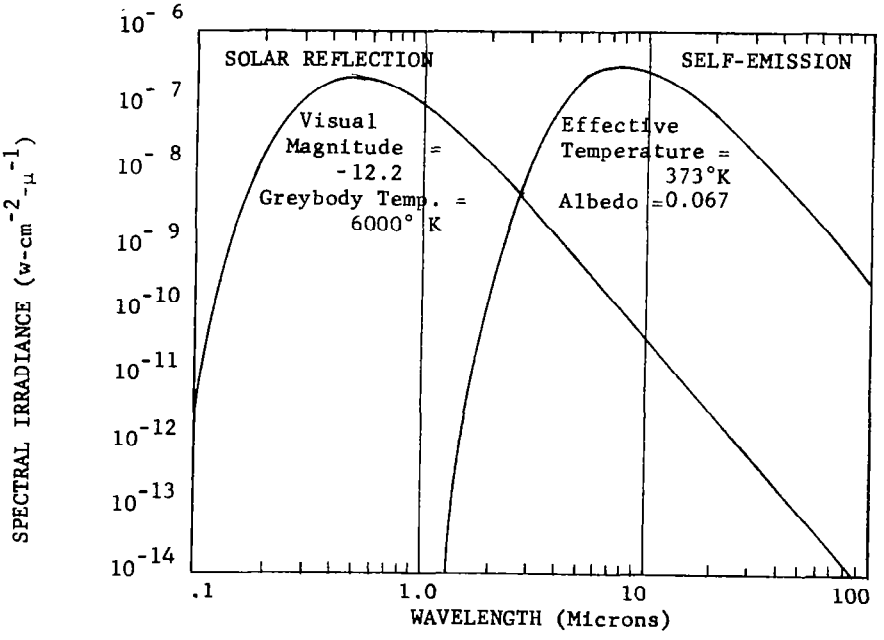

Figure 7-22. Calculated Maximum Irradiance from the Full Moon Outside the Earth's Atmosphere (Moon to earth at minimum distance of 384.4(10^3) km.)

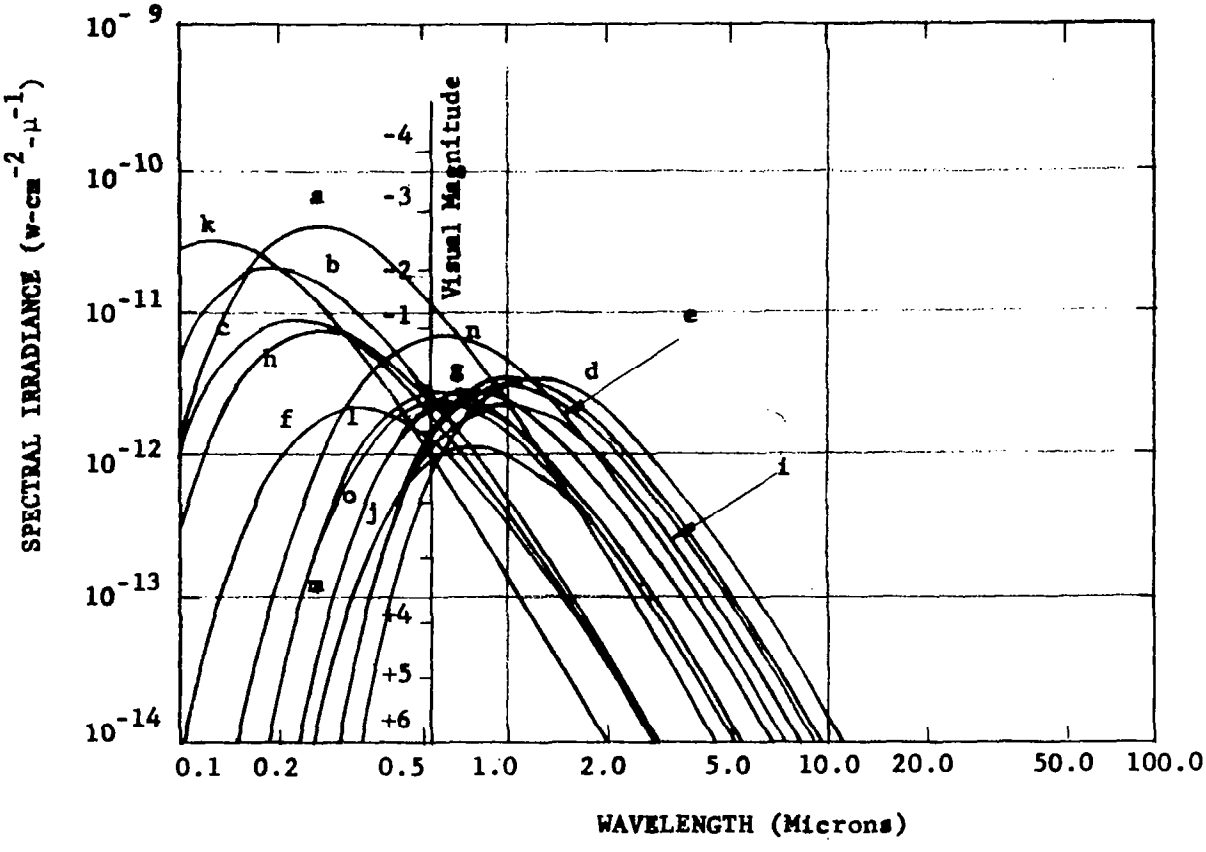

Figure 7-23 Calculated Irradiance from Fifteen of the Brightest Stars Outside the Earth's Atmosphere

a - Sirius A
b - Achornar
c - Rigel
d - Mira
e - Acrux (α Crucis)
f - Altair
g - Betelgeuse
h - Vega
i - Antares
j - Pollux
k - Agena (β Centauri)
l - Canopus
m - Arcturus
n - Rigil Kent
o - Capella

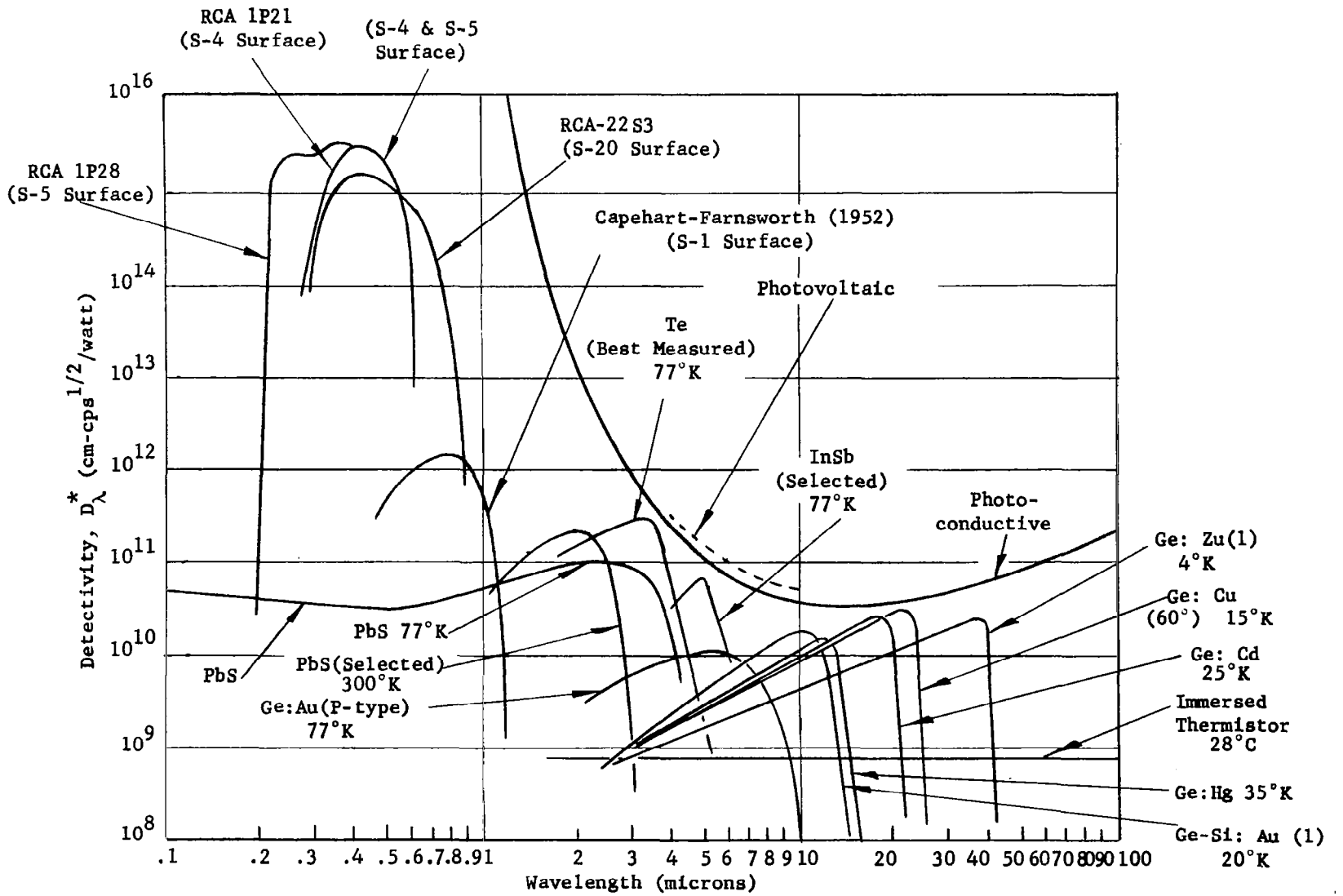

Figure 7-24. Detectivity Versus Wavelength for the Best Detectors

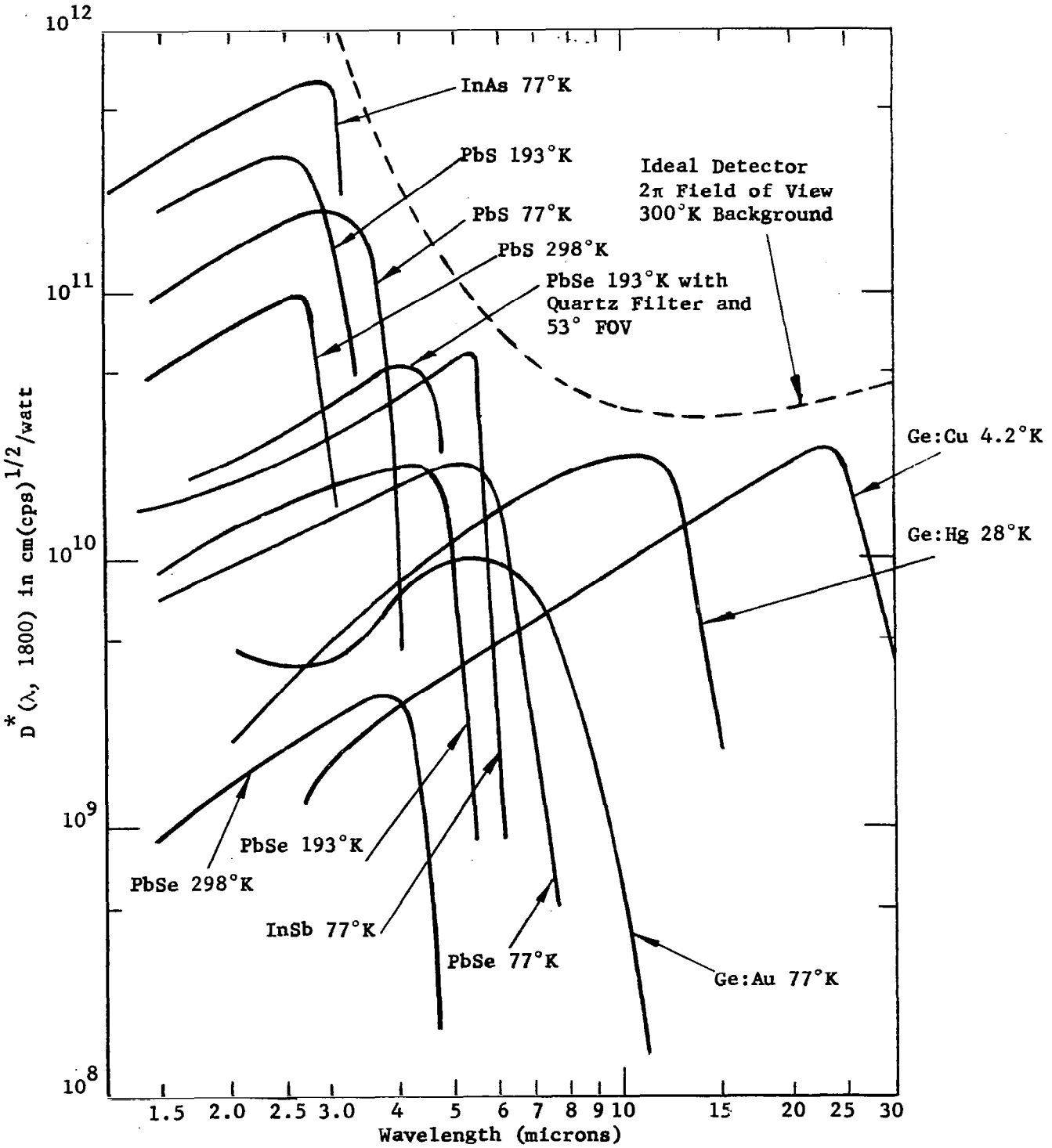

Figure 7-25. Optimum Spectral Detectivities of Infrared Detectors Prepared by Santa Barbara Research Center

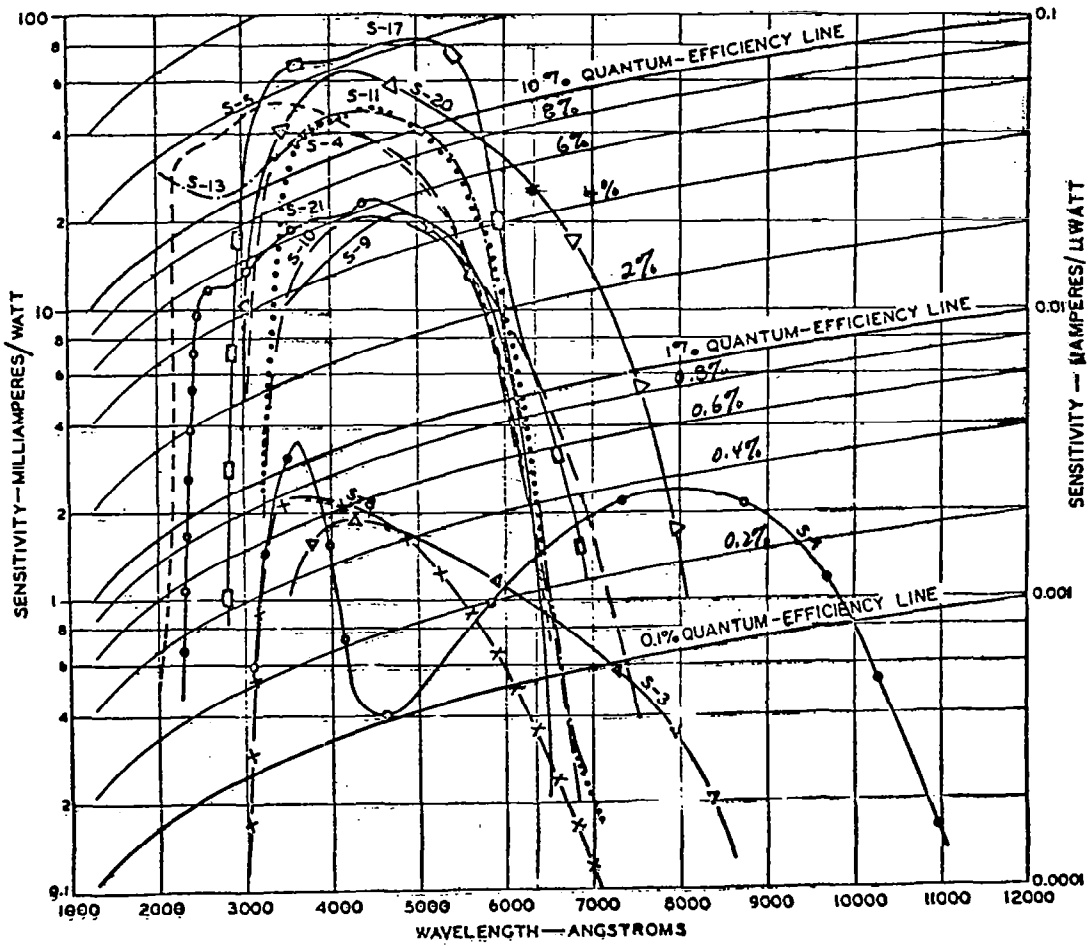

Figure 7-26. Spectral Response Characteristics

cathode dark current (21.9×10^{-16} amperes at 25°C and 0.505×10^{-16} amperes at -70°C). The results were plotted in terms of equivalent input watts as a function of wavelength and are shown in Figure 7-27, along with a similar curve based upon manufacturer's published data for the EMR 543C-51 photomultiplier. It should be noted that the 7265 measured dark currents at +25°C are nearly equivalent to the published data for the EMI 9558-S20 photomultiplier. It is felt that the curves presented represent achievable performance.

Tubes with smaller photocathode areas should exhibit proportionally less dark current and should be considered, if available and applicable, for specific optical system designs.

7.4 ACQUISITION PHOTOMETRY

The problem of earth beacon acquisition by a deep-space vehicle shall now be investigated to establish whether a simple approach exists. Considered will be a system in which the following rather reasonable assumptions exist:

(1) The receiver aperture area is one square meter.

(2) The earth beacon output power is one watt at 6328Å and the beacon beamwidth (including atmospheric spreading) is ten arc-seconds.

(3) Initial ground station tracking of the vehicle allows prediction of the vehicle's future angular position to within 3.6 arc-seconds.

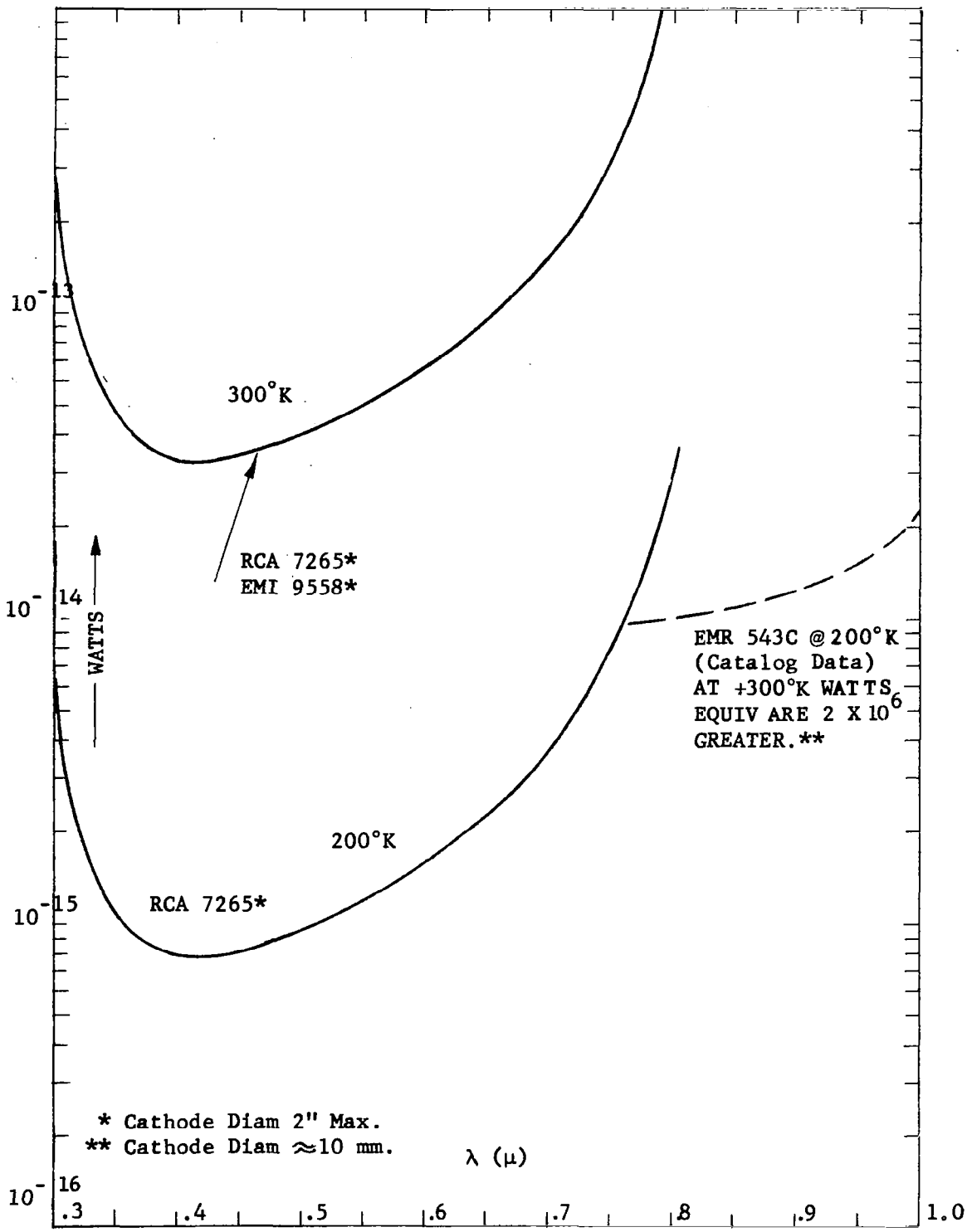

Figure 7-27. Photomultiplier Photocathode Dark Current Equivalent Watts

TABLE 7-3

PMT PERFORMANCE SUMMARY FOR S20 RCA 7265
(AS MEASURED BY PERKIN-ELMER)

Tube Code No.	Anode Sens. (a/ℓ)***	Cathode Sens. ($\mu a/\ell$)***	Anode Dark Current* (Nanoamps or Equiv. Lumens)	Cathode Dark Current (Amperes)	Temperature (°C)
11.1.407	3160	145	8×10^{-12} $.247\times10^{-12}$	1160×10^{-18} 35.8×10^{-18}	+25 -70
6.2.185	1000	141	20×10^{-12} $.2\times10^{-12}$	2820×10^{-18} 28.2×10^{-18}	+25 -70
6.2.183	1070	95	4×10^{-12} $.6\times10^{-12}$	380×10^{-18} 57×10^{-18}	+25 -70
6.2.173	2500	142	13×10^{-12} $.08\times10^{-12}$	1845×10^{-18} 125×10^{-18}	+25 -70
6.2.154	1760	126	56×10^{-12} $.51\times10^{-12}$	7060×10^{-18} 64.3×10^{-18}	+25 -70
2.2.417	3800	134	20 na 2 na	705×10^{-18} 70.5×10^{-18}	+25 -70
12.1.41	960	123	18 na .15 na	2300×10^{-18} 19.2×10^{-18}	+25 -70
2.2.440	4500	135	22.6×10^{-12} .6 na	3050×10^{-18} 18×10^{-18}	+25 -70
2.2.537	2780	102	4.1×10^{-12} 1.0 na	418×10^{-18} 36.7×10^{-18}	+25 -70

Average cathode current at 25°C**: 21.90×10^{-16}

Average cathode current at -70°C: 0.505×10^{-16}

*Tubes were specifically selected for low dark current and spatial uniformity. Spatial uniformity was ±20% from nominal value over a 1-inch diameter photocathode area.

**This is almost identical to that quoted (16×10^{-16}) for the EMI S20 9558 @ 25°C.

***Utilizing a 2870°K (color temperature) tungsten light source.

(4) The vehicle can predict earth location with an accuracy in the order of one or two degrees.

The first rather basic question is whether the receiver can have a sufficiently wide field of view so that the earth beacon can be acquired without resort to narrow fields of view and scanning techniques. Considering, therefore, that the system's field of view is one square degree, the S/N ratio (including noise in signal, noise due to expected background illumination, and detector noise) shall be computed for a 10^8 mile range. According to Figure 7-2, the signal power density at the receiver is 2.1×10^{-18}, corresponding to a received power of 2.1×10^{-14} watts. The maximum earthshine irradiance at this distance from Figure 7-23 will be:

$$\frac{1.5 \times 10^{-5} \ (238{,}000)}{(10^8)^2} = 8.5 \times 10^{-11} \text{ watts/cm}^2/\mu \ ,$$

indicating that the earthshine power received will be a maximum of 8.5×10^{-7} watts/μ or 8.5×10^{-11} watts/Å. The assumption that only a one square degree of stellar background exists, in addition to earthshine, leads to an additional component of received power which is (from Figure 7-14) 8×10^{-14} watts/cm^2/μ, representing a received power of 8×10^{-10} watts/μ or 8×10^{-14} watts/Å.

For this situation the contribution from the starfield is one thousand times less than earthshine and can be neglected. An RCA 7265 uncooled photosensor (from Figure 7-27) used as a photodetector, will contribute an additional 8.3×10^{-13} watts of equivalent input power, and operation at -70°C could reduce this to 2×10^{-15} watts equivalent input at 6328Å. Table 7-4 summarizes these results for systems using various spectral filters and phototube temperatures, taking into account estimated spectral filter losses.

TABLE 7-4

RELATIVE POWER LEVELS AT PHOTODETECTOR FOR 6328Å OPERATION

Condition / Component of Power at Detector (watts)	1 PMT @ 25°C, 1Å Spectral Filter	2 PMT @ 25°C, 0.1Å Spectral Filter	3 PMT @ -70°C, 1Å Spectral Filter	4 PMT @ -70°C, 0.1Å Spectral Filter
Signal	10^{-14}	2×10^{-15}	10^{-14}	2×10^{-15}
Earthshine	4.2×10^{-11}	8×10^{-13}	4.2×10^{-11}	8×10^{-13}
Stellar Power	4×10^{-14}	8×10^{-16}	4×10^{-14}	8×10^{-16}
PMT (7265)	8.3×10^{-13}	8×10^{-13}	2×10^{-15}	2×10^{-15}

NOTES: Transmissions of 1Å and .1Å spectral filters have been assumed as 50% and 10%, respectively. Atmospheric transmission has been assumed as unity.

The calculated signal-to-noise ratios for conditions one through four of Table 7-4 are 0.6, 0.62, 0.607, and 0.875, respectively (based on Equation (3), page 7-5, a $\Delta f = 1/2$ cps ($\Delta t = 1$), and an S20 quantum efficiency of 5%). These results lead to the following conclusions for the assumed system:

(1) Reduction of spectral filter width need not result in a substantial increase of S/N ratio, because PMT dark current equivalent power is constant and the total photon arrival rate is decreased due to higher filter losses, thus, tending to lower S/N ratio.

(2) An increase of beacon power to 10 watts will increase signal-to-noise by a factor of ten for the same bandwidth or will allow bandwidth to be increased by a factor of one hundred while maintaining the same S/N ratio. Alternatively, both bandwidth and S/N ratio could be increased.

(3) The total field of view of the system can be substantially decreased without noticeable effect on S/N ratio since starfield background contributions are very small. Hence, acquisition can be performed with a large field of view and subsequent efforts to increase S/N ratio by field narrowing techniques will be largely ineffective.

(4) Earthshine input power can be reduced only by reducing the field of view (FOV) to less than the 16-arc-second apparent earth diameter at 10^8 miles. Roughly speaking, reduction of the FOV to 8 (or 4) arc-seconds will result in S/N ratio improvement factors of two (or four) since noise is mainly determined by earthshine input power. S/N ratio improvement with range reduction will be substantial as range is reduced below that at which the tracking FOV is equivalent to the earth's angular subtense. At larger ranges S/N ratio should remain constant.

(5) System operation at approximately 8400Å would decrease earthshine input by a factor of less than two (refer to Figure 7-16), but photosensor dark current equivalent would increase by a factor of at least five. While there are more photons/sec corresponding to 1 watt at 8400Å, an overall loss in S/N ratio should be expected since quantum efficiency will be at least ten times less.

(6) More accurate ground prediction of vehicle angular position would allow a S/N ratio increase, through reduction of beamwidth, to attain higher signal power density at the receiver. It is doubtful, however, that this will lead to ratio improvement factors exceeding four.

(7) Larger diameter receiving apertures, in all four cases considered above, will increase S/N ratio at least proportionally due to increasing the total photon arrival rate.

(8) Smaller PMT photocathodes will increase the S/N ratio appreciably only when phototubes are not cooled and narrow spectral filters are being used (viz: in case 2 the S/N ratio could be increased to a maximum of $.62 \times \sqrt{2} = .875$, identical with case 4).

(9) Inclusion of optical heterodyning apparatus should result in much better signal-to-noise ratios since very small spectral bandwidth is achieveable without further reduction of photon arrival rate, as in the case of the spectral filters assumed above. Further, it is theoretically possible to increase the S/N of the foregoing examples, through use of high local oscillator power, to effectively approach sensor conditions corresponding to higher quantum efficiency. With this approach, local oscillator shifting will be required to compensate for the Doppler shift expected ($\approx$ .3Å) due to vehicle velocity with respect to earth. Such shifts appear prohibitively large compared to those available from present lasers (viz: $\approx$ .06Å utilizing Zeeman Effect), while in the case of narrow spectral filters such shifts are readily produced by thermal control. Another approach is to tune the IF channel, but even the use of traveling wave photomultiplier tubes (3,000-megacycle response) allows only a 0.06Å shift.

(10) Without earthshine, the signal-to-noise ratio can be large enough to permit direct beacon detection with large stellar background fields. With earthshine conditions which result in low beacon detection signal-to-noise ratio, the earth can be located with earthshine sensors.

The possibility of coronal light background exists only for conditions where earthshine is essentially zero (refer to Figure 7-12). Let us consider, therefore, what coronal area will introduce the same quantity of light as produced by earthshine in the previous four systems since, under this condition, the former S/N ratios are directly applicable.

At 6328Å the solar irradiance is 0.17 watts/cm^2/μ (Figure 7-11) at 1 AU where the sun's angular subtense is 32 arc-minutes. The maximum earthshine irradiance at 10^8 miles ($\approx$ 1 AU) and 6328Å is 8.4×10^{-11} watts/cm^2/μ. At this distance the earth subtends 16 arc-seconds. Hence, light from the photosphere must be reduced by $\left(\frac{8.4 \times 10^{-11}}{.17} = .5 \times 10^{-9}\right)$ in order to be equivalent to earthshine. Such a brightness reduction occurs (Figure 7-12) at a distance of 6.4 solar radii ($\approx$1.68°) from the center of the sun and four times this brightness reduction occurs at 12 radii ($\approx$3.2°). It is concluded that a half degree (or one degree) FOV can be used during initial acquisition without additionally degrading S/N* if the edge of the field does not approach within 1.68° (or 3.2°) of the sun's center. This does not appear to be a significant limitation. In contrast with the case of earthshine background, subsequent field narrowing will significantly improve the signal-to-noise ratio.

A second system in which the earth beacon frequency is 8400Å shall now be considered. Since coronal light and earthshine are assumed to have nearly the same spectral distribution, the preceding comments related to coronal effects are also relevant here. Table 7-5 summarizes the results for this case, based on the same assumptions as Table 7-4.

*The basic assumption is that coronal light induced degradation should not exceed that for the case of maximum earthshine.

TABLE 7-5

RELATIVE POWER LEVELS AT PHOTODETECTOR FOR 8400Å OPERATION

CONDITION	Case 1 / Case 2 PMT AT 25°C		Case 3 / Case 4 PMT AT -70°C	
Component of Power at Detector (Watts)	1Å Spectral Filter	0.1Å Spectral Filter	1Å Spectral Filter	0.1Å Spectral Filter
Signal	10^{-14}	$2x10^{-15}$	10^{-14}	$2x10^{-15}$
Earthshine	$3x10^{-11}$	$6x10^{-13}$	$3x10^{-11}$	$6x10^{-13}$
Stellar Power	$2.5x10^{-14}$	$5x10^{-16}$	$2.5x10^{-14}$	$5x10^{-16}$
PMT (EMR)	$2.2x10^{-8}$	$2.2x10^{-8}$	$1.1x10^{-14}$	$1.1x10^{-14}$

The signal-to-noise ratios in the first two cases are negligible, while those for cases 3 and 4 are 0.213 and 0.302, respectively. An increase of power by a factor of 10 (or 100) would raise these S/N ratios to 2.13 and 3.02, respectively (or, accomplish this end and also allow simultaneous increase of bandwidth from 1/2 cps to 50 cps). The 8400Å systems examined above appear to be the most practical since 3- to 4-watt Ga As lasers are a reality, while current He Ne lasers are in the order of 200 milliwatts. For the specific case of a 4-watt 8400Å earth beacon and a vehicle following a trajectory to Mars, the earthshine will be that corresponding to an earth-illumination phase exceeding 90 degrees. Under such circumstances the S/N ratio will be increased at least 1.78 times due to lower earthshine and approximately four times due to higher laser power. The S/N ratio during acquisition can thus exceed 2.14 for a 1/2-cps bandwidth. This is great enough to detect the beacon and commence field narrowing without beacon loss. As the field is reduced, excluding more and more

earthshine, pointing servo bandwidth can be increased to avoid beacon loss due to high frequency torque disturbances which, being of small amplitude because of system inertia, would otherwise cause beacon loss for narrow field conditions.

SECTION VIII

OPTICAL COMMUNICATIONS

8.1 GENERAL CONSIDERATIONS APPLICABLE TO DEEP-SPACE AND SATELLITE COMMUNICATIONS

An optical communications system in a space application must meet a number of diverse requirements. Foremost among these is the requirement that it permit reliable communications over interplanetary distances at information rates substantially greater than those possible utilizing microwave systems. As indicated earlier in the introduction to this report, the development of an optical communications system for a deep-space application is justified only if it can be demonstrated that the advantages it enjoys overshadow the inherent difficulties of precise acquisition and tracking.

Although the potential afforded by broadband optical communications has long been recognized, the problem of achieving the practical implementation of such a system has yet to be completely analyzed.

It is necessary to fully evaluate the promising transmission, modulation, and detection techniques against the particular constraints imposed by a space application. These constraints are: minimum size, weight, and power consumption and high performance and reliability in a space environment. The comparatively extensive experience with microwave systems can only partly be applied by analogy to optical communications. At the low signal levels characteristic of deep-space communications, the quantum nature of light requires the use of new analytical tools to evaluate or predict performance. Techniques applicable to

the analysis of continuous channel microwave communications must be modified for the case of optical communications.

This section of the report will introduce criteria for judging the performance of an optical communications system, together with a procedure for comparing different optical communications techniques. Several possible modulation techniques are evaluated in terms of communication performance and hardware implementation.

One particular optical communications system is analyzed numerically both to illustrate the analytical procedures involved and to demonstrate the order of performance which can be expected. Both the deep space and synchronous orbit cases are treated. In no sense does this preliminary communications system analysis represent an optimum choice.

In addition, another optical communications system is described which appears as a suitable candidate for the synchronous satellite case where high signal levels are possible.

8.2 INFORMATION CAPACITY OF AN OPTICAL CHANNEL

In order to meaningfully assess the capability of various optical modulation and detection schemes, it is necessary to establish a theoretical standard for comparison. Analytical approaches dealing with the information capacity of a quantum channel have only been investigated in recent years.

J. P. Gordon[38] has considered the theoretical information capacity of an optical communications channel and has taken into account the quantum high-frequency effects which are not dominant in a lower frequency r.f. channel.

Gordon has shown that the maximum rate at which information can be transmitted over a single quantum channel can be expressed as:

$$C_W = \Delta f \log_2 \left[1+\frac{P_s}{P_b+h\nu\Delta f}\right] + \left[\frac{P_s+P_b}{h\nu}\right] \log_2 \left[1+\frac{h\nu\Delta f}{P_s+P_b}\right] - \frac{P_b}{h\nu} \log_2 \left[1+\frac{h\nu\Delta f}{P_b}\right]$$

This is the capacity of an electromagnetic wave, C_W, expressed in bits per second as a function of:

(1) Channel bandwidth, Δf cps

(2) Average signal power, P_s

(3) Average noise power, P_b

(4) Carrier frequency, ν cps.

It is assumed for the derivation of C_W that the noise is additive white noise and that the available average signal power is attained when the signal has the characteristics of white noise. The values of P_s and P_b used in the equation for C_W are all referenced to the optical receiver input.

It is interesting to note that if the noise power P_b is much greater than $h\nu\Delta f$, C_W approaches the classical channel capacity formulation:

$$C = \Delta f \log_2 \left[1+\frac{P_s}{P_b}\right]$$

If there is no additive noise, i.e. $P_b = 0$, and the signal is much larger than $h\nu\Delta f$, one obtains an approximate equivalence to the above classical formulation by assuming the presence of an equivalent "zero-point" noise power, $h\nu\Delta f/e$, where e is the natural logarithm base.

It is necessary to point out that the above expression for C_{wave} is limited to waves existing in a transmission system for which only a single transmission mode of the field is used.

For the case considered below, of pulse code modulation utilizing left and right polarization, an analogous expression for the wave capacity must

be derived. This is true since the analysis by Gordon does not take into account the information obtained from the knowledge of field polarization.

Work is currently in progress on the derivation of a wave capacity expression for this case which will permit an evaluation of the information extraction ability of this modulation technique.

8.3 SIGNAL AND NOISE LEVELS AT THE OPTICAL RECEIVER

The average power, P, radiated by the transmitting telescope depends upon the choice of laser transmitter power, modulation techniques, and the optical efficiency of the transmitting telescope. The signal energy density at the receiving telescope aperture depends upon the atmospheric transmission, the range and the divergence of the transmitted beam. The amount of signal collected depends upon the receiver aperture.

Finally, the signal having an average power, P_s, arrives at the detector after suffering losses as it passed through the receiver optics and pre-detection noise filter. The receiver is also subject to noise due to a number of background sources previously described in detail in this report. In addition to the above attenuation factors, the average noise power, P_b, at the receiver detector is further limited by the narrow bandpass of the pre-detection noise filter and the field stop which restricts the receiver field of view.

The following equations express P_s and P_b in terms of these factors. The signal power may be expressed as:

$$P_s = P_i \times A_r \times \tau_o \tau_f$$

where

P_i = power density incident on the receiving telescope aperture;

A_r = area of the receiving telescope aperture equal to $\frac{\pi D_r^2}{4}$ where D_r is the diameter of the receiving aperture;

τ_o = optical transmission of the receiving telescope; and

τ_f = transmission through the narrow-band pre-detection filter.

P_i, in turn, can be written as:

$$\frac{4KP}{\pi R^2 \alpha_t^2} \tau_A$$

where:

K = the factor converting uniform power density to that for a circular diffraction pattern at the half-width point of the central maximum. (K=0.45);

R = range;

P = power radiated by the transmitter;

τ_A = atmospheric transmission; and

α_t = transmitted angular beam divergence which may be considered diffraction limited for transmission from space to earth, i.e., $\alpha_t = 1.22 \frac{\lambda}{D_t}$ where D_t is the diameter of the transmitting aperture.

Rewriting the expression for P_s and grouping factors yields:

$$P_s = \left[\frac{K}{(1.22)^2} \right] \times \left[\frac{D_t^2 D_r^2}{R^2} \right] \times \left[\frac{P \tau_A \tau_o \tau_f}{\lambda^2} \right]$$

(geometric factors) (wavelength dependent factors)

for a ground station receiving a signal from space, and:

$$P_s = \left[K \right] x \left[\frac{D_r^2}{R^2 \alpha_t^2} \right] x \left[P \tau_A \tau_o \tau_f \right]$$

(geometric factors) (wavelength dependent factors)

for a space station receiving a ground transmission where α_t is not necessarily diffraction limited, but has a minimum value of about three arc-seconds due to atmospheric effects.

The parameters involved in the expression for received average noise power P_b, may also be divided into the same two categories:

$$P_b = \left(\frac{\pi}{4} \right)^2 x \left[D_r^2 \alpha_r^2 \Delta\lambda \right] x \left[N_\lambda \tau_o \tau_f \right]$$

(geometric factors) (wavelength dependent factors)

where:

α_r = receiver angular field of view;

$\Delta\lambda$ = pre-detection filter bandpass; and

N_λ = spectral radiance of the noise sources.

If a photomultiplier tube is used as the photodetector, then the rates at which signal and noise photoelectrons, n_s and n_b respectively, are generated by the cathode surface is given by:

$$n_s = \frac{P_s}{hc/\lambda} \epsilon$$

$$n_n = \frac{(P_b + P_D)}{hc/\lambda} \epsilon$$

where:

P_D = radiant input power equivalent to photomultiplier dark current;

ϵ = detector quantum efficiency;

h = Planck's constant; and

c = velocity of light.

Both the quantum efficiency and the dark current equivalent power are strongly wavelength dependent. The quantum efficiency alone can vary from a fraction of 1 percent for ultraviolet wavelengths to nearly 100 percent for super-cooled detectors in the infrared region. In addition, P_D is greatly dependent on the temperature of the photomultiplier tube.

8.4 SELECTION OF OPTICAL SYSTEM PARAMETERS

This section presents a possible systematic procedure for choosing the optical system parameters which meet the requirements for a particular space application.

It appears necessary to first examine potential laser transmitters to determine the applicable characteristic emission frequencies and maximum power output associated with each. Latitude in this selection is necessary to allow for the rapid change in the state of the art. Engineering judgment must be employed at this step to reject those sources which are obviously unsatisfactory in terms of power consumption, weight, cost, or reliability.

In order to determine the average signal and noise power incident on the detector, it is necessary to select values for the factors involved in the receiving and transmitting telescope design. These are chiefly: receiver and transmitter aperture diameters, transmitter beam divergence, receiver field of view, and optical rejection filter bandwidth. These parameters should be clearly achievable but not necessarily the most advantageous for the final application. A more detailed consideration of these factors is involved in the final choice.

The wavelength dependent factors necessary for the calculation of the average signal and noise power incident on receiver photodetector can be evaluated for each potential transmitter wavelength. Sufficient experimental data and analytical methods exist which permit an evaluation of the following factors: optical transmittance of the transmitting and receiving telescope, transmittance of the atmosphere, background spectral radiances, and noise filter transmittance.

It is then necessary to identify possible encoding and decoding systems, again using engineering judgment to make a preliminary selection.

In accordance with a potential user's requirement for channel capacity and error rate, the bandwidth required for each candidate system can be evaluated for each potential laser transmitter frequency, and the associated values of P_s and P_b may be referenced to the receiver input. The subset of bandwidths calculated in this manner will be further limited by hardware considerations.

At this stage, the error rates are computed for each candidate modulation scheme and remaining possible laser transmitter frequencies. Only those communications systems for which the computed error rate is less than or equal to the desired error rate are retained.

The above procedure will have to be repeated for other initial choices of system parameters such as those involved in the transmitter and receiver telescope design.

The communications systems which meet or exceed the desired performance criteria must be more closely evaluated in terms of their comparative desirability concerning cost, size, weight, power consumption, and reliability. In addition, it is necessary to insure that the communications system is compatible with the acquisition and tracking requirements.

8.5 MODULATION SYSTEM CONSIDERATIONS

Candidate Modulation Systems - Two promising candidate modulation systems have been studied in some detail. They are:

(1) Pulse Position Modulation with the highest received pulse marking the pulse position (PPM-HP or briefly, PPM); and

(2) Pulse Code Modulation using left or right circular polarization to mark the binary "one" or "zero" (PCM-PL).

These two systems have been analyzed by other investigators,[39] but we believe the analysis presented here is a suitable point of departure from the previous work for several reasons:

(1) Poisson statistics were used rather than Gaussian statistics. For the optical communication systems from deep space, the photon arrival rate is so low that a Poisson statistical model should be used.

(2) Since this analysis has the benefit of the previous work, the communication system chosen for the analysis is intentionally less conservative in order to permit clear comparisons between one approach or the other (PPM versus PCM).

To illustrate these points specifically, we have analyzed a PPM system in which the the pulse location is marked by the highest pulse received (PPM-HP) and compared the performance of this approach with a PPM system in which the first pulse to exceed a threshold marks the pulse position. The comparison of these two approaches is shown in Figure 8-1. Note the significant advantage of the PPM-HP approach over the PPM-Bias Level approach in the presence of large background radiation. (The cusps in the PPM-Bias Level Curves are due to discrete changes in the bias level in the analysis.) On the basis of this improvement, further study on the PPM and PCM-PL communication approaches was initiated.

The following steps were taken in analyzing the PPM and the PCM-PL systems:

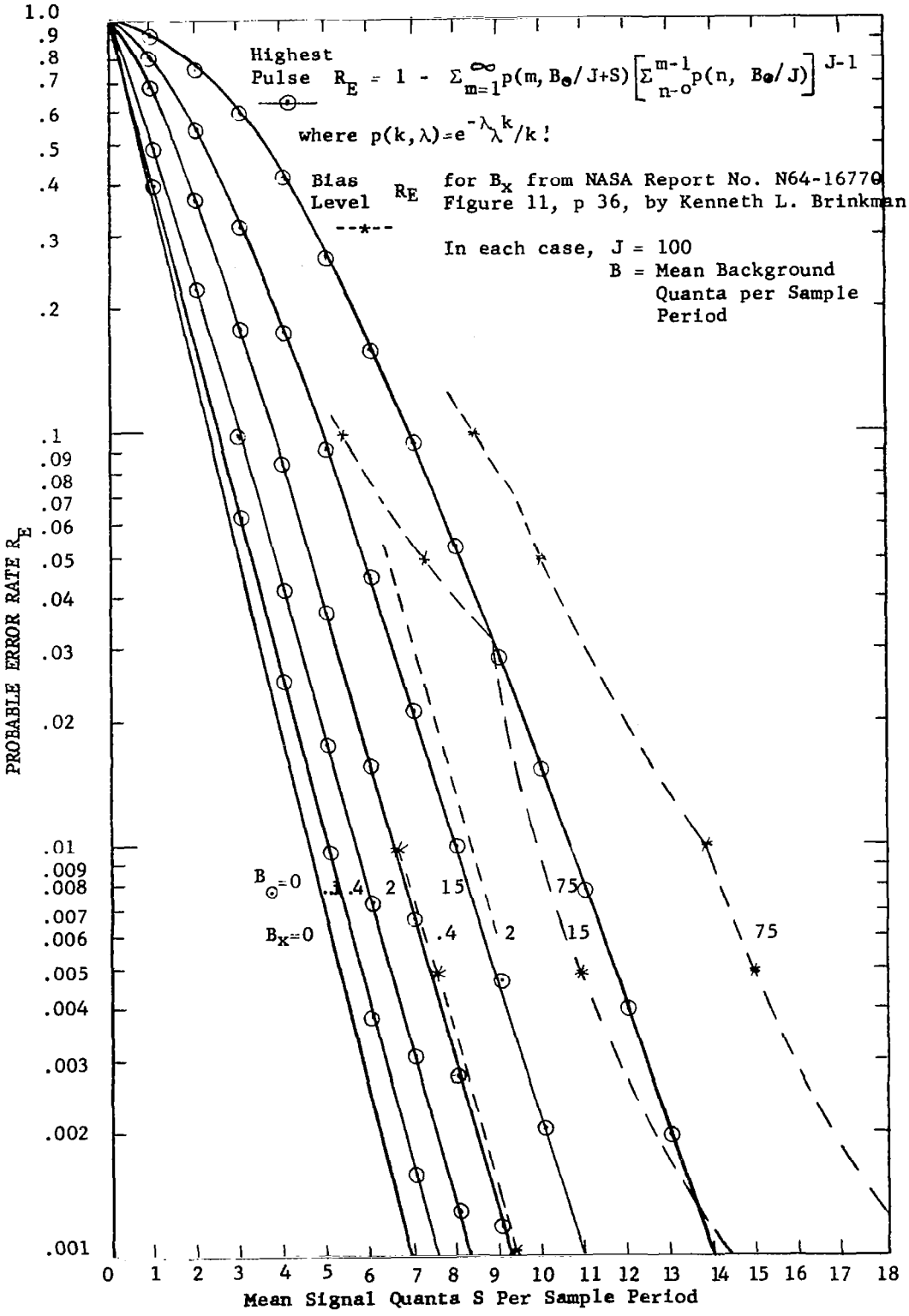

Figure 8-1. Pulse Position Modulation Error Rate Comparison

(1) A near optimal configuration was chosen and a model was defined.

(2) Poisson photoelectron statistics were assumed for both signal and background sources.

(3) An equation for probable error rate as a function of mean number of received signal photoelectrons S per sample period, mean number of received background photoelectrons B per sample period, and a system parameter was derived from each model. These equations are presented and discussed in Appendix D. For PPM the parameter J was the number of distinguishable pulse positions in a sample period as limited by receiver bandwidth. The error rate R_E for PPM was the probability that a wrong pulse position was received in the sample period. For PCM-PL the error rate R was the error rate per bit, i.e., the probability that any particular code bit is incorrectly received. The parameter K for PCM-PL was the number of code bits in a word. One word is to be transmitted for each sample.

(4) Two computer programs were written for each system. One program ("Error Rate Analysis") computed probable error rate as a function of S with B as a parameter for selected values of the system parameter. The other program ("Equal Error Rate Curves") computed the minimum S required to

maintain a selected error rate ±1 percent as a function of B with a selected value of the system parameter.

(5) Computer runs of these programs were made and the results were plotted. See Figures 8-2 through 8-9. Examining the lower portions of all these figures, it will be noted that the logarithm of the error rate approaches asymptotically a state in which it decreases linearly with increasing signal. In all cases the asymptote depends upon the three independent variables, S, B, and K or J. The maximum error rate per bit for PCM-PL is 1/2 for zero signal. Such an error rate corresponds to the recovery of zero information. Of course, one could obtain an equal amount of information by flipping a coin to decide what binary digit is received, and that is precisely analogous to what the system internal noise and the received background quanta actually do when no signal quanta are received! The error rate for PPM is 1 if neither signal nor noise quanta are received, and the information recovered is zero. If no signal quanta are received during a particular sample period there is a slight probability that any background quanta received may mark the correct pulse position. Hence, the error rate drops slightly below 1 when background quanta are received. Operation in the region of high error rates is not anticipated

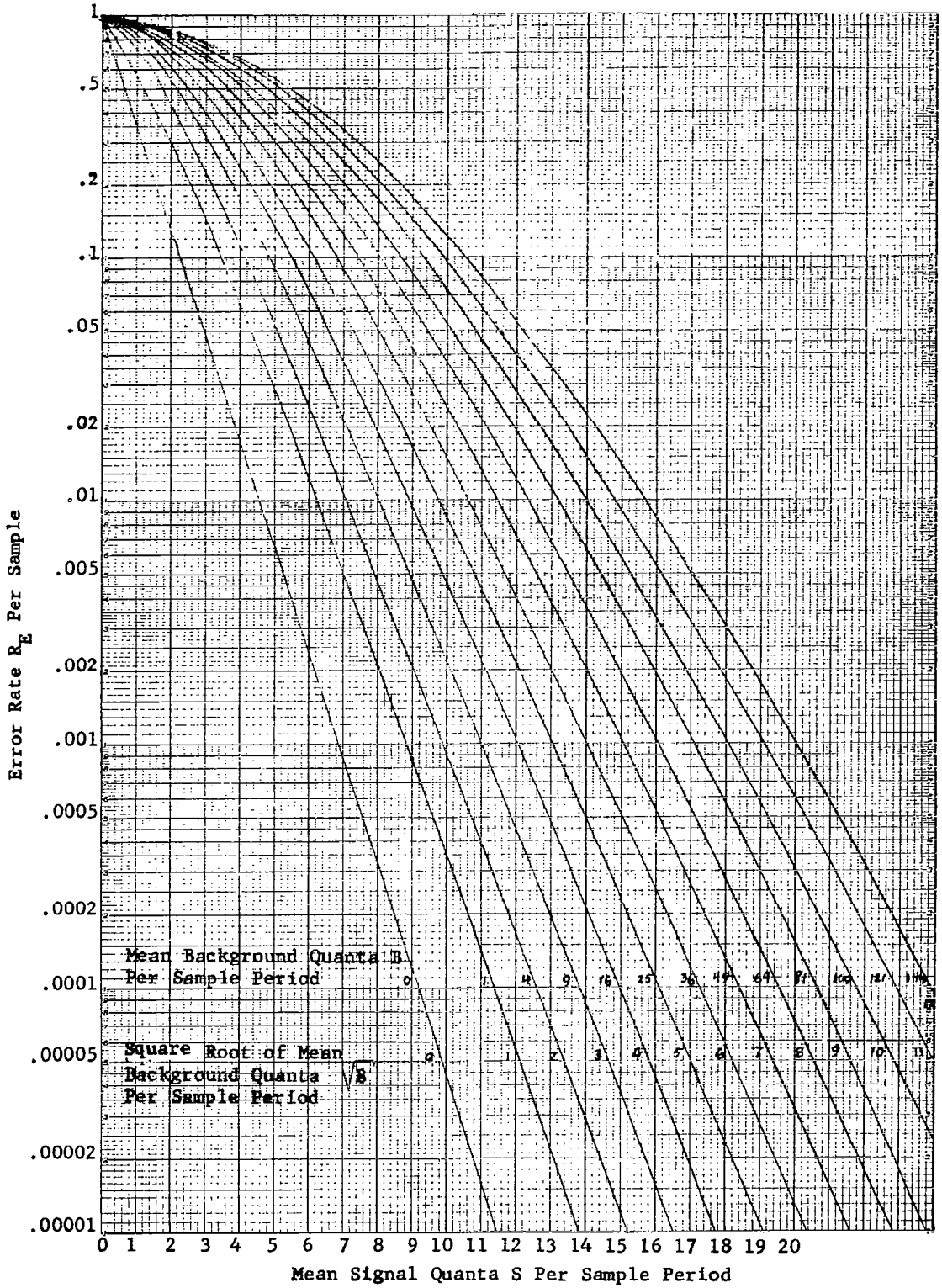

Figure 8-2. Pulse Position Modulation - Highest Pulse Error Rates, 32 Resolvable Positions

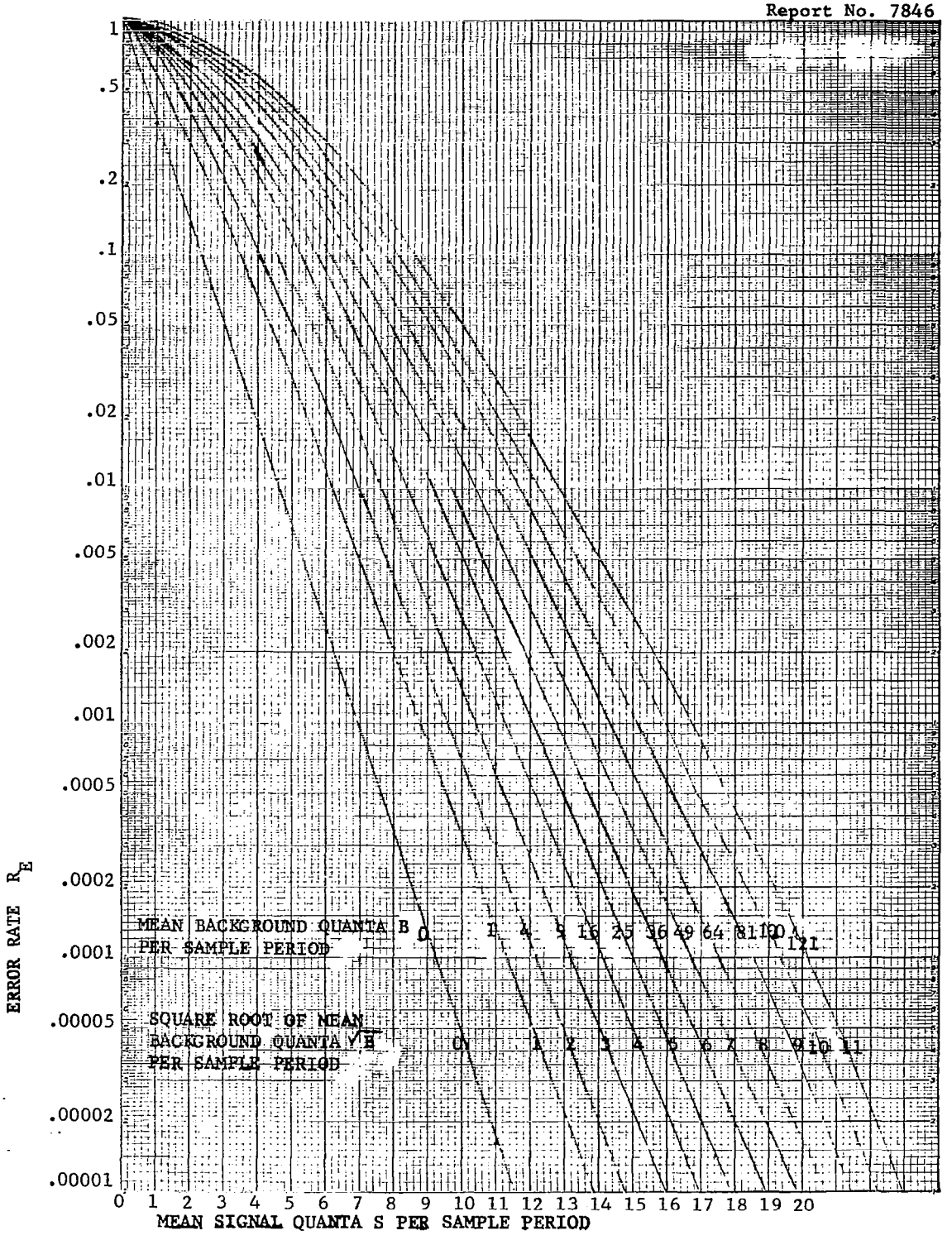

Figure 8-3. Pulse Position Modulation - Highest Pulse Error Rates 64 Resolvable Positions

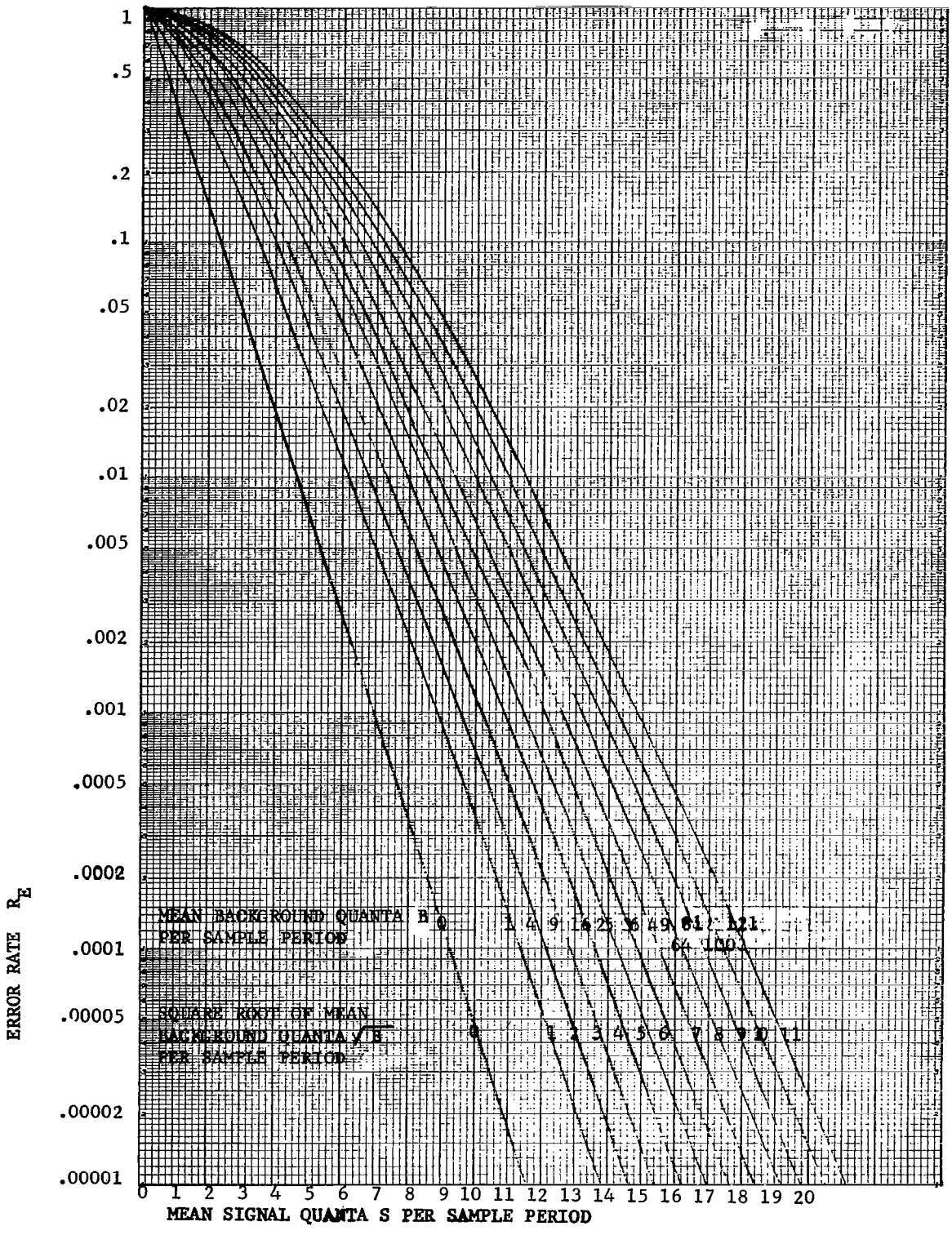

Figure 8-4. Pulse Position Modulation - Highest Pulse Error Rates, 128 Resolvable Positions

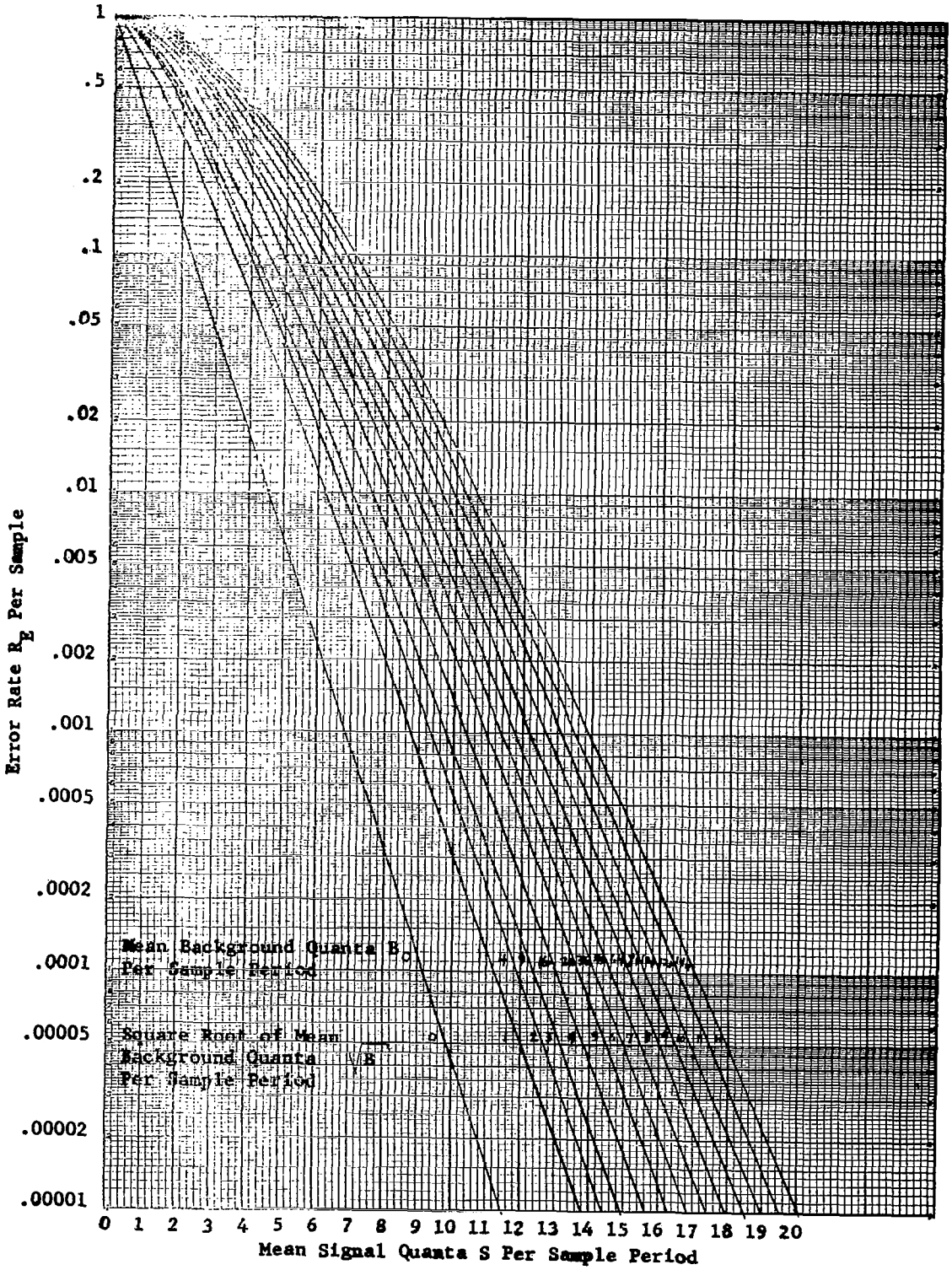

Figure 8-5. Pulse Position Modulation - Highest Pulse Error Rates, 256 Resolvable Positions

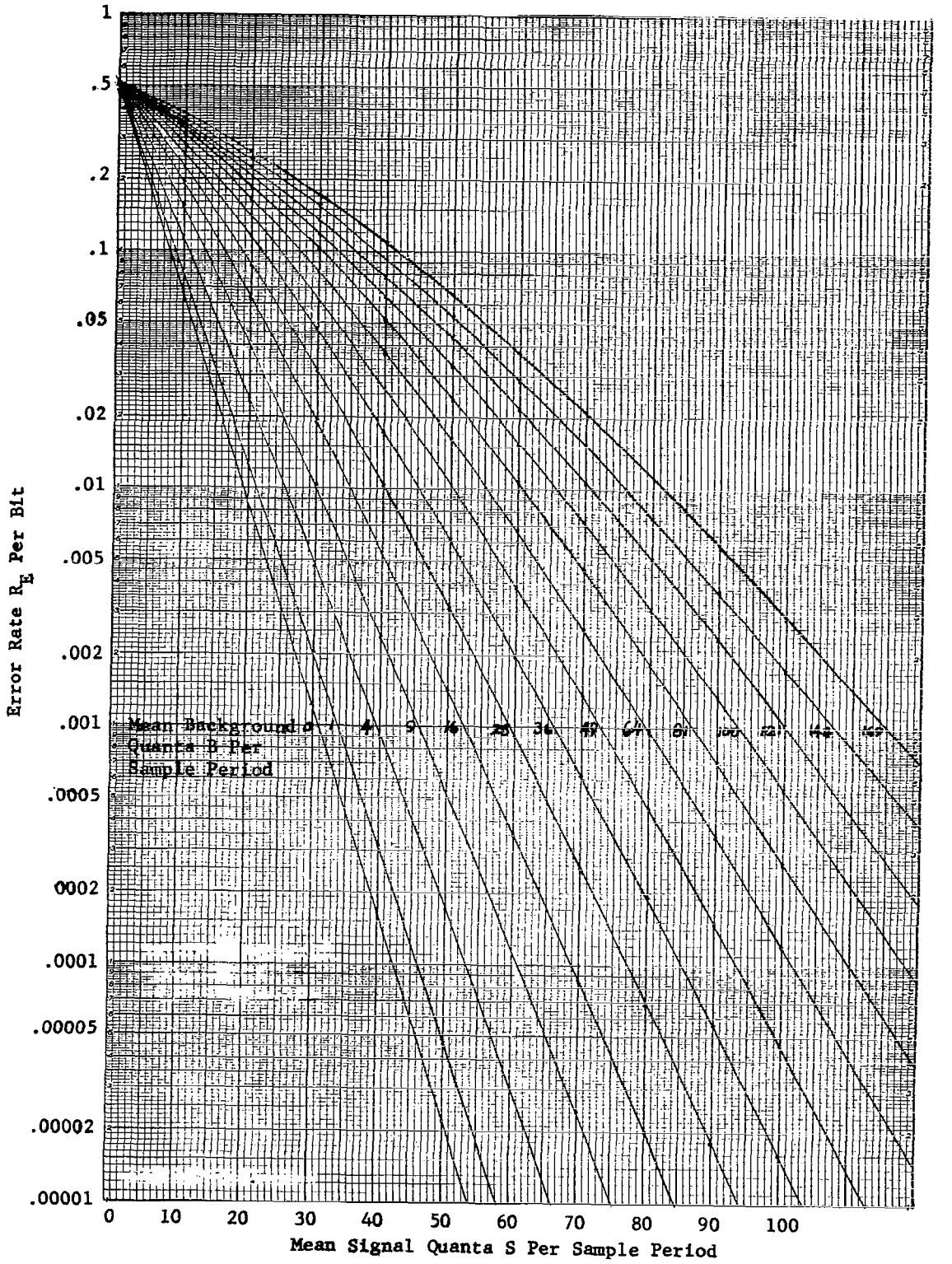

Figure 8-6. Pulse Code Modulation Error Rates, Five-Bit Code

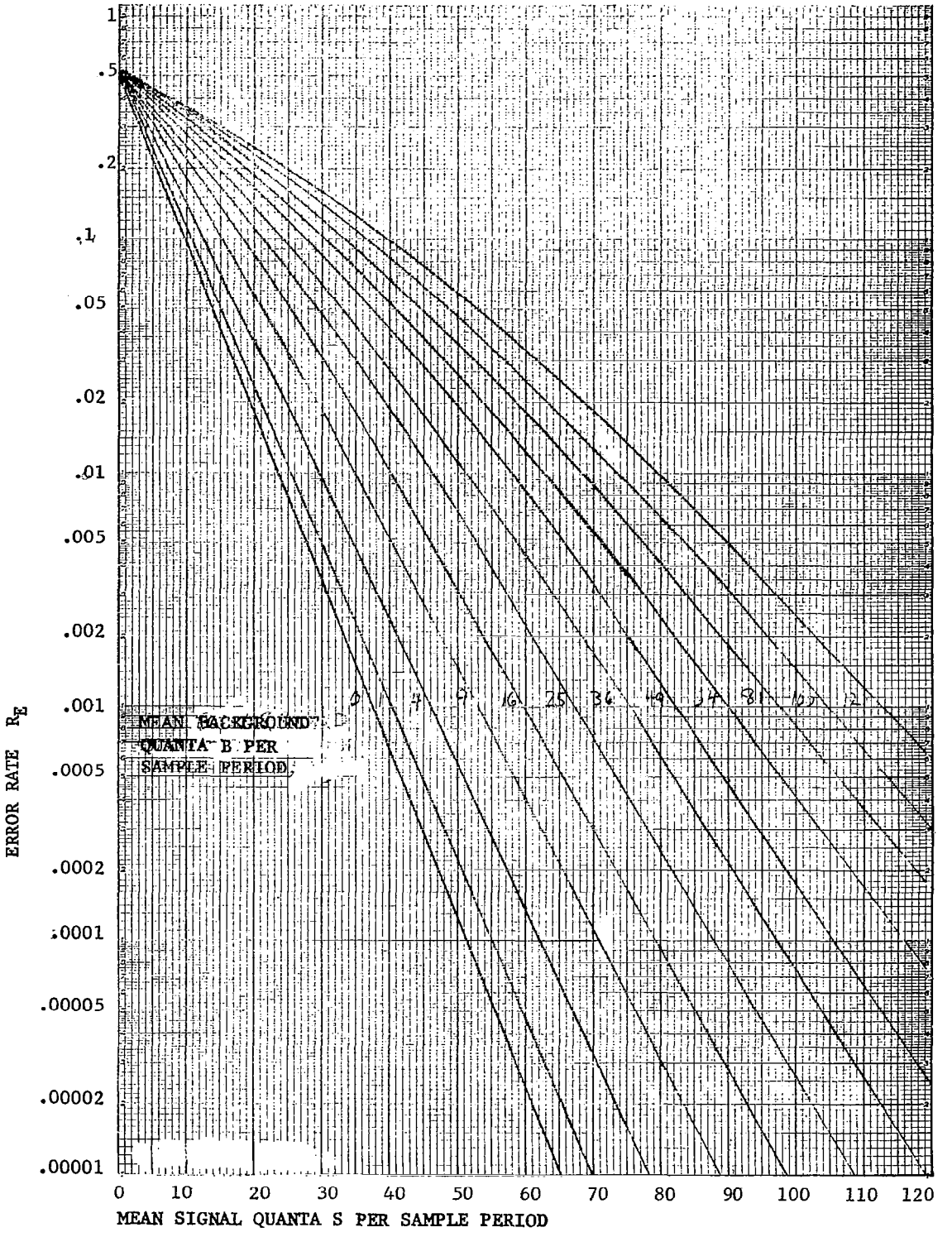

Figure 8-7. Pulse Code Modulation Error Rates, Six-Bit Code

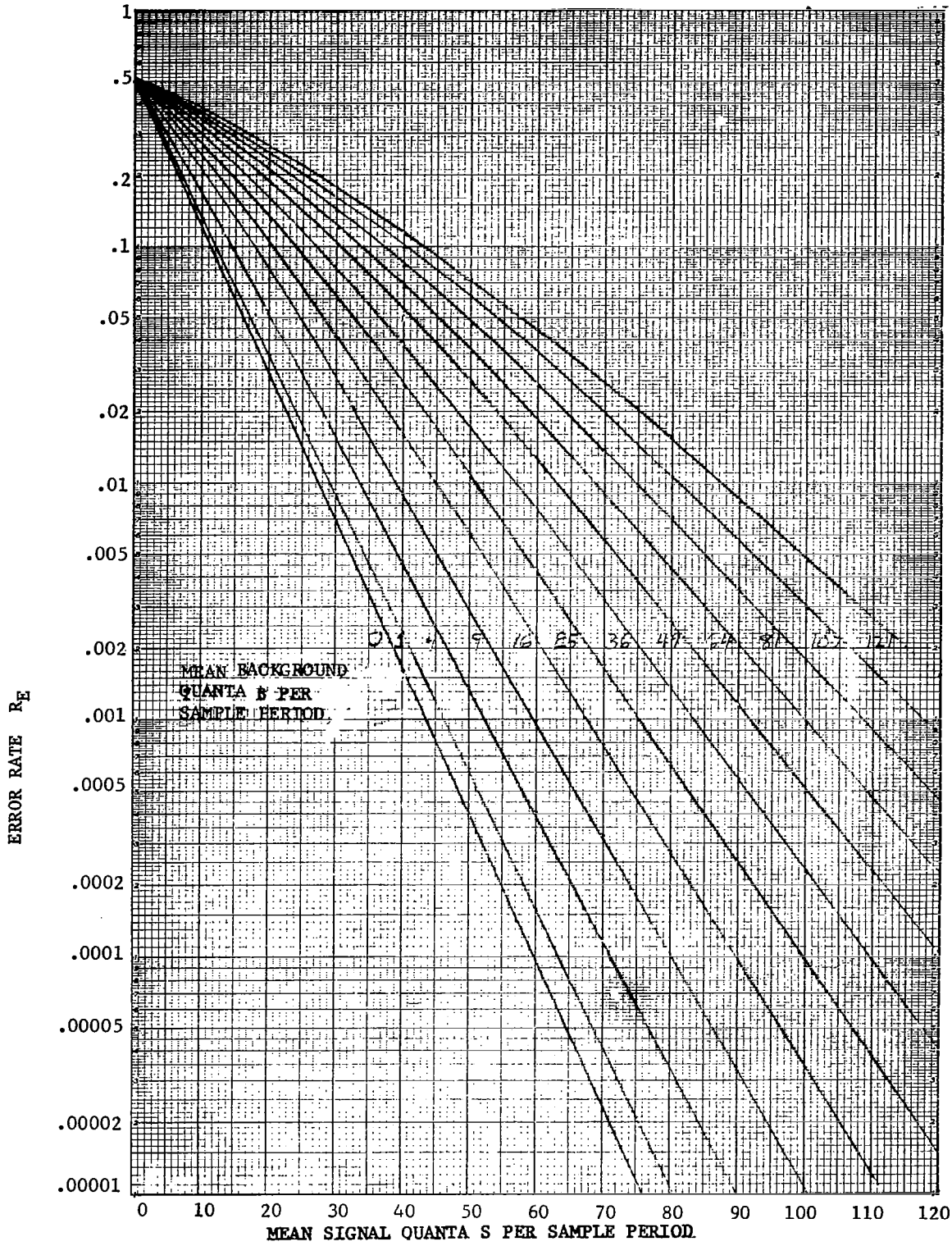

Figure 8-8. **Pulse Code Modulation Error Rates, Seven-Bit Code**

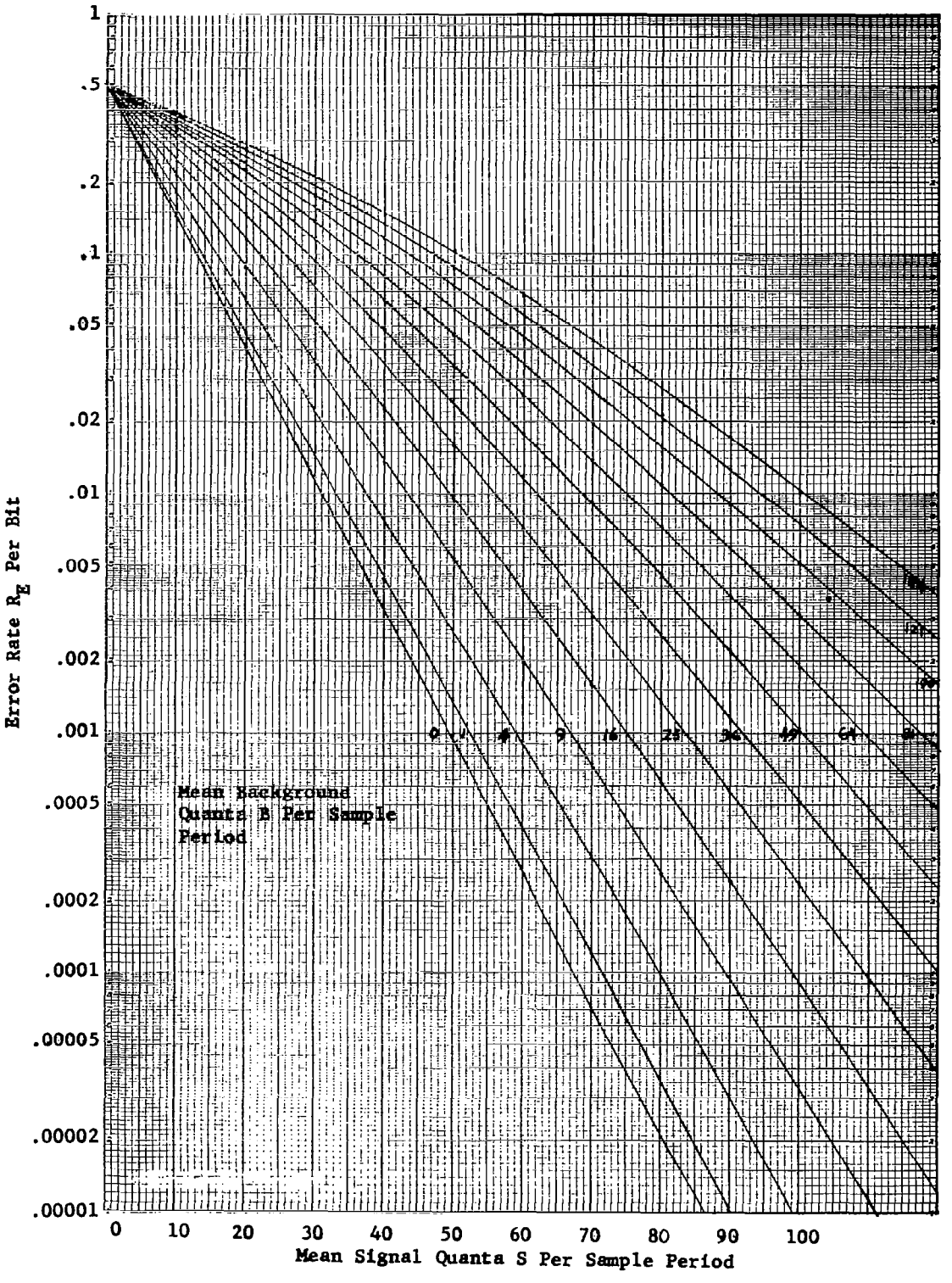

Figure 8-9. Pulse Code Modulation Error Rates, Eight-Bit Code

unless error correcting codes are used, or it is decided to superimpose a pulse amplitude modulated signal upon the PCM-PL or PPM signals with a low maximum frequency. The latter possibility is particularly suited to PPM or PCM-PL, since for both the average signal power is constant, independent of the signal waveform.

(6) Tentative comparisons of these systems were made.

Comparison Considerations - In comparing these systems there are several considerations involved.

(1) Power Limitation - If S for PPM is taken equal to S for PCM-PL, then the systems are being compared on the basis of an average power limitation and no peak power limitation (e.g., with reference to a pulsed solid state laser system). If S for PCM-PL is taken equal to S times J for PPM, then the systems may be compared on the basis of a peak power limitation (e.g., with reference to a gas laser and high speed shutter system).

(2) Bandwidth - For equal sample periods the bandwidth required by J-position PPM can be shown to be $J/K = 2^K/K$ times as great as that required for a K-bit PCM-PL system.

(3) Sample Quantization - For equal sample resolution the number of resolvable positions for PPM is 2^K, when a K-bit code is used with the PCM-PL system.

(4) Information Capacity - The error rate per sample R_E in PPM is not, in general, equal to the error rate R per bit in PCM-PL for equal information capacity. The probability of receiving a PPM sample correctly is $1-R_E$. The probability of receiving a PCM-PL sample correctly is $(1-R)^K$.

It may be desired to compare the signal power required to maintain a specified information capacity for the two systems. If so, error rates for the two systems should be chosen which give an equivalent information capacity. If each system parameter is chosen properly as in (3) above for equal resolution, then the error rates must be chosen for equal equivocation. The choice may be made conveniently by referring to Figures 8-10 and 8-11. For a derivation of the equations plotted in Figures 8-10 and 8-11 refer to Appendix D.

(5) Sample Error Rate - On the other hand, it may be desired to compare the signal power required to maintain equal sample error rates for the two systems. This should also be done for systems with equal sample resolution,

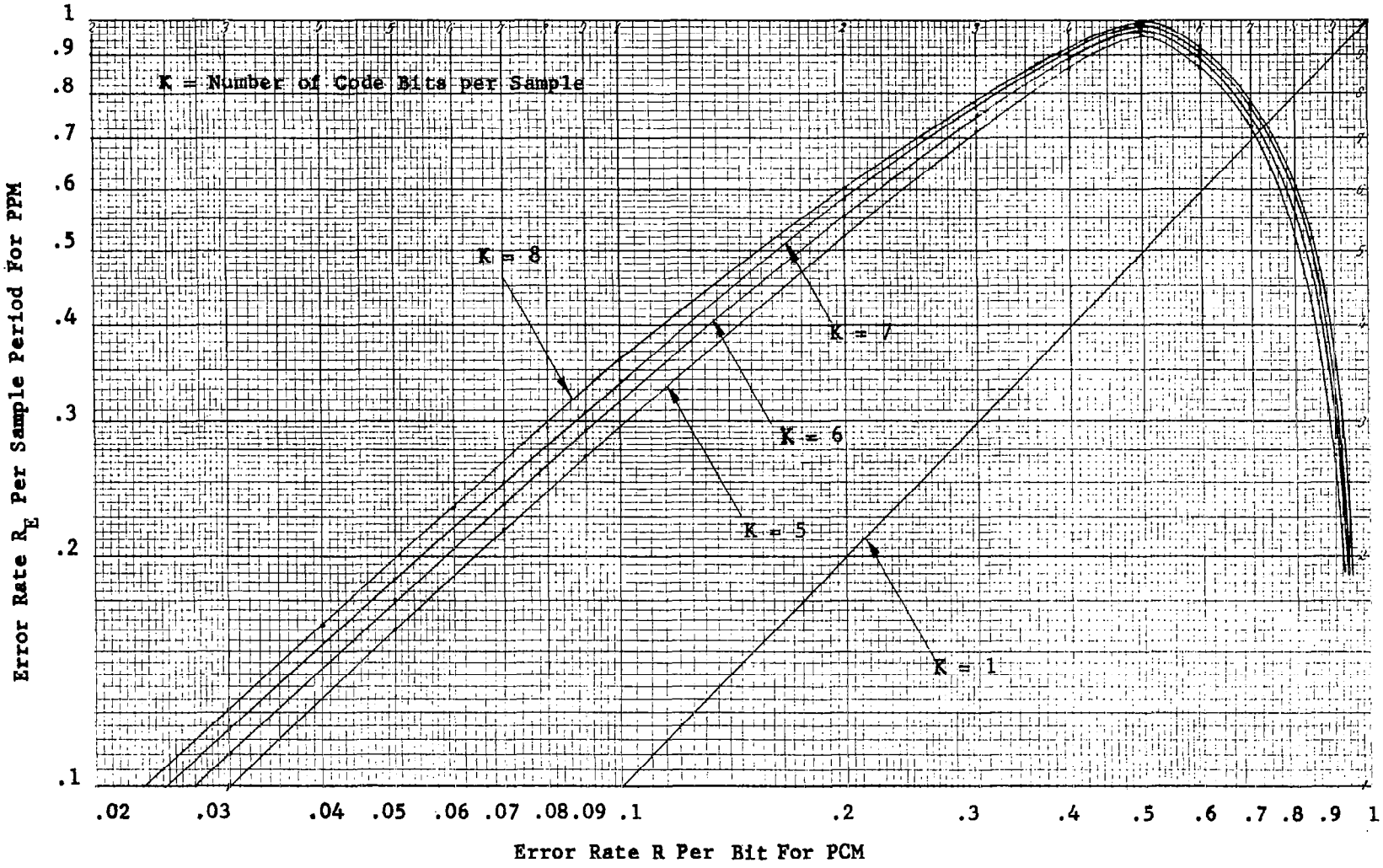

Figure 8-10. Equal Equivocation Curves for PCM and PPM-Large Error Rates

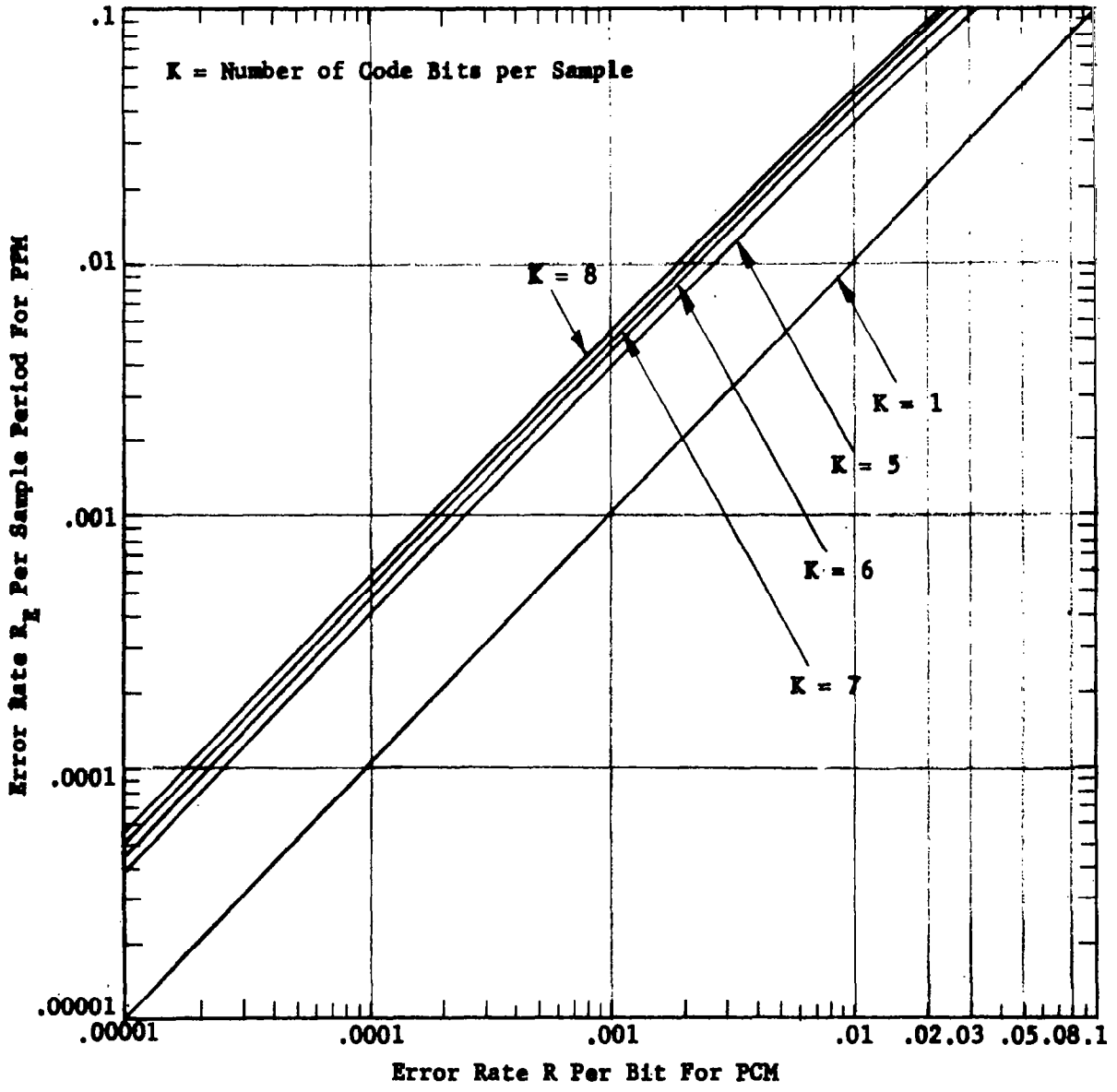

Figure 8-11. Equal Equivocation Curves For PCM and PPM-Small Error Rates

i.e., $J = 2^K$ as above. The probability of error for PPM is R_E and the probability of a sample error in PCM-PL is $R'_E = 1 - (1-R)^K$ (provided an error correcting code is not used).

(6) Realizability and Complexity - Obviously, even if one system may be shown to have many theoretical advantages over the other, the choice of a system is an engineering choice. The choice must be partly based on the relative practicality of the systems with reference to the state of the art at the time of the choice.

Examples of System Comparison - Let us first compare PCM-PL and PPM for the case of equal information capacity and then for the case of equal sample error rates. Refer to Figure 8-12 throughout the following discussion.

It will be necessary to choose a sample period for a quantitative comparison. A 500-nanosecond sample period is chosen because of the following considerations. The OTS requirement is a 10 Mcps optical information bandwidth. The information capacity C of an ideal continuous Shannon communication channel with a signal-to-noise ratio of 1 and a bandwidth of 10 Mcps is:

$$C = \Delta f \log_2 (1 + S/N) = 10 \text{ M bits/sec}$$

Neither PPM nor PCM-PL are continuous communication systems. They are sampled systems, and for optical frequencies and low signal and background levels they are also quantized systems. Hence, their information capacity cannot be calculated with Shannon's formula, and it is meaningless to speak of a signal-to-noise

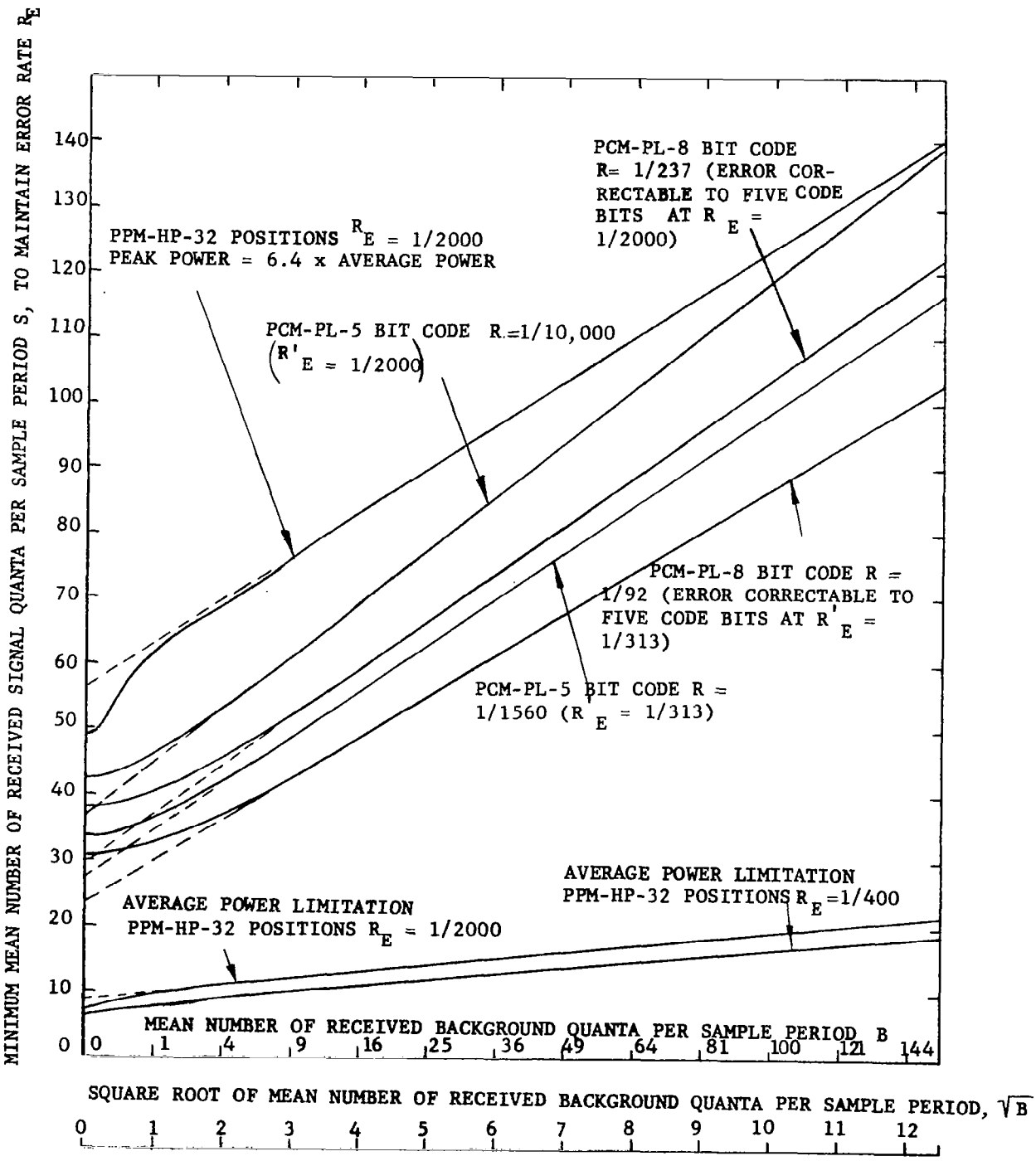

Figure 8-12. Comparison of Pulse Code Modulation - Polarization With Pulse Position Modulation - Highest Pulse

ratio in any ordinary sense. However, PPM and PCM-PL do have a definite information capacity which can be calculated from the entropy of the signal encoding scheme and the equivocation, provided the sample period and some error rate per sample or bit is known. Let us, therefore, choose a sample period for the two systems which gives a 10 M bit/second channel information capacity. For the transmission of television pictures it may be sufficient to transmit every resolution element with only 32 possible gray levels. Let each resolution element constitute one sample, and then $\log_2 32 = 5$ bits per sample will be transmitted. This can be done by using PCM-PL with a 5-bit code, or PPM with 32 resolvable positions. Now, if 2×10^6 samples per second are transmitted, the information transmitted is 10 M bits/second. For a sampling rate of 2 M samples/second the sample period is 500 nanoseconds.

Note that if an analog waveform is to be transmitted with a sampling system the Nyquist sample period should be used to prevent loss of information and waste of power. If the sample period is T, the maximum significant frequency f_{max} in the analog waveform should be no greater than 1/2T. Thus, if $T = .5\mu$ sec, $f_{max} = 1$ M cps.

The optical bandwidth may have to be greater than 10^7 cps to receive recognizable pulses.

Having chosen the sample period, we may now compare PPM and PCM-PL for the two cases desired.

Case I: Equal Information Capacity - Suppose it is desired to transmit samples with an error rate of roughly 1/400. This may be a suitable error rate for TV pictures. Then for 32-position PPM the error rate per sample is just $R_E = 1/400$. The minimum S to maintain R_E for various amounts of background B is plotted in Figure 8-12. Note that for an average power limitation, as shown, all the signal

quanta would have to be transmitted during the pulse time (1/32 of 500 nanoseconds) and none before or after. For equal information capacity with straight 5-bit coding, a PCM-PL system would have to maintain an error rate of R = 1/1560 per bit. This corresponds to an error rate R'_E per sample of 1/313. It would also be possible for the PCM-PL system to transmit eight code bits in the sample period, where the coding is so chosen that all words transmitted may be corrected at the receiver if no more than one of the code bits has been incorrectly received. The sample resolution remains at 32 levels (5 bits) since the extra three bits are error correction bits and do not add information. Then the sample error rate R'_E will not be higher than 1/313 as long as the probable error R per bit is not greater than 1/92. Reference to Figure 8-12 will show that fewer signal quanta per sample period are required to maintain this R for an 8-bit code than for R = 1/1560 and a 5-bit code. However, the required bandwidth has been increased by 8/5, since now eight separate pulses must be transmitted in the same period of time as was allowed for five. The complexity of the coding and decoding equipment has been increased somewhat also.

Case II: Equal Sample Error Rates - Let the sample error rate now be fixed at 1/2000, i.e., $R_E = R'_E = 1/2000$. Suppose a signal having low redundancy is to be transmitted. If an error occurs in a received sample it will then not be possible to correct the sample by referring to the samples immediately preceding or following it. Hence, a low sample error rate may be required. Given that $R'_E = 1/2000$, reference to the formula for R in terms of R'_E in Appendix D gives R = 1/10,000. The equation for the straight line portion of the PCM-PL 5-bit code curve for $R'_E = 1/2000$ in Figure 8-12 is $S = 8.24\sqrt{B} + 35.9$. Arbitrarily choosing S/B = 1 and solving for S we have S = 130. (Note that R may

be maintained equal to 1/10,000 for varying ratios of S to B, depending on the value of B, merely by making S large enough. The ratio S/B = 1 is chosen purely for purposes of illustration.)

If an 8-bit error correcting code is employed, then $R'_E = 1/2000$ implies that R = 1/237. See Appendix D. The equation of the straight line portion of the PCM-PL 8-bit code curve for $R'_E = 1/2000$ is $S = 7.28\sqrt{B} + 30.1$ and S/B = 1 implies that S = 94.6. Note that (130-94.6) x 100%/130 = 27.2% less signal power is required for error correcting coding than for simple coding with equal signal-to-background ratios. As an alternative comparison, if S = 94.6, the error correcting system maintains $R'_E = 1/2000$ with B = 94.6, while the simple coding system cannot maintain $R'_E = 1/2000$ if B is greater than 50.7. Thus the background tolerance for the error correcting system is (94.6-50.7) x 100%/50.7 = 86.6% greater than that for the simple coding system, when S = 94.6. These results are summarized briefly in Table 8-1.

TABLE 8-1

COMPARISON OF SIMPLE CODING AND ERROR CORRECTING CODING

Condition	Five-Bit System	Eight-Bit System With Error Correction	Percentage
S/B = 1	S = 130	S = 94.6	-27.2%
S = 94.6	B ≤ 50.7	B ≤ 94.6	86.6%
Bandwidth Required	F = 1 unit	F = 8/5 unit	60%
Complexity	1 unit	> 1 unit	

We may conclude that the advantage of the error correcting system is only clearly apparent when: (1) background is high and/or signal power is quite restricted; and (2) bandwidth is available.

A curve for 32-position PPM with an average power limitation and R'_E = 1/2000 has been plotted on Figure 8-12 also. Since in PPM all the signal power is concentrated in one pulse, for 32 possible positions and rectangular pulses the peak power is 32 times the average power. (In comparing PCM-PL systems it is not necessary to consider differences between peak power and average power, since for rectangular pulses they are equal.) Gas lasers are likely to be limited by their peak power to no more than about ten times their average power, and even then the average pulse repetition frequency is much too low for the sample rates contemplated. Furthermore, the pulses may not be easily located in the sample period. Giant pulse ruby lasers are limited only by their average power, but once again the pulse repetition rate is much too low for the PPM system envisioned. In addition, a 32-position PPM system requires $\cdot 32/5 =$ 6.4 times more bandwidth than a five-bit PCM system.

If some laser is developed which may be operated with a 1/32 duty cycle and a (say) 2 Mc average repetition rate, then the advantage of the PPM system over PCM-PL is remarkable. It may also be more possible to obtain a laser whose peak power is as much as (say) 6.4 times its average power, with the same duty cycle and average repetition rate as before. (Such a system might be realized if the laser had a duty cycle somewhat greater than 1/32 and a fast shutter were used to shape and precisely locate the pulse.) The curve for PPM-32 positions and peak power = 6.4 x average power shows the minimum required signal for R'_E = 1/2000. For this system only a little more signal power is

required than for PCM-PL-5 bits. Now if a system is found for which peak power = C x average power, where $6.4 > C > 1$, its characteristic will fall between the two PPM characteristics on Figure 8-12, and may give some advantage over PCM-PL. The exact characteristic may be found simply by multiplying S for each point on the PPM-average power limitation curve by C, and plotting the resulting points.

The PPM and PCM-PL systems were analyzed in detail since they are promising candidates for the envisioned optical communications system. The literature has very little modulation systems comparison for any other conditions than Gaussian distributed signal processes operating against additive white Gaussian noise. In particular, analyses of fading effects for the various systems are lacking. It appears that these questions could bear much further investigation. Due partly to its awkwardness the Poisson Distribution has not been used much in analytical investigation. The studies we have presented here of communications systems with a low photon rate were enhanced due to the availability of a digital computer. The area is hardly exhausted and considerably more work must be done before a system is evolved which is identified as near optimum.

8.6 COMMUNICATIONS IN DEEP SPACE

Discussion - Calculations have been carried out to demonstrate the procedure for selecting optical system parameters for communications to and from deep space at interplanetary distances of the order of 100 million miles. A first indication of system performance is also provided by these calculations.

Selection of System Parameters - The system parameters that have been chosen for this initial analysis are presented in Table 8-2, and will be discussed briefly.

TABLE 8-2

Design Parameters for Laser Communications Between a Deep-Space Probe and Earth

Input Parameters	Symbol	Reception on Earth of Space Transmission		Reception in Space of Earth Transmission	
		Day	Night	Day	Night
Range (Statute Miles)	R	10^8		10^8	
Wavelength Received (Å)	λ	6328.		8400.	
Transmitted Power (Watts)	P	0.1		200.	
Transmitted Beam Divergence (Radians)	α_t	$1.22 \frac{\lambda}{D_t}$		1.45×10^{-5} (3 Arc-Sec)	
Diameter of Transmitting Aperture (CM)	D_t	100.		—	
Diameter of Receiving Aperture (CM)	D_R	1000.		100.	
Receiver Field of View (Radians)	α_R	9.7×10^{-5} (20 Arc-Sec)		145×10^{-5} (3 Arc-Sec)	
Atmospheric Transmission (60° From the Zenith)(%)	τ_A	70.(40)		85.(40)	
Optical System Transmission (%)	τ_o	50.		50.	
Pre-Detection Filter Transmission (%)	τ_f	15.(41)		50.	
Pre-Detection Filter Bandpass (Å)	$\Delta\lambda$	0.5(41)		1.0	
Background Brightness Blue Sky at 6328Å $\left(\frac{\text{Watts}}{\text{CM}^2\text{-Ster-}\mu}\right)$	$N_{\lambda B}$	5.0×10^{-3}(42)	0	—	
Background Brightness Earthshine at 8400Å $\left(\frac{\text{Watts}}{\text{CM}^2\text{-Ster-}\mu}\right)$	$N_{\lambda E}$	—		1.2×10^{-2}(††)	~0
Background Brightness Average Starfield Toward Ecliptic Plane $\left(\frac{\text{Watts}}{\text{CM}^2\text{-Ster-}\mu}\right)$	$N_{\lambda S}$	3.3(*) $\times 10^{-10}$		—	
Receiving Photomultiplier Tube		RCA 7265		EMR543C	
Dark Current Radiant Input Power Equiv. @ -70°C (Watts)	$P_{d_{-70°C}}$	2.0×10^{-15}(†)		1.1×10^{-14}(†)	
Dark Current Radiant Input Power Equiv. @ 25°C (Watts)	$P_{d_{25°C}}$	—		—	
PMT Quantum Efficiency (%)	ϵ	5(**)		0.36(**)	

*Derived from Figure 7-14
†See Figure 7-27
**See Figure 7-26
††Derived from Figure 7-7

The space vehicle transmitter is a helium-neon laser which radiates a diffraction-limited beam at 6328Å through a one-meter diameter optical system. Laser transmitters presently exist which are capable of radiating the 100 milliwatts of cw power assumed here.

There appear to be a number of important advantages in sharing one optical system for receiving and transmitting functions in space. Cost and weight are reduced by utilizing a common optical transceiver rather than separate transmitting and receiving telescopes. Precise boresight alignment between the optical axes of the two telescopes required for accurate point ahead is eliminated. Narrow-band pre-detection filtering and two separate widely spaced laser frequencies will substantially reduce the mutual interference.

Thus, the space-borne receiver utilizes the same telescope as a light collector, together with an EMR 543C photomultiplier tube which has an S-1 surface for maximum quantum efficiency at the received wavelength of 8400Å. Values assumed for the optical system transmission and the noise filter bandpass and transmission are realistic. Limiting the receiver field of view to 3 arc-seconds is considered feasible as a means of restricting earthshine, which is the dominant noise source when the receiver views the earth during the day. At night, the thermal radiation from the earth can be shown to be negligible at 6328Å.

The earth station communication system, in turn, consists of a 10-meter-diameter receiving telescope which functions only as a light collector and, therefore, may consist of multiple elements, since precise optical alignment is not required. The received wavelength of 6328Å is detected

with an RCA 7265 photomultiplier tube which has an S-20 surface. A Lyot filter is considered to reject noise at a bandpass half that assumed for the space receiver, since the additional complexity of this device is justified at the earth station for daylight communications. Atmospheric turbulence during the daylight hours and the inability to stabilize the thermal environment will cause large image motion at the ground and require restriction of the field of the receiving telescope to greater than 3 arc-seconds (perhaps as large a field of view as 20 arc-seconds, which is used for these calculations).

In the daytime the dominant noise source is specular radiance of the blue sky, for which a maximum value has been assumed. On a moonless night viewing well off the horizon, the only background noise is due to the star field, for which an average spectral radiance has been computed (see page 7-23 of this report).

Transmission takes place through a separate telescope aperture, but the radiated beam is not diffraction limited because of atmospheric scattering which limits the beam divergence to about 3 arc-seconds. A radiated power of 200 watts at 8400Å is assumed to be possible in the near future through the use of a number of ganged lasers operating in parallel.

A number of factors are common to both the earth-based and space-borne systems. Both photomultiplier tubes require cooling to limit dark current noise. This is especially true for the EMR 543C photomultiplier tube for which a temperature of -70°C is assumed. Admittedly, it remains to be seen if cooling to this extent is possible by passive means in space. Atmospheric transmission is high at an angle 60 degrees off the zenith for both laser wavelengths.

Finally, a PCM-PL, 5-bit code modulation system is assumed for the communication system encoder analysis. In order to permit meaningful comparisons of the channel capacities and error rates of the PCM-PL modulation system, the quantum efficiencies of the previously mentioned photomultiplier tubes are assumed to be equal to unity. The actual values differ markedly and would prevent meaningful performance comparisons between up-looking and down-looking cases.

Sample Calculations of Communications Performance - The analytical procedures presented in the preceding sections will now be used, together with the parameters chosen, to define the optical communicating system under study. Sample calculations are presented which derive system performance step by step for daytime communications in both directions between earth and deep space. Performance during the nighttime has been similarly calculated, but only the results are presented. These calculations begin with the determination of the average signal and noise powers incident on the detector, and end in the calculation of the information capacity of the PCM-PL modulation system, together with corresponding error rates.

Calculations for the daytime case of reception on earth of space transmission is presented in the following steps, 1 through 11:

(1) Transmitted beam divergence, α_t:

$$\alpha_t = 1.22\,\lambda/D$$

$$= \frac{1.22\ (.63\mu)\ \times 10^{-6}}{1\ \text{m}}\ \frac{\text{m}}{\mu}$$

$$= 0.77\times 10^{-6}\ \text{radians} = \underline{0.16\ \text{arc-second}}$$

(2) Signal power density incident on the receiver aperture, P_i:

From Figure 7-2, for $\alpha_t = 0.16$ arc-second, $R = 10^8$ miles, and $P = 2.2$ watts, $P_i = 1.0\times10^{-14}$ watt. However, $P = 0.1$ watt here, therefore:

$$P_i = \frac{0.1}{2.2} \times 1.0\times10^{-14} \ \frac{\text{watt}}{\text{cm}^2} = \underline{4.6\times10^{-16}} \ \text{watt/cm}^2$$

(3) Signal power incident on the photodetector, P_s:

$$P_s = P_i \, A \, \tau_A \tau_o \tau_f$$

$$= \left(4.6\times10^{-16} \ \frac{\text{watt}}{\text{cm}^2}\right) \left(7.86\times10^5 \ \text{cm}^2\right) (0.7)(0.5)(0.15)$$

$$= \underline{1.9\times10^{-11} \ \text{watt}}$$

(4) Arrival rate of signal photons at the photodetector, n_s:

$$n_s = \frac{P_s}{hc/\lambda}$$

$$= P_s \times \frac{6328\text{Å}\times10^{-10} \ \frac{\text{m}}{\text{Å}}}{\left(6.62\times10^{-34} \ \text{joule-sec}\right)\left(3\times10^8 \ \frac{\text{m}}{\text{sec}}\right)}$$

$$= 1.9\times10^{-11} \ \text{watts} \times 3.18\times10^{18} \ \text{joule}^{-1}$$

$$= \underline{6.0\times10^7 \ \frac{\text{photons}}{\text{sec}}}$$

(5) Background noise power incident on the photodetector, P_b:

$$P_b = N_\lambda A \frac{\pi}{4} \alpha_R^2 \Delta\lambda \tau_o \tau_f$$

$$(N_\lambda = N_{\lambda B} + N_{\lambda s}), \simeq N_{\lambda B})$$

$$P_b = \left(5.0\text{x}10^{-3} \frac{\text{watt}}{\text{cm}^2\text{-ster-}\mu}\right)\left(7.86\text{x}10^{5}\ \text{cm}^2\right)\left(\frac{\pi}{4}\right)\left(9.70\text{x}10^{-5}\ \text{rad}\right)^2$$

$$\text{x}\ (.5\text{x}10^{-4}\mu)\ (.5)\ (.15)$$

$$= \underline{1.1\text{x}10^{-10}}\ \text{watt}$$

(6) Signal-to-noise ratio in terms of radiant power incident on the photodetector SNR_p:

$$SNR_p = \frac{P_s}{P_b + P_d}$$

$$= \frac{1.9\text{x}10^{-11}\ \text{watt}}{\left(1.1\text{x}10^{-10} + 2.0\text{x}10^{-15}\right)\text{watt}}$$

$$= \underline{0.17}$$

(7) Arrival rate of background noise photons at the photodetector, n_B:

$$n_B = \frac{P_b}{hc/\lambda}$$

$$= 1.1\text{x}10^{-10}\ \text{watt x}\ 3.18\text{x}10^{18}\ \text{joule}^{-1}$$

$$= \underline{3.5\text{x}10^{8}}\ \text{photons/sec}$$

(8) Equivalent arrival rate of dark current photons, n_d:

$$n_d = \frac{P_d}{hc/\lambda}$$

$$= 2.0\times10^{-15} \text{ watt} \times 3.18\times10^{18} \text{ joule}^{-1}$$

$$= \underline{6.4\times10^{3}} \text{ photons/sec}$$

(9) Generation rate of signal and noise photoelectrons, n_{es} and n_{en}:

$$n_{es} = n_s \times \epsilon$$

$$= 6.0\times10^{7} \frac{\text{photons}}{\text{sec}} \times .05 \frac{\text{photoelectrons}}{\text{photon}}$$

$$= \underline{3.0\times10^{6}} \frac{\text{photoelectrons}}{\text{sec}}$$

$$n_{en} = (n_b + n_d)\,\epsilon$$

$$= (3.5\times10^{8} + 6.4\times10^{3}) \frac{\text{photons}}{\text{sec}} \times .05 \frac{\text{photoelectrons}}{\text{photon}}$$

$$= \underline{1.8\times10^{7}} \frac{\text{photoelectrons}}{\text{sec}}$$

(10) Information capacity, C_{PCM-PL}, and probable rate of error per bit, R, of PCM-PL 5-bit code (without photodetector) where Δf, the information bandwidth, equals 10^7 cps:

The bit time, τ, equals $1/\Delta f$, where Δf is the information bandwidth. The sample period, T, in turn, is equal to 5τ. Therefore, $T = 5/\Delta f$. In this case, $\Delta f = 10^7$ cps, and $T = 5\times10^{-7}$ sec.

S, mean signal quanta per sample period,

$$= n_s T$$

$$= \left(6.0\text{x}10^{7} \ \frac{\text{photons}}{\text{sec}}\right) \left(5\text{x}10^{-7} \text{ sec}\right)$$

$$= \underline{30 \text{ photons}}$$

B, mean noise quanta per sample period

$$= n_b T$$

$$= \left(3.5\text{x}10^{8} \ \frac{\text{photons}}{\text{sec}}\right) \left(5\text{x}10^{-7} \text{ sec}\right)$$

$$= \underline{175 \text{ photons}}$$

From Figure 8-6, page 8-18, the probable rate of error per bit, R, for these values of S and B is 0.18.

Channel capacity is equal to the coding entropy minus the equivocation, divided by the sample period. (See Page D-16 for the derivation of PCM-PL equivocation using a 5-bit code.) Then:

$$C = \frac{5}{T} \left\{1 + \log_2 \left[R^R (1-R)^{1-R}\right]\right\}$$

Substituting,

$$C = \frac{5}{5\text{x}10^{-7}} \left\{1 + \log_2 \left[.18^{.18} \ (1-.18)^{1-.18}\right]\right\}$$

$$= \underline{3.2\text{x}10^{6}} \quad \frac{\text{bits}}{\text{sec}}$$

(11) Information capacity, $C_{\text{PCM-PL}}$, and information bandwidth, Δf, of PCM-PL 5-bit code (without photodetector) where the probable rate of error per bit, R, equals 10^{-4}:

The curve in Figure 8-12 for signal quanta versus noise quanta where $R = 10^{-4}$ may be represented for large values of B by the expression $S = 8.24\sqrt{B} + 35.9$ (refer to page 8-29).

Now $S = n_s T$ and $B = n_b T$;

therefore,

$$S = \frac{n_s}{n_b} B = \frac{6.0 \times 10^7}{35 \times 10^7} B,$$

$$S = .172\ B.$$

Finding the simultaneous solution to these equations yields:

$$S = 464,\ B = 2,700.$$

Now $T = 5/n_s$, and $C \simeq 5/T$ where

$R = 10^{-4}$; therefore,

$$C = \frac{5n_s}{S} = \frac{5(6.0 \times 10^7)}{464} = \underline{6.4 \times 10^{-5}}\ \frac{\text{bits}}{\text{sec}},$$

and

$$\Delta f = \frac{5}{T} = \frac{5n_s}{S} = C = \underline{6.4 \times 10^5}\ \frac{\text{bits}}{\text{sec}}.$$

The calculations for the daytime case of reception in deep space of earth transmission is presented in the following steps 1 through 11:

(1) Transmitted beam divergence, α_t, is independent of transmitter aperture because atmospheric affects limit the emerging beam to a minimum divergence angle of 3 arc-seconds.

(2) Signal power density incident on the receiver aperture, P_i:

In a manner similar to that shown on page 8-37, P_i can be calculated for 3 arc-seconds, where P equals 200 watts and R = 10^8 miles:

$$P_i = \underline{1.8\text{x}10^{-15}} \text{ watt/cm}^2$$

(3) Signal power incident on the photodetector, P_s:

$$P_s = P_i A \tau_A \tau_o \tau_f$$

$$= \left(1.8\text{x}10^{-15} \frac{\text{watt}}{\text{cm}^2}\right) \left(7.85\text{x}10^3 \text{cm}^2\right) \left(.85\right) \left(.5\right) \left(.5\right)$$

$$= \underline{3.1\text{x}10^{-12}} \text{ watt}$$

(4) Arrival rate of signal photons at the photodetector, n_s:

$$n_s = \frac{P_s}{hc/\lambda}$$

$$= 3.1\text{x}10^{-12} \text{ watt x } 4.22\text{x}10^{18} \text{ joule}^{-1}$$

$$= \underline{1.3\text{x}10^7} \quad \frac{\text{photons}}{\text{sec}}$$

(5) Background noise power incident on the photodetector, P_b:

$$P_b = N_{\lambda E} A \frac{\pi}{4} \alpha_R^2 \Delta\lambda \tau_o \tau_f$$

(5) Continued -

$$P_b = \left(1.2\times10^{-2}\ \frac{\text{watt}}{\text{cm}^2\text{-ster-}\mu}\right)\left(7.85\times10^{3}\ \text{cm}^2\right)\left(\frac{\pi}{4}\right)\left(1.45\times10^{-5}\ \text{rad}\right)^2$$

$$\times\ (1.0\times10^{-4}\ \mu)\ (.5)\ (.5)$$

$$= \underline{3.9\times10^{-13}}\ \text{watt}$$

(6) Signal-to-noise ratio in terms of radiant power incident on the photodetector SNR_p:

$$SNR_p = \frac{P_s}{P_b+P_d}$$

$$SNR_{p\ -70°C} = \frac{3.1\times10^{-12}\ \text{watt}}{\left(3.9\times10^{-13}+1.1\times10^{-14}\right)\ \text{watt}}$$

$$= \underline{7.8}$$

$$SNR_{p\ \ 25°C} = \frac{3.1\times10^{-12}\ \text{watt}}{\left(3.9\times10^{-13}+2.2\times10^{-8}\right)\ \text{watt}}$$

$$= \underline{1.4\times10^{-4}}$$

(7) Arrival rate of background noise photons at the photodetector, n_B:

$$n_B = \frac{P_b}{hc/\lambda}$$

$$= 3.9\times10^{-13}\ \text{watt} \times 4.22\times10^{18}\ \text{joule}^{-1}$$

$$= \underline{1.6\times10^{6}}\ \frac{\text{photons}}{\text{sec}}$$

(8) Equivalent arrival rate of dark current photons, n_d:

$$n_d = 1.1\times10^{-14}\ \text{watt} \times 4.22\times10^{18}\ \text{joule}^{-1}$$

$$= \underline{4.6\times10^{4}}\ \frac{\text{photons}}{\text{sec}}$$

(9) Generation rate of signal and noise photoelectrons, n_{es} and n_{en}:

$$n_{es} = n_s \times \epsilon$$

$$= \left(1.3\times10^{7} \ \frac{\text{photons}}{\text{sec}}\right) \ (.0036) \ \frac{\text{photoelectron}}{\text{photon}}$$

$$= 4.7\times10^{4} \ \frac{\text{photoelectrons}}{\text{sec}}$$

$$n_{en} = (n_B + n_d) \epsilon$$

$$n_{en} = \left(1.6\times10^{6} + 4.6\times10^{4}\right) \frac{\text{photons}}{\text{sec}} \times .0036 \ \frac{\text{photoelectron}}{\text{photon}}$$

$$= \underline{5.8\times10^{3}} \ \frac{\text{photoelectrons}}{\text{sec}}$$

(10) Information capacity of PCM-PL 5-bit code, C_{PCM-PL} (calculated for a photodetector of unit quantum efficiency):

The bit time, τ, equals $1/\Delta f$, where Δf is the information bandwidth. The sample period, T, in turn, is equal to 5τ. Therefore, $T = 5/\Delta f$. In this case, $\Delta f = 10^{5}$ cps and $T = 5\times10^{-5}$ sec.

S, mean signal quanta per sample period,

$$= n_s T$$

$$= \left(1.3\times10^{7} \ \frac{\text{photons}}{\text{sec}}\right) \left(5\times10^{-5} \text{ sec}\right)$$

$$= \underline{650. \text{ photons}}$$

B, mean noise quanta per sample period,

$$= n_b T$$

$$= \left(1.5\text{x}10^{6} \ \frac{\text{photons}}{\text{sec}}\right) \left(5\text{x}10^{-7} \text{ sec}\right)$$

$$= \underline{80. \text{ photons}}$$

Although these values of S and B are off scale in Figure 8-6, page 8-18, the probable rate of error per bit, R, for these values of S and B is $< 10^{-5}$. Channel capacity is given by

$$C = \frac{5}{T} \left\{ 1 + \log_2 \left[R^R (1-R)^{1-R} \right] \right\}$$

For very small values of R, $\log_2 \left[R^R (1-R)^{1-R} \right] \simeq 0$

Therefore, $C \simeq 5/T$

$$C = \frac{5}{5\text{x}10^{-5}}$$

$$= \underline{10^5} \quad \frac{\text{bits}}{\text{sec}} .$$

(11) Information capacity, $C_{\text{PCM-PL}}$, and information bandwidth, Δf, of PCM-PL 5-bit code (without photodetector) where the probable rate of error per bit, R, equals 10^{-4}:

$$S = \frac{n_s}{n_b} B = \frac{1.3\text{x}10^{7}}{1.6\text{x}10^{6}} B,$$

$$S = 8.1 B$$

From Figure 8-6, page 8-18, this equation is satisfied for $R = 10^{-4}$ when $S = 55$, $B = 6.8$.

Then,

$$C = 5/T = \frac{5\, n_s}{S} = \frac{5 \times 1.3 \times 10^7}{55} = \underline{1.18 \times 10^6} \frac{\text{bits}}{\text{sec}}$$

$$\Delta f = 5/T = \underline{1.18 \times 10^6} \text{ cps.}$$

Discussion of Results - These calculations are summarized and expanded in Table 8-3 to include both day and night operation in both directions between earth and deep space.

The results for earth reception will be discussed first. The signal-to-noise ratio, SNR_p, increases markedly from .17 in the day to 950 at night. This increase is due to the large reduction in noise power, since at night twenty arc-seconds of blue sky brightness are no longer viewed by the receiving telescope. In this case the dominant noise term is the dark current equivalent noise power incident of the photomultiplier tube equal to 2.0×10^{-15} watts.

The large reduction in noise at night also leads to a greater channel capacity of 9.9×10^6 bits/sec compared to 3.2×10^6 bits/sec in the day for an assumed information bandwidth of 10^7 cps. However, a probable rate of error per bit of 0.18 is too large for useful daytime communications.

Conversely, system channel capacity and information bandwidth have been calculated for a low error rate of 10^{-4}, which is probably acceptable for most communications purposes. The steps carried out in the sample calculations show that for such a low error rate the channel capacity and

TABLE 8-3

Laser Communications Performance Between a Deep-Space Probe and Earth

Computed Parameters	Symbol	Reception on Earth of Space Transmission		Reception in Space of Earth Transmission	
		Day	Night	Day	Night
Signal Power Density Incident on the Receiver Aperture (Watts /CM^2)	P_i	4.6×10^{-16}		1.8×10^{-15}	
Signal Power Incident on the Photo-Detector (Watts)	P_S	1.9×10^{-11}		3.1×10^{-12}	
Background Noise Power Incident on the Photodetector (Watts)	P_B	1.1×10^{-10}	7.3×10^{-18}	3.9×10^{-13}	~ 0
Dark Current Equivalent Power Incident on the Photodetector (Watts)	P_D	$.2.0 \times 10^{-14}$ @-70°C		1.1×10^{-14} @-70°C	
Signal-to-Noise Ratio of Signal Radiant Power Incident on the Photodetector to Noise Power	SNR_P	0.17	950.	7.8	280.
Arrival Rate at Photodetector of Signal Photons (#/Sec)	n_s	6.0×10^{7}		1.3×10^{7}	
Arrival Rate at Photodetector of Background Noise Photons (#/Sec)	n_b	3.5×10^{8}	25.	1.6×10^{6}	~ 0
Arrival Rate at Photodetector of Equivalent Dark Current Photons (#/Sec)	n_d	6.4×10^{3}		4.6×10^{4}	
Emission Rate of Signal Photoelectrons (#/Sec)	n_{es}	3.0×10^{6}		4.7×10^{4}	
Emission Rate of Noise (Background + Dark Current) Photoelectrons (#/Sec)	n_{en}	1.8×10^{7}	3.2×10^{2}	5.8×10^{3}	1.7×10^{2}
*Capacity for PCM-PL 5-BIT Code Modulation System $\left(\frac{BITS}{SEC}\right)$	C_{PCM-PL}	3.2×10^{6}	9.9×10^{6}	1.0×10^{5}	
*Probable Rate of Error Per Bit	R	0.18	0.0012	$< 10^{-5}$	
†Capacity for PCM-PL 5-BIT Code Modulation System $\left(\frac{BITS}{SEC}\right)$	C_{PCM-PL}	0.64×10^{6}	7.2×10^{6}	1.2×10^{6}	1.6×10^{6}
†Information Bandwidth Δf (CPS)	Δf	0.64×10^{6}	7.2×10^{6}	1.2×10^{6}	1.6×10^{6}

* Calculated for an Information Bandwidth of 10^7 CPS for Earth reception, and 10^5 CPS for space reception.

†Calculated for a probable rate of error per bit of 10^{-4}.

information bandwidth are numerically equal. Table 8-3 shows that the information bandwidth or channel capacity increases from 0.64×10^6 in the day to 7.2×10^6 for nighttime earth reception of deep-space transmission.

The photon shot noise power for the optical communication system can be expressed as $h\nu\Delta f$ watts. For the earth reception of deep-space communications the bandwidth Δf is 10^7 cps and the attendant photon shot noise power is 3.13×10^{-12} watts. The received signal power is 1.9×10^{-11} watts, which is approximately six times the possible minimum noise level.

Next, consider the performance of the space receiving system at 10^8 miles from earth. As with earth reception, signal-to-noise ratio increases markedly for night reception over daytime operations when earthshine is the dominant noise contribution. At night, SNR_p equals 280, while in the day, SNR_p equals 7.8.

The information bandwidths for communication to the spacecraft need not be as great as 10^7 cps, since it is anticipated that control functions can be encompassed with an information bandpass of 10^5 cps. For example, no need is envisioned for real time television transmission to the spacecraft which would require an information capacity in excess of 10^5 cps.

For reception in deep space, the photon shot noise power is now 2.37×10^{-14} watts. The received signal power is 3.1×10^{-12} watts, which is approximately 130 times greater than this value.

A bandwidth of 10^5 cps leads to a channel capacity of 10^5 bits/sec, at an error rate per bit less than 10^{-5} for both day and night cases.

For an error rate per bit of 10^{-4} the calculated channel capacities and bandwidths increase, equalling 1.2×10^6 for daytime reception and 1.6×10^6 for the nighttime case.

The performance derived in the above sample calculations reflect optimistic bandwidths and channel capacities. Actual design implementation will degrade the performance by introducing the effects of photodetector quantum efficiencies less than unity, multiplication disturbances due to atmospheric turbulence, and noise contributions from communication circuitry.

8.7 COMMUNICATIONS WITH A SYNCHRONOUS SATELLITE

Selection of System Parameters - The communications system analyzed for the deep-space situation is modified to represent accurately the case of a satellite in synchronous orbit, 23,000 miles from earth. Table 8-4 lists the design parameters used in the performance evaluation for this case.

Several system parameters have been relaxed in accordance with the greatly increased signal power available due to the great reduction in range. The space laser transmitter power has been reduced from 100 milliwatts to 10 milliwatts, and the earth transmitter has been greatly reduced to 0.5 watt from 200 watts. The earth receiver aperture is reduced to 12 inches and the space receiver noise filter bandpass is increased to 5.0Å. The temperature of the EMR 543C photomultiplier tube is considered to be 25°C, since cooling does not appear feasible for the satellite case.

Discussion of Results - Comparing the communications performance for the synchronous satellite presented in Table 8-5 against that for deep space, it is

TABLE 8-4

Design Parameters for Laser Communications Between Satellite in Synchronous Orbit and Earth

Input Parameters	Symbol	Reception on Earth of Satellite Transmission		Reception by Satellite of Earth Transmission	
		Day	Night	Day	Night
Range (Statute Miles)	R	2.3×10^4		2.3×10^4	
Wavelength Received (Å)	λ	6328.		8400.	
Transmitted Power (Watts)	P	0.01		0.5	
Transmitted Beam Divergence (Radians)	α_t	$1.22 \frac{\lambda}{D_t}$		1.45×10^{-5} (3 Arc-Sec)	
Diameter of Transmitting Aperture (Cm)	D_t	100.		—	
Diameter of Receiving Aperture (Cm)	D_R	30. (12 Inches)		100.	
Receiver Field of View (Radians)	α_R	9.7×10^{-5} (20 Arc-Sec)		1.45×10^{-5} (3 Arc-Sec)	
Atmospheric Transmission (%) (60° from the Zenith)	τ_A	70.		85.	
Optical System Transmission (%)	τ_o	50.		50.	
Pre-Detection Filter Transmission (%)	τ_f	15.		50.(43)	
Pre-Detection Filter Bandpass (Å)	$\Delta\lambda$	0.5		5.0(43)	
Background Brightness Blue Sky at 6328Å $\left(\frac{\text{Watts}}{\text{CM}^2\text{-Ster-}\mu}\right)$	$N_{\lambda B}$	5.0×10^{-3}	0	—	
Background Brightness Earthshine at 8400Å $\left(\frac{\text{Watts}}{\text{CM}^2\text{-Ster-}\mu}\right)$	$N_{\lambda E}$	—		1.2×10^{-2}	0
Background Brightness Average Star Field Toward Ecliptic Plane $\left(\frac{\text{Watts}}{\text{CM}^2\text{-Ster-}\mu}\right)$	$N_{\lambda S}$	3.3×10^{-10}		—	
Receiving Photomultiplier Tube		RCA 7265		EMR 543C	
Dark Current Radiant Input Power Equivalent at -70°C (Watts)	$P_{d_{-70°C}}$	2.0×10^{-15}		—	
Dark Current Radiant Input Power Equivalent at 25°C (Watts)	$P_{d_{25°C}}$	—		2.2×10^{-8}	
PMT Quantum Efficiency (%)	ϵ	5.		0.36	

TABLE 8-5

Laser Communications Performance Between Satellite in Synchronous Orbit and Earth

Computed Parameters	Symbol	Reception on Earth of Satellite Transmission		Reception by Satellite of Earth Transmission	
		Day	Night	Day	Night
Signal Power Density Incident on the Receiver Aperture (Watts/CM^2)	P_I	8.6×10^{-10}		8.6×10^{-11}	
Signal Power Incident on the Photodetector (Watts)	P_S	3.3×10^{-8}		1.5×10^{-7}	
Background Noise Power Incident of the Photodetector (Watts)	P_B	1.0×10^{-13}	6.6×10^{-21}	2.0×10^{-12}	0
Dark Current Equivalent Power Incident on the Photodetector (Watts)	P_D	$.2.0 \times 10^{-14}$ @-70°C		2.2×10^{-8} @25°C	
Signal-To-Noise Ratio of Signal Radiant Power Incident on the Photodetector to Noise Power	SNR_P	3.3×10^{5}	1.6×10^{7}	6.8	
Arrival Rate at Photodetector of Signal Photons (#/Sec)	n_s	1.0×10^{11}		6.3×10^{11}	
Arrival Rate at Photodetector of Background Noise Photons (#/Sec)	n_b	3.2×10^{5}	4.7×10^{-4}	8.2×10^{6}	0
Arrival Rate at Photodetector of Equipment Dark Current Photons (#/Sec)	n_d	6.4×10^{3}		9.3×10^{10}	
Emission Rate of Signal Photoelectrons (#/Sec)	n_{es}	5.0×10^{9}		2.3×10^{9}	
Emission Rate of Noise (Background + Dark Current) Photoelectrons (#/Sec)	n_{en}	1.6×10^{4}	3.2×10^{2}	3.4×10^{8}	
*Capacity for PCM-PL 5-Bit Code Modulation System $\left(\frac{BITS}{SEC}\right)$	C_{PCM-PL}	1.0×10^{7}		1.0×10^{5}	
* Probable Rate of Error Per Bit	R	$<< 10^{-5}$		$<< 10^{-5}$	
†Capacity for PCM-PL 5-bit Code Modulation System $\left(\frac{BITS}{SEC}\right)$	C_{PCM-PL}	1.2×10^{10}		7.5×10^{10}	
†Information Bandwidth Δf	Δf	1.2×10^{10}		7.5×10^{10}	

* Calculated for an Information Bandwidth of 10^7 CPS for Earth reception, and 10^5 CPS for space reception.

† Calculated for a probable rate of error per bit of 10^{-4}.

CR-252

clear that the large reduction in range for the synchronous orbit leads to greatly increased signal power levels. The signal power at the photodetector for earth reception is 1700 times greater for the satellite than for deep space. Similarly, in the case of satellite reception, the average signal power is approximately 50,000 times greater for the synchronous orbit case than for the deep-space situation.

The signal-to-noise ratios are substantial for both day and night earth reception. However, the signal-to-noise ratio of 6.8 at the satellite is somewhat smaller, compared to the value of 7.8 obtained for deep-space reception. The reason for this decrease is that the dark current contribution to the noise at 25°C is nearly one million times greater than at the -70°C temperature of the photodetector in deep space.

The higher signal powers do not lead to an appreciable increase in channel capacity, calculated for information bandwidths of 10^7 cps and 10^5 cps, in the satellite case, compared to the results for deep space. However, the probable error rate per bit has been reduced to a vanishingly small value, $<< 10^{-5}$ for communications in the synchronous satellite case.

A marked increase in information bandwidth and channel capacity occurs when these values are calculated for an error rate equal to 10^{-4}. At this error rate, both information bandwidths and channel capacity exceed 10^{10} for both earth and satellite reception.

Modulator Hardware - An external modulator built up around a Pockels cell using KDP as the working substance can be used as a modulator at 6328Å in the space-to-ground experiment. Perkin-Elmer and other companies have experience with

this form of modulator. The Perkin-Elmer modulator includes low-pass and band-pass operation and capability for both single and multiple transits of the crystal. The prism arrangement for a modulator employing three passes through the crystal is shown in Figures 8-13 and 8-14, and an exciter used with it at 100 megacycles per second is shown in Figure 8-15.

The final choice of modulator for the space-to-ground experiment should be deferred as long as is reasonable in order to maximize the efficiency of the modulation subsystem. Since GaAs lasers are used aboard the synchronous satellite for the basic experiment, the modulator requirement for these devices is an order of magnitude less difficult, and the efficiency problems of the Pockels cell are now insignificant. The difficulties of cooling the GaAs laser to liquid-hydrogen temperatures or even to liquid-nitrogen temperatures are now present. Further, the output of the GaAs lasers available is not diffraction-limited (the gas laser beams are nearly diffraction-limited) and, as a consequence, the spread of the beam is greater. However, the development of these semiconductor lasers is rapid, and one can hope that by the time a system freeze must be made, improved hardware will be available in either or both of these areas — modulators for gas lasers, or lower dispersion diode lasers.

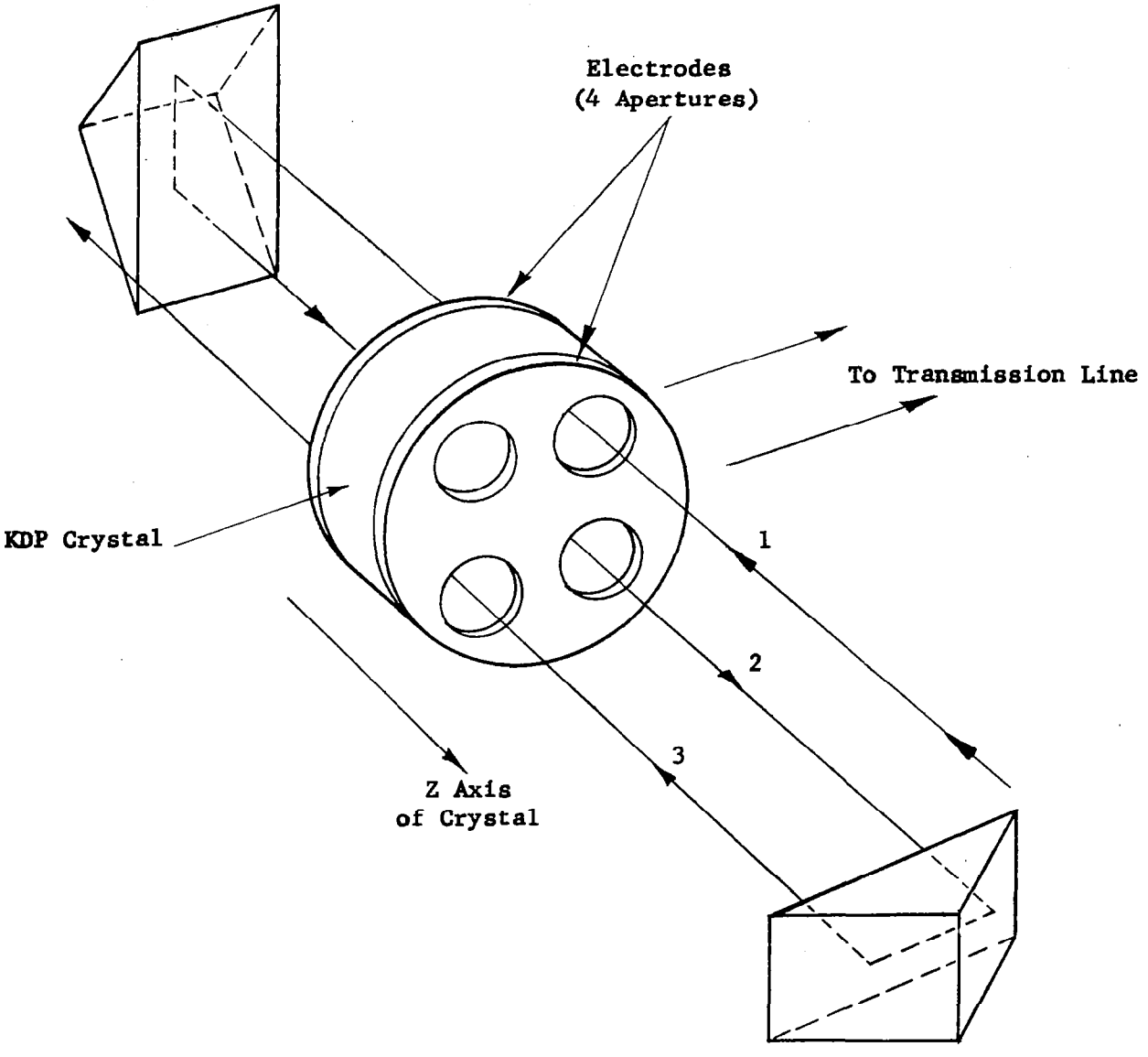

Figure 8-13. Three-Pass Modulator Optical Diagram

CR-252

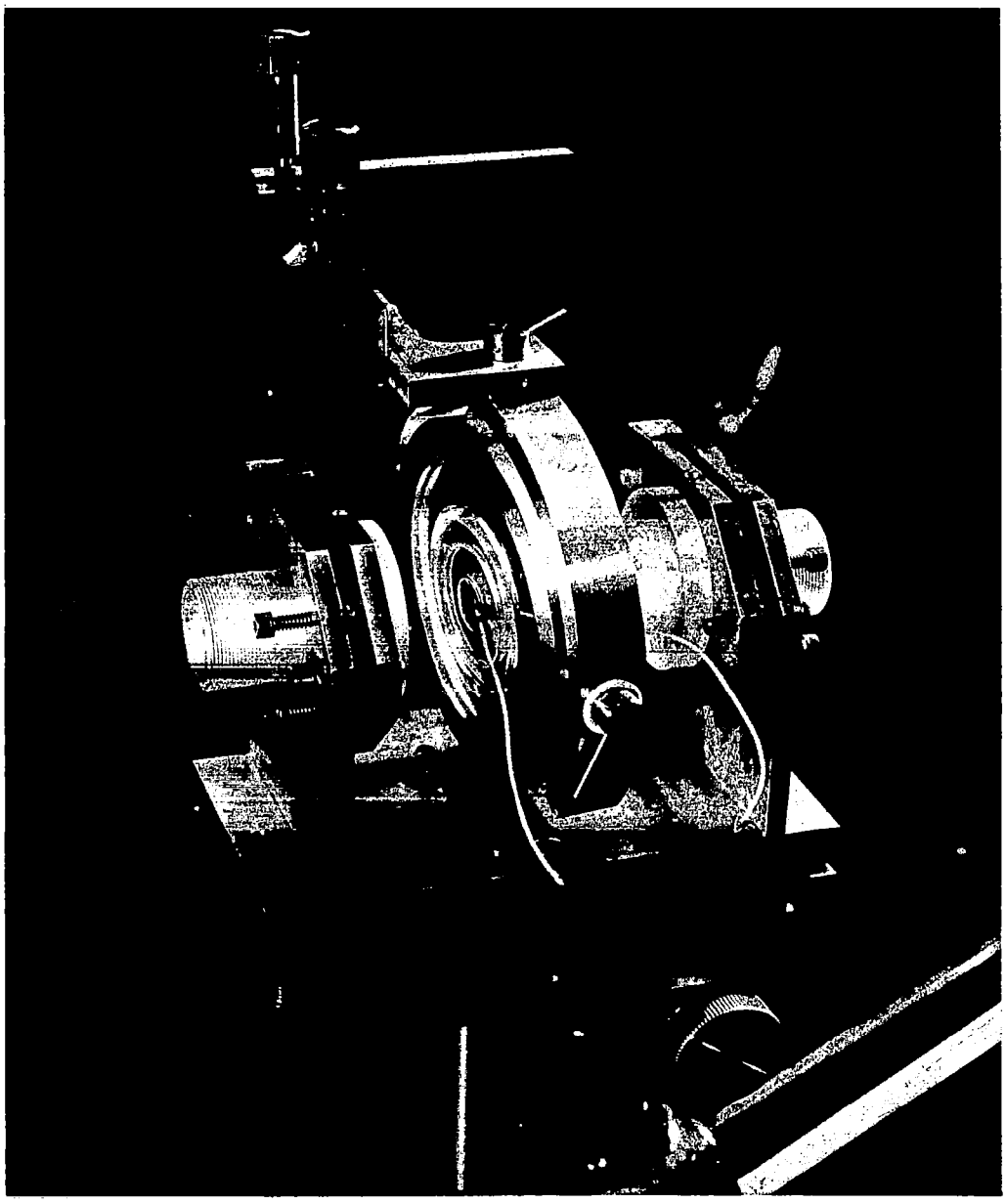

Figure 8-14. Prototype Multipass Modulator

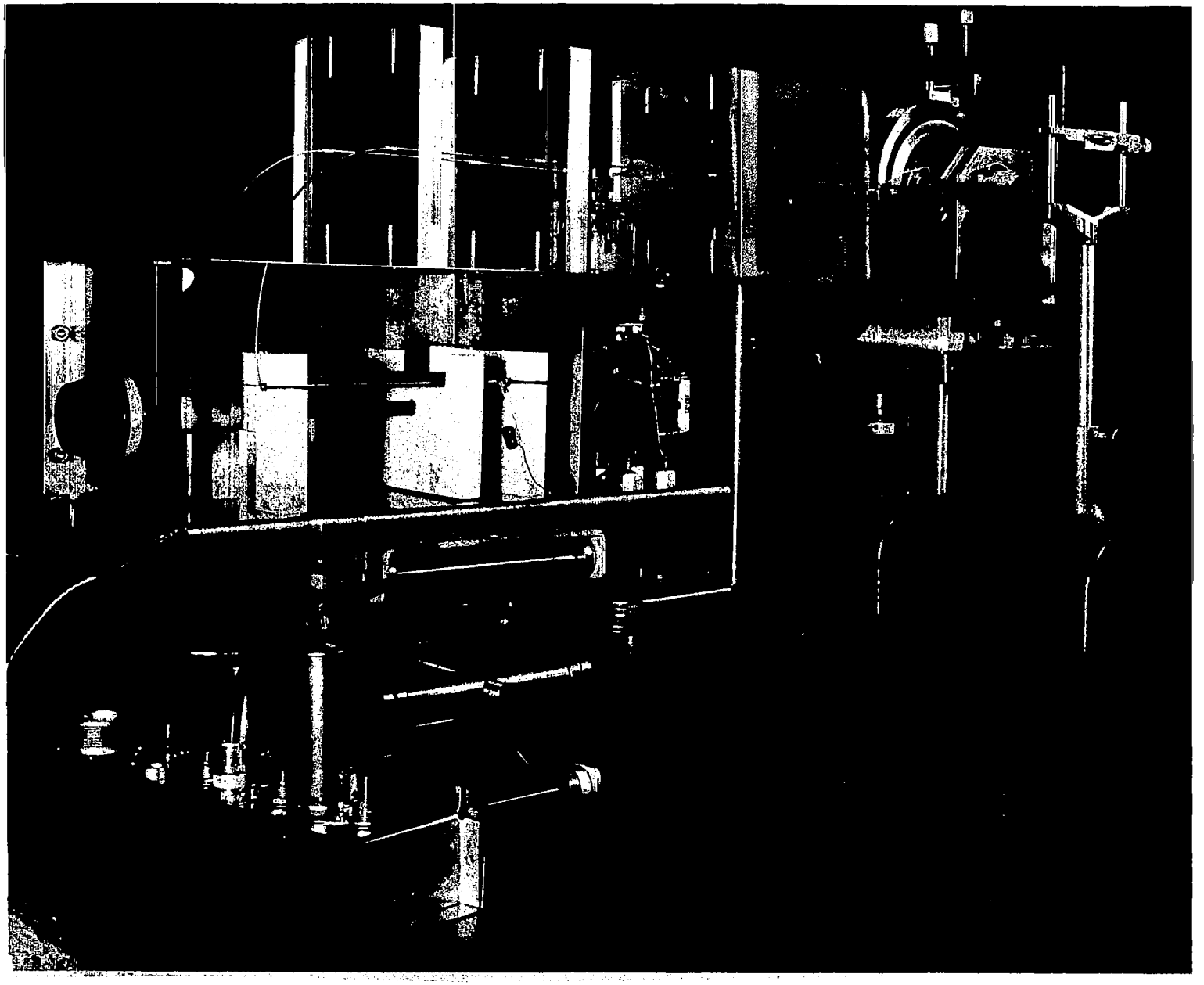

Figure 8-15. Multipass Modulator with Resonant Line Exciter

8.8 A COMMUNICATION APPROACH FOR THE OPTICAL TECHNOLOGY SATELLITE

System Considerations - Ideally, the communications approach for the satellite experiments should be capable of being extrapolated to predict system performance in deep space. Also, the hardware that is developed for the experiments in near earth space should be capable of being used with little or no modifications. Practically, this ideal situation has pitfalls. The bandwidth that is desired with present state-of-the-art components for near earth space is 10 megacycles with a very adequate signal-to-noise ratio and using conservative ratings for each element in the system. The chief difficulty is the external modulator efficiency for the gas laser.[44,45,46] The modulator subsystem is available today, although its efficiency is still not high. Power inputs as low as 12 watts have been obtained for a KDP modulator. However, this device attenuates incoming laser light so that the output light level is reduced by a factor of four.[45]

Based on an anticipated three-year launch cycle for the OTS payload, a subsystem freeze on even this component is at least one year off. As a consequence, the development status of a more efficient external modulator for the gas laser seems like a reasonable assumption. If that is the case, the preliminary design efforts on the OTS for Phase II will turn out to be conservative approaches and the probability of success for the mission will be enhanced further.

While the external modulator is, at present, a technical limiting item from an efficiency viewpoint, an alternate course is to consider the prospective improvements in solid state (diode) lasers like gallium arsenide (GaAs). These devices are several orders of magnitude more efficient (typically, 20 percent efficiency) than gas lasers and are considerably easier to modulate (Reference 47, page 46). Thus, the diode laser communication experiments will have much higher optical power generated and at a lower power input level. The modulator power and even the hardware itself will be an order of magnitude better than that for the gas laser. The limitations in today's GaAs lasers are the low temperature requirement and the non-diffraction-limited optical beam output. Perhaps the low temperature problem can be solved practically by evaporative cooling techniques (Reference 48, page 23) or by passive radiant cooling techniques in the spacecraft. This area requires further investigation.

The remaining problem is then the beam dispersion from the crystal (a narrow-beam laser might have a dispersion of 4 degrees[49]). For near-space experiments this dispersion is of limited significance. For deep space, however, the advantages of an optical communication system are absolutely dependent upon the dispersion angle. For even with large-aperture transmitting telescopes, if the light source is not diffraction-limited, the beam will not traverse the interplanetary distances in a tightly collimated bundle. At this point in time, the choice of an optical communication system for the satellite experiments is contingent upon judgments of need of developments of diode

lasers operating with more nearly diffraction-limited performance and gas laser modulators of higher efficiency.

The Phase I efforts for the experiments are predicated upon the testing of both gas and solid-state lasers.

One further observation of the future deep-space communications system should be permitted. Error rate calculations shown in Table 8-5 indicate that a 10-megacycle deep-space signal is not possible now because of the limited power output of gas laser transmitters and/or lack of a narrow-beam powerful diode laser. Yet, for the satellite case, we persist in considering 10 megacycles. The justification for our recommendation is that improvements in modulators, gas laser power, and/or GaAs laser beam widths will permit deep-space bandwidths of 10 megacycles. Since the operational mission in deep space is many years off, the collection of the data to operate an optical communication system at 10 megacycles should proceed for the satellite case, since 10-megacycle bandwidth can be obtained at reasonable signal-to-noise ratios.

With this type of logic, we proceed to recommend an optical communication system for the OTS. In the discussion, below, of engineering experiment (13), the recommendation is based on a 10-megacycle bandwidth. The material developed in the previous paragraph on pulse code modulation is one of the possible communication systems which can be considered. For the deep-space case, this form of digital communications system is developed with the use of the Poisson statistics necessary for optical communication techniques

at long ranges, rather than the more common Gaussian statistics which apply to the microwave communication systems. Yet, for the satellite case, the range is comparatively short, the signal levels are high and the Poisson models simplify to Gaussian models. Thus, classical microwave statistical and communication approaches are applicable.

We have chosen to discuss one of these well developed systems for the satellite case for which the Gaussian model is applicable. It is presented as a considered communications approach for the satellite case even though it is probably not optimum for the deep-space case.

A Suppressed Subcarrier Communication Technique for the OTS - An experiment for transmitting toward earth with a modulated laser with a 10-megacycle bandwidth and a suitable signal-to-noise ratio is a primary experiment.* Therefore, a decision basic to the design of any optical communication system is the manner in which the temporal and spatial coherence of the radiant output of the laser is to be employed. The spatial coherence of the laser beam (regularity of wavefront) is the property which allows collimation to extremely small divergences, and it will be employed in this communication system in that context only (i.e. as the source of a very high equivalent antenna gain). The temporal coherence is the property which accounts for the very narrow linewidth characteristic of lasers, and will be employed as a property which allows the use of a narrow (less than 1 Å) spectral filter before envelope detection of the received light. The first detection will be performed in a photomultiplier tube. Coherent (heterodyne) detection will not be employed in this basic experiment for

*NASA MSFC Work Statement

telescope 1.* The second detection, the detection of the modulation, will be coherent.

Modulation in Baseband - The simplest modulation system would employ amplitude modulation of the light with the information bearing waveform. This modulation technique would be applicable to lasers exhibiting a low-pass self-modulation characteristic, such as gallium arsenide at 77°K, and to other lasers when combined with an external modulator possessing a low-pass characteristic. A combination possessing low absorption and scattering losses in the atmosphere and good detectability with photomultiplier tubes is the helium-neon laser operating at 6328Å with an external modulator. The most suitable photocathode for a wavelength of 6328Å is the trialkali cathode with S-20 response.

The self-modulation characteristic of gallium arsenide, the modulation characteristic of the Pockels cell, and the detector characteristic of photomultiplier tubes are nonlinear for amplitude-modulated signal purposes. The distortion resulting from a combination of these elements will impair an analog link to some degree. A digital link will be insensitive to this distortion but will require excess bandwidth. For example, a signal whose amplitude can vary over a 32:1 range in Δt seconds can be coded as a 5-digit binary number every Δt second. This coding will require five times the bandwidth and five times as much noise power will be admitted through the pre-detector passband, but this excess noise is more than compensated for in the detection process.

---

*Heterodyne detection is an experiment for telescope 2.

Modulation with a Sub-Carrier - Should modulation of a sub-carrier be desirable, perhaps because of the availability of an attractive modulator possessing a bandpass characteristic, the modulation situation becomes more complex and the number of choices becomes greater. The recommended method within the sub-carrier category is described in the following paragraphs.

For systems employing a sub-carrier, the information in the base-band will be impressed on the sub-carrier in a symmetrical form, i.e., both sets of sidebands will be employed. The sub-carrier will be suppressed because it conveys no information. A double-sideband system will be employed because of the relative ease with which Doppler shifts associated with a signal originating at a moving source can be accommodated. A more detailed discussion of the possible modulation techniques and the specific recommendation of a system follows.

Two broad categories of modulated signal can be identified as those which occupy one baseband on either or both sides of the carrier (hereafter used to refer to the sub-carrier, not the light) and those which are expanded in bandwidth occupancy and occupy more than one baseband around the carrier. The expanded bandwidth signals involve a trade in bandwidth occupancy for an improvement in signal-to-noise ratio in the post-detector passband over signal-to-noise ratio in the pre-detector pass band. Wideband FM, such as broadcast FM, is the best known example. The communication efficiency of expanded-bandwidth systems, when compared with the efficiency of normal bandwidth systems is not considered to be a favorable trade. This is especially true when consideration is given to the difficulty of reducing such a system to laser hardware. For a particular condition in the communication link, an expanded-bandwidth transmission

will be recommended, but this case involves maintaining the bandwidth occupancy at 10 megacycles while reducing the information rate as the minimum signal strength threshold is approached.

Communication efficiency requires minimum redundancy in the signal. Any carrier power is totally redundant. Single-sideband modulation is generally carrier-suppressed and not easily employed in an environment in which Doppler shifts will be encountered. Transmitting the carrier makes accommodating Doppler shifts easier but introduces redundancy. The minimum redundancy goal and the tractability in the presence of Doppler shifts dictate against conventional amplitude modulation (AM) and single-sideband modulation (SSB). These same reasons identify double-sideband suppressed-carrier amplitude modulation as a sound choice for the OTS communication system.

The performance of any communication system is dependent on the efficiency of detection. The envelope (diode) detector is acknowledged to be an inefficient detector because the signal-to-noise ratio in the detected signal is dependent upon the pre-detector bandwidth. Envelope detection is suited to double-sideband suppressed-carrier (DSBSC) signals because, in the absence of a carrier, the sidebands beat against one another instead of against the strong carrier and this beating produces 100 percent second-harmonic distortion.

Detection of a DSBSC signal requires that the carrier which was suppressed in the original modulation process be recreated in proper phase. Fortunately, the symmetry of the sideband structure in a DSBSC signal contains information about the frequency and phase of the missing carrier. The synchronous detector illustrated in Figure 8-16 provides the missing carrier for demodulation.

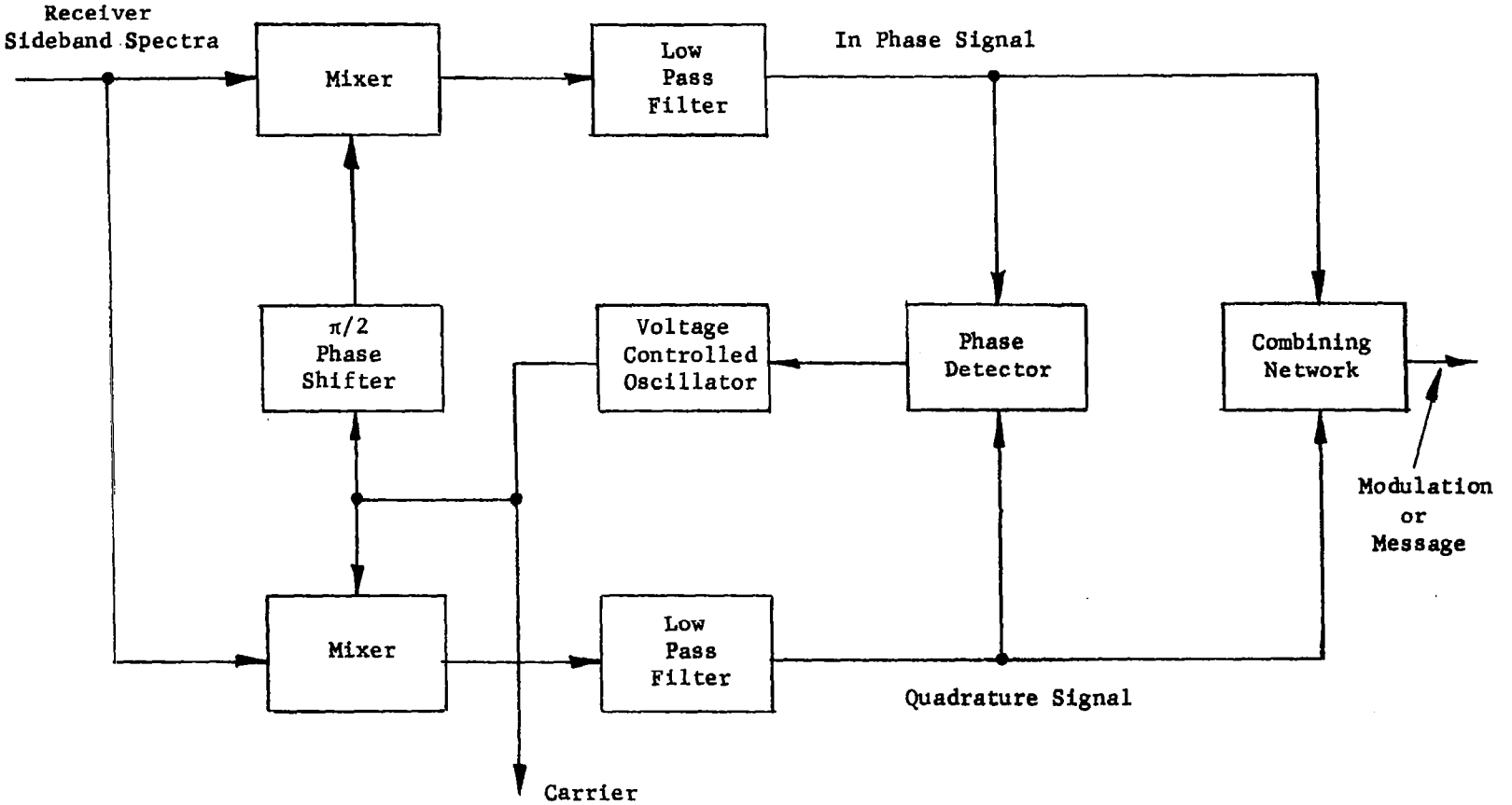

Figure 8-16. Synchronous Detector

Two phases of the carrier are used, one in phase with the suppressed carrier and one in quadrature with it. Each phase of the local carrier, in beating against the incoming signal, produces a demodulated signal. When these demodulated signals are mutually phase detected, the dc term in the resultant output contains the necessary information for completion of a phase lock to the suppressed carrier. This technique is described in detail in the literature (Reference 50; Reference 51, pages 534-537; Reference 52, pages 1383-1385). The block diagram of a laser communication system employing a synchronous detector is shown in Figure 8-17. It is suitable for analog or digital signals.

In describing a DSBSC communication system operating with binary signals it is generally called phase-shift keying (PSK) because the two binary levels each correspond to transmission of the carrier at one of two phases. This phase characteristic exists with bipolar analog signals also, but with the additional property that the amplitude of the carrier at one phase must duplicate the amplitude of the analog signal in the polarity associated with that phase.

Every communication system has a threshold, a level of received power for which weaker signals are detected with an insufficient signal-to-noise ratio or with excessive error rate if the message is digital. Often it is desirable to maintain the link operating at a reduced message rate (bandwidth) rather than accept failure of the link at its maximum bandwidth. This can be best accomplished for digital messages by encoding the characters so that a "zero" consists of N elements in code A and a "one" consists of N elements of code B. Very efficient correlation detectors exist for signals of this sort. A block diagram of such a detector is shown in Figure 8-18 and a

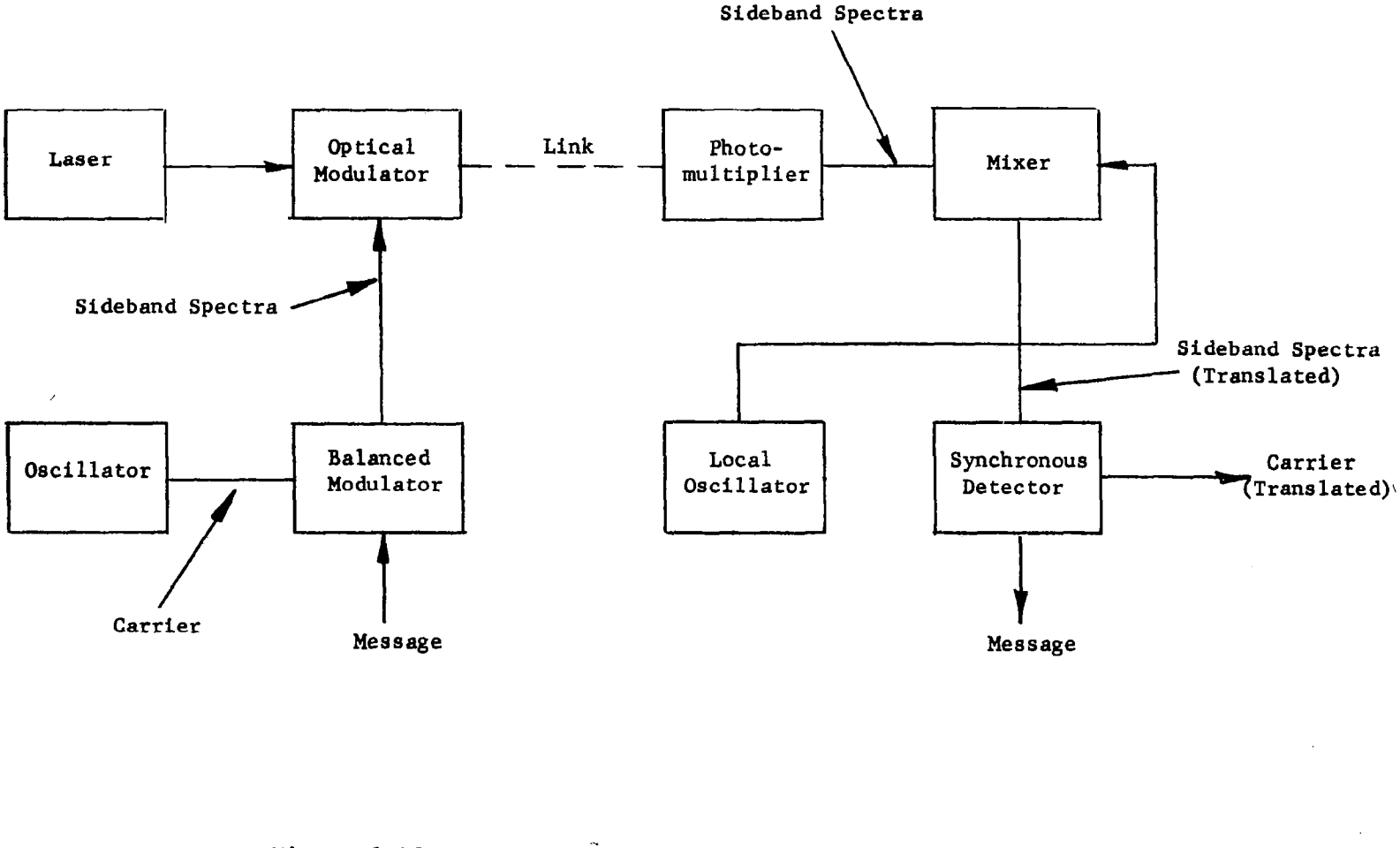

Figure 8-17. Block Diagram - Communication System - Uncoded

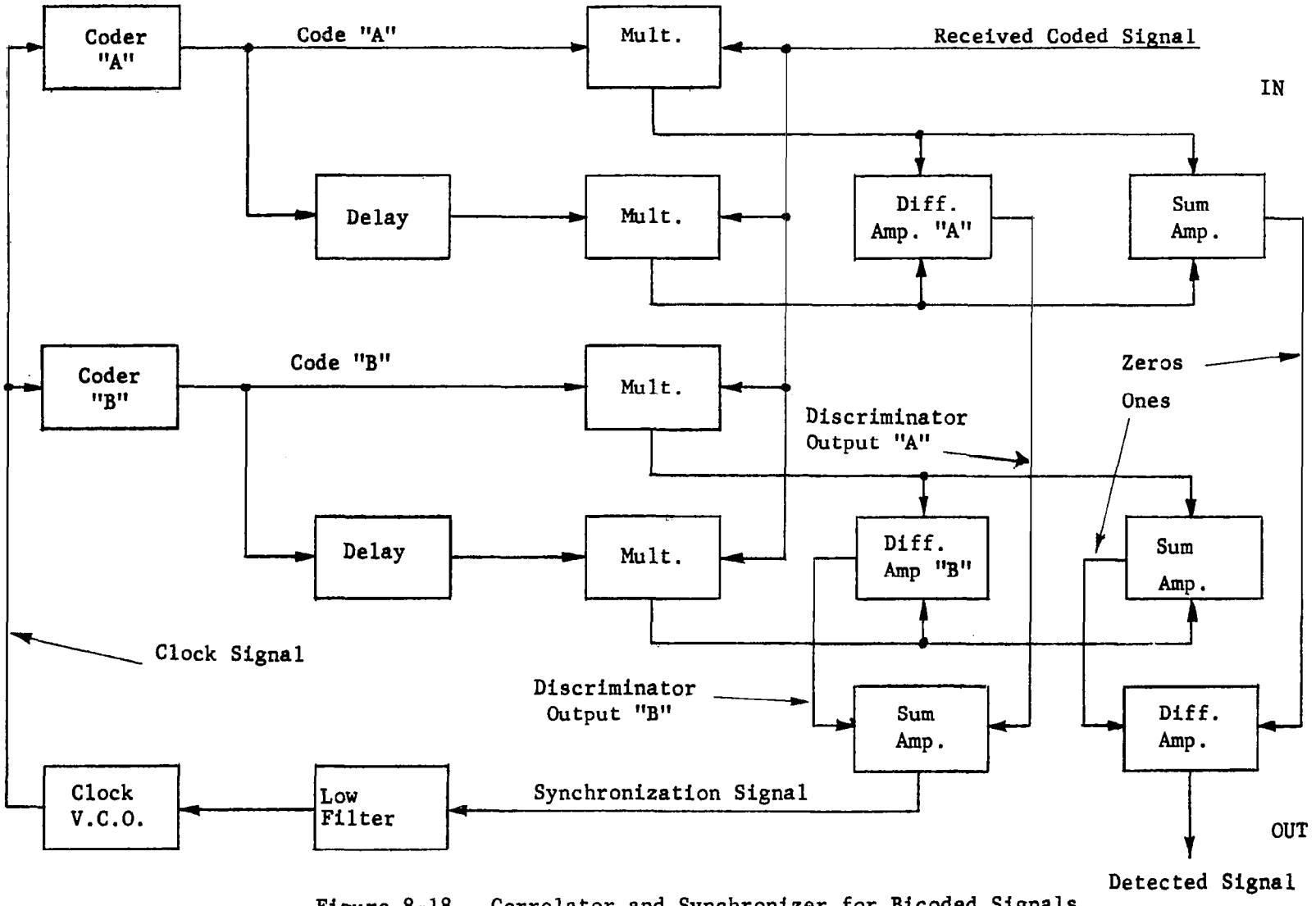

Figure 8-18. Correlator and Synchronizer for Bicoded Signals

and a block diagram of a communication system employing a correlation detector is shown in Figure 8-19.

In a coded communication system, as the detectability threshold is approached, the message rate (character rate) is reduced but the bandwidth occupancy is maintained by continuing to send elements at the same rate but reducing the information value of an element from 1 to 1/N. The optimum bandwidth (generally) for any detector is that which matches the message rate (character rate). This match is maintained without change to any of the major transmission elements of the system such as the optical modulator, modulator driver or the receiver. The changes are limited entirely to the low level message handling input and output elements.

Codes with desirable characteristics for this type of system exist (Reference 53, pages 153-161), as do simple means for their generation.[54]

The most important characteristic sought in a code is an autocorrelation function with low sidelobes. The most common method of generating the code employs a clock driver shift register with feedback. For defining a character, the number of elements (N) available from a register of (n) stages is:

$$N = 2^n - 1$$

Signals with symmetrical sideband spectra and a suppressed carrier have been identified as most desirable for reasons centering on signal efficiency. A method of obtaining range information from a spacecraft will be described as an indicator of the versatility of a coded DSBSC system. Envision an earth-spacecraft instrumentation which includes an earth-to-spacecraft

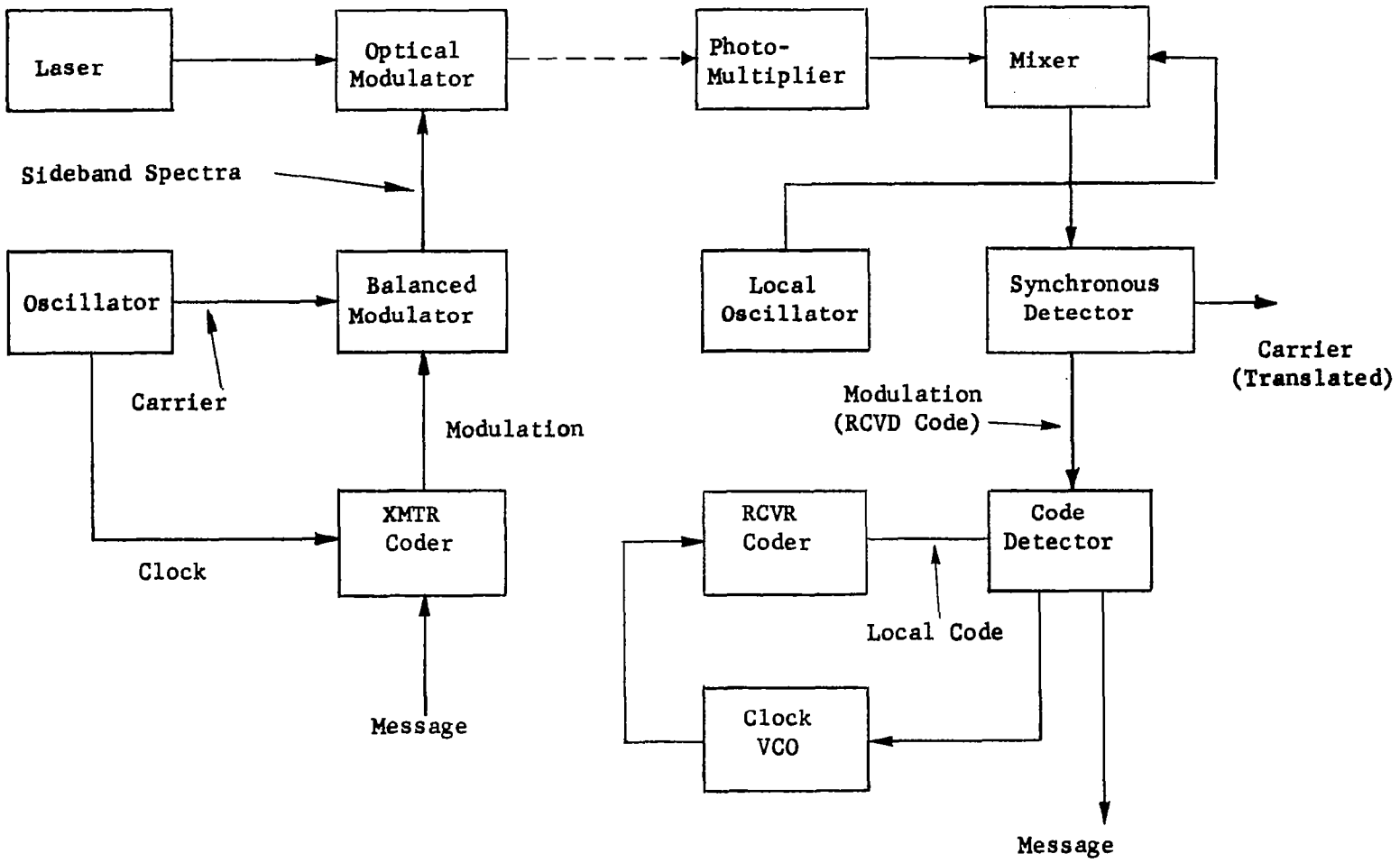

Figure 8-19. Block Diagram - Communication System - Coded

microwave link and a spacecraft-to-earth laser link. An uncertainty, of some size, about range to the spacecraft exists. Suppose that a code character of M elements is transmitted continuously to the spacecraft via the microwave link and retransmitted to earth via the laser link. If this character had a duration greater than the transit time of light through the range uncertainty distance, the range uncertainty distance can be reduced to 1/M of its initial value, i.e., the range increment associated with a transit time of one element duration. For the case of complete range uncertainty, a character duration would have to equal or exceed a complete, round-trip, transit time, including transponding delays. The use of coded cw transmissions for range measurement has been employed successfully in the Courier program.[55] Simultaneous transponding via microwave and via light could conceivably yield new information on relative radio and optical refractive indices.

REFERENCES

[1] Cameron, A.G.W. (ed.) Interstellar Communication. New York: W.A. Benjamin, Inc., 1963; Article by R.N. Schwartz and C.H. Townes, pp. 223-231.

[2] Potter, P., Stevens, R., and Wells, W. "Radio and Optical Space Communications". Light and Heat Sensing. Edited by H.J. Merrill. New York: Macmillan Co., 1963, p. 235

[3] Ligda, M. "Meterological Observations With Lidar," Stanford Research Institute, Menlo Park, California. Paper presented at the First Conference on Laser Technology, San Diego, California, November 12-14, 1963.

[4] Elterman, L. "A Series of Stratospheric Temperature Profiles Obtained with the Searchlight Technique," Journal of Geophysical Research, 58:4, December, 1953.

[5] Long, R.K. "Atmospheric Attenuation of Ruby Lasers," Proceedings of the Institute of Electrical and Electronics Engineers, May, 1963.

[6] Allen, C.W. Astrophysical Quantities. London: The Athlene Press, 1963.

[7] Tatarski, V.I. Wave Propagation in a Turbulent Medium. New York: McGraw-Hill Book Co., 1961.

[8] Chernov, L.A. Wave Propagation in a Random Medium. New York: McGraw-Hill Book Co., 1961.

[9] Optical Space Communications System Study. NASA Report CR-53466, Final Report (February, 1964). Vol. III, System Topics, Part II, Spacecraft Department, Missile and Space Division, General Electric Company, Valley Forge Space Technology Center, Philadelphia, Pennsylvania.

[10] Sedgwick, J.B. Amateur Astronomer's Handbook (Pulkova Refraction Table). London: Faber and Faber, Ltd., 1955.

[11] Smart, W. Text Book in Spherical Astronomy. 4th ed., Cambridge: Cambridge University Press, 1944.

[12] Brown, D.G. "A Treatment of Analytical Photogrammetry with Emphasis on Ballistic Camera Application," RCA Data Reduction Technical Report No. 39 (ASTIA Document No. 124144), August, 1957.

[13] Connaissance des Temps ou des Mouvements Célestes. publiee par le Bureau des Longitudes. Gauthier-Villars, Paris Anually.

[14] Hufnagel, R.E. Understanding the Physics of Seeing Through Turbulent Atmospheres. Abstracted from Advanced Range Instrumentation Presentation made by Perkin-Elmer Corporation at Patrick AFB, Florida, November 20, 1963.

[15] Hufnagel, R.E. and Stanley, N.R. "Modulation Transfer Function Associated with Image Transmission Through Turbulent Media," Journal of the Optical Society of America, January, 1964.

[16] Handbook of Chemistry and Physics. 42nd ed. Chemical Rubber Publishing Company, 1961.

[17] O'Neal, John B., Jr. A Theory of Quantum Communications. ASTIA Document No. AD 429721.

[18] Jones, R. Clark, "Information Capacity of a Beam of Light," Journal of the Optical Society of America, L11, No. 5, May, 1962.

[19] Russel, H.N., Dugan, R.S., and Stewart, J.Q. Astronomy. Boston: Ginn and Co., 1945.

[20] Erway, D.E. Direct Use of Solar Energy for Communication, Part I. ASTIA Document No. AD-269430, Electro-Optical Systems, Inc., Pasadena, California, September, 1961.

[21] Strandberg, M.W.P. "Inherent Noise of Quantum Mechanical Amplifiers," Physical Review, Vol. 106, May 15, 1957.

[22] Oliver, B.M. "Signal-To-Noise Ratios in Photoelectric Mixing," Proceedings of the Institute of Radio Engineers, December, 1960.

[23] Investigation of Optical Spectral Regions for Space Communications. ASTIA Document No. AD 410537 Prepared by the Institute of Science and Technology. Ann Arbor: the University of Michigan.

[24] Chatterton, E.J. Infrared Modulation Noise - Radiometry, Characteristics and Applications. Technical Report No. 229, Lincoln Laboratory, Bedford, Massachusetts, September 8, 1960 (SECRET).

[25] Gilmore, H.F. Use of Radiation from the Sun to Measure Ranges in Space. Proprietary Internal Memorandum of the University of Michigan, August 3, 1962.

[26] Gardner, S. "Some Effects of Atmospheric Turbulence on Optical Heterodyne Communications" Paper presented at the 1964 International Convention of the Institute of Electrical and Electronics Engineers.

[27] Fried, D.L. and Cloud, J.D. "Theoretical Examination of the Effect of Atmospheric Turbulence on Optical Propagation," Technical Memorandum No. 94. Paper presented at the 1964 Spring Meeting of the Optical Society of America, Washington, D.C., April 3, 1964.

[28]Brinkman, Kenneth L. Deep Space Optical Communications Study. NASA Contractor Report No. CR-73, Hughes Aircraft Company, El Segundo, California, July,1964.

[29]Condon and Odishaw. Handbook of Physics. New York: McGraw-Hill Book Co., 1958.

[30]Born and Wolf. Principles of Optics. 2nd ed. New York: Pergamon Press, 1964.

[31]"Etudes Des Effets Combines Des Aberrations Et D'une Obturatien Centrale De Lu Pupille Sur Se Contraste Des Images Optiques," translated by W.H. Steel. Revue D'Optique, Vol. 32, No. 1, 1953.

[32]Newton, Gould, and Kaiser. Analytical Design of Linear Feedback Controls. New York: John Wiley & Sons, Inc., 1957.

[33]Spitzer, L. "The Beginnings and Future of Space Astronomy," American Scientist, Vol. 50, No. 3, 1962.

[34]Investigation of Optical Spectral Regions for Space Communications. ASTIA Document No. AD 410537. Ann Arbor: University of Michigan, May, 1963.

[35]Ramsey, R.C. "Spectral Irradiance from Stars and Planets, Above the Atmosphere, from 0.1 to 100.0 Microns," Applied Optics, Vol. 1, No. 4, July, 1962.

[36]Kruse, McGlauchlin, and McQuistan. Elements of Infrared Technology. New York: John Wiley & Sons, Inc., 1962.

[37]Santa Barbara Research Corporation Catalogue No. 64CM.

[38]Gordon, J.P. "Quantum Effects in Communication Systems," Proceedings of the Institute of Radio Engineers. 50:1898; 1962.

[39]Brinkman, Kenneth L. Study on Optical Communications from Deep Space: Interim Progress Report: 27 March 1963 Through 31 May 1963. NASA Report No. N64-16770, Hughes Aircraft Company.

[40]Survey and Evaluation of Phenomena and Techniques in the Ultraviolet Visible and Submillimeter Region for Application to Detectors and Astrosurveillance. First Report, Part 1. Geophysics Corporation of America, July 1, 1961, p. 30.

[41]Lyot Filter for Hydrogen Alpha Wavelength, Perkin-Elmer Report No. 7682.

[42]Survey and Evaluation of Phonomena and Techniques in the Ultraviolet, Visible and Submillimeter Region for Application to Detectors and Astrosurveillance. First Report, Part 1. Geophysics Corporation of America, July 1, 1961, pp. 50-59.

[43]Baumeister, P.W. "Interference Coatings for Astronomical Optical Instruments," The Astronomical Journal, Vol. 69, No. 5 (June, 1964) p. 341.

[44]Modulator and Mechanical Scanner for Laser Display System. Perkin-Elmer Report No. 7551.

[45]Peters, C.J. "Traveling Wave Amplitude Modulator," Proceedings of the Northeast Electronics Research and Engineering Meeting, November, 1964.

Peters, C.J., "Gigacycle Bandwidth Coherent Light Traveling Wave Phase Modulator," Proceedings of the Institute of Radio Engineers, January, 1963.

[46]Fried, D., Read, W.S., and Pollock, D. An Interferometric Optical Modulator. First Conference on Laser Technology, San Diego, California, November 12, 1963.

[47]Keyes, R.W. "Injection Lasers," Industrial Research, October, 1964.

[48]Gross, U.E. and Weinstein, A.I. "A Cyrogenic-Solid Cooling System," Proceedings of the Infrared Information Symposium, Vol. 9, No. 1, January, 1964.

[49]RCA Developmental Laser TA2393, Data Sheet.

[50]Costas, John P. "Synchronous Communication," Proceedings of the Institute of Radio Engineers, December, 1956.

[51]Costas, John P. "Double Sideband vs. Single Sideband Systems," Proceedings of the Institute of Radio Engineers, April, 1957.

[52]Costas, John P. "Some Notes on Space Communication," Proceedings of the Institute of Radio Engineers, April, 1959.

[53]Craig, S.E., Fishbein, W., and Rittenbach, O.E. "Continuous-Wave Radar with High Range Resolution and Unambiguous Velocity Determination," Transactions of the Institute of Radio Engineers, Mil-6, April, 1962.

[54]Birdsall, T.G. and Ristenbatt, M.P. Introduction to Linear Shift-Register Generated Sequences. Technical Report No. 90. Ann Arbor: Research Institute, University of Michigan, 1958.

[55]Easterling, M. A Long-Range Precision Ranging System. Jet Propulsion Laboratories Technical Report No. 32-80.

APPENDIX A

FLOW CHART SHOWING METHOD OF PERFORMING PHASE I TASKS

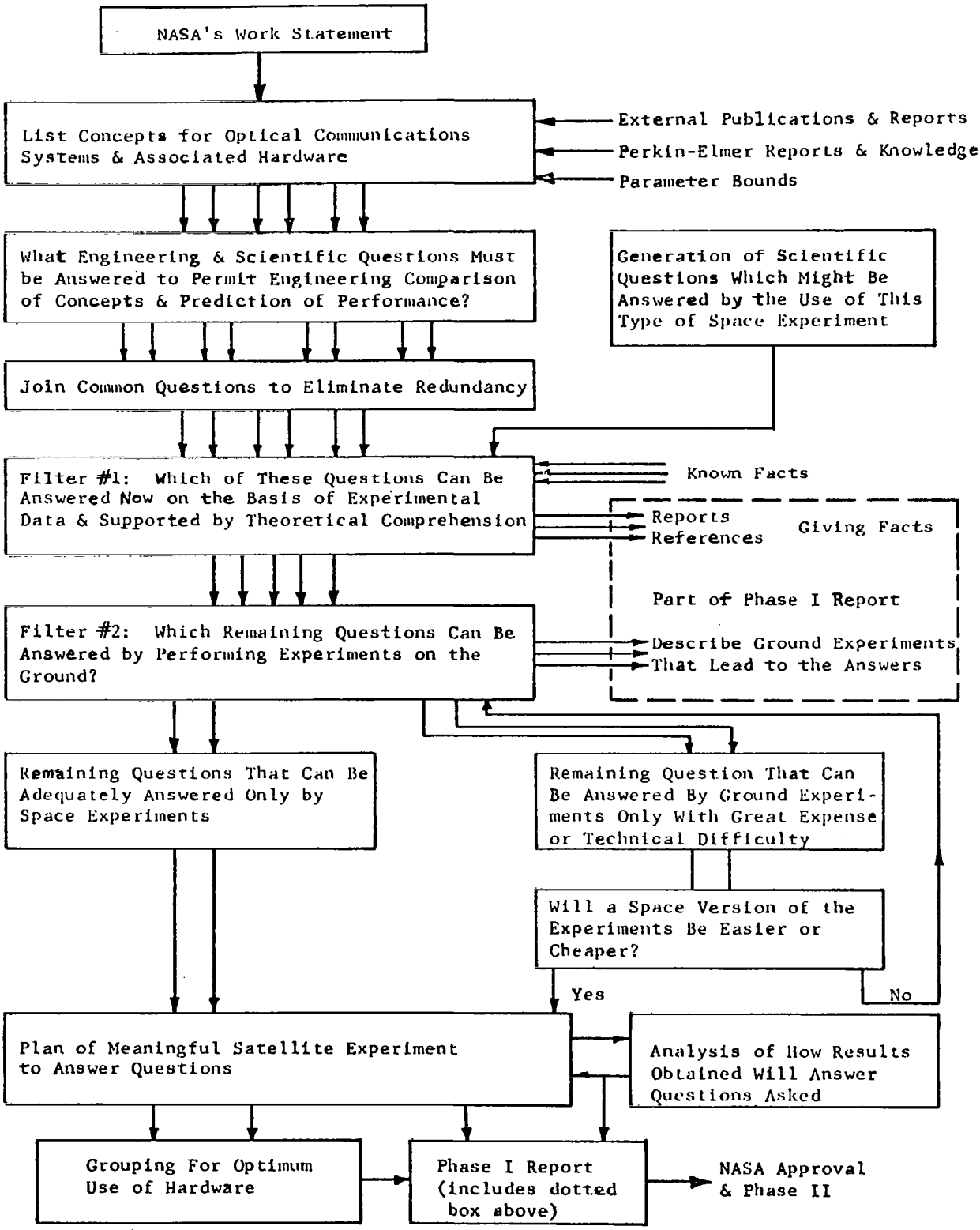

Figure A-1. Flow Chart Showing Method of Performing Phase One Tasks

APPENDIX B

ORBITAL CONSIDERATIONS

APPENDIX B

ORBITAL CONSIDERATIONS

The orbiting technology satellite must revolve in a nearly synchronous orbit in order to simulate properly the low angular velocities which occur between the ground station and a space vehicle traveling at interplanetary distances from earth. This analysis evaluates the angular velocity of a satellite as measured by an observer at the equator for a number of orbital choices.

In each case, the satellite is considered to revolve in the same direction as the earth along a circular orbit at constant tangential speed. Only the earth's rotation is considered in deriving the relative angular velocity between observer and satellite; other minor perturbations are ignored. At any instant the relative angular velocity of the ground station viewed from the satellite has the same magnitude as that measured by an earth observer.

A mathematical expression for the velocity of the satellite in the sky as measured by the observer at the equator can be derived in the following manner. Consider a set of inertial coordinates located so that the earth rotates about the Z axis. A second set of coordinates is fixed to the revolving earth with the origin at the observer's site (see Figure B-1).

The general expression[1] relating the velocity of a point measured in two coordinate systems accelerating with respect to each other is:

[1] R.A. Becker, Introduction to Theoretical Mechanics (1st ed. New York: McGraw-Hill Book Co., 1954), pp. 248-251.

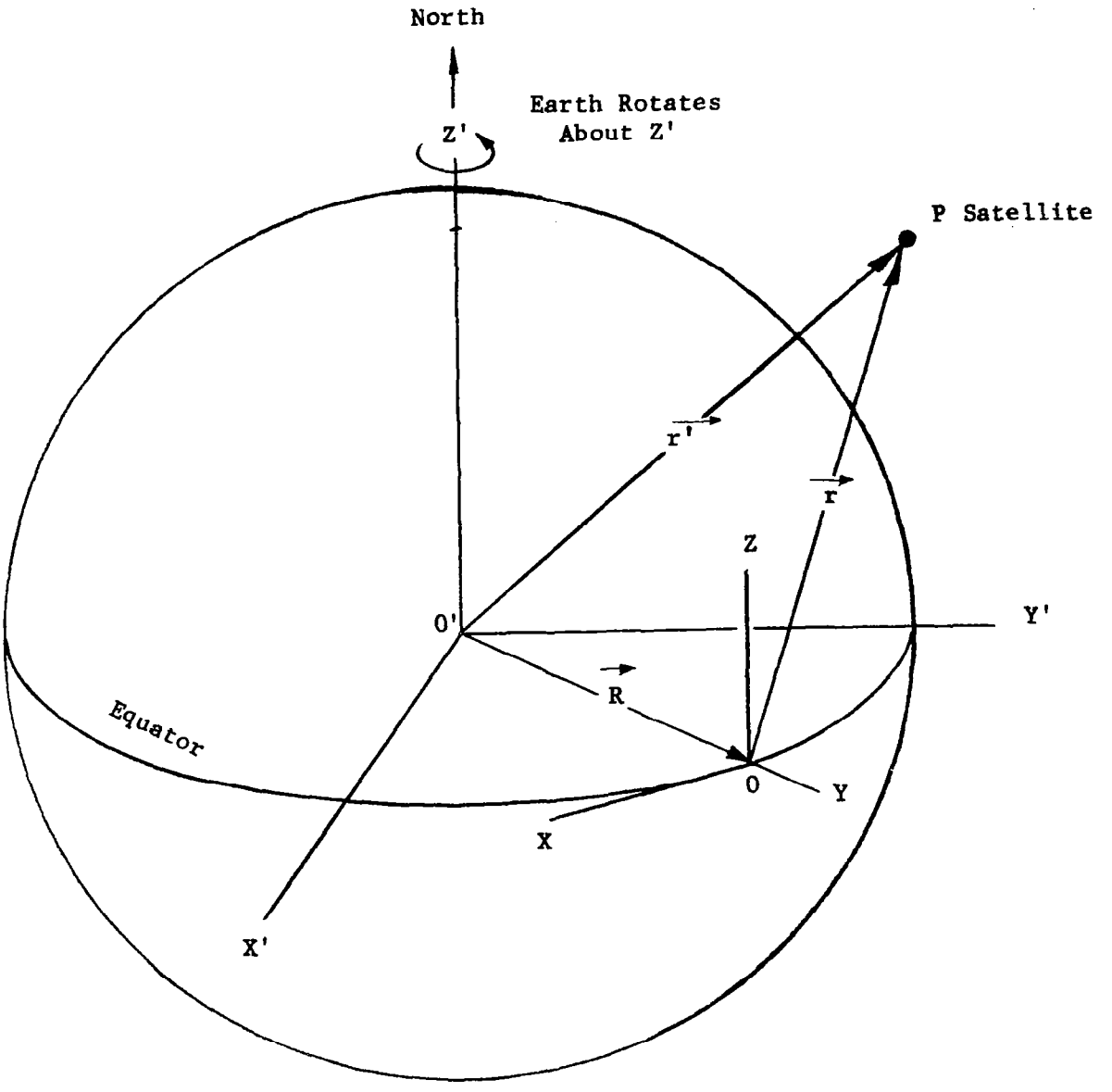

Primed Coordinate System Fixed

Unprimed Coordinate System Accelerates
(Rotates with Earth)

Figure B-1. Inertial and Rotating Coordinate Systems

$$\dot{\vec{r}}' = \dot{\vec{R}}' + \vec{\omega} \times \vec{r} + \dot{\vec{r}} \qquad (1)$$

where, with respect to the primed, fixed coordinate system:

$\dot{\vec{r}}'$ = the vector velocity of the moving point, P,

$\dot{\vec{R}}'$ = the vector velocity of the origin of the unprimed coordinate system,

and, with respect to the unprimed, accelerating coordinate system:

$\vec{\omega}$ = the vector rotational velocity of the unprimed coordinate system,

$\vec{r}$ = the position vector of the point, P, and

$\dot{\vec{r}}$ = the vector velocity of the point, P.

Consider first the case of a satellite in an orbit in the equatorial plane at an altitude, h, as shown in Figure B-2. Then the observed angular velocity of the satellite, ω_s, is given as:

$$\omega_s = \left| \frac{\dot{\vec{r}}}{h} \right| \qquad (2)$$

and

$$\left| \dot{\vec{r}} \right| = \left| \dot{\vec{r}}' \right| - \left| \dot{\vec{R}}' \right| - \left| \vec{\omega} \times \vec{r} \right|, \qquad (3)$$

since the above vectors are parallel to each other.

The absolute value of each term on the right side of Equation (3) is:

$\left| \dot{\vec{r}}' \right|$ = v_s, the speed of the satellite along its orbital path,

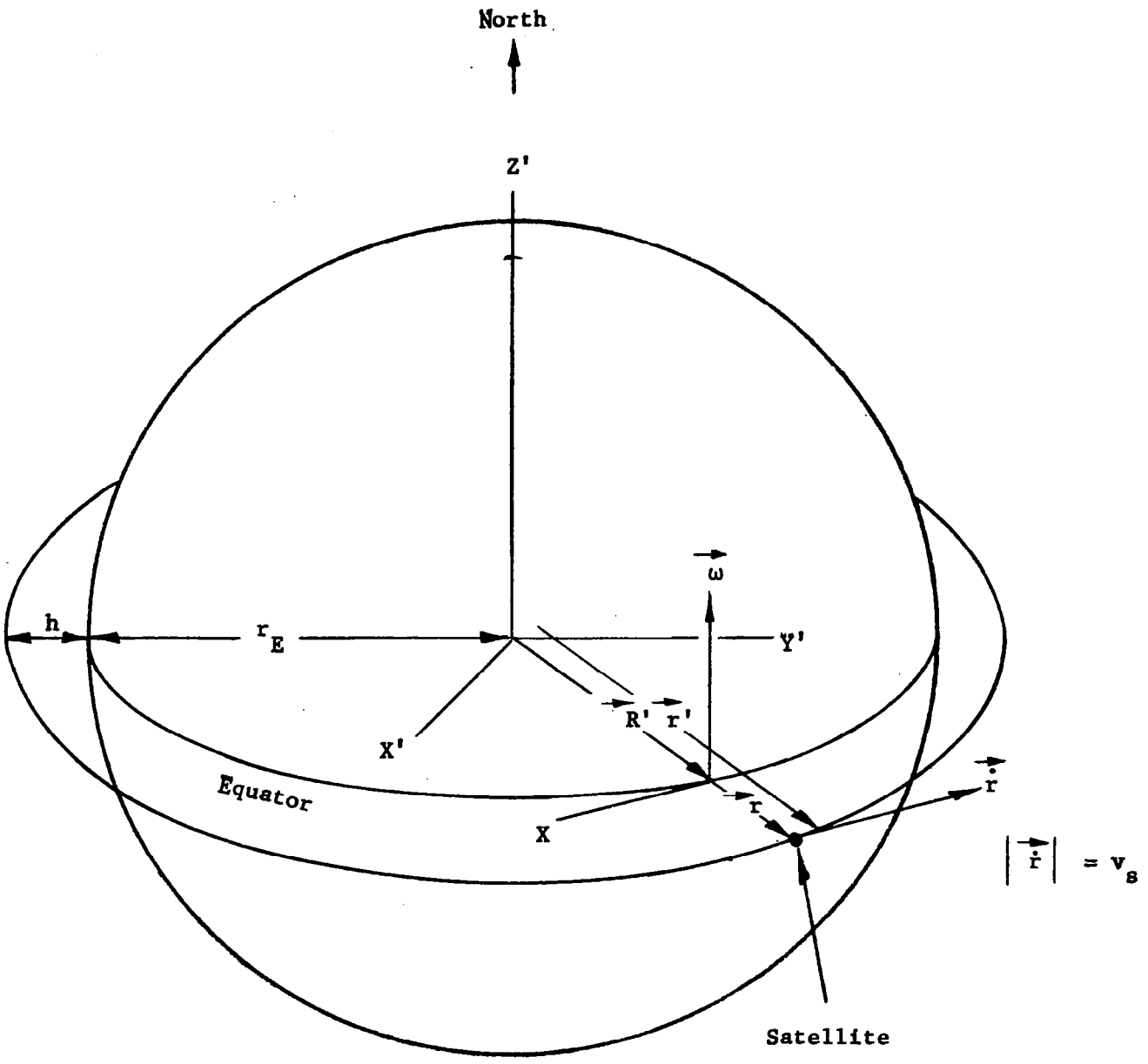

Figure B-2. Geometry of the Equatorial Angular Rate Determination; Orbit at Zero Inclination Angle

$\left|\dot{\vec{R}}'\right|$ = $\omega_E r_E$, the speed of the observer at the equator where ω_E is the earth's rotational speed and r_E is the earth's radius,

and

$\left|\vec{\omega} \times \vec{r}\right|$ = $\omega_E h$, the apparent speed of the satellite due to rotation of the observer's (unprimed) coordinate system.

Thus, on substitution,

$$\omega_s = \frac{v_s - \omega_E(r_E+h)}{h} \tag{4}$$

The value for v_s may be found by setting the centripetal force acting on the satellite equal to the gravitational force of attraction:

$$\frac{Gm_s m_E}{(r_E+h)^2} = \frac{m_s v_s^2}{(r_E+h)},$$

and solving for v_s yields:

$$v_s = \sqrt{\frac{Gm_E}{(r_E+h)}} \tag{5}$$

where

m_E = mass of the earth = 5.98×10^{27} gms;

m_s = mass of the satellite; and

G = gravitational constant = 6.67×10^{-8} $\frac{\text{dyne-cm}^2}{\text{gm}^2}$

The altitude of a satellite in synchronous orbit in the equatorial plane may be calculated by substituting Equation (5) into Equation (4) and solving for $r_E + h$, where $\omega_s = 0$:

$$r_E + h = \left[\frac{Gm_E}{\omega_E^2} \right]^{1/3} \qquad (6)$$

This expression is evaluated using the above numerical values of G and m_E, together with $\omega_E = 7.29 \times 10^{-5}$ rad/sec.

$$r_E + h = \left\{ \frac{\left(6.67\times10^{-8}\ \frac{\text{dyne-cm}^2}{\text{gm}^2} \times \frac{\text{gm-cm-sec}^{-2}}{\text{dyne}}\right)\left(5.98\times10^{27}\ \text{gms}\right)}{\left(7.29\times10^{-5}\ \text{rad/sec}\right)^2} \right\}^{1/3}$$

$$r_E + h = 4.22 \times 10^9 \text{ cm} = 13.8 \times 10^7 \text{ ft.}$$

Since

$$r_E = 2.09 \times 10^7 \text{ ft,}$$

$$h = 13.8 \times 10^7 \text{ ft} - 2.09 \times 10^7 \text{ ft,}$$

$$= 11.7 \times 10^7 \text{ ft,}$$

it is now possible to calculate v_s as:

$$v_s = \sqrt{\frac{\left(6.67\times10^{-8}\ \frac{\text{cm}^3}{\text{gm-sec}^2}\right)\left(5.98\times10^{27}\ \text{gms}\right)}{\left(4.22\times10^{9}\ \text{cm}\right)}}$$

$$v_s = 3.07 \times 10^5 \text{ cm/sec} = 10{,}100 \text{ ft/sec.}$$

Figure B-3 illustrates how the observed angular velocity, ω_s, varies at altitudes other than the one for synchronous orbit. At low altitudes the satellite appears to move rapidly in the direction of the earth's rotation.

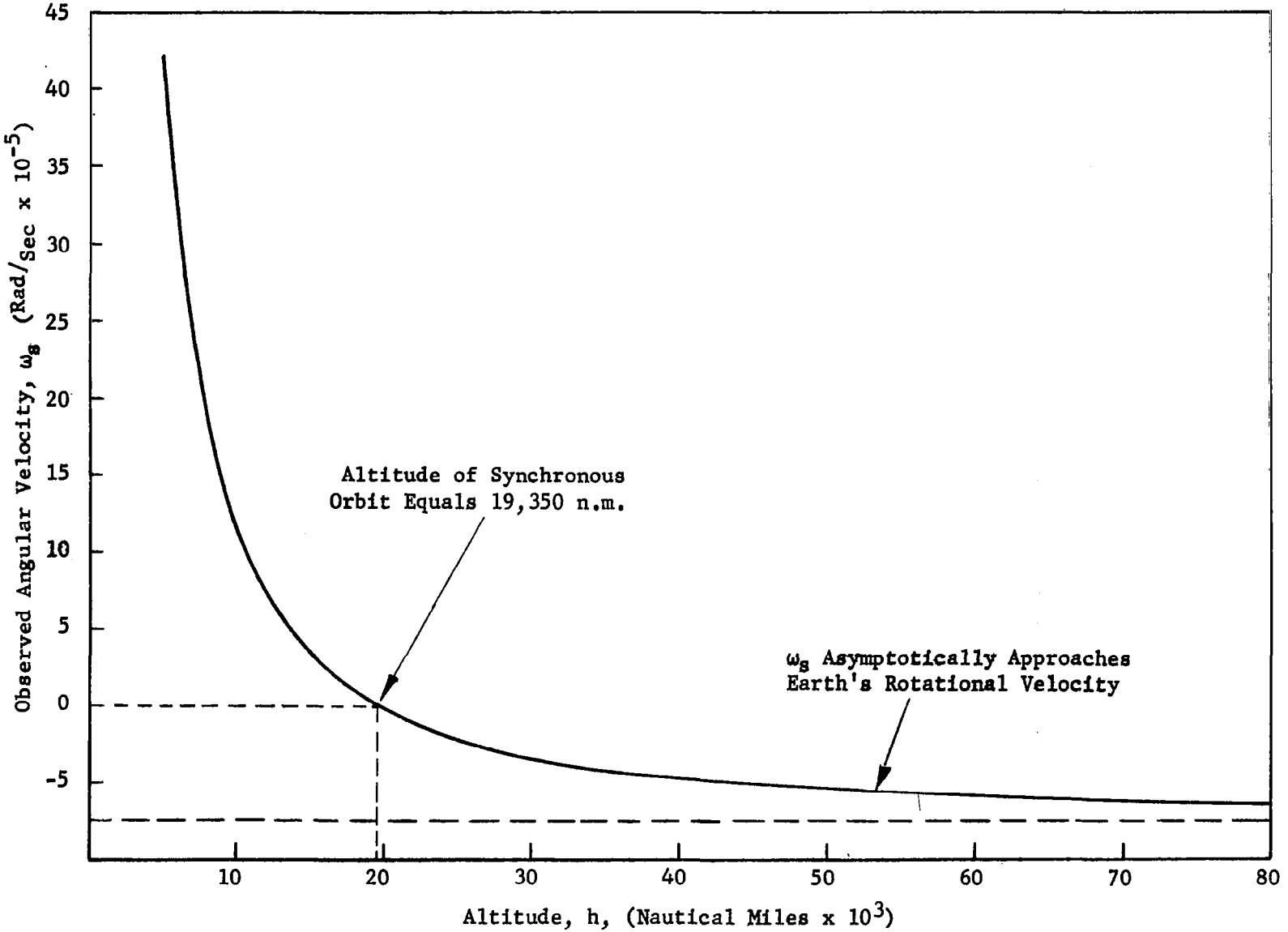

Figure B-3. Angular Velocity of a Satellite in an Equatorial Orbit Viewed from the Equator

At higher than synchronous altitudes the satellite appears to move in a direction opposite to the earth's rotation and, as expected, ω_s approaches $-\omega_E$, the earth's rotational velocity, as h approaches infinity.

If the synchronous altitude is maintained but the angle of inclination, θ, between the equatorial and the orbital planes is varied, figure "8" patterns will appear to be generated in the sky; the satellite will move around the "8" once in 24 hours. These will extend in a north-south direction with the center of the "8" on the equator. The maximum east-west angular velocity, $\omega_{s/E\text{-}W}$, will occur at the top and bottom of the "8" when the satellite velocity vector is parallel to the east-west direction. At these points, all the vectors of Equation (1) are parallel to one another, and, in a case similar to Equation (3), one may write:

$$\left|\dot{\vec{r}}\right| = v_s - \omega_E r_E - \left|\vec{\omega} \times \vec{r}\right|, \qquad (7)$$

and from Figure B-4,

$$\left|\vec{\omega} \times \vec{r}\right| = \omega_E d \sin\beta$$

$$\alpha = 90° - \beta$$

$$\left|\vec{\omega} \times \vec{r}\right| = \omega_E d \cos\alpha \qquad (8)$$

where d equals $\left|\vec{r}\right|$, the distance from the observer to the satellite. Substituting Equation (8) in Equation (7),

$$\left|\dot{\vec{r}}\right| = v_s - \omega_E (r_E + d\cos\alpha),$$

but

$$r_E + d\cos\alpha = (r_E + h)\cos\theta$$

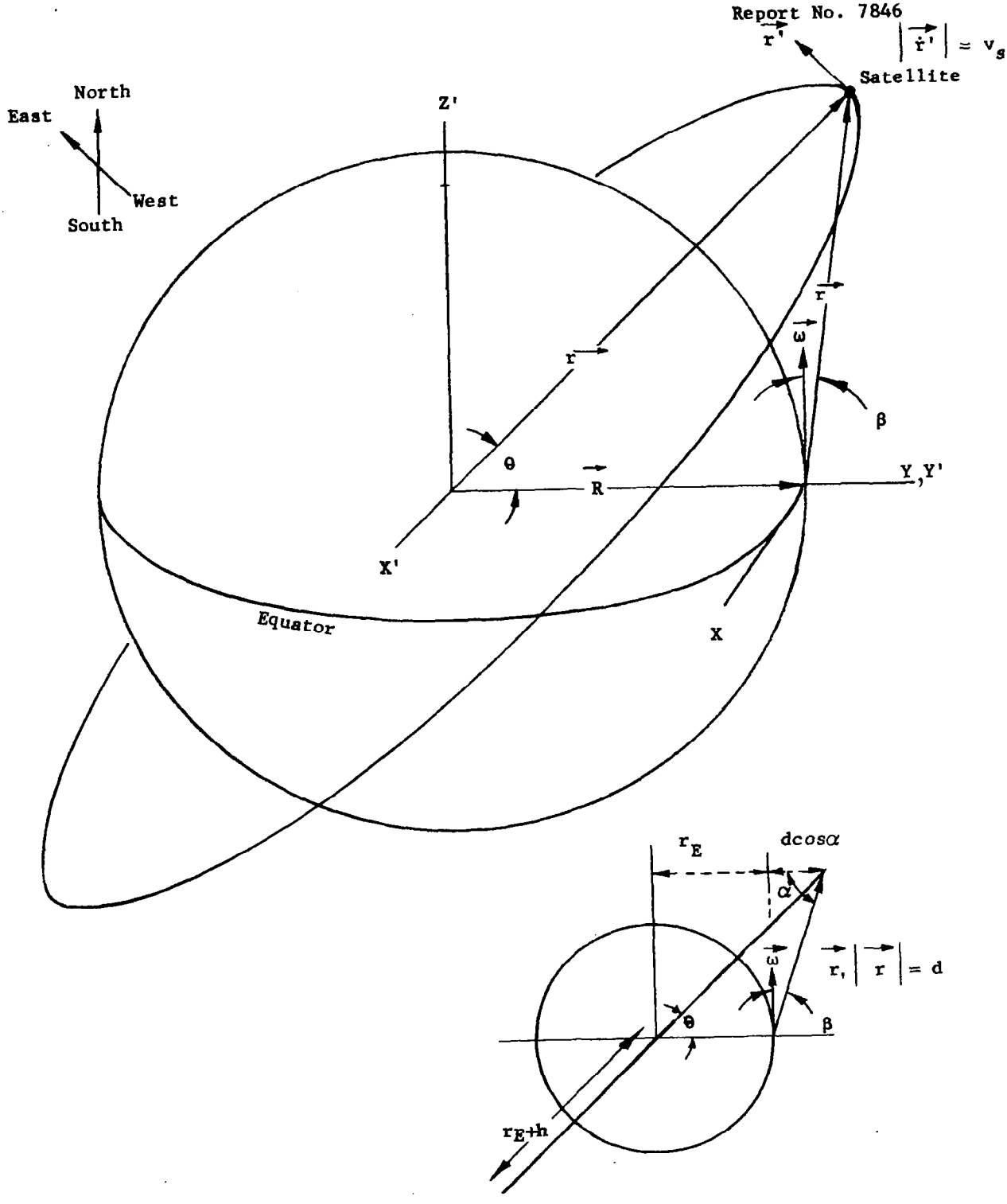

Figure B-4. Geometry of the East/West Angular Rate Determination; Orbit at Inclination Angle θ

and, therefore,

$$\left|\vec{\dot{r}}\right| = v_s - \omega_E\,(r_E+h)\,\cos\theta. \qquad (9)$$

Finally,

$$\omega_{s/E\text{-}W} = \left|\frac{\vec{\dot{r}}}{d}\right|,$$

and

$$\omega_{s/E\text{-}W} = \frac{v_s - \omega_E(r_E+h)\cos\theta}{d} \qquad (10)$$

When $\theta = 0°$, d becomes equal to the altitude, h, and Equation (10) reduces to Equation (4), as it should.

As a sample calculation, the value of $\omega_{s/E\text{-}W}$ will be calculated for an inclination angle, θ, of 60°. From the synchronous orbit calculation,

$$r_E+h = 13.8 \times 10^7 \text{ft} \qquad \omega_E = 7.29 \times 10^{-5}\ \frac{\text{rad}}{\text{sec}}$$

$$v_s = 10{,}100 \text{ ft/sec}$$

$$r_E = 2.09 \times 10^7 \text{ft}.$$

From the law of cosines,

$$d = \left[r_E^{\,2} + (r_E+h)^2 - 2r_E(r_E+h)\cos\theta\right]^{1/2}$$

$$= \left[(2.09\text{x}10^7)^2 + (13.8\text{x}10^7)^2 - 2(2.09\text{x}10^7)(13.8\text{x}10^7)(.5)\right]^{1/2} \text{ft}$$

$$= 12.9\text{x}10^7 \text{ ft}.$$

On substitution,

$$\omega_{s/E\text{-}W} = \frac{10{,}000 \text{ ft/sec} - \left(7.29\text{x}10^{-5}\ \frac{\text{rad}}{\text{sec}}\right)\ (13.8\text{x}10^7 \text{ft})(.5)}{12.9\text{x}10^7 \text{ ft}},$$

$$\omega_{s/E\text{-}W} = 3.94\text{x}10^{-5} \text{ rad/sec}.$$

The maximum east-west angular velocity is plotted in Figure B-5 for other inclination angles up to 60°

The maximum angular velocity, $\omega_{s/N-S}$, in the north-south direction occurs at the point where the path of the satellite crosses the equatorial plane, as shown in Figure B-6. At this point, the satellite is radially opposite the observation point and directly overhead, which facilitates the computation. It is clear from Figure B-6 that

$$\omega_{s/N-S} = \frac{v_s \sin\theta}{h} \qquad (11)$$

As a sample calculation, again consider $\theta = 60°$. Then,

$$\omega_{s/N-S} = \frac{(10{,}100 \text{ ft/sec})(.866)}{11.7 \times 10^7 \text{ ft}}$$

$$\omega_{s/N-S} = 7.48 \times 10^{-5} \text{ rad/sec.}$$

The north-south angular velocity at inclination angles up to 60° is shown in Figure B-7.

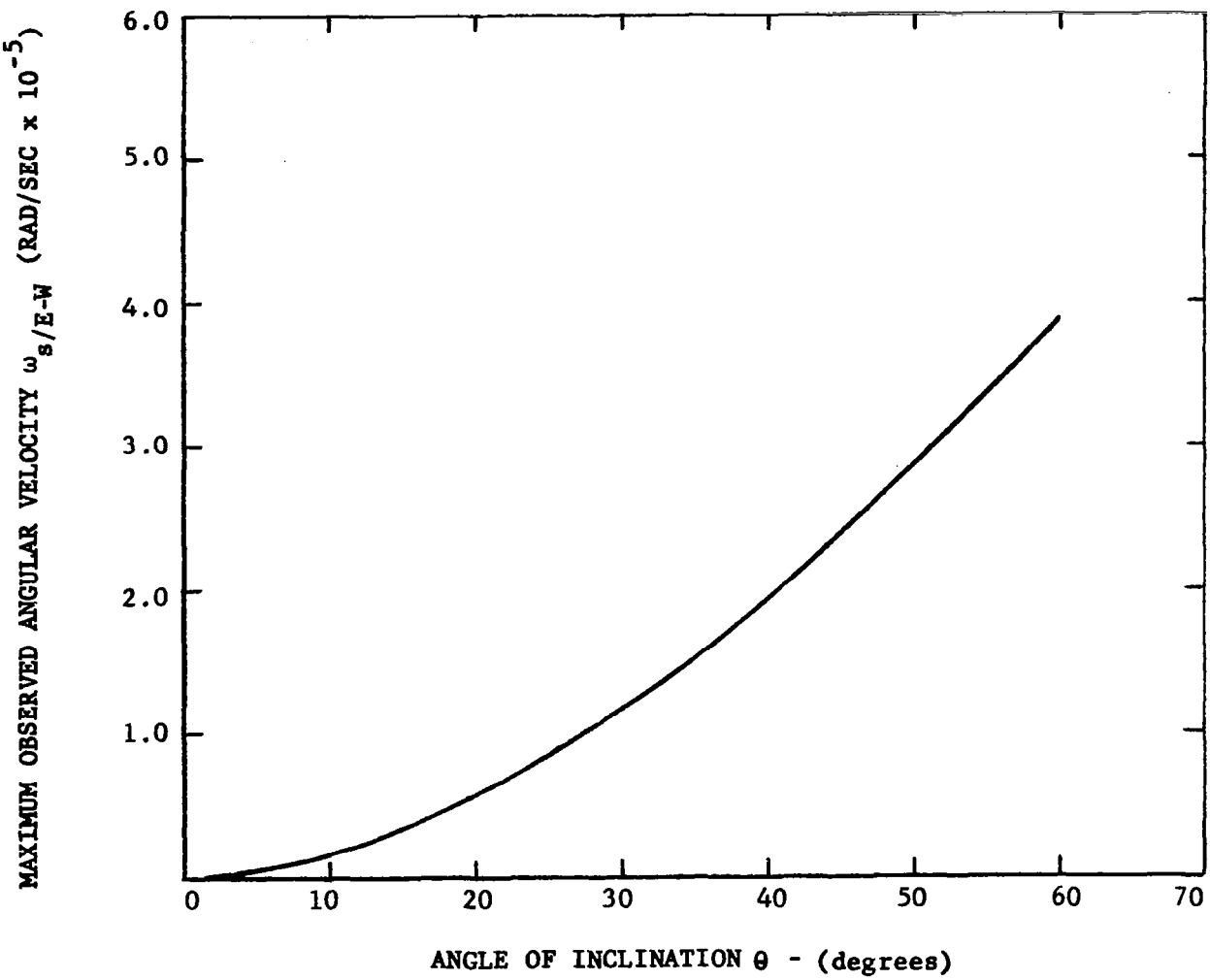

Figure B-5. Maximum Angular Velocity in the East-West Direction Viewed From the Equator Versus Angle of Inclination of the Orbital Plane

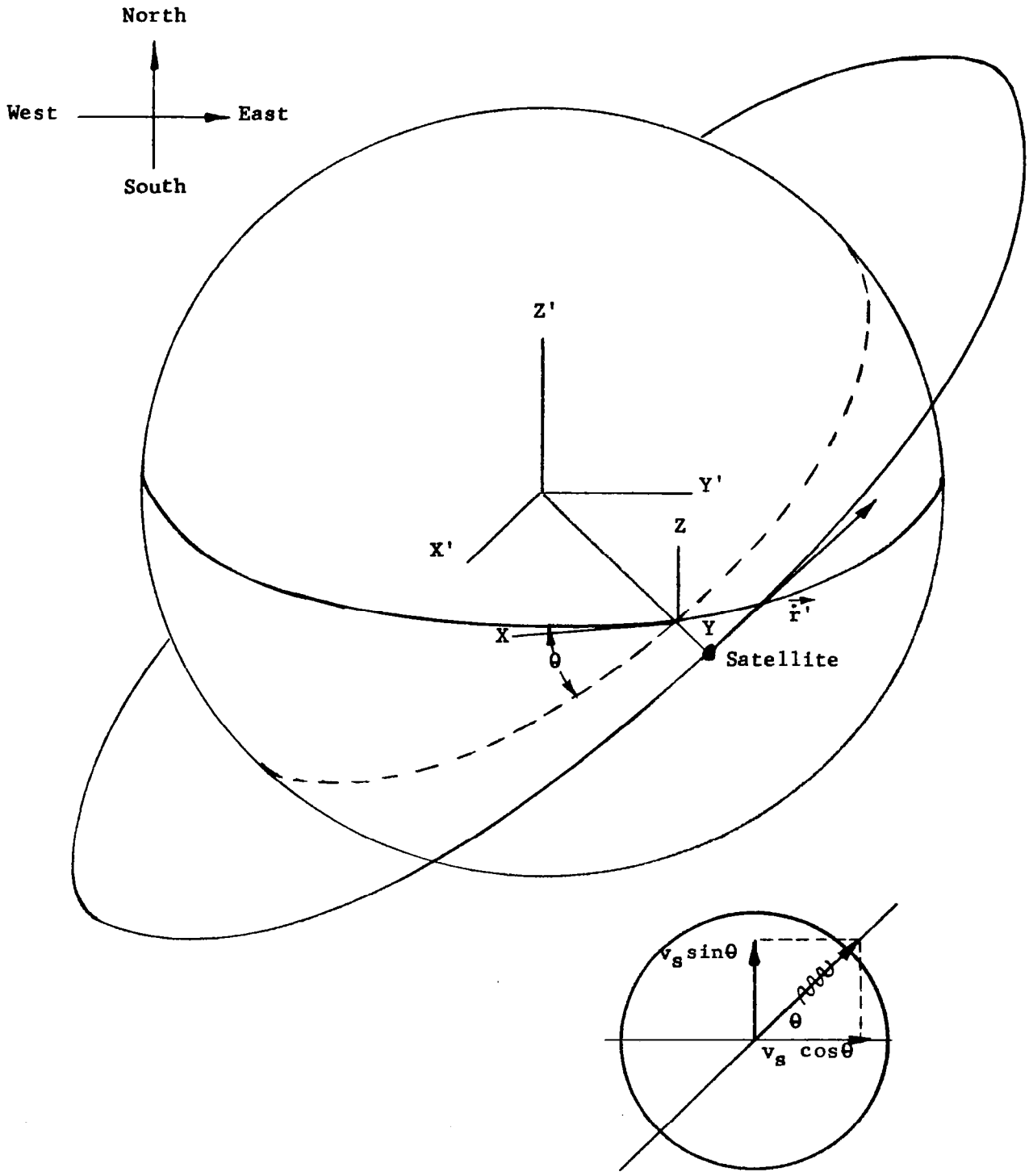

Figure B-6. Geometry of the North/South Angular Rate Determination; Orbit at Inclination Angle θ

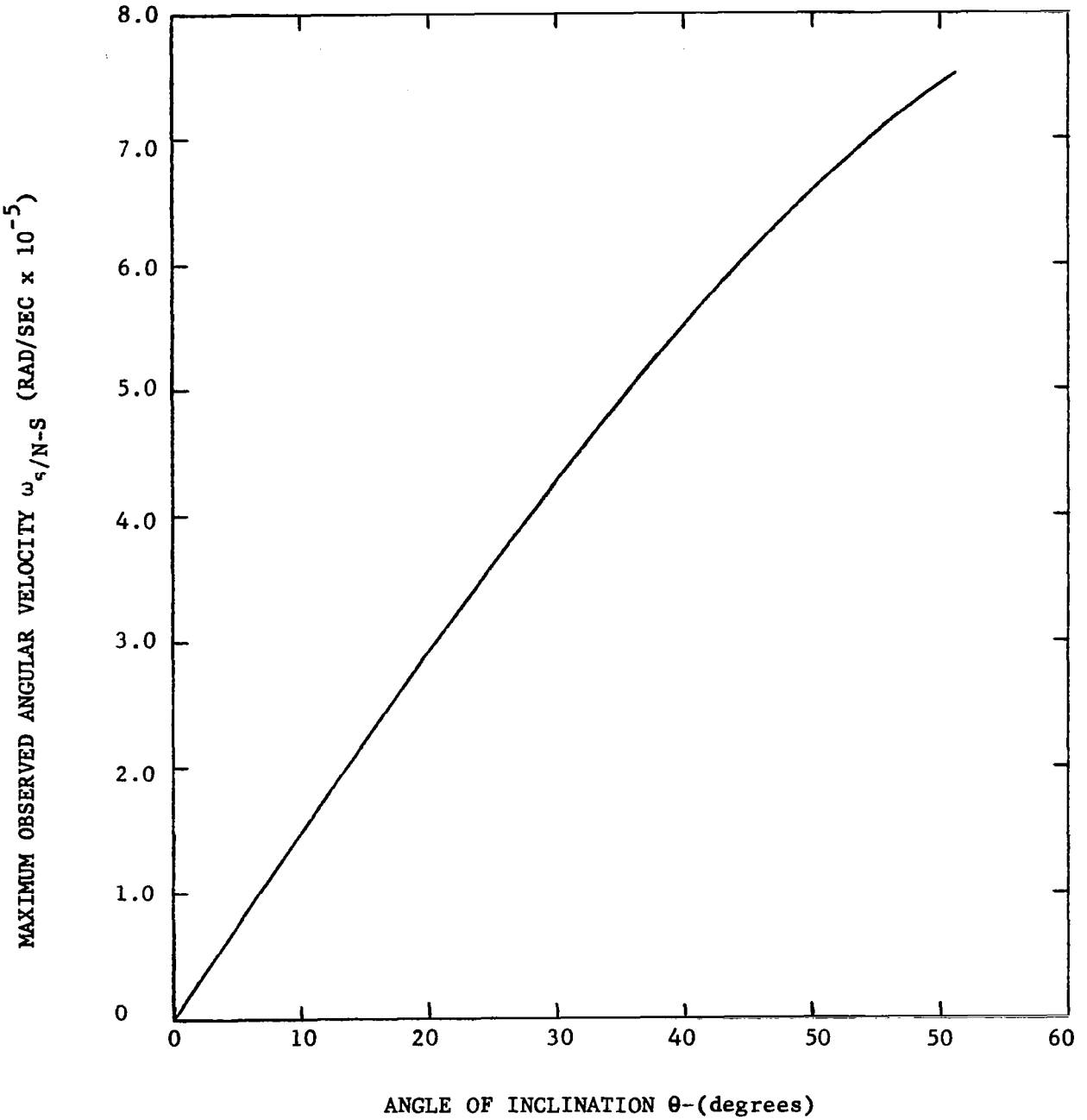

Figure B-7. Maximum Angular Velocity in the North-South Direction Viewed From the Equator Versus Angle of Inclination of the Orbital Plane

APPENDIX C

REFLECTOR STUDY

APPENDIX C

REFLECTOR STUDY

I. REFLECTOR PARAMETER RELATIONSHIPS

A. Introduction

A reflector intended for use as part of the space-borne optical or microwave system should generally represent the best possible combination of the following characteristics:

(1) Light weight

(2) Sufficient rigidity to permit fabrication and testing on the ground (in a gravity environment) to the degree of accuracy necessary to assure correct dimensional properties in gravity-free operation

(3) Sufficient strength to survive the rigors of launch vehicle environments with no permanent deformations

(4) Surface accuracy, resistance to thermal and other environmental effects, and dimensional stability consistent with the performance requirements of the system.

It is apparent, of course, that the cell or support system is a critical factor in all of the above characteristics. It is thus virtually

impossible to realistically consider reflectors without simultaneously considering their support systems either implicitly or explicitly. The support systems for fabrication, testing, launch, and operation may all be different. Each must meet different requirements and must operate in a particular environment.

Selection of materials for reflector fabrication invariably requires a compromise between conflicting requirements. Desirable properties include high stiffness-to-weight ratio, high thermal conductivity, low thermal expansion, ease of fabrication, dimensional stability, mechanical strength, and suitability for the degree of surface finish required.

B. Summary

The relationship between reflector diameter, reflector weight, and operating wavelength is of considerable interest in the evaluation of overall system characteristics. The following discussion attempts to arrive at a reasonable means of reducing the many variables suggested by the above paragraphs to a point where meaningful relationships between aperture, weight, and wavelength may be discerned.

Three approaches have been considered. In each case, it has been assumed that diffraction-limited systems are required, i.e., that the allowable departure from the ideal surface must be limited to a specific small fraction of the operating wavelength. The first of the three approaches effectively assumes geometrically similar support systems for reflectors of various diameters. In so doing, the full responsibility for maintaining constant deflections as diameter increases is placed on improved stiffness characteristics

of the reflector. The second approach assumes that the number of support points would increase in direct proportion to the area of the reflector. This assumption assigns full responsibility for maintaining constant deflections to the support system, and results in reflector stiffness requirements being independent of diameter. The third approach represents a compromise between the first two, and yields relationships which require both the support system and the stiffness characteristics of the reflector to improve as diameter increases.

The three alternative approaches are discussed in detail in the following paragraphs.

C. Approach No. 1

Perhaps the most difficult characteristic to define for a reflector to be used in the absence of gravity or inertia forces is required stiffness. Operational stiffness requirements, assuming a support system which does not introduce constraining loads, are nil. The stiffness requirements are thus determined by ground fabrication and testing requirements and, indirectly, by the need for resistance to launch loads. If it may be assumed that satisfying requirements for fabrication and testing will automatically result in a workable solution to the launch problem, the latter may be neglected.

How stiff must a reflector be to permit fabrication and testing? Ideally, a very good support system, consisting, for example, of a large number of precisely adjusted counterweights, could be provided to balance out the weight and hence eliminate gravity deflections, permitting testing of even the most flexible of reflectors. The extent to which this ideal situation may be

approached is determined by a variety of practical considerations, including the accuracy with which the various supports may be located and adjusted.

Since it is difficult to predict the cumulative effect of support system imperfections, let us make the admittedly arbitrary but seemingly reasonable assumption that the net effect is equivalent to one percent of the mirror weight acting at its center and reacted uniformly over the reflector area. For a circular, homogeneous plate of uniform thickness, the deflection due to such a load is:

$$(1)^* \qquad \delta = \frac{3(0.01W)\ K\ d^2}{64\pi E\ t^3}$$

where W = reflector weight $= \frac{\rho\pi d^2 t}{4}$;

$$K = \frac{(m-1)(7m+3)}{m^2};$$

$$m = \frac{1}{\nu^2} = \frac{1}{(\text{Poisson's ratio})^2};$$

d = reflector diameter;

E = Young's modulus;

t = reflector thickness $= \frac{4W}{\rho\pi d^2}$; and

ρ = material density.

If it is further assumed that the allowable value of this deflection is 1/50 of the operating wavelength, the above expression may be reduced to:

$$(2) \qquad \frac{d^2}{t\sqrt{\lambda}} = \sqrt{\frac{171\ E}{\rho\ K}} \qquad \text{where } \lambda = \text{wavelength}$$

or, expressing t in terms of W,

*From Roark, Formulas for Stress and Strain, Table X, Case 11.

$$(3) \qquad d = \left[\frac{276\ E}{K\rho^3}\right]^{1/8} W^{1/4} \lambda^{1/8}$$

Equation (2) shows that, for a given material, the stated assumptions require that:

$$(4) \qquad \frac{d^2}{t\sqrt{\lambda}} = \text{constant} = k_1$$

Similarly, it is evident from Equation (3) that the attainable aperture varies with a constant determined by material properties, with the fourth root of the allowable weight, and with the eighth root of the selected wavelength.

The above relations apply only to solid plates of uniform thickness. Such a configuration is probably not of much interest for space applications because of the weight penalties involved. In order to adapt the expressions to lightweight configurations, let us assume that a solid plate of specified thickness may be replaced by a lightweight structure, of approximately the same thickness, with the same stiffness-to-weight ratio (i.e., with identical gravity deflection characteristics), but with only 25 percent of the weight of the solid plate. This approximation is in general agreement with actual state-of-the-art experience on a variety of optical reflectors. If the weight of the lightweight mirror is designated by W_L, Equation (3) thus becomes:

$$(5) \qquad d = \sqrt{2}\left[\frac{276\ E}{K\rho^3}\right]^{1/8} W_L^{1/4} \lambda^{1/8}$$

Figure C-1 charts Equations (2) and (5) in terms of diameter versus wavelength curves for fused silica reflectors and for various values of t and W_L, respectively. Also shown are curves for various values of beamwidth, where the angular width of the transmitted beam is taken as:

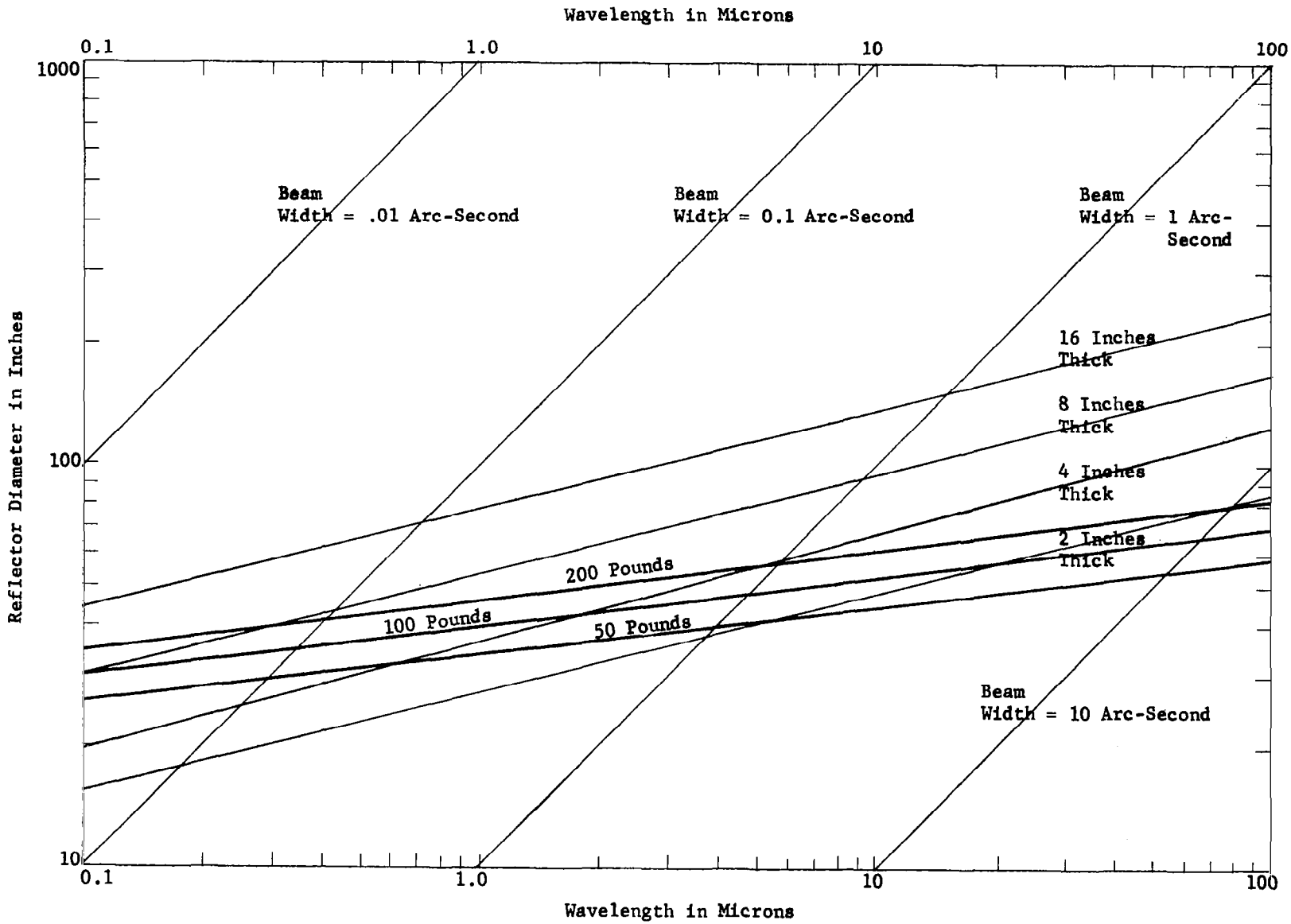

Figure C-1. Reflector Parameter Chart for $\frac{d^2}{t\,\lambda^{1/2}} = 5.84 \times 10^4\ in^{1/2}$

$\rho = 0.08\ Lb/In^3$

(6) $$\theta_s = \frac{1.22\,\lambda}{d}$$

The most prominent characteristic demonstrated by Figure C-1 is the rate at which thickness and weight increase with diameter. This phenomenon results from the fact that the way in which required rigidity was defined is equivalent to assuming that the support systems for all diameters are geometrically similar. This assumption leads directly to Equation (2).

The effect of different reflector materials is evident from Table C-1 which shows the values of the constants in Equations (2) and (5) for the most frequently considered reflector materials.

TABLE C-1

Values of Material Constants - Approach No. 1

MATERIAL	$\sqrt{\frac{171\ E}{\rho K}}$	$\left[\frac{276\ E}{K\rho^3}\right]^{1/8}$
Fused Silica	5.8×10^4 in$^{1/2}$	31.0 in$^{7/8}$ lb$^{-1/4}$
Beryllium	12.4×10^4	39.4
Aluminum	5.6×10^4	29.0
Magnesium	5.6×10^4	32.4

It is apparent that the various materials are nearly equivalent with the exception of beryllium which, at a particular wavelength, permits an aperture increase to $\sqrt{\frac{12.4}{5.8}} = 1.46 = 146\%$ for the same thickness or $\frac{39.4}{31.0} = 1.27 = 127\%$ for the same weight when compared with corresponding values for fused silica.

D. Approach No. 2

A very different approach to the problem of specifying stiffness requirements is suggested by the trend towards multiple support points for large mirrors. Examples include the 15-point support system for the Stratoscope II primary and the 36-point system which supports the 200-inch Palomar mirror. Suppose the assumption is made that the number of uniformly spaced support points will increase with the square of aperture diameter, i.e., that the ratio of aperture area to the number of support points is constant. This being true, the maximum gravity deflections will be proportional to the reflector weight over each support, which in turn is proportional to mirror thickness and material density. Similarly, the deflections will be inversely proportional to flexural rigidity, which is defined as $Et^3/12(1-\nu^2)$. If it is again assumed that the allowable deflection is proportional to wavelength:

$$\delta = \frac{k'\rho t(12)(1-\nu^2)}{Et^3} = k''\lambda \tag{7}$$

Equation (7) may be reduced to:

$$\frac{1}{t\sqrt{\lambda}} = k_2 \sqrt{\frac{E}{\rho(1-\nu^2)}} \tag{8}$$

Again, it is evident that, for a given material:

$$\frac{1}{t\sqrt{\lambda}} = \text{constant} = k_3 \tag{9}$$

The thickness requirements are thus independent of diameter. This, of course, results from the initial assumption which, in effect, requires the penalties of increased diameter to be compensated entirely by the support system.

Using the relationship $W = \rho \frac{\pi d^2}{4} t$, Equation (8) may be re-written as:

$$(10) \qquad d = k_4 \left[\frac{E}{\rho^3 (1-\nu^2)} \right]^{1/4} W^{1/2} \lambda^{1/4}$$

If the assumption is again made that the weight of an equivalent lightweight mirror will be $W_L = 0.25\ W$, Equation (10) becomes:

$$(11) \qquad d = 2k_4 \left[\frac{E}{\rho^3 (1-\nu^2)} \right]^{1/4} W_L^{1/2} \lambda^{1/4}$$

The attainable aperture diameter is thus proportional to a constant determined by material properties, to the square root of allowable weight, and to the fourth root of the selected wavelength.

Figure C-2 charts Equations (8) and (11) in terms of diameter versus wavelength curves for fused silica reflectors and for various values of t and W_L. The various proportionality constants were determined for this figure by taking the thickness (5.0 inches) and operating wavelength (20×10^{-6} inches) of the fused silica Stratoscope II primary mirror as a reference point. Thus:

$$k_2 = 0.004 \text{ in}^{-2}$$
$$k_3 = 44.8 \text{ in}^{-3/2}$$
$$k_4 = 0.071 \text{ in}^{-1}$$

Curves of d versus λ for various values of beamwidth, identical with those of Figure C-1, are also shown.

Comparison with Figure C-1 indicates that approach No. 2 yields much more optimistic results in terms of weight and thickness requirements,

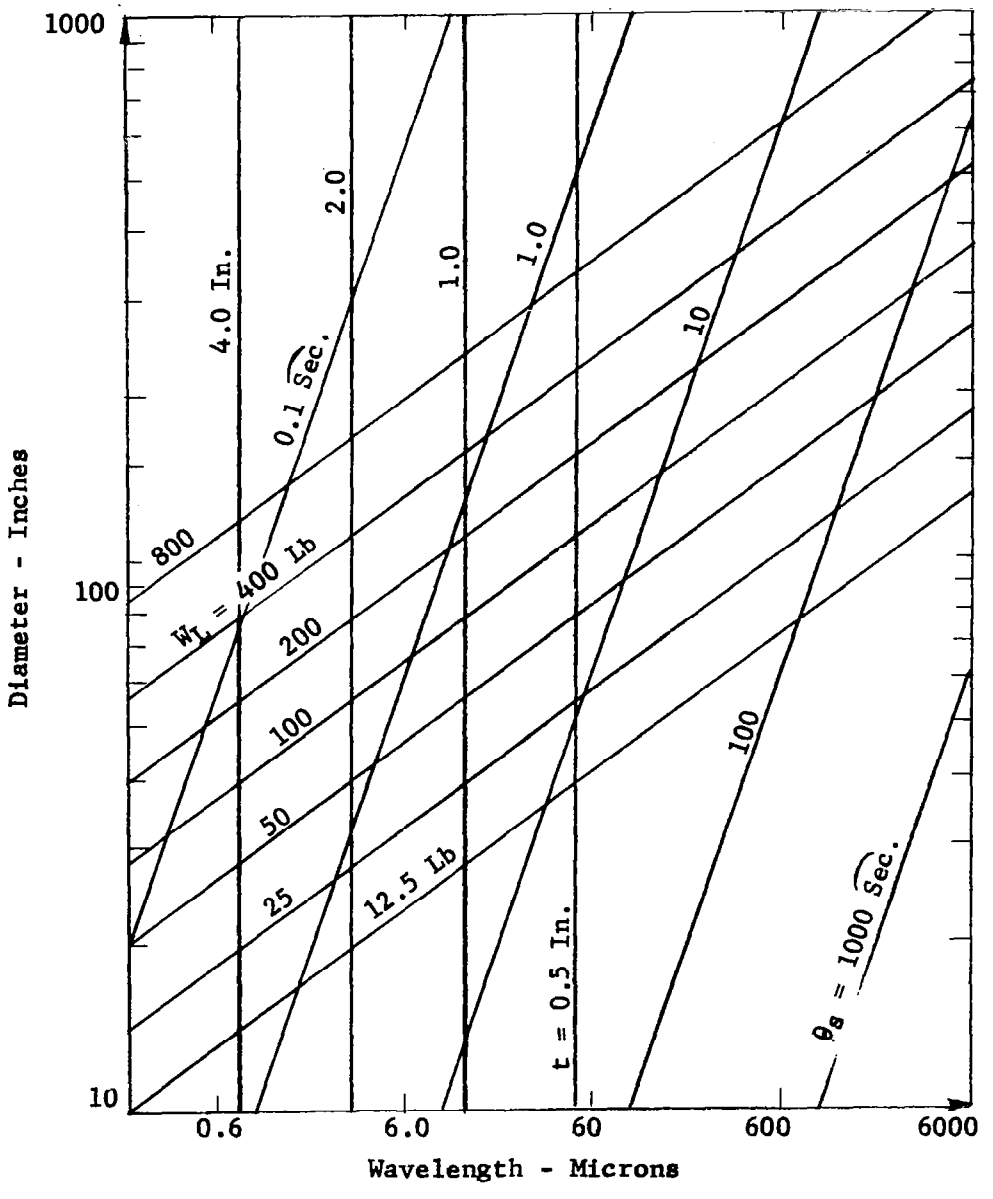

Figure C-2. Reflector Parameter Chart For $\frac{1}{d\sqrt{\lambda}}$ = Const. = 448 in $^{-3/2}$ ρ = .0.08 Lb/In^3

particularly for large diameters and relatively long wavelengths. This result stems directly from the comparison of Equations (4) and (9).

The degree to which varying material properties affect the results of this approach may be deduced from Table C-2, which shows the values of the material constants in Equations (8) and (11) for the most frequently considered reflector materials.

TABLE C-2

Values of Material Constants - Approach No. 2

MATERIAL	$\sqrt{\frac{E}{\rho(1-\nu^2)}}$	$\left[\frac{E}{\rho^3(1-\nu^2)}\right]^{1/4}$
Fused Silica	11.3×10^3 $in^{1/2}$	376 $in^{7/4}$ $lb^{-1/2}$
Beryllium	24.8×10^3	617
Aluminum	10.5×10^3	324
Magnesium	10.5×10^3	403

Again comparing fused silica and beryllium, it is evident that at a given wavelength, the latter permits a thickness decrease to $\frac{11.3}{24.8} = 0.46 = 46\%$ and, for the same weight, an aperture increase to $\frac{617}{376} = 1.64 = 164\%$ of the corresponding values for fused silica.

E. Approach No. 3

The two approaches discussed above involve assumptions which, in effect, require the entire burden of increased aperture to be borne by the rigidity characteristics of the reflector in one case or by the support system in the other. It is of interest to consider a compromise between these

extremes, i.e., an approach in which the problems of increased diameter are shared by the reflector itself and by the support system.

Examination of Equations (4) and (9) shows that Approach No. 1 requires $\frac{d^2}{t\sqrt{\lambda}}$ to be a constant, while Approach No. 3 requires $\frac{1}{t\sqrt{\lambda}}$ $\left(\text{or } \frac{d^0}{t\sqrt{\lambda}}\right)$ to be held constant. An evident compromise between these approaches would be to define $\frac{d}{t\sqrt{\lambda}}$ as constant.

$$\frac{d}{t\sqrt{\lambda}} = \text{constant} = K_5 \tag{12}$$

It is difficult to assign a specific and logical interpretation to such a definition beyond the fact that it is a compromise between two approaches which do have explicit derivations. However, at a constant wavelength, Equation (12) says that the ratio of diameter to thickness is constant. The latter statement has long been used as an empirical or "rule-of-thumb" design guide for optical mirrors. Again, noting that $W = \rho \frac{\pi d^2}{4} t$, Equation (12) may be rewritten as:

$$d = k_6 W^{1/3} \lambda^{1/6} \tag{13}$$

Repeating the assumption that the weight of an equivalent lightweight mirror is $W_L = 0.25W$, Equation (13) becomes:

$$d = 1.59\, k_6 W^{1/3} \lambda^{1/6} \tag{14}$$

Figure C-3 charts Equations (12) and (14) in terms of diameter versus wavelength curves for fused silica reflectors and for various values

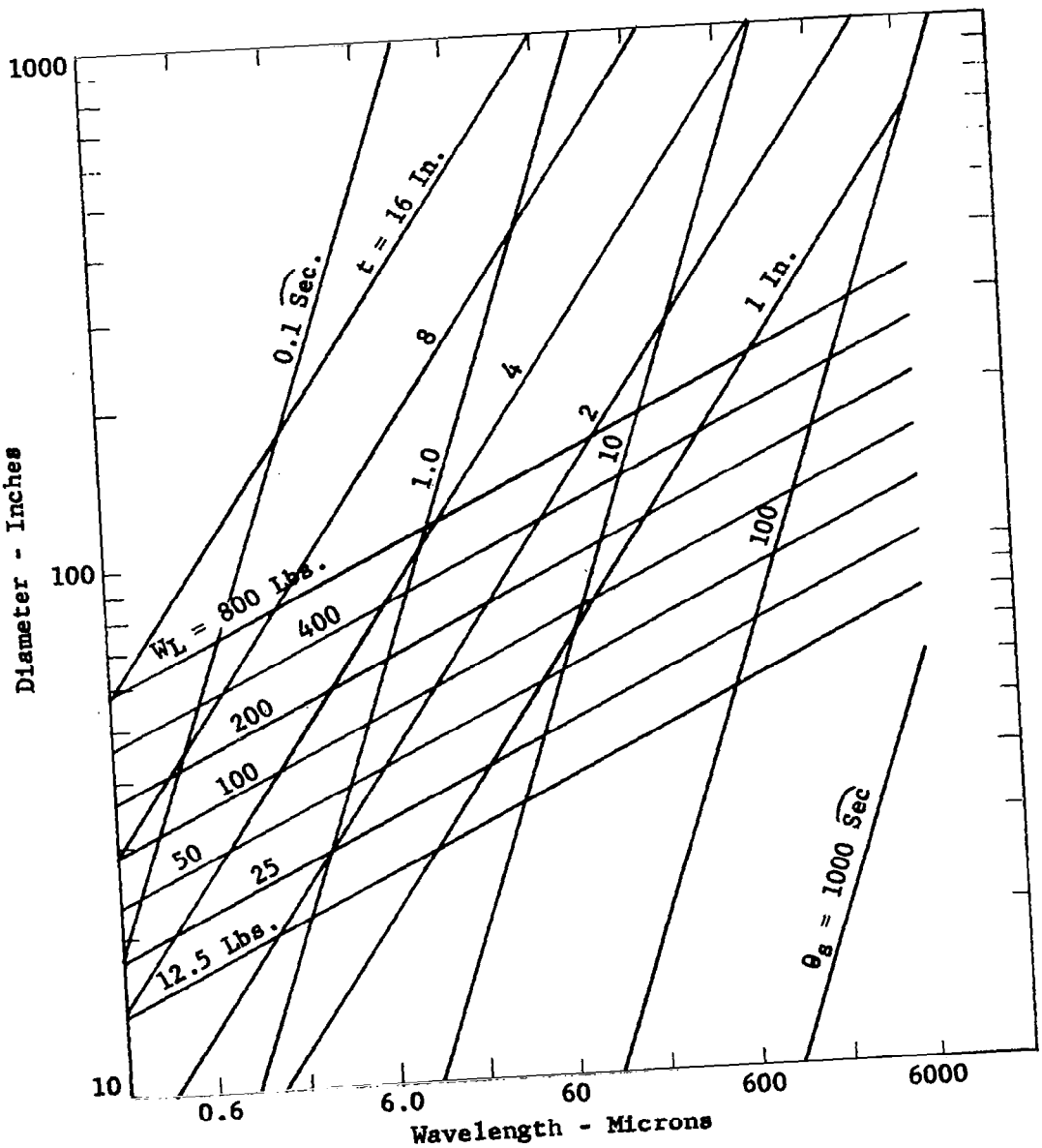

Figure C-3. Reflector Parameter Chart For $\frac{d}{t\sqrt{\lambda}}$ =

Const. = 1340 $in^{-1/2}$ ρ = 0.08 Lb/In^3

of t and W_L. The constant k_5 was found to be 1340 $in^{-1/2}$ by assuming a diameter/thickness ratio of 6.0 at a wavelength of 20 x 10^{-6} inches (0.5 micron). The corresponding value of k_6 is 27.8 $in^{5/6}$ $lb^{-1/3}$ for fused silica. The curves of d versus λ for various values of angular beamwidth are again included.

F. Conclusions

Three alternative approaches to the problem of describing the relationships between important reflector parameters have been presented. Each is based on a different assumption of the extent to which the support system used for ground testing will reduce the need for reflector rigidity.

It is important to note that Figures C-1 through C-3 are plotted on the basis of proportionality constants derived from arbitrary judgments or by reference to existing reflectors of known characteristics. The numerical data obtained from these figures must thus be subject to some variation. The character of the relationships, however, is valid for the conditions defined in each case.

While specific evaluation of the relative merits of the three approaches is not feasible, some tentative conclusions may be drawn. Perhaps the most evident is that Approach No. 1 is not consistent with the inevitable trend for support systems to become more sophisticated as aperture diameters increase. This is particularly true since the support system of primary concern here is that employed for testing on the ground, where support system weight is of little consequence. Overall system objectives would seem to warrant all practical emphasis on ground test support systems in order to reduce the weight of the mirror and, hence, of its flight support system and back-up structure.

Approach No. 2 is most consistent with this concept. A relationship which shows reflector thickness to be independent of diameter is admittedly surprising in terms of the thinking applied to ground-based applications. There appears to be no real reason, however, why development of fabrication and testing procedures specifically directed at this objective should not yield favorable results. Since efforts in this direction are demanding increasingly serious attention, Approach No. 2 might reasonably be considered as a projection of future developments.

Conversely, Approach No. 3 is most representative of the present state-of-the-art. It assumes that both reflector rigidity and support system sophistication must increase as aperture diameter increases. It does not take full advantage of the gravity-free operating environment, but also does not impose severe requirements on the ground test support system.

Each of the alternative approaches considers only the reflector itself. This, of course, is only part of the story. The characteristics of the reflector are unavoidably related to those of the launch and operational support systems and to the structural requirements of the vehicle.

II. SUPPORT SYSTEMS

Consideration of support systems for space reflectors must include at least four distinct situations: fabrication, ground testing, launch, and operation. These situations may require four separate support systems or may be adequately provided for by a smaller number of multi-purpose systems.

Support of a reflector during fabrication is perhaps the least difficult to provide. It is almost inevitable that significant distortions

will result from fabricating forces or thermal inputs. As long as the reflector can be accurately tested and dimensional errors located, however, these errors may be repeatedly reduced until successful results are attained. It is true, of course, that large deflections of the reflector during fabrication will considerably complicate and protract this procedure.

The importance of the support system employed for ground testing was emphasized in the discussion of reflector parameter relationships. The degree to which extremely effective test support systems can be developed is a key to successful fabrication of thin mirrors. Ideally, such support systems must negate the effects of gravity, i.e., eliminate all deflections caused by the weight of the reflector material. One way of approximating this ideal is with a system of counterweights, each of which is adjusted to exactly react the weight of its share of the reflector. Such a system is employed to support the 36-inch diameter primary mirror of Stratoscope II. Figure C-4 shows a portion of the fifteen counterweights in the Stratoscope II primary cell. Various schemes employing gas or liquid pressure are of considerable interest where the reflector geometry is such that the pressure distribution may be made to match the weight distribution.

The function of the support system used during launch is simply to ensure that the reflector survives the rigors of acceleration, vibration, and shock with no non-elastic deformations. Resonant frequencies of the reflector and of the reflector/mount combination are a problem of increasing severity as aperture diameter increases, and the system must be adequately damped to prevent excessive stresses and amplitudes. The operational mounting system must define the position of the reflector relative to the rest of the system.

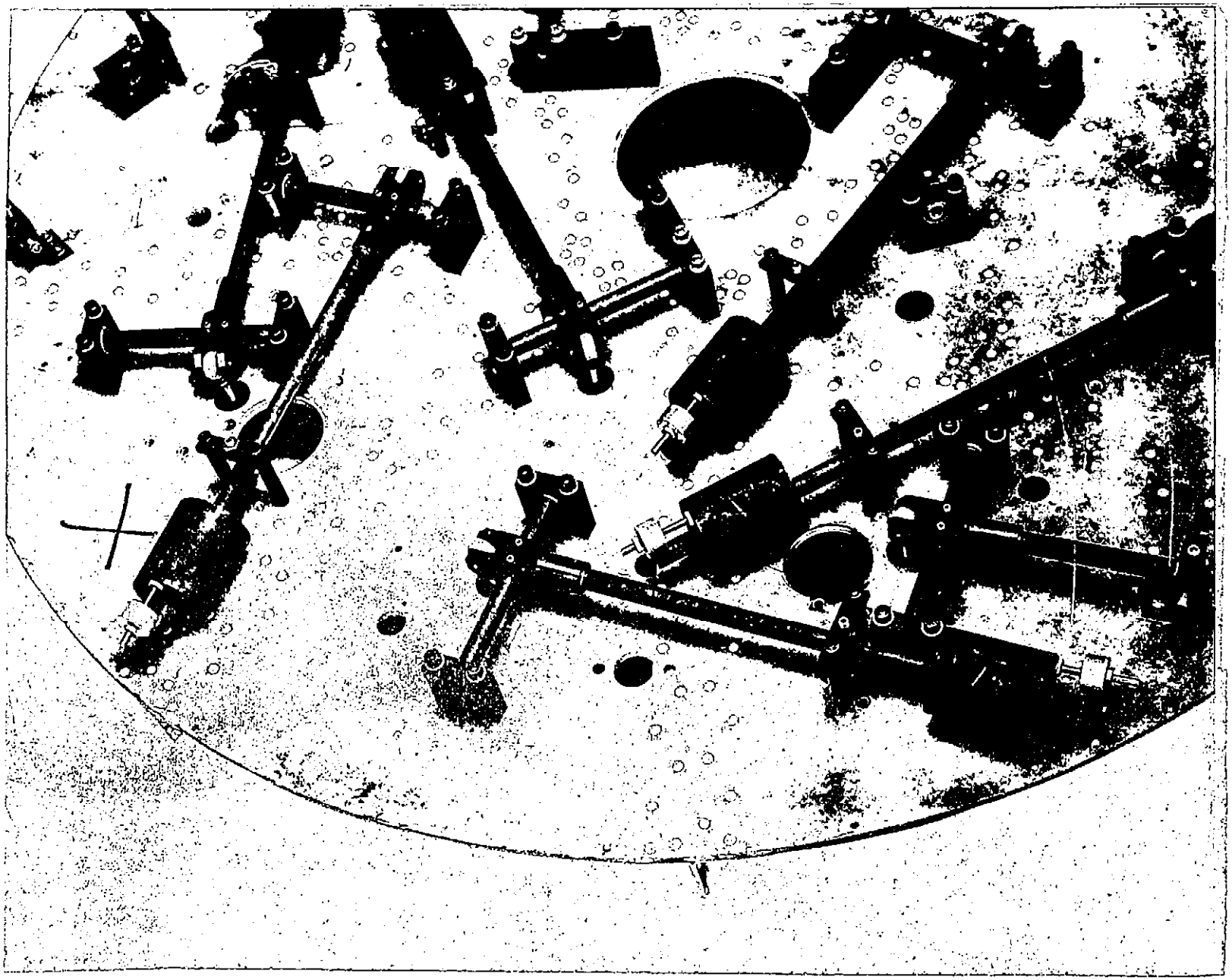

Figure C-4. A Sample of the Fifteen Counterweights Which Support The Stratoscope II Primary Mirror

Since inertial forces are negligible in the applications under consideration, the supports need have no appreciable load-carrying capability. Freedom for relative thermal expansion between the reflector and the mount must be provided. The supports should, in fact, be incapable of applying any restraining load or bending moment which might strain the reflector. Thermal effects must also be considered; the supports should not contribute to temperature gradients in the reflector.

An example of a support system which provides for launch environments and for operation is that used for the 32-inch diameter primary mirror in the Princeton Experiment Package for the Orbiting Astronomical Observatory. This fused silica mirror, which is of "egg-crate" sandwich construction, is positioned laterally (perpendicular to optical axis) by three equally spaced tangential links, as shown in Figures C-5 and C-6. These links are fastened to the mirror and to the mirror cell with ball-joints so that no bending moments may be transmitted to the mirror. The links permit the aluminum cell to thermally contract with respect to the mirror, but accurately maintain the concentricity of the two. In order to minimize localized thermal conduction paths, the links are of titanium.

In the axial direction, the mirror is supported during launch on three vibration isolators. The isolators attach to extensions or "feet" on the tangential links, as shown in Figures C-6 and C-7, and effectively protect the mirror from axial resonances.

Whereas the tangential links carry launch loads as well as defining position, the axial isolators are not suitable for the latter function. Hence,

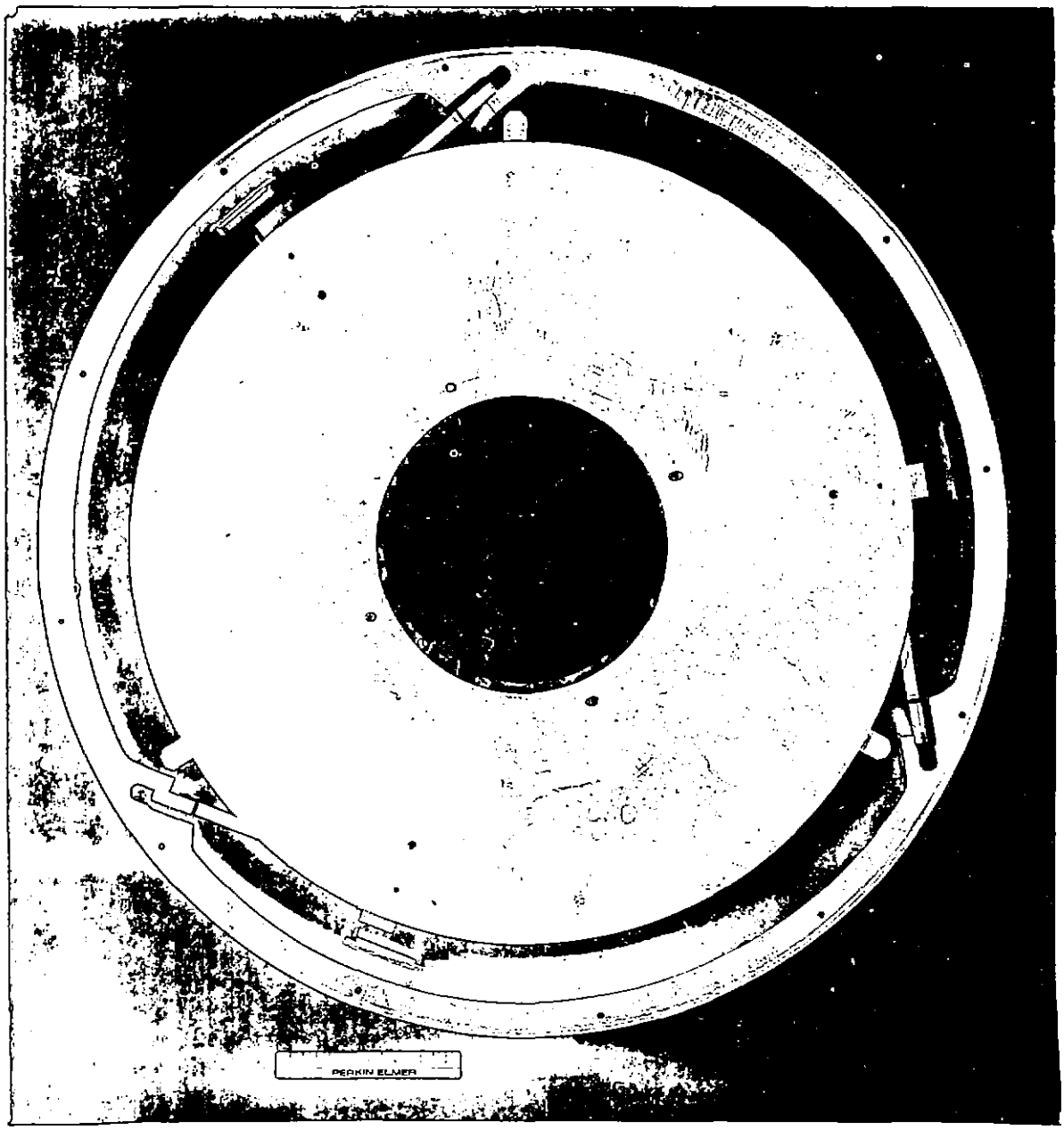

Figure C-5. Front View of (Dummy) OAO-PEP Mirror Showing Tangential Links

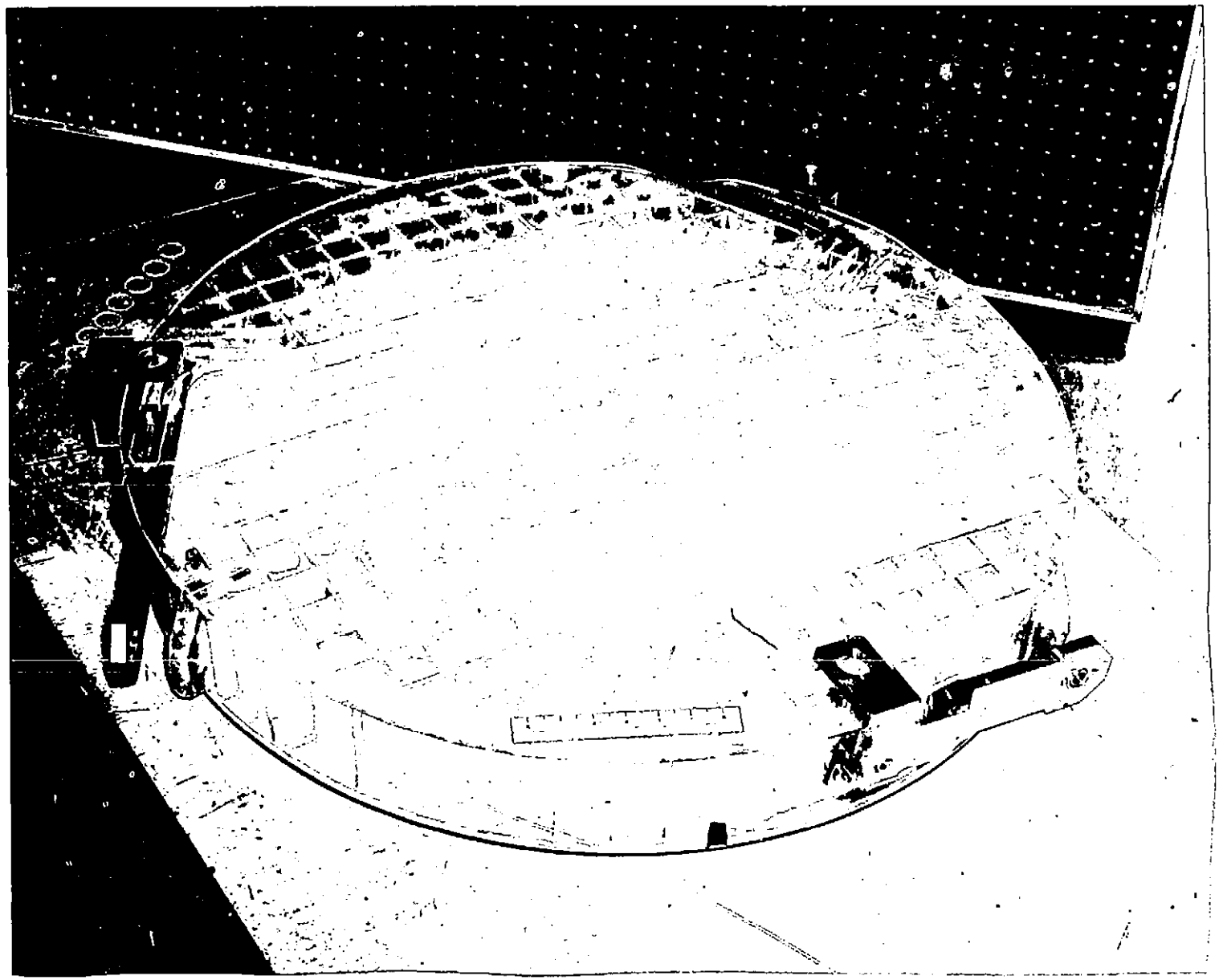

Figure C-6. OAO-PEP Mirror With Support Links Attached

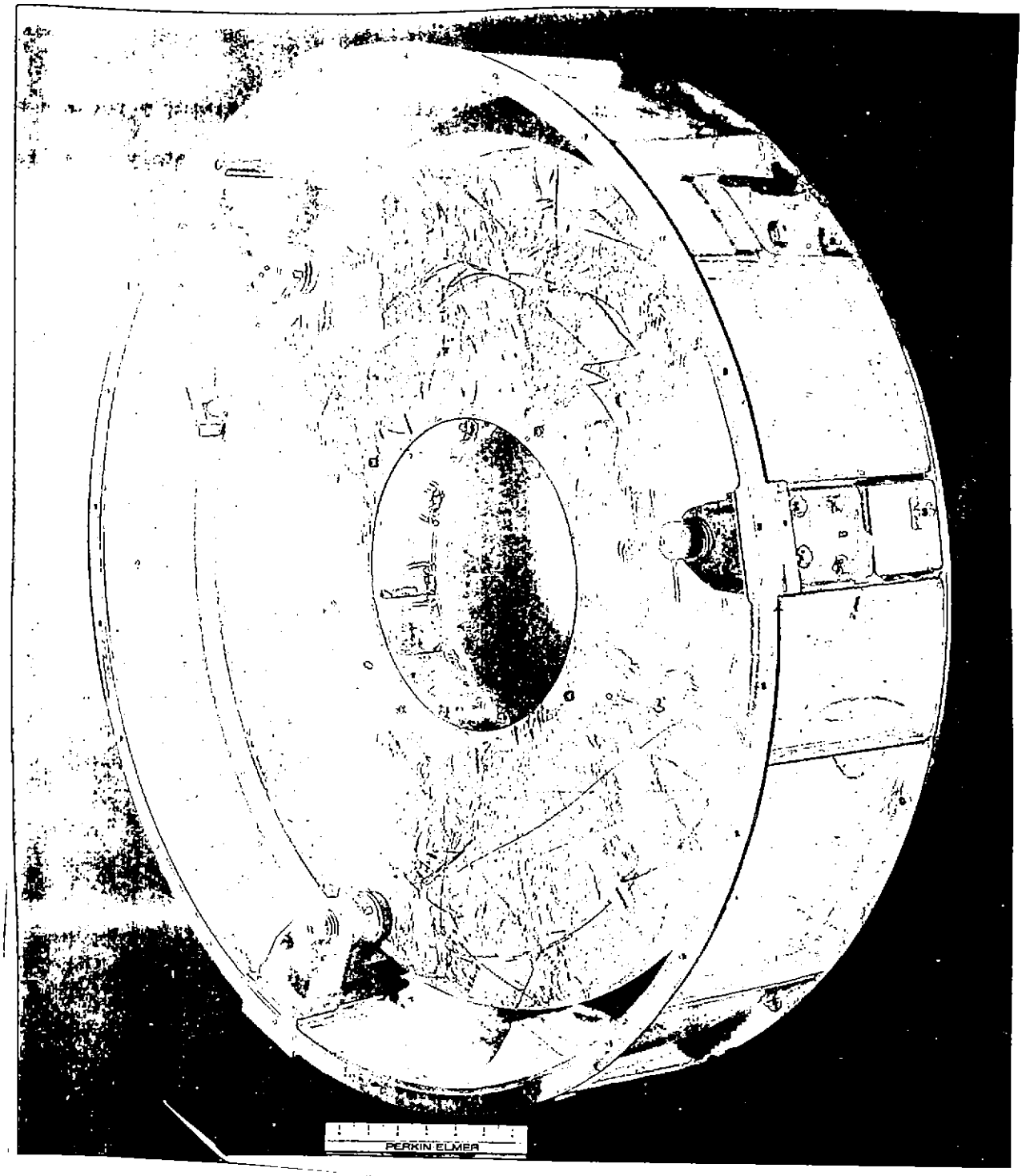

Figure C-7. Rear View of (Dummy) OAO-PEP Mirror Showing Vibration Isolators

they are disengaged after launch and the mirror is moved slightly forward by light springs until it contacts three quartz rods which accurately establish the spacing between primary and secondary mirrors.

In the axial direction, therefore, the OAO-PEP primary mirror has separate support systems for launch and for operation. In the lateral direction, a single system serves a dual function.

APPENDIX D

COMMUNICATIONS SYSTEMS AND PROBABILITY FORMULAE

APPENDIX D

COMMUNICATIONS SYSTEMS AND PROBABILITY FORMULAE

The derivations and sources of various formulae used in the analysis of pulse code modulation (PCM) and pulse position modulation (PPM) systems are given in this appendix.

A. Nyquist Sample Period

The signal to be transmitted from a deep-space probe to earth or back will very likely be either a continuous waveform or a pulsed waveform. A pulsed waveform, in which the pulse height may only assume certain discrete amplitudes to within some tolerance, may be easily encoded to a string of binary pulses or some other desired coding. The string of binary pulses then lends itself readily to transmission by a PCM system. A continuous waveform, on the other hand, may assume any amplitude within a certain range and may vary with time slowly or rapidly. The waveform will not, of course, be able to change from one amplitude to another in an infinitesimal time because of the finite rise time of all practical circuits. It will, therefore, have a maximum frequency f_{max} in its frequency spectrum. This property permits us to encode the waveform in the following way. Samples of the waveform must be taken at regular intervals. Each sample will be some amplitude value. This sample amplitude may then be transmitted directly by PPM or it may be encoded again as a string of binary digits and transmitted by PCM.

The question remains: How often must samples be taken from the continuous waveform in order to insure that the waveform may be reconstructed

accurately? The answer is as follows: If samples are taken periodically (with a period T) at a rate which is twice the highest significant signal frequency, f_{max}, then the samples contain all the information of the original continuous waveform. The period is then:

$$T = 1/2\ f_{max}$$

and is called the Nyquist sample period, or briefly, the sample period. These two remarkable statements may be found in many textbooks, and are based on the so-called Temporal Sampling Theorem. Black devotes a chapter to the discussion of sampling[1] and Woodward has given a concise proof of the Temporal Sampling Theorem.[2]

B. Pulse Code Modulation - Polarization

A pulse code modulation system (PCM) is first of all a sampled data system. Samples must be taken as in Paragraph A above to insure the recoverability of the information.

After the samples are taken, it is further necessary to quantize them. If they are voltage samples, a voltage discriminator may be used to determine whether or not the sample amplitude is equal to n(V-1/2) ±V/2 for all permitted values of n. Thus, if the sample amplitude range is zero volts to 31 volts and it is desired to quantize the amplitude to 32 possible levels, then we have V = 1 volt and n = 1,2,3...,32. The voltage discriminator then indicates the proper value of n for the input sample.

---

[1] Harold S. Black, Modulation Theory, (Princeton, New Jersey: D. Van Nostrand Company, Inc., 1953), pp. 37-58.

[2] P.M. Woodward, Probability and Information Theory, With Applications to Radar, (New York: Pergamon Press, Macmillan Co., 1953), pp. 33 f.

A binary code is assigned to each of the n levels. For instance, the code 10001 might be assigned to n = 17.

A pulse code modulation system then transmits the binary code. The system designer chooses some method of modulating the carrier wave to mark the binary ones and zeros. He may send pulses of two different heights, thus modulating the carrier amplitude (PCM-AM). He may shift the frequency to one of two different frequencies, as in frequency shift keying (PCM-FSK). He may shift the phase similarly (PCM-PSK). For optical communication from deep space an especially attractive method is to change the polarization of the laser light to left-circular polarization for one binary digit (say "1") and to right-circular polarization for the other binary digit ("0"). This last system is designated PCM-PL in this report.

A block diagram of a PCM-PL optical system appears in Figure D-1. Continuous signals are sampled, quantized, encoded, and transmitted. Pulsed data may or may not need to be quantized, depending on its nature. It must then be encoded and transmitted. The modulator may be a Kerr or Pockel Cell. The quarter-wave plates convert light back and forth between linear and circular polarization. The narrow-band filter admits some background photons along with the signal photons. All signal photons received during the transmission of a particular code bit will have the same polarization, but the background photons will, in general, have either polarization with equal probability. The prism separates the photons according to their polarization and they enter the two separate photomultiplier and amplifier channels. The outputs are differenced and discriminated. If the difference is positive, we assume the signal photons were so polarized that they entered the left channel.

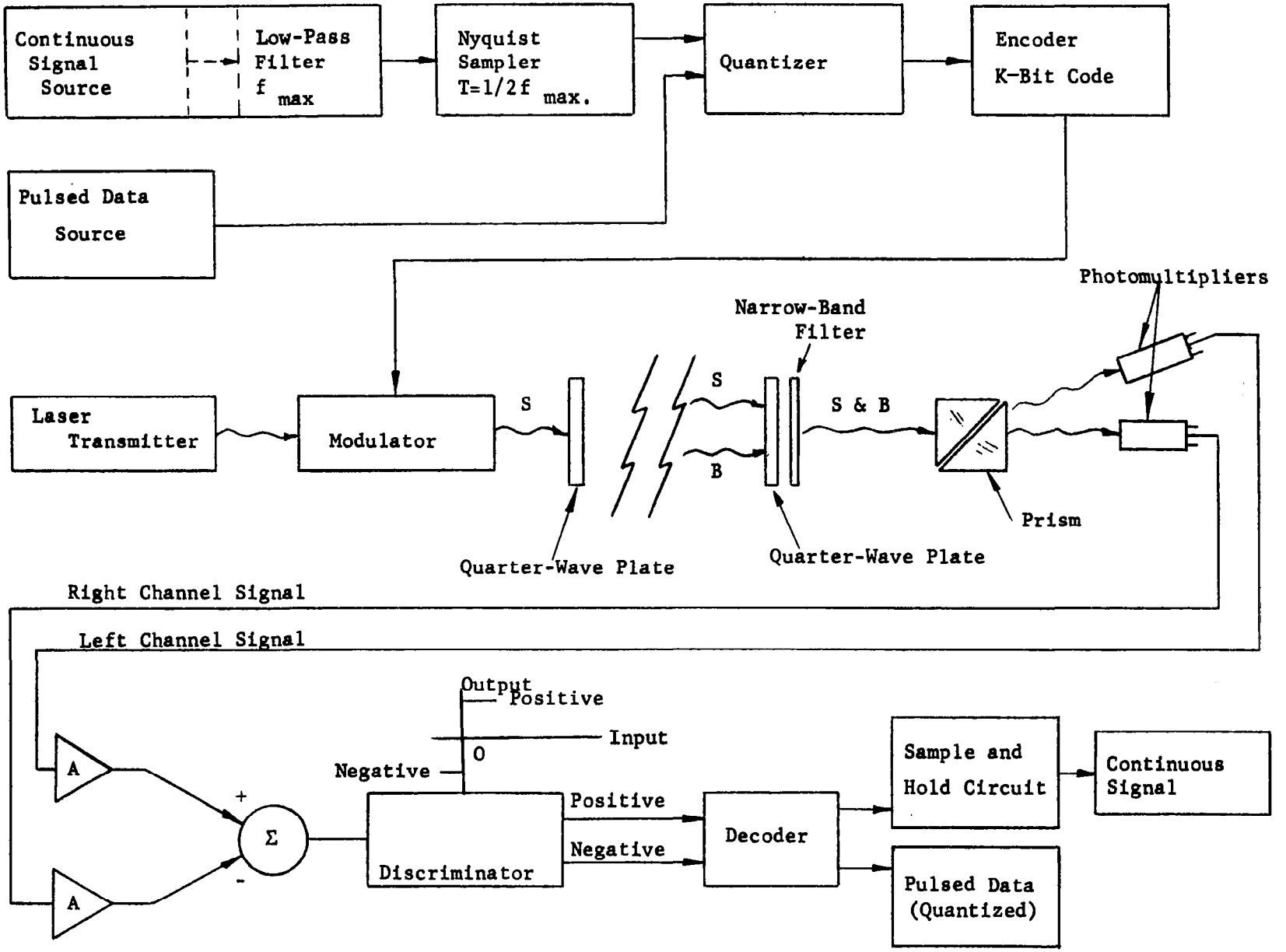

Figure D-1. Pulse Code Modulation - Polarization System

If it is negative, assume the signal was meant for the right channel. The selection of right or left is a binary choice and hopefully corresponds to the binary digit being transmitted. It will, in fact, correspond if the number of received signal photons plus the number of received background photons polarized the same way is at least one greater than the number of received background photons polarized the opposite way. A probability analysis to determine what the error rate per bit will be for various numbers of received signal and background photons per code bit time is now in order.

Let us be specific and analyze the PCM-PL system when the signal is being transmitted in the left, or positive channel. The mean number of signal quanta received during a sample period is S. If K code bits are sent as one word and one word represents the encoding of a sample then S/K signal quanta will be received in the left channel in one code bit-time, on the average. During the same code bit-time an average B/2K background quanta will be received in each channel, when the mean number of background quanta received per sample period is B.

The bit will be correctly detected if the actual number of quanta ℓ received in the left channel is at least 1 greater than the number r received in the right channel during the particular code bit-time. The bit will be incorrectly detected if ℓ is at least one less than r. We have not defined what the system will do if $r = \ell$.* However, if it is equally likely from one code bit-time to the next that the binary digit to be transmitted is zero or one, it does not matter what the system does, nor does it matter if the system does it consistently or not, when $r = \ell$. The probability of correct detection will be

1/2 when $r = \ell$. To state this point in another way, if $r = \ell$ one can gain just as much information about the transmitted signal by flipping a coin as he can by looking at the receiver output. Therefore in the following discussion, let us assume that system internal noise causes an output, and that the output will be correct with 50 percent probability.

A list of events may now be set up. If $r = \ell$ the event E_o has occurred. If $r = \ell + 1$, the event E_1 has occurred, and an error has occurred. If $r = \ell + m$, the event E_m, an error event, has occurred. The probability of an event is denoted P(E). Since the events just listed above are mutually exclusive (if one occurs none of the others can) the probability of error per code bit, R, is obtained by adding the probabilities of all the error events, plus (as we said earlier) one half the probability of the event E_o. Thus,

$$R = 1/2\ P(E_o) + P(E_1) + P(E_2) + \ldots + P(E_m) + P(E_{m+1}) + \ldots$$

$$= 1/2\ P(E_o) + \Sigma_{m=1}^{\infty}\ P(E_m)$$

Clearly R will only be finite if

$$\lim_{m \to \infty} P(E_m) = 0$$

although fulfilling this condition does not guarantee the finiteness of R.

It is now only necessary to determine $P(E_o)$ and $P(E_m)$, both of which are functions of S,B,K, and the statistics of the physical process by which quanta are transmitted and received. The simplest physical assumptions lead to the following result: if the mean number of observations of an event (such as the reception of a photon) in unit time (such as a code bit-time) is λ, then the probability of exactly k such events in unit time is

$$p(k;\lambda) = e^{-\lambda} \lambda^k / k!$$

For the left channel $\lambda = S/K + B/2K$ and for the right channel $\lambda = B/2K$, as we said earlier. Now, assuming that the number of photons received in the left channel is independent of the number received in the right channel, the probability of receiving ℓ photons in the left and r in the right is

$$\begin{aligned} P(\ell, r) &= p(\ell;\ S/K + B/2K) \cdot p(r;\ B/2K) \\ &= \left[\frac{e^{-(S/K + B/2K)} (S/K + B/2K)^{\ell}}{\ell!} \right] \cdot \left[\frac{e^{-B/2K} (B/2K)^{r}}{r!} \right] \\ &= \frac{e^{-(S + B)/K} (S/K + B/2K)^{\ell} (B/2K)^{r}}{\ell!\ r!} \end{aligned}$$

Both ℓ and r may independently assume any of the values $0, 1, 2, \ldots$ Hence the probability of the event E_o that $\ell = r$ is

$$\begin{aligned} P(E_o) &= P(0,0) + P(1,1) + P(2,2) + \ldots \\ &= \Sigma_{n=o}^{\infty} P(n,n) \\ &= \Sigma_{n=o}^{\infty} e^{-(S + B)/K} \left[(S/K + B/2K)\ (B/2K) \right]^n / (n!)^2 \\ &= e^{-(S + B)/K} \Sigma_{n=o}^{\infty} \left[(S/K + B/2K)\ (B/2K) \right]^n / (n!)^2 \end{aligned}$$

If the event E_m occurs, then by definition $r = \ell + m$. If $\ell = 0$, $r = m$; if $\ell = 1$, $r = 1 + m$, etc. Thus, the probability of the event E_m is

$$P(E_m) = P(0,m) + P(1,1+m) + P(2,2+m) + \ldots$$

$$= \sum_{n=0}^{\infty} P(n,n+m)$$

$$= \sum_{n=0}^{\infty} \frac{e^{-(S+B)/K} (S/K + B/2K)^n (B/2K)^{n+m}}{n!\,(n+m)!}$$

$$= e^{-(S+B)/K} \sum_{n=0}^{\infty} \frac{[(S/K + B/2K)(B/2K)]^n}{(n!)^2} \left[\frac{(B/2K)^m n!}{(n+m)!}\right]$$

Now, substituting $P(E_o)$ and $P(E_m)$ in the equation for R above, we have

$$R = 1/2\ e^{-(S+B)/K} \sum_{n=0}^{\infty} \left[(S/K + B/2K)(B/2K)\right]^n/(n!)^2$$

$$+ \sum_{m=1}^{\infty} e^{-(S+B)/K} \sum_{n=0}^{\infty} \frac{[(S/K + B/2K)(B/2K)]^n}{(n!)^2} \left[\frac{(B/2K)^m n!}{(n+m)!}\right]$$

$$= e^{-(S+B)/K} \sum_{n=0}^{\infty} \frac{[(S/K + B/2K)(B/2K)]^n}{(n!)^2} \left[1/2+n!\ \sum_{m=1}^{\infty} \frac{(B/2K)^m}{(n+m)!}\right]$$

For the degenerate case of B = 0 we have $R = (1/2)e^{-S/K}$. This result might be obtained finding the limit of R as B approaches zero. However it is much simpler to rederive the formula for R when B = 0. In that case the error events E_1, E_2, E_3, --- cannot occur. The event E_o can occur if, during the code bit-time, no signal photons are received. The probability of E_o is then

$$P(E_o) = p(0,S/K) = e^{-S/K} \quad \text{and} \quad R = (1/2)e^{-S/K} \quad \text{for } B = 0.$$

These formulae have been plotted for K = 5, 6, 7, and 8 in Figures 8-6 through 8-9.

The probability of receiving a bit correctly is 1-R. The probability of receiving a K-bit word correctly is $(1-R)^K$ and is denoted R'_E. The probability of receiving a K-bit code with no more than one error is

$$\binom{K}{0}(1-R)^K + \binom{K}{1} R \quad (1-R)^{K-1}$$

$$= (1-R)^K + KR\,(1-R)^{K-1}$$

$$= \left[1+(K-1)R\right]\,(1-R)^{K-1}$$

C. Pulse Position Modulation

A pulse position modulation (PPM) system is a sampled system like the PCM system. It is not ordinarily considered to be a quantized system at radio frequencies, although it may be used that way. At optical frequencies and for low signal levels it appears best to analyze the PPM system as a quantized system. Receiver and transmitter bandwidth in any case limit the resolution of a PPM to some finite number of resolvable positions. Hence in this report the PPM system discussed is a system in which one signal pulse is transmitted per sample period and in which only J positions may be resolved. Furthermore J has been chosen equal to 2^K, where K is an integer, for comparison with PCM-PL. The position of the signal pulse in the sample period as measured from the beginning of the period is then proportional to the quantized value of the sample.

Let S equal the mean number of received signal photons per sample period. These will all be received during the pulse time, i.e., at the pulse position. Let B equal the mean number of received background photons per sample period. Because a Poisson process is assumed for both signal and background sources, the mean number of received background photons per resolution element of the sample period is B/J. Hence, S+B/J photons will be received, on the average, during the pulse time.

Correct detection will occur if the number of quanta received during the pulse time is at least one greater than the number of quanta received during any other resolvable position. Otherwise an error may occur. The formula which has been used for the probable error rate, R_E, is then

$$R_E = 1 - \sum_{n=1}^{\infty} p(n;\ S+B/J) \left[\sum_{m=o}^{n-1} p(m;\ B/J) \right]^{J-1} \qquad CR-252$$

This formula is known to be slightly conservative, i.e., the actual error rate is lower than the R_E from the formula. The model is still under study. Therefore no derivation will be given. Note, however, that the power required to maintain a given error rate is then even less than that implied by the formula. Even so, reference to Figure 8-12 shows that PPM requires far less power than PCM-PL to transmit the same information or to maintain the same error rate.

D. Equal Information Capacity

The information capacity of a quantized communications channel, such as a PCM channel or a PPM channel with limited resolution, is given by

$$C = -\Sigma_i P_i \log P_i + \Sigma_i P'_i \Sigma_j P_{ij} \log P_{ij}$$

where P_i = a priori probability of sending the ith signal (relative frequency of sending the ith code word or of transmitting a pulse in the ith position. The first term of H is called the entropy of the signal).

P'_i = a priori probability of receiving the ith signal.

P_{ij} = conditional probability of receiving the jth signal, given that the ith signal has been transmitted. The second term of H is the equivocation. The information capacity is measured in bits per sample period if logarithms are taken to the base 2.

It is desirable to choose a coding scheme which maximizes the first term and to choose a modulation system which minimizes the second, for maximum information capacity.

The first term is maximized if all possible signals have equal a priori probabilities of transmission (so called "random" signaling). Assuming

that a coding scheme is chosen in this ideal way, we have for PCM

$$P_i = 1/2^K$$

and for PPM with $J = 2^K$

$$P_i = 1/J = 1/2^K$$

(We may choose $J = 2^K$, where K is the same K as for PCM, for equal sample resolution.) The signal entropy

$$C_S = -\Sigma_{i=1}^{2^K} (1/2^K) \log_2 (1/2^K)$$

$$= K \text{ bits/sample.}$$

The PCM system sends K code bits per sample. From the calculation above we see that K information bits would be sent with K code bits if there were zero equivocation. We shall see that zero equivocation implies an error rate per bit of zero or one.*

Neither the PPM system nor the PCM-PL system is more likely to receive one signal than another if the probabilities of transmitting each signal are equal. (This statement is not true for PCM-AM.) Hence

$$P'_i = P_i = 1/2^K \text{ for both systems.}$$

The P_{ij} for the two systems are different.

In the PPM system only background radiation can cause the signal to appear to be in the jth position when it was transmitted in the ith position. Given that background radiation does do that, it can make the signal appear to

---

*If it is known that the natives of some island always lie, accurate information may be obtained from them by asking questions answerable only with a "yes" or a "no."

be in any of the $J-1 = 2^K-1$ wrong positions with equal probability. The probability of an error is R_E, so the probability of reception in a particular wrong position is

$P_{ij} = R_E/(J-1) = R_E/(2^K-1)$ for $i \neq j$. The probability of reception in the correct position, P_{ii}, is the probability of making no error. Hence

$$P_{ii} = 1-R_E$$

Then for PPM the equivocation

$$C_E = \Sigma_{i=1}^{2^K} (1/2^K) \left[\Sigma_{\substack{j=1 \\ j\neq i}}^{2^K} P_{ij} \log_2 P_{ij} + P_{ii} \log_2 P_{ii} \right]$$

$$= (1/2^K) \Sigma_{i=1}^{2^K} \left\{ \left[R_E/(2^K-1) \right] \log_2 \left[R_E/(2^K-1) \right] \Sigma_{\substack{j=1 \\ j\neq i}}^{2^K} 1 + (1-R_E) \log_2 (1-R_E) \right\}$$

$$= (1/2^K)2^K \left\{ (2^K-1) \left[R_E/(2^K-1) \right] \log_2 \left[R_E/(2^K-1) \right] + (1-R_E) \log_2 (1-R_E) \right\}$$

$$= R_E \log_2 \left[R_E/(2^K-1) \right] + (1-R_E) \log_2 (1-R_E)$$

$$= \log_2 \left[R_E^{R_E} (1-R_E)^{(1-R_E)}/(2^K-1)^{R_E} \right]$$

for $R_E \neq 0$ and $R_E \neq 1$. If $R_E = 0$ or 1 the equivocation is zero.

In the PCM-PL system, background radiation and lack of signal power can cause a particular code bit to be received wrongly, with probable error rate R. The ith code word will be some sequence of binary ones and zeros. Let T denote the event that a code bit is received correctly, and let F denote incorrect reception. Let p denote the probability of correct reception of a code bit and q of incorrect reception. Then

$p = P(T) = 1-R$ and $q = P(F) = R$. The event T is a success.

The probability of having n successes in the reception of a K-bit code word is then

$$P_n = p^n q^{K-n}$$

There are $\binom{K}{n}$ ways of having n successes, where $\binom{K}{n}$ is the binomial coefficient.

$$\binom{K}{n} = K!/(K-n)!\, n! \quad \text{and} \quad 0! = 1$$

Although the equivocation for PCM-PL could be summed as the formula indicates, it is much more convenient to note that the equivocation is also equal to

$$C_E = \Sigma_{n=o}^{K} P_n \log_2 (P_n)$$

It will also be convenient to use the following identities:

$$\Sigma_{n=o}^{K} \binom{K}{n} p^n q^{K-n} = (p+q)^K = 1$$

$$\Sigma_{n=o}^{K} n \binom{K}{n} p^n q^{K-n} = Kp = K-KR$$

Now,

$$C_E = \Sigma_{n=o}^{K} \binom{K}{n} p^n q^{K-n} \log_2 \left[p^n q^{K-n} \right]$$

$$= \log_2 p \; \Sigma_{n=o}^{K} n \binom{K}{n} p^n q^{K-n}$$

$$+ K \log_2 q \; \Sigma_{n=o}^{K} \binom{K}{n} p^n q^{K-n}$$

$$- \log_2 q \; \Sigma_{n=o}^{K} n \binom{K}{n} p^n q^{K-n}$$

$$= Kp \log_2 p + K(1-p) \log_2 q$$

$$= K \log_2 p^p q^q$$

$$= K \log_2 \left[R^R (1-R)^{(1-R)} \right]$$

$$= \log_2 \left[R^{KR} (1-R)^{K(1-R)} \right]$$

for the case $R \neq 0$ and $R \neq 1$. If R = 0 or 1 the equivocation is zero.

If it is desired to have equal information capacity for PPM and PCM-PL systems with equal sample resolution it is only necessary to equate the equivocations to determine the equivalent error rates. Thus,

$$\frac{R_E^{R_E} (1-R_E)^{(1-R_E)}}{(2^K-1)^{R_E}} = R^{KR} (1-R)^{K(1-R)}$$

This implicit equation may appear to be a bit formidable when $K \neq 1$. It has been plotted in Figures 8-10 and 8-11. Note that for $K = 1$ the solution is $R_E = R$, as one might expect by considering a binary interpretation of a two-position PPM system.

E. Error Correcting Codes

There is some literature available on the general subject of error correcting codes.

A 5-bit simple code will be received correctly only if all five code bits are received correctly. However, if three extra code bits are added to each code as a check on the five code bits used to carry the information, it will be possible to correct any received code-word in which one of the code bits has been received incorrectly. One may then say that the 8-bit error correcting code word is received correctly if all eight codes are received correctly or if only seven code bits are received correctly.

If the error rate per bit is R for five-bit code words, then the equivalent error rate per code word is

$$_5R'_E = 1 - (1 - R)^5$$

Let the error rate per bit be Q for eight-bit code words. Then

$$_8R'_E = 1 - (1 - Q)^8 - 8Q\,(1 - Q)^7$$

For equivalent error rates per code word or per sample we have

$$_5R'_E = {}_8R'_E$$

$$5R - 10R^2 + 10R^3 - 5R^4 + R^5 =$$

$$28Q^2 - 112Q^3 + 210Q^4 - 224Q^5 + 140Q^6 - 48Q^7 + 7Q^8$$

CR252

For small R and Q we have

$$5R \cong 28Q^2.$$

APPENDIX E

ATMOSPHERIC EFFECTS ON SIGNAL WAVEFORMS

APPENDIX E

ATMOSPHERIC EFFECTS ON SIGNAL WAVEFORMS

One suggested experiment was the measurement of the rise time of a coherent optical pulse after passing through the whole atmosphere, or equivalently, to determine the impulse response of the atmosphere. Some study was made to determine what the order of magnitude of the result of such an experiment might be on the basis of known physical theory. Of all the possible effects only one was found which could conceivably cause the rise time to be as great as about one nanosecond. That effect was the anomalous dispersion effect. It is thought to be quite unlikely to occur.

The effect of anomalous dispersion on the rise time of a signal waveform is best illustrated by a numerical example. Anomalous dispersion is the variation of the refractive index of a gas in the vicinity of certain absorption lines. A very strong absorption line may cause a variation $\Delta N = 3 \times 10^{-5}$ over a frequency difference of about 1 Gcps. Optical communications systems are unlikely to be operated in the region of a strong absorption line, but suppose that some large Doppler effect were to shift the laser frequency over the absorption line. If a pulse as short as one nanosecond were transmitted, its frequency spectrum would have sidebands extending beyond 1 Gcps on either side of the laser frequency. Strong anomalous dispersion would cause the sidebands to experience differential time delays of $\Delta t = \Delta NL/C$, where L = 8Km is the scale height of the atmosphere and C is the velocity of light. Thus, $\Delta t = (3 \times 10^{-5} \times 8 \times 10^{3}/3 \times 10^{8})$ sec = 0.8 nanosecond. We conclude that anomalous dispersion in

the vicinity of a strong absorption line could cause the width of a 1-nanosecond optical pulse to approximately double.

Since the shortest pulses likely to be used in an optical communications system are about 50 nanoseconds long, and the optical frequency chosen would certainly not be one close enough to a strong absorption line to be shifted over the line by Doppler effects, it is thought that anomalous dispersion will not be a serious drawback to optical communications through the atmosphere. Although the question, "What is the rise time of a coherent optical pulse after passing through the whole atmosphere?" remains valid and a question of scientific interest, we feel that no experiment requiring highly specialized vehicle equipment should be made until experiments on the ground indicate that some (as yet unknown) atmospheric effect may be troublesome to optical communications.

"The aeronautical and space activities of the United States shall be conducted so as to contribute . . . to the expansion of human knowledge of phenomena in the atmosphere and space. The Administration shall provide for the widest practicable and appropriate dissemination of information concerning its activities and the results thereof."

—NATIONAL AERONAUTICS AND SPACE ACT OF 1958

NASA SCIENTIFIC AND TECHNICAL PUBLICATIONS

TECHNICAL REPORTS: Scientific and technical information considered important, complete, and a lasting contribution to existing knowledge.

TECHNICAL NOTES: Information less broad in scope but nevertheless of importance as a contribution to existing knowledge.

TECHNICAL MEMORANDUMS: Information receiving limited distribution because of preliminary data, security classification, or other reasons.

CONTRACTOR REPORTS: Technical information generated in connection with a NASA contract or grant and released under NASA auspices.

TECHNICAL TRANSLATIONS: Information published in a foreign language considered to merit NASA distribution in English.

TECHNICAL REPRINTS: Information derived from NASA activities and initially published in the form of journal articles.

SPECIAL PUBLICATIONS: Information derived from or of value to NASA activities but not necessarily reporting the results of individual NASA-programmed scientific efforts. Publications include conference proceedings, monographs, data compilations, handbooks, sourcebooks, and special bibliographies.

Details on the availability of these publications may be obtained from:

SCIENTIFIC AND TECHNICAL INFORMATION DIVISION

NATIONAL AERONAUTICS AND SPACE ADMINISTRATION

Washington, D.C. 20546